NCSAC-42

484

NCSAC-42
EANDC(US)-165"U"
INDC(USA)-36"U"

Reports to...

THE AEC NUCLEAR CROSS SECTIONS ADVISORY COMMITTEE

Meeting at

BROOKHAVEN NATIONAL LABORATORY

17-19 NOVEMBER 1971

Compiled by...
H. E. Jackson, Secretary, NCSAC
Physics Division

U of C-AUA-USAEC

Argonne National Laboratory

Printed in the United States of America
Available from
National Technical Information Service
U.S. Department of Commerce
5285 Port Royal Road
Springfield, Virginia 22151
Price: Printed Copy $3.00; Microfiche $0.95

NCSAC-42
EANDC(US)-165"U"
INDC(USA)-36"U"

REPORTS TO THE AEC NUCLEAR CROSS SECTIONS ADVISORY COMMITTEE

BROOKHAVEN NATIONAL LABORATORY

17-19 NOVEMBER 1971

Compiled by

H. E. Jackson, Secretary

NCSAC

ARGONNE NATIONAL LABORATORY

PREFACE

The reports in this document were submitted to the AEC Nuclear Cross Sections Advisory Committee (NCSAC) at the meeting at Brookhaven, New York, November 15—17, 1971. The reporting laboratories are those having a substantial effort in measuring neutron and nuclear cross sections of relevance to the U. S. applied nuclear energy program. The material contained in these reports is to be regarded as comprised of informal statements of recent developments and preliminary data. Appropriate subjects are listed as follows:

1. Microscopic neutron cross sections relevant to the nuclear energy program, including shielding. Inverse reactions where pertinent are included.

2. Charged particle cross sections, where they are relevant to 1) above, and where relevant to developing and testing nuclear models.

3. Gamma-ray production, radioactive decay, and theoretical developments in nuclear structure which are applicable to nuclear energy programs.

4. Proton and alpha-particle cross sections, at energies of up to 1 GeV, which are of interest to the space program.

These reports cannot be regarded as a complete summary of the nuclear research efforts of the AEC. A number of laboratories, whose research is less programmatically oriented do not submit reports; neither do the submitted reports reflect all the work related to nuclear cross sections in progress at the submitting laboratory. Budgetary limitations have made it mandatory to follow more strictly the subject guidelines described above and therefore to restrict the size of this document.

Persons wishing to make use of these data should contact the individual experimenter for further details. The data which appear in this document should be quoted only by permission of the contributor and should be referenced as private communication, and not by this document number.

This compilation has been produced almost completely from master copies prepared by the individual contributors listed in the Table of Contents. It is a pleasure to acknowledge their help in the preparation of these reports.

H. E. Jackson
Secretary, NCSAC
Argonne National Laboratory
Argonne, Illinois 60439

TABLE OF CONTENTS

Previously submitted Reports to the AEC Nuclear Cross Sections Advisory Committee include the following:

May 1971 Meeting at Duke University	NCSAC- 38 EANDC(US)-156U INDC(USA)- 30U
December 1970 Meeting at Lawrence Radiation Laboratory	NCSAC- 33 EANDC(US)-150U INDC(US)- 25U
May 1970 Meeting at Argonne National Laboratory	NCSAC- 31 EANDC(US)-143U INDC(US)- 22U
September 1969 Meeting at Rice University	WASH-1136 EANDC(US)-122U INDC(US)- 14U
April 1969 Meeting at Oak Ridge, Tennessee	WASH-1127 EANDC(US)-120U INDC(US)- 10U
October 1968 Meeting at Columbia University	WASH-1124 EANDC(US)-111U INDC(US)- 9U
April 1968 Meeting at Los Alamos, New Mexico	WASH-1093 EANDC(US)-105U INDC(US)- 2U
October 1967 Meeting at Idaho Falls, Idaho	WASH-1079 EANDC(US)-104U INDC(US)- 12U
April 1967 Meeting at Brookhaven, New York	WASH-1074 EANDC(US)- 99U INDC(US)- 9U
November 1966 Meeting at Argonne, Illinois	WASH-1071 EANDC(US)- 91U INDC(US)- 5U
March 1966 Meeting at Washington, D. C.	WASH-1068 EANDC(US)- 85U INDC(US)- 3U

The following is an index to measurements in NCSAC 42 pertinent to entries listed in NCSAC-35, "Compilation of Requests for Nuclear Cross Section Measurements", (March 1971). A CINDA-type index, prepared by L. T. Whitehead, of the Division of Technical Information, follows on page viii.

NCSAC-35 REQUEST NO.	MATERIAL	X-SECTION	NCSAC-42 PAGE NO.
1	H-1	Total	213
4	H-3	Elastic	154
7	He-3	Elastic	158
17	Li-7	Total	213
32	C	Elastic	8
33	C	Elastic	190
33	C	Elastic	256
34	C	Emission	190
35	C	Total $\bar{g}$ Prod.	181
37	C-12	Polariz.	260
38,39	N	Elastic	181,191,256
40	N	Emission	181,191
42	N	Total $\bar{g}$ Prod.	181
43	O	Elastic	181,256
44	O	Emission	181
46	O	Total $\bar{g}$ Prod.	181
54	Na	Total	61
58	Na	N, Gamma	185
60	Al	Elastic	181
61	Al	Emission	181
63	Al	Total $\bar{g}$ Prod.	105,181,191
65	Al	Elastic	181
66	Al	Emission	181
71	Ca	Elastic	181
72	Ca	Emission	181
73	Ca	Total $\bar{g}$ Prod.	192
78,79,80	Ti	Total $\bar{g}$ Prod.	195
82	Ti-47	N, proton	10
84	V	Elastic	8,10
97	Fe	Elastic	215

NCSAC-35 REQUEST NO.	MATERIAL	X-SECTION	NCSAC-42 PAGE NO.
97,98	Fe	Elastic	8,181,256
101	Fe	Emission	181
104	Fe	Total $\bar{g}$ Prod.	181
107	Fe-54	N, Gamma	219
111	Fe-58	N, Gamma	219
117	Ni	Total	172
118	Ni	Elastic	8
119	Ni	Emission	8
122,123	Ni	Total $\bar{g}$ Prod.	195
129	Cu-63	N, Gamma	185
131	Cu-65	N, Gamma	185
153	Zr	Elastic	10
169	Zr-90	N, Gamma	185
176	Zr-91	N, Gamma	185
185	Zr-92	N, Gamma	185
192	Zr-94	N, Gamma	185
203	Nb	Elastic	8,10
205	Nb	Emission	8
208	Nb	Cap. Spect.	29
209	Nb	Total $\bar{g}$ Prod.	195
253	Sm-152	Res. Int.	61
278	Gd-154	Res. Params	61
290	Gd-158	Res. Params	61
292	Gd-160	Res. Params	61
322	Ta	Total $\bar{g}$ Prod.	195
358,359	U-233	Fission	100,130
361,362	U-233	Nu Bar	130
400	U-235	Res. Params	48,98,153
388,389	U-235	Fission	16,17,98
388,389,390,391	U-235	Fission	130,160
388,389,390	U-235	Fission	199
393	U-235	Alpha	199
395	U-235	Nu Bar	130,219
396	U-235	Fis n Y	15
398	U-235	Cap. Spect.	48

NCSAC-35 REQUEST NO.	MATERIAL	X-SECTION	NCSAC-42 PAGE NO.
427	U-238	Total	61
427	U-238	Res. Params	71
412	U-238	Elastic	8
413	U-238	Inelastic	8
417	U-238	Fission	17,130
419	U-238	Nu Bar	130
425	U-238	Delayed $\bar{g}$ Y	142
436,437,438	Pu-238	Fission	130
444	Pu-239	Elastic	9
449,450,451	Pu-239	Fission	130
451	Pu-239	Fission Ratio	199
452	Pu-239	Nu Bar	130
455	Pu-239	Alpha	199
456	Pu-239	Delayed $\bar{g}$ Y	117,142
463	Pu-240	Emission	9
464,466	Pu-240	Fission, Nu Bar	130
468,469	Pu-240	N, Gamma	213
471	Pu-240	Res. Params	213
474,476	Pu-241	Fission, Nu Bar	130
499	Am-242	Fission	135
506	Cm-243	Fission	135
515	Cm-245	Fission	135
521	Cm-247	Fission	135
528	Cf-249	Fission	135

ELEMENT S	A	QUANTITY	TYPE	ENERGY MIN	MAX	DOCUMENTATION REF	VOL	PAGE	DATE	LAB	COMMENTS	SERIAL NO.
H	001	TOTAL XSECT	EXPT-PROG	5.0 5	1.2 7	NCSAC-42	213		N/71	RPI	STOLER+. TRANS. LINAC. CURVE	60374
H	001	DIFF ELASTIC	EXPT-PROG	5.0 6	2.0 7	NCSAC-42	260		N/71	YAL	FIRK+. LEFT-RIGHT ASYMETTRY. NO DATA	60379
H	001	POLARIZATION	EXPT-PROG	5.0 6	2.0 7	NCSAC-42	260		N/71	YAL	FIRK+. LEFT-RIGHT ASYMETTRY. NO DATA	59921
D	002	TOTAL XSECT	EXPT-PROG	5.5 6	4.6 7	NCSAC-42	154		N/71	LAS	SEAGRAVE+. TABLE 10ES. TBP AP	60166
D	002	TOTAL XSECT	EXPT-PROG	5.0 5	1.2 7	NCSAC-42	213		N/71	RPI	STOLER+. TRANS. LINAC. CURVE	60373
D	002	ELASTIC	EXPT-PROG	5.5 6	4.6 7	NCSAC-42	154		N/71	LAS	SEAGRAVE+. TABLE 10ES. TBP AP	60165
D	002	NONELASTIC	EXPT-PROG	5.5 6	4.6 7	NCSAC-42	154		N/71	LAS	SEAGRAVE+. TABLE 10ES. TBP AP	60164
D	002	N2N REACTION	EXPT-PROG	1.4 7		NCSAC-42	158		N/71	LAS	GRAVES+. PROTON SPECTRUM SHOWN.	60159
T	003	TOTAL XSECT	EXPT-PROG	6.0 6	2.3 7	NCSAC-42	154		N/71	LAS	SEAGRAVE+. TABLE 7 ES. TBP AP	60163
T	003	ELASTIC	EXPT-PROG	6.0 6	2.3 7	NCSAC-42	154		N/71	LAS	SEAGRAVE+. TABLE 7 ES. TBP AP	60162
T	003	NONELASTIC	EXPT-PROG	6.0 6	2.3 7	NCSAC-42	154		N/71	LAS	SEAGRAVE+. TABLE 7 ES. TBP AP	60161
HE	003	EVALUATION	EVAL-PROG		2.0 7	NCSAC-42	170		N/71	LAS	BATTAT+. NO DATA GIVEN	60357
HE	003	DIFF ELASTIC	EXPT-PROG	7.9 6	2.4 7	NCSAC-42	158		N/71	LAS	DROSG+. TOF. ANG DIST MEASD. NO DATA	60160
LI	006	EVALUATION	EVAL-PROG		2.0 7	NCSAC-42	170		N/71	LAS	BATTAT+. NO DATA GIVEN	60356
LI	006	TOTAL XSECT	EVAL-PROG		2.0 7	NCSAC-42	170		N/71	LAS	BATTAT+. NO DATA GIVEN	60354
LI	006	DIFF ELASTIC	EVAL-PROG		2.0 7	NCSAC-42	170		N/71	LAS	BATTAT+. NO DATA GIVEN	60353
LI	007	TOTAL XSECT	EXPT-PROG	1.5 7	2.5 7	NCSAC-42	213		N/71	RPI	STOLER+. TRANS. LINAC. CURVE	60372
BE	009	DIFF ELASTIC	EXPT-PROG	7.6 6		NCSAC-42	256		N/71	ABD	HOLLANDSWORTH+. 2-150EG. TO BE DONE	60392
B	010	EVALUATION	EVAL-PROG		2.0 7	NCSAC-42	170		N/71	LAS	BATTAT+. NO DATA GIVEN	60355
B	010	DIFF ELASTIC	EVAL-PROG		2.0 7	NCSAC-42	170		N/71	LAS	BATTAT+. NO DATA GIVEN	60351
B	010	N,ALPHA	THEO-PROG	NDG		NCSAC-42	31		N/71	ANL	HAUSLADEN+. R-MATRIX CALC. NO DATA	59932
B	010	N,ALPHA	EXPT-PROG	NDG		NCSAC-42	114		N/71	GA	FRIESENHAHN+. MEAST NOT MADE YET	60198
B	010	N,ALPHA	EVAL-PROG		2.0 7	NCSAC-42	170		N/71	LAS	BATTAT+. NO DATA GIVEN	60352
C		TOTAL XSECT	EXPT-PROG	1.7 6	2.4 6	NCSAC-42	12		N/71	ANL	WHALEN+. OVER 2.08-EV RESON. CURVE.	60012
C		DIFF ELASTIC	EXPT-PROG	1.5 6	3.0 6	NCSAC-42	8		N/71	ANL	GUENTHER+. 20-160DEG. TBC. NO DATA	59959
C		DIFF ELASTIC	EXPT-PROG	5.2 6	8.7 6	NCSAC-42	190		N/71	ORL	PEREY+. ANAL TBC. NO DATA GIVEN	60282
C		DIFF ELASTIC	EXPT-PROG	1.0 7	1.4 7	NCSAC-42	256		N/71	ABD	HOLLANDSWORTH+. SMALL ANG.TO BE DONE	60383
C		DIFF ELASTIC	EXPT-PROG	7.6 6	9.5 6	NCSAC-42	256		N/71	ABD	HOLLANDSWORTH+.TBL+CURV.2.8-150EG CM	60386
C		NONEL GAMMAS	EXPT-PROG	1.0 6	1.5 7	NCSAC-42	195		N/71	ORL	MORGAN+. NAI DET. GAM SPECT. NO DATA	60415
C		DIFF INELAST	EXPT-PROG	1.5 6	3.0 6	NCSAC-42	8		N/71	ANL	GUENTHER+. 20-160DEG. TBC. NO DATA	59946
C		DIFF INELAST	EXPT-PROG	5.2 6	8.7 6	NCSAC-42	190		N/71	ORL	PEREY+. ANAL TBC. NO DATA GIVEN	60281
C		INELST GAMMA	EXPT-PROG	1.5 7		NCSAC-42	181		N/71	TNC	NELLIS+. NO DATA GIVEN. TBP NSE	60285
C	012	DIFF ELASTIC	EXPT-PROG	2.0 6	5.0 6	NCSAC-42	260		N/71	YAL	FIRK+. POL AT 50DEG LAB. CURVES	60378
C	012	POLARIZATION	EXPT-PROG	2.0 6	5.0 6	NCSAC-42	260		N/71	YAL	FIRK+. POL AT 50DEG LAB. CURVES	60377
C	012	SPECT NGAMMA	EXPT-PROG	THR		NCSAC-42	163		N/71	LAS	JURNEY. PRELIMINARY ES GIVEN	60157
N		EVALUATION	EVAL-PROG	1.0-5	2.0 7	NCSAC-42	169		N/71	LAS	YOUNG+. COMPLETE RE-EVAL. TBP LA4725	60154
N		TOTAL XSECT	EVAL-PROG	1.0-5	2.0 7	NCSAC-42	169		N/71	LAS	YOUNG+. COMPLETE RE-EVAL. TBP LA4725	60151
N		DIFF ELASTIC	EVAL-PROG	1.0-5	2.0 7	NCSAC-42	169		N/71	LAS	YOUNG+. COMPLETE RE-EVAL. TBP LA4725	60148
N		DIFF ELASTIC	EXPT-PROG	6.0 6	8.5 6	NCSAC-42	191		N/71	ORL	PEREY+. 6ES. NO DATA GIVEN	60268
N		DIFF ELASTIC	EXPT-PROG	9.0 6	1.1 7	NCSAC-42	181		N/71	TNC	TUCKER+. NO DATA GIVEN. REPORT TBP	60291
N		DIFF ELASTIC	EXPT-PROG	1.0 7	1.4 7	NCSAC-42	256		N/71	ABD	HOLLANDSWORTH+. SMALL ANG.TO BE DONE	60381
N		DIFF ELASTIC	EXPT-PROG	7.6 6	9.5 6	NCSAC-42	256		N/71	ABD	HOLLANDSWORTH+.2ES.TBL 2.8-150EG C-M	60384
N		NONELASTIC	EXPT-PROG	6.0 6	8.5 6	NCSAC-42	191		N/71	ORL	PEREY+. NO DATA GIVEN	60267
N		NONEL GAMMAS	EVAL-PROG	1.0-5	2.0 7	NCSAC-42	169		N/71	LAS	YOUNG+. COMPLETE RE-EVAL. TBP LA4725	60360
N		DIFF INELAST	EVAL-PROG	1.0-5	2.0 7	NCSAC-42	169		N/71	LAS	YOUNG+. COMPLETE RE-EVAL. TBP LA4725	60145
N		DIFF INELAST	EXPT-PROG	9.0 6	1.1 7	NCSAC-42	181		N/71	TNC	TUCKER+. NO DATA GIVEN. REPORT TBP	60280
N		INELST GAMMA	EXPT-PROG	9.0 6	1.1 7	NCSAC-42	181		N/71	TNC	TUCKER+. NO DATA GIVEN. REPORT TBP	60274
N		INELST GAMMA	EXPT-PROG	1.5 7		NCSAC-42	181		N/71	TNC	NELLIS+. NO DATA GIVEN. TBP NSE	60284

ELEMENT S	A	QUANTITY	TYPE	ENERGY MIN	MAX	DOCUMENTATION REF	VOL	PAGE	DATE	LAB	COMMENTS	SERIAL NO.
O		EVALUATION	EVAL-PROG	1.0-5	2.0 7	NCSAC-42	169		N/71	LAS	YOUNG+. COMPLETE RE-EVAL. TBP LA4780	60153
O		TOTAL XSECT	EXPT-PROG	5.0 5	2.0 7	NCSAC-42	172		N/71	NBS	SCHWARTZ+. TRANSMISSION. CURVE	60142
O		TOTAL XSECT	EVAL-PROG	1.0-5	2.0 7	NCSAC-42	169		N/71	LAS	YOUNG+. COMPLETE RE-EVAL. TBP LA4780	60150
O		DIFF ELASTIC	EVAL-PROG	1.0-5	2.0 7	NCSAC-42	169		N/71	LAS	YOUNG+. COMPLETE RE-EVAL. TBP LA4780	60147
O		DIFF ELASTIC	EXPT-PROG	9.0 6	1.1 7	NCSAC-42	181		N/71	TNC	TUCKER+. NO DATA GIVEN. REPORT TBP	60290
O		DIFF ELASTIC	EXPT-PROG	1.0 7	1.4 7	NCSAC-42	256		N/71	ABD	HOLLANDSWORTH+. SMALL ANG.TO BE DONE	60382
O		DIFF ELASTIC	EXPT-PROG	7.6 6	9.5 6	NCSAC-42	256		N/71	ABD	HOLLANDSWORTH+.2ES.TBL 2.8-15DEG C-M	60385
O		NONEL GAMMAS	EVAL-PROG	1.0-5	2.0 7	NCSAC-42	169		N/71	LAS	YOUNG+. COMPLETE RE-EVAL. TBP LA4780	60359
O		DIFF INELAST	EVAL-PROG	1.0-5	2.0 7	NCSAC-42	169		N/71	LAS	YOUNG+. COMPLETE RE-EVAL. TBP LA4780	60144
O		DIFF INELAST	EXPT-PROG	9.0 6	1.1 7	NCSAC-42	181		N/71	TNC	TUCKER+. NO DATA GIVEN. REPORT TBP	60269
O		INELST GAMMA	EXPT-PROG	9.0 6	1.1 7	NCSAC-42	181		N/71	TNC	TUCKER+. NO DATA GIVEN. REPORT TBP	60275
O		INELST GAMMA	EXPT-PROG	1.5 7		NCSAC-42	181		N/71	TNC	NELLIS+. NO DATA GIVEN. TBP NSE	60283
F	019	TOTAL XSECT	EXPT-PROG	1.0 2	2.0 5	NCSAC-42	69		N/71	COL	SINGH+. R-MATRIX FIT TO1970DATA,CURV	60046
F	019	RESON PARAMS	EXPT-PROG	2.7 4	9.7 4	NCSAC-42	69		N/71	COL	SINGH+. L J PI WN WIGNER LMT 3 RESON	60215
F	019	STRNTH FNCTN	EXPT-PROG	1.0 2	2.0 5	NCSAC-42	69		N/71	COL	SINGH+. S1 VALUE GIVEN	60039
NE		TOTAL XSECT	EXPT-PROG	NDG		NCSAC-42	61		N/71	COL	HACKEN+. TRANS. ANAL TBC. NO DATA	60090
NA	023	EVALUATION	EVAL-PROG	NDG		NCSAC-42	210		N/71	ORL	KINNEY+. NO DATA GIVEN	60413
NA	023	TOTAL XSECT	EXPT-PROG	NDG		NCSAC-42	61		N/71	COL	HACKEN+. TRANS. ANAL TBC. NO DATA	60098
NA	023	N,GAMMA	EXPT-PROG	3.0 3	5.0 5	NCSAC-42	185		N/71	ORL	MACKLIN+. DRELA. ANAL TBC. NO DATA	60340
MG		TOTAL XSECT	EXPT-PROG	1.0 2	5.0 5	NCSAC-42	69		N/71	COL	SINGH+. R-MATRIX FIT TO1970DATA,NDG	60045
MG		TOTAL XSECT	EXPT-PROG	NDG		NCSAC-42	61		N/71	COL	HACKEN+. TRANS. ANAL TBC. NO DATA	60097
MG	024	RESON PARAMS	EXPT-PROG	8.2 4	4.3 5	NCSAC-42	69		N/71	COL	SINGH+. L J PI WN WIGNER LMT 3 RESON	60214
MG	024	STRNTH FNCTN	EXPT-PROG	1.0 2	5.0 5	NCSAC-42	69		N/71	COL	SINGH+. S1 VALUE GIVEN	60038
MG	025	RESON PARAMS	EXPT-PROG	2.0 4		NCSAC-42	69		N/71	COL	SINGH+. L J PI WN WIGNER LMT	60213
MG	025	STRNTH FNCTN	EXPT-PROG	1.0 2	5.0 5	NCSAC-42	69		N/71	COL	SINGH+. S1 VALUE GIVEN	60037
AL	027	EVALUATION	EVAL-PROG	1.0-5	2.0 7	NCSAC-42	169		N/71	LAS	YOUNG+. COMPLETE RE-EVAL. TBP LA4726	60152
AL	027	TOTAL XSECT	EXPT-PROG	1.0 2	2.2 5	NCSAC-42	69		N/71	COL	SINGH+. R-MATRIX FIT TO1970DATA,CURV	60044
AL	027	TOTAL XSECT	EXPT-PROG	NDG		NCSAC-42	61		N/71	COL	HACKEN+. TRANS. ANAL TBC. NO DATA	60096
AL	027	TOTAL XSECT	EVAL-PROG	1.0-5	2.0 7	NCSAC-42	169		N/71	LAS	YOUNG+. COMPLETE RE-EVAL. TBP LA4726	60149
AL	027	TOTAL XSECT	EXPT-PROG	5.0 5	6	NCSAC-42	172		N/71	NBS	SCHRACK. INTERMEDIATE STRUCT.NDG.TBP	60300
AL	027	RESON PARAMS	EXPT-PROG	5.9 3	2.1 5	NCSAC-42	69		N/71	COL	SINGH+. L J PI WN D(AVG) 8 RESON	60209
AL	027	STRNTH FNCTN	EXPT-PROG	1.0 2	2.2 5	NCSAC-42	69		N/71	COL	SINGH+. S0 AND S1 VALUES GIVEN	60036
AL	027	DIFF ELASTIC	EXPT-PROG	2.0 6		NCSAC-42	10		N/71	ANL	COX. NO DATA GIVEN.	60011
AL	027	DIFF ELASTIC	EVAL-PROG	1.0-5	2.0 7	NCSAC-42	169		N/71	LAS	YOUNG+. COMPLETE RE-EVAL. TBP LA4726	60146
AL	027	DIFF ELASTIC	EXPT-PROG	9.0 6	1.1 7	NCSAC-42	181		N/71	TNC	TUCKER+. NO DATA GIVEN. REPORT TBP	60289
AL	027	DIFF ELASTIC	EXPT-PROG	7.6 6		NCSAC-42	256		N/71	ABD	HOLLANDSWORTH+. 2-15DEG. TO BE DONE	60391
AL	027	POLARIZATION	EXPT-PROG	2.0 6		NCSAC-42	10		N/71	ANL	COX. NO DATA GIVEN	59991
AL	027	NONEL GAMMAS	EXPT-PROG	8.6 5	1.7 7	NCSAC-42	105		N/71	GA	ORPHAN+. GAMMA PRODUCTION SIGS GIVEN	60199
AL	027	NONEL GAMMAS	EVAL-PROG	1.0-5	2.0 7	NCSAC-42	169		N/71	LAS	YOUNG+. COMPLETE RE-EVAL. TBP LA4726	60358
AL	027	DIFF INELAST	EVAL-PROG	1.0-5	2.0 7	NCSAC-42	169		N/71	LAS	YOUNG+. COMPLETE RE-EVAL. TBP LA4726	60143
AL	027	DIFF INELAST	EXPT-PROG	9.0 6	1.1 7	NCSAC-42	181		N/71	TNC	TUCKER+. NO DATA GIVEN. REPORT TBP	60270
AL	027	INELST GAMMA	EXPT-PROG	5.3 6	9.0 6	NCSAC-42	191		N/71	ORL	DICKENS. BES. GE(LI) DET. CURVES	60241
AL	027	INELST GAMMA	EXPT-PROG	9.0 6	1.1 7	NCSAC-42	181		N/71	TNC	TUCKER+. NO DATA GIVEN. REPORT TBP	60276
SI		TOTAL XSECT	EXPT-PROG	5.0 5	6	NCSAC-42	172		N/71	NBS	SCHRACK. INTERMEDIATE STRUCT.NDG.TBP	60295
SI		RESON PARAMS	EXPT-PROG	1.9 2	1.6 3	NCSAC-42	228		N/71	OKE	PINEO+. WN GIVEN FOR 10 RESONANCES	60361
SI		DIFF ELASTIC	EXPT-PROG	9.0 6	1.1 7	NCSAC-42	181		N/71	TNC	TUCKER+. NO DATA GIVEN. REPORT TBP	60288
SI		DIFF INELAST	EXPT-PROG	9.0 6	1.1 7	NCSAC-42	181		N/71	TNC	TUCKER+. NO DATA GIVEN. REPORT TBP	60271
SI		INELST GAMMA	EXPT-PROG	9.0 6	1.1 7	NCSAC-42	181		N/71	TNC	TUCKER+. NO DATA GIVEN. REPORT TBP	60277

ELEMENT S A	QUANTITY	TYPE	ENERGY MIN	ENERGY MAX	DOCUMENTATION REF VOL PAGE DATE	LAB	COMMENTS	SERIAL NO.
SI 028	N,GAMMA	EXPT-PROG	3.0 3	5.0 5	NCSAC-42 185 N/71	ORL	MACKLIN+. ORELA. ANAL TBC. NO DATA	60339
SI 029	TOTAL XSECT	EXPT-PROG	1.0 3	5	NCSAC-42 183 N/71	ORL	GOOD+. TOF. 3 NEW RESON ES GIVEN	60305
SI 029	RESON PARAMS	EXPT-PROG	1.0 3	5	NCSAC-42 183 N/71	ORL	GOOD+. TOF. 3 NEW RESON ES GIVEN	60245
S	TOTAL XSECT	EXPT-PROG	1.0 2	4.0 5	NCSAC-42 69 N/71	COL	SINGH+. R-MATRIX FIT TO1970DATA,NDG	60043
S 032	RESON PARAMS	EXPT-PROG	3.0 4	3.8 5	NCSAC-42 69 N/71	COL	SINGH+. L J PI WN WIGNER LMT 6 RESON	60212
S 032	STRNTH FNCTN	EXPT-PROG	1.0 2	4.0 5	NCSAC-42 69 N/71	COL	SINGH+. SO AND S1 VALUES GIVEN	60035
CL	TOTAL XSECT	EXPT-PROG	1.0 2	2.0 5	NCSAC-42 69 N/71	COL	SINGH+. R-MATRIX FIT TO1970DATA,CURV	60042
CL	TOTAL XSECT	EXPT-PROG	NDG		NCSAC-42 61 N/71	COL	HACKEN+. TRANS. ANAL TBC. NO DATA	60095
CL 035	RESON PARAMS	EXPT-PROG	-2. 2	1.9 5	NCSAC-42 69 N/71	COL	SINGH+. L J PI WN D(AVG) 24RESON	60207
CL 035	STRNTH FNCTN	EXPT-PROG	1.0 2	2.0 5	NCSAC-42 69 N/71	COL	SINGH+. SO AND S1 VALUES GIVEN	60034
CL 037	RESON PARAMS	EXPT-PROG	1.1 3	1.4 5	NCSAC-42 69 N/71	COL	SINGH+. L J PI WN D(AVG) 21RESON	60208
CL 037	STRNTH FNCTN	EXPT-PROG	1.0 2	2.0 5	NCSAC-42 69 N/71	COL	SINGH+. SO AND S1 VALUES GIVEN	60033
K	TOTAL XSECT	EXPT-PROG	1.0 2	2.0 5	NCSAC-42 69 N/71	COL	SINGH+. R-MATRIX FIT TO1970DATA,NDG	60041
K	TOTAL XSECT	EXPT-PROG	NDG		NCSAC-42 61 N/71	COL	HACKEN+. TRANS. ANAL TBC. NO DATA	60094
K 039	RESON PARAMS	EXPT-PROG	-1. 3	2.0 5	NCSAC-42 69 N/71	COL	SINGH+. L J PI WN D(AVG) 31RESON	60206
K 039	STRNTH FNCTN	EXPT-PROG	1.0 2	2.0 5	NCSAC-42 69 N/71	COL	SINGH+. SO AND S1 VALUES GIVEN	60032
K 041	RESON PARAMS	EXPT-PROG	1.1 3	9.3 4	NCSAC-42 69 N/71	COL	SINGH+. L J PI WN D(AVG) 39RESON	60205
K 041	STRNTH FNCTN	EXPT-PROG	1.0 2	2.0 5	NCSAC-42 69 N/71	COL	SINGH+. SO AND S1 VALUES GIVEN	60031
CA	EVALUATION	EVAL-PROG	NDG		NCSAC-42 210 N/71	ORL	KINNEY+. NO DATA GIVEN	60412
CA	TOTAL XSECT	EXPT-PROG	1.0 2	3.0 5	NCSAC-42 69 N/71	COL	SINGH+. R-MATRIX FIT TO1970DATA,NDG	60040
CA	TOTAL XSECT	EXPT-PROG	NDG		NCSAC-42 61 N/71	COL	HACKEN+. TRANS. ANAL TBC. NO DATA	60093
CA	TOTAL XSECT	EXPT-PROG	5.0 5	2.0 7	NCSAC-42 172 N/71	NBS	SCHWARTZ+. TRANSMISSION. CURVE	60141
CA	TOTAL XSECT	EXPT-PROG	5.0 5	6	NCSAC-42 172 N/71	NBS	SCHRACK. INTERMEDIATE STRUCT.NDG.TBP	60299
CA	DIFF ELASTIC	EXPT-PROG	9.0 6	1.1 7	NCSAC-42 181 N/71	TNC	TUCKER+. NO DATA GIVEN. REPORT TBP	60287
CA	NONEL GAMMAS	EXPT-PROG	4.8 6	8.0 6	NCSAC-42 192 N/71	ORL	DICKENS+. GE(LI) DET. NO DATA GIVEN	60237
CA	DIFF INELAST	EXPT-PROG	9.0 6	1.1 7	NCSAC-42 181 N/71	TNC	TUCKER+. NO DATA GIVEN. REPORT TBP	60272
CA	INELST GAMMA	EXPT-PROG	9.0 6	1.1 7	NCSAC-42 181 N/71	TNC	TUCKER+. NO DATA GIVEN. REPORT TBP	60278
CA 040	TOTAL XSECT	EXPT-PROG		1.0 4	NCSAC-42 183 N/71	ORL	HARVEY+. NO DATA GIVEN. TRANSMISSION	60260
CA 040	RESON PARAMS	EXPT-PROG	2.0 4	2.9 5	NCSAC-42 69 N/71	COL	SINGH+. L J PI WN WIGNER LMT 10RESON	60211
CA 040	RESON PARAMS	EXPT-PROG	NDG		NCSAC-42 183 N/71	ORL	HARVEY+. TRANS. ANAL TBC. NO DATA	60320
CA 040	STRNTH FNCTN	EXPT-PROG	1.0 2	3.0 5	NCSAC-42 69 N/71	COL	SINGH+. SO AND S1 VALUES GIVEN	60030
CA 040	N,GAMMA	EXPT-PROG	3.0 3	5.0 5	NCSAC-42 185 N/71	ORL	MACKLIN+. ORELA. ANAL TBC. NO DATA	60338
CA 042	TOTAL XSECT	EXPT-PROG		1.0 4	NCSAC-42 183 N/71	ORL	HARVEY+. NO DATA GIVEN. TRANSMISSION	60246
CA 042	RESON PARAMS	EXPT-PROG	NDG		NCSAC-42 183 N/71	ORL	HARVEY+. TRANS. ANAL TBC. NO DATA	60319
CA 042	N,GAMMA	EXPT-PROG	3.0 3	5.0 5	NCSAC-42 185 N/71	ORL	MACKLIN+. ORELA. ANAL TBC. NO DATA	60337
CA 043	TOTAL XSECT	EXPT-PROG		1.0 4	NCSAC-42 183 N/71	ORL	HARVEY+. NO DATA GIVEN. TRANSMISSION	60247
CA 043	RESON PARAMS	EXPT-PROG	NDG		NCSAC-42 183 N/71	ORL	HARVEY+. TRANS. ANAL TBC. NO DATA	60318
CA 044	TOTAL XSECT	EXPT-PROG		1.0 4	NCSAC-42 183 N/71	ORL	HARVEY+. NO DATA GIVEN. TRANSMISSION	60248
CA 044	RESON PARAMS	EXPT-PROG	1.1 4	1.0 5	NCSAC-42 69 N/71	COL	SINGH+. L J PI WN WIGNER LMT 4 RESON	60210
CA 044	RESON PARAMS	EXPT-PROG	NDG		NCSAC-42 183 N/71	ORL	HARVEY+. TRANS. ANAL TBC. NO DATA	60317
CA 044	STRNTH FNCTN	EXPT-PROG	1.0 2	3.0 5	NCSAC-42 69 N/71	COL	SINGH+. SO AND S1 VALUES GIVEN	60029
TI	TOTAL XSECT	EXPT-PROG	5.0 5	6	NCSAC-42 172 N/71	NBS	SCHRACK. INTERMEDIATE STRUCT.NDG.TBP	60298
TI	DIFF ELASTIC	EXPT-PROG	1.5 6	3.0 6	NCSAC-42 8 N/71	ANL	GUENTHER+. 20-160DEG. TBC. NO DATA	59957
TI	DIFF ELASTIC	EXPT-PROG	2.0 6		NCSAC-42 10 N/71	ANL	COX. CURVE	60009
TI	POLARIZATION	EXPT-PROG	2.0 6		NCSAC-42 10 N/71	ANL	COX. CURVE	59974
TI	NONEL GAMMAS	EXPT-PROG	6.0 6		NCSAC-42 195 N/71	ORL	DICKENS+. NO DATA GIVEN	60427
TI	DIFF INELAST	EXPT-PROG	1.5 6	3.0 6	NCSAC-42 8 N/71	ANL	GUENTHER+. 20-160DEG. TBC. NO DATA	59948
TI 046	NONEL GAMMAS	EXPT-PROG	6.0 6		NCSAC-42 195 N/71	ORL	DICKENS+. NO DATA GIVEN	60417

ELEMENT S A	QUANTITY	TYPE	ENERGY MIN	ENERGY MAX	DOCUMENTATION REF VOL PAGE	DATE	LAB	COMMENTS	SERIAL NO.
TI 047	TOTAL XSECT	EXPT-PROG	1.0 3	5	NCSAC-42 183	N/71	ORL	GOOD+. TOF. 7 NEW RESON ES GIVEN	60304
TI 047	RESON PARAMS	EXPT-PROG	1.0 3	5	NCSAC-42 183	N/71	ORL	GOOD+. TOF. 7 NEW RESON ES GIVEN	60244
TI 047	N,PROTON	EXPT-PROG	1.2 6	4.5 6	NCSAC-42 10	N/71	ANL	MEADOWS+. ACT. GE(LI)+NAI DET. CURVE	59943
TI 048	NONEL GAMMAS	EXPT-PROG	6.0 6		NCSAC-42 195	N/71	ORL	DICKENS+. NO DATA GIVEN	60418
TI 049	TOTAL XSECT	EXPT-PROG	1.0 3	5	NCSAC-42 183	N/71	ORL	GOOD+. TOF. NO NEW RESON BELOW 30KEV	60303
TI 049	RESON PARAMS	EXPT-PROG	1.0 3	5	NCSAC-42 183	N/71	ORL	GOOD+. TOF. NO NEW RESON BELOW 30KEV	60243
V	DIFF ELASTIC	EXPT-PROG	1.5 6	3.0 6	NCSAC-42 8	N/71	ANL	GUENTHER+. 20-160DEG. TBC. NO DATA	59955
V	DIFF ELASTIC	EXPT-PROG	2.0 6		NCSAC-42 10	N/71	ANL	COX. NO DATA GIVEN.	60010
V	POLARIZATION	EXPT-PROG	2.0 6		NCSAC-42 10	N/71	ANL	COX. NO DATA GIVEN	59990
V	DIFF INELAST	EXPT-PROG	1.5 6	3.0 6	NCSAC-42 8	N/71	ANL	GUENTHER+. 20-160DEG. TBC. NO DATA	59967
V 051	STRNTH FNCTN	EXPT-PROG	3	5	NCSAC-42 221	N/71	RPI	BLOCK+. S1 VALUE GIVEN	60403
CR 050	STRNTH FNCTN	EXPT-PROG	3	5	NCSAC-42 221	N/71	RPI	BLOCK+. S1 VALUE GIVEN	60404
CR 052	STRNTH FNCTN	EXPT-PROG	3	5	NCSAC-42 221	N/71	RPI	BLOCK+. S1 VALUE GIVEN	60405
CR 053	STRNTH FNCTN	EXPT-PROG	3	5	NCSAC-42 221	N/71	RPI	BLOCK+. S1 VALUE GIVEN	60406
CR 054	STRNTH FNCTN	EXPT-PROG	3	5	NCSAC-42 221	N/71	RPI	BLOCK+. S1 VALUE GIVEN	60407
FE	EVALUATION	EVAL-PROG	NDG		NCSAC-42 210	N/71	ORL	KINNEY+. NO DATA GIVEN	60411
FE	TOTAL XSECT	EXPT-PROG	2.1 4	4.7 5	NCSAC-42 61	N/71	COL	HACKEN+. TRANS. CURVES. TBC	60026
FE	TOTAL XSECT	EXPT-PROG	NDG		NCSAC-42 61	N/71	COL	HACKEN+. TRANS. ANAL TBC. NO DATA	60092
FE	TOTAL XSECT	EXPT-PROG	5.0 5	6	NCSAC-42 172	N/71	NBS	SCHRACK. INTERMEDIATE STRUCT.NDG.TBP	60297
FE	TOTAL XSECT	EXPT-PROG	2.5 4		NCSAC-42 221	N/71	RPI	BLOCK+. SIG MINIMUM AT 24.7KEV GIVEN	60363
FE	DIFF ELASTIC	EXPT-PROG	1.5 6	3.0 6	NCSAC-42 8	N/71	ANL	GUENTHER+. 20-160DEG. TBC. NO DATA	59956
FE	DIFF ELASTIC	EXPT-PROG	9.0 6	1.1 7	NCSAC-42 181	N/71	TNC	TUCKER+. NO DATA GIVEN. REPORT TBP	60286
FE	DIFF ELASTIC	EXPT-PROG	3	5	NCSAC-42 215	N/71	RPI	ZUHR+. ANAL TBC. NO DATA GIVEN	60371
FE	DIFF ELASTIC	EXPT-PROG	7.6 6		NCSAC-42 256	N/71	ABD	HOLLANDSWORTH+. 2-15DEG. TO BE DONE	60390
FE	SCATTERING	EXPT-PROG	5.0 4	6.5 5	NCSAC-42 215	N/71	RPI	ZUHR+. CURVE. CFD OTHERS	60370
FE	NONEL GAMMAS	EXPT-PROG	8.6 5	1.7 7	NCSAC-42 105	N/71	GA	ORPHAN+. GAMMA PRODUCTION SIGS GIVEN	60200
FE	NONEL GAMMAS	EXPT-PROG	4.9 6	9.0 6	NCSAC-42 194	N/71	ORL	DICKENS+. NO DATA GIVEN	60231
FE	DIFF INELAST	EXPT-PROG	1.5 6	3.0 6	NCSAC-42 8	N/71	ANL	GUENTHER+. 20-160DEG. TBC. NO DATA	59968
FE	DIFF INELAST	EXPT-PROG	9.0 6	1.1 7	NCSAC-42 181	N/71	TNC	TUCKER+. NO DATA GIVEN. REPORT TBP	60273
FE	INELST GAMMA	EXPT-PROG	9.0 6	1.1 7	NCSAC-42 181	N/71	TNC	TUCKER+. NO DATA GIVEN. REPORT TBP	60279
FE 054	TOTAL XSECT	EXPT-PROG		1.0 4	NCSAC-42 183	N/71	ORL	HARVEY+. NO DATA GIVEN. TRANSMISSION	60249
FE 054	RESON PARAMS	EXPT-PROG	NDG		NCSAC-42 183	N/71	ORL	HARVEY+. TRANS. ANAL TBC. NO DATA	60316
FE 054	DIFF ELASTIC	EXPT-PROG	5.5 6	8.5 6	NCSAC-42 191	N/71	ORL	PEREY+. ANG. DIST. 3ES. NO DATA GIVN	60240
FE 054	DIFF INELAST	EXPT-PROG	5.5 6	8.5 6	NCSAC-42 191	N/71	ORL	PEREY+. ANG. DIST. 3ES. NO DATA GIVN	60233
FE 054	DIFF INELAST	EXPT-PROG	5.5 6	8.5 6	NCSAC-42 191	N/71	ORL	PEREY+. 500KEV STEPS. NO DATA GIVEN	60266
FE 054	N,GAMMA	EXPT-PROG	2.0 1	4.0 5	NCSAC-42 219	N/71	RPI	HOCKENBURY+. TO BE COMPL. NO DATA	60369
FE 056	TOTAL XSECT	EXPT-PROG		1.0 4	NCSAC-42 183	N/71	ORL	HARVEY+. NO DATA GIVEN. TRANSMISSION	60250
FE 056	RESON PARAMS	EXPT-PROG	NDG		NCSAC-42 183	N/71	ORL	HARVEY+. TRANS. ANAL TBC. NO DATA	60315
FE 056	STRNTH FNCTN	EXPT-PROG	3	5	NCSAC-42 221	N/71	RPI	BLOCK+. S1 VALUE GIVEN	60400
FE 056	N,PROTON	EXPT-PROG	3.8 6	5.0 6	NCSAC-42 10	N/71	ANL	MEADOWS+. ACT. GE(LI)+NAI DET. CURVE	59941
FE 057	TOTAL XSECT	EXPT-PROG		1.0 4	NCSAC-42 183	N/71	ORL	HARVEY+. NO DATA GIVEN. TRANSMISSION	60251
FE 057	RESON PARAMS	EXPT-PROG	NDG		NCSAC-42 183	N/71	ORL	HARVEY+. TRANS. ANAL TBC. NO DATA	60314
FE 058	N,GAMMA	EXPT-PROG	2.0 1	3.0 5	NCSAC-42 219	N/71	RPI	HOCKENBURY+. NO DATA GIVEN	60368
CO 059	TOTAL XSECT	EXPT-PROG	NDG		NCSAC-42 144	N/71	LOK	FISHER.SPIN-SPIN EFF.SEE PL 35B 573	60170
CO 059	TOTAL XSECT	EXPT-PROG	3.0 5	1.5 7	NCSAC-42 142	N/71	LOK	FISHER. DEFORMATN EFFECT TO BE MEASD	60171
CO 059	DIFF ELASTIC	EXPT-PROG	1.5 6	3.0 6	NCSAC-42 8	N/71	ANL	GUENTHER+. 20-160DEG. TBC. NO DATA	59958
CO 059	DIFF ELASTIC	EXPT-PROG	2.0 6		NCSAC-42 10	N/71	ANL	COX. NO DATA GIVEN.	60008
CO 059	POLARIZATION	EXPT-PROG	2.0 6		NCSAC-42 10	N/71	ANL	COX. NO DATA GIVEN	59989

ELEMENT S A	QUANTITY	TYPE	ENERGY MIN	ENERGY MAX	DOCUMENTATION REF	VOL	PAGE	DATE	LAB	COMMENTS	SERIAL NO.
CO 059	DIFF INELAST	EXPT-PROG	1.5 6	3.0 6	NCSAC-42	8		N/71	ANL	GUENTHER+. 20-160DEG. TBC. NO DATA	59947
NI	TOTAL XSECT	EXPT-PROG	5.0 5	6	NCSAC-42	172		N/71	NBS	SCHRACK. INTERMEDIATE STRUCT.NDG.TBP	60296
NI	DIFF ELASTIC	EXPT-PROG	1.5 6	3.0 6	NCSAC-42	8		N/71	ANL	GUENTHER+. 20-160DEG. TBC. NO DATA	59961
NI	NONEL GAMMAS	EXPT-PROG	6.0 6		NCSAC-42	195		N/71	ORL	DICKENS+. NO DATA GIVEN	60419
NI	DIFF INELAST	EXPT-PROG	1.5 6	3.0 6	NCSAC-42	8		N/71	ANL	GUENTHER+. 20-160DEG. TBC. NO DATA	59944
NI 058	STRNTH FNCTN	EXPT-PROG	3	5	NCSAC-42	221		N/71	RPI	BLOCK+. S1 VALUE GIVEN	60401
NI 058	N,PROTON	EXPT-PROG	1.5 6	4.5 6	NCSAC-42	10		N/71	ANL	MEADOWS+. ACT. GE(LI)+NAI DET. CURVE	59942
NI 060	STRNTH FNCTN	EXPT-PROG	3	5	NCSAC-42	221		N/71	RPI	BLOCK+. S1 VALUE GIVEN	60402
NI 060	NONEL GAMMAS	EXPT-PROG	6.0 6		NCSAC-42	195		N/71	ORL	DICKENS+. NO DATA GIVEN	60420
NI 061	N,GAMMA	EXPT-PROG	NDG		NCSAC-42	219		N/71	RPI	HOCKENBURY+. TO BE DONE	60367
NI 064	N,GAMMA	EXPT-PROG	NDG		NCSAC-42	219		N/71	RPI	HOCKENBURY+. TO BE DONE	60366
CU	TOTAL XSECT	EXPT-PROG	NDG		NCSAC-42	61		N/71	COL	HACKEN+. TRANS. ANAL TBC. NO DATA	60091
CU	DIFF ELASTIC	EXPT-PROG	2.0 6		NCSAC-42	10		N/71	ANL	COX. NO DATA GIVEN.	60007
CU	DIFF ELASTIC	EXPT-PROG	7.6 6		NCSAC-42	256		N/71	ABD	HOLLANDSWORTH+. 2-15DEG. TO BE DONE	60389
CU	POLARIZATION	EXPT-PROG	2.0 6		NCSAC-42	10		N/71	ANL	COX. NO DATA GIVEN	59988
CU 063	DIFF ELASTIC	EXPT-PROG	5.5 6	8.5 6	NCSAC-42	191		N/71	ORL	PEREY+. ANG. DIST. 3ES. NO DATA GIVN	60239
CU 063	NONEL GAMMAS	EXPT-PROG	6.0 6		NCSAC-42	195		N/71	ORL	DICKENS+. NO DATA GIVEN	60421
CU 063	DIFF INELAST	EXPT-PROG	5.5 6	8.5 6	NCSAC-42	191		N/71	ORL	PEREY+. ANG. DIST. 3ES. NO DATA GIVN	60234
CU 063	DIFF INELAST	EXPT-PROG	5.5 6	8.5 6	NCSAC-42	191		N/71	ORL	PEREY+. 500KEV STEPS. NO DATA GIVEN	60265
CU 063	N,GAMMA	EXPT-PROG	3.0 3	5.0 5	NCSAC-42	185		N/71	ORL	MACKLIN+. ORELA. ANAL TBC. NO DATA	60336
CU 065	DIFF ELASTIC	EXPT-PROG	5.5 6	8.5 6	NCSAC-42	191		N/71	ORL	PEREY+. ANG. DIST. 3ES. NO DATA GIVN	60238
CU 065	NONEL GAMMAS	EXPT-PROG	6.0 6		NCSAC-42	195		N/71	ORL	DICKENS+. NO DATA GIVEN	60422
CU 065	DIFF INELAST	EXPT-PROG	5.5 6	8.5 6	NCSAC-42	191		N/71	ORL	PEREY+. ANG. DIST. 3ES. NO DATA GIVN	60235
CU 065	DIFF INELAST	EXPT-PROG	5.5 6	8.5 6	NCSAC-42	191		N/71	ORL	PEREY+. 500KEV STEPS. NO DATA GIVEN	60261
CU 065	N,GAMMA	EXPT-PROG	3.0 3	5.0 5	NCSAC-42	185		N/71	ORL	MACKLIN+. ORELA. ANAL TBC. NO DATA	60335
ZN	DIFF ELASTIC	EXPT-PROG	2.0 6		NCSAC-42	10		N/71	ANL	COX. NO DATA GIVEN.	60006
ZN	POLARIZATION	EXPT-PROG	2.0 6		NCSAC-42	10		N/71	ANL	COX. NO DATA GIVEN	59987
ZN 064	NONEL GAMMAS	EXPT-PROG	6.0 6		NCSAC-42	195		N/71	ORL	DICKENS+. NO DATA GIVEN	60423
ZN 068	NONEL GAMMAS	EXPT-PROG	6.0 6		NCSAC-42	195		N/71	ORL	DICKENS+. NO DATA GIVEN	60424
SE	TOTAL XSECT	EXPT-PROG	NDG		NCSAC-42	61		N/71	COL	HACKEN+. TRANS. ANAL TBC. NO DATA	60089
SE	DIFF ELASTIC	EXPT-PROG	2.0 6		NCSAC-42	10		N/71	ANL	COX. NO DATA GIVEN.	60005
SE	POLARIZATION	EXPT-PROG	2.0 6		NCSAC-42	10		N/71	ANL	COX. NO DATA GIVEN	59986
RB 087	N,GAMMA	EXPT-PROG	PILE		NCSAC-42	5		N/71	MTR	HARMER+. ACT. CFRMF INTEGRAL MEAST	59971
SR	TOTAL XSECT	EXPT-PROG		6	NCSAC-42	228		N/71	OKE	MALAN+. R-MATRIX ANAL TBC. NO DATA	60362
Y 089	DIFF ELASTIC	EXPT-PROG	2.0 6		NCSAC-42	10		N/71	ANL	COX. NO DATA GIVEN.	60004
Y 089	POLARIZATION	EXPT-PROG	2.0 6		NCSAC-42	10		N/71	ANL	COX. NO DATA GIVEN	59985
ZR	DIFF ELASTIC	EXPT-PROG	2.0 6		NCSAC-42	10		N/71	ANL	COX. NO DATA GIVEN.	60003
ZR	POLARIZATION	EXPT-PROG	2.0 6		NCSAC-42	10		N/71	ANL	COX. NO DATA GIVEN	59984
ZR 090	STRNTH FNCTN	EXPT-PROG	3	5	NCSAC-42	221		N/71	RPI	BLOCK+. S1 VALUE GIVEN	60399
ZR 090	N,GAMMA	EXPT-PROG	3.0 3	5.0 5	NCSAC-42	185		N/71	ORL	MACKLIN+. ORELA. ANAL TBC. NO DATA	60334
ZR 091	STRNTH FNCTN	EXPT-PROG	3	5	NCSAC-42	221		N/71	RPI	BLOCK+. S1 VALUE GIVEN	60398
ZR 091	N,GAMMA	EXPT-PROG	3.0 3	5.0 5	NCSAC-42	185		N/71	ORL	MACKLIN+. ORELA. ANAL TBC. NO DATA	60333
ZR 092	STRNTH FNCTN	EXPT-PROG	3	5	NCSAC-42	221		N/71	RPI	BLOCK+. S1 VALUE GIVEN	60397
ZR 092	N,GAMMA	EXPT-PROG	3.0 3	5.0 5	NCSAC-42	185		N/71	ORL	MACKLIN+. ORELA. ANAL TBC. NO DATA	60332
ZR 094	STRNTH FNCTN	EXPT-PROG	3	5	NCSAC-42	221		N/71	RPI	BLOCK+. S1 VALUE GIVEN	60396
ZR 094	N,GAMMA	EXPT-PROG	3.0 3	5.0 5	NCSAC-42	185		N/71	ORL	MACKLIN+. ORELA. ANAL TBC. NO DATA	60331
NB 093	DIFF ELASTIC	EXPT-PROG	1.5 6	3.0 6	NCSAC-42	8		N/71	ANL	GUENTHER+. 20-160DEG. TBC. NO DATA	59960
NB 093	DIFF ELASTIC	EXPT-PROG	2.0 6		NCSAC-42	10		N/71	ANL	COX. NO DATA GIVEN.	60002

ELEMENT S A	QUANTITY	TYPE	ENERGY MIN	ENERGY MAX	DOCUMENTATION REF	VOL	PAGE	DATE	LAB	COMMENTS	SERIAL NO.
NB 093	POLARIZATION	EXPT-PROG	2.0 6		NCSAC-42	10		N/71	ANL	COX. NO DATA GIVEN	59983
NB 093	NONEL GAMMAS	EXPT-PROG	6.0 6		NCSAC-42	195		N/71	ORL	DICKENS+. NO DATA GIVEN	60425
NB 093	DIFF INELAST	EXPT-PROG	1.5 6	3.0 6	NCSAC-42	8		N/71	ANL	GUENTHER+. 20-160DEG. TBC. NO DATA	59945
NB 093	SPECT NGAMMA	EXPT-PROG	THR	2	NCSAC-42	29		N/71	ANL	BOLLINGER+. THERMAL+AVG RES SPEC.NDG	59931
MO	DIFF ELASTIC	EXPT-PROG	2.0 6		NCSAC-42	10		N/71	ANL	COX. NO DATA GIVEN.	60001
MO	POLARIZATION	EXPT-PROG	2.0 6		NCSAC-42	10		N/71	ANL	COX. NO DATA GIVEN	59982
MO 092	SPECT NGAMMA	EXPT-PROG	NDG		NCSAC-42	43		N/71	BNL	CHRIEN+. S-WAVE CAPTURE. NO DATA GVN	60109
MO 092	SPECT NGAMMA	EXPT-PROG	NDG		NCSAC-42	40		N/71	BNL	CHRIEN+. ANAL TBC. NO DATA GIVEN	60117
MO 096	SPECT NGAMMA	EXPT-PROG	NDG		NCSAC-42	43		N/71	BNL	CHRIEN+. S-WAVE CAPTURE. NO DATA GVN	60108
MO 098	TOTAL XSECT	EXPT-PROG		1.0 4	NCSAC-42	183		N/71	ORL	HARVEY+. NO DATA GIVEN. TRANSMISSION	60252
MO 098	RESON PARAMS	EXPT-PROG	NDG		NCSAC-42	183		N/71	ORL	HARVEY+. TRANS. ANAL TBC. NO DATA	60313
MO 098	RESON PARAMS	EXPT-PROG	4.0 2	4.8 3	NCSAC-42	185		N/71	ORL	COLE+. J FOR 10 L#1 RES. WG FOR GND	60321
MO 098	SPECT NGAMMA	EXPT-PROG	NDG		NCSAC-42	43		N/71	BNL	CHRIEN+. S-WAVE CAPTURE. NO DATA GVN	60107
MO 098	SPECT NGAMMA	EXPT-PROG	1.2 1	4.8 3	NCSAC-42	40		N/71	BNL	CHRIEN+. GAMMA SPECTRA SHOWN	60116
MO 098	SPECT NGAMMA	EXPT-PROG	1	3	NCSAC-42	185		N/71	ORL	COLE+. P-WAVE CAPTURE SPECTRA.	60322
MO 100	SPECT NGAMMA	EXPT-PROG	NDG		NCSAC-42	43		N/71	BNL	CHRIEN+. S-WAVE CAPTURE. NO DATA GVN	60106
TC 099	SPECT NGAMMA	EXPT-PROG	THR	2	NCSAC-42	59		N/71	BNL	COCHAVI+. THR+RESON CAPT. NO DATA	60079
RU 102	N,GAMMA	EXPT-PROG	PILE		NCSAC-42	5		N/71	MTR	HARHER+. ACT. CFRMF INTEGRAL MEAST	59970
RU 104	N,GAMMA	EXPT-PROG	PILE		NCSAC-42	5		N/71	MTR	HARHER+. ACT. CFRMF INTEGRAL MEAST	59969
RH 103	SPECT NGAMMA	EXPT-PROG	THR	2	NCSAC-42	29		N/71	ANL	BOLLINGER+. THERMAL+AVG RES SPEC.NDG	59930
PD	TOTAL XSECT	EXPT-PROG	1.0 5	1.5 6	NCSAC-42	10		N/71	ANL	SMITH+. 2KEV RESOL. NDG SEE ANL-7869	60015
PD	DIFF ELASTIC	EXPT-PROG	3.0 5	1.5 6	NCSAC-42	10		N/71	ANL	SMITH+. NO DATA GIVEN. SEE ANL-7869	60014
PD	DIFF-INELAST	EXPT-PROG	3.0 5	1.5 6	NCSAC-42	10		N/71	ANL	SMITH+. NO DATA GIVEN. SEE ANL-7869	60013
AG	DIFF ELASTIC	EXPT-PROG	2.0 6		NCSAC-42	10		N/71	ANL	COX. NO DATA GIVEN.	59999
AG	POLARIZATION	EXPT-PROG	2.0 6		NCSAC-42	10		N/71	ANL	COX. NO DATA GIVEN	59981
CD	TOTAL XSECT	EXPT-PROG	NDG		NCSAC-42	61		N/71	COL	HACKEN+. TRANS. ANAL TBC. NO DATA	60088
CD	DIFF ELASTIC	EXPT-PROG	2.0 6		NCSAC-42	10		N/71	ANL	COX. CURVE.	60000
CD	POLARIZATION	EXPT-PROG	2.0 6		NCSAC-42	10		N/71	ANL	COX. CURVE	59973
CD 110	TOTAL XSECT	EXPT-PROG	NDG		NCSAC-42	61		N/71	COL	HACKEN+. TRANS. ANAL TBC. NO DATA	60062
CD 110	N,GAMMA	EXPT-PROG	3.0 3	5.0 5	NCSAC-42	185		N/71	ORL	MACKLIN+. ORELA. ANAL TBC. NO DATA	60330
CD 111	N,GAMMA	EXPT-PROG	3.0 3	5.0 5	NCSAC-42	185		N/71	ORL	MACKLIN+. ORELA. ANAL TBC. NO DATA	60329
CD 112	TOTAL XSECT	EXPT-PROG	NDG		NCSAC-42	61		N/71	COL	HACKEN+. TRANS. ANAL TBC. NO DATA	60060
CD 114	TOTAL XSECT	EXPT-PROG	NDG		NCSAC-42	61		N/71	COL	HACKEN+. TRANS. ANAL TBC. NO DATA	60059
CD 116	TOTAL XSECT	EXPT-PROG	NDG		NCSAC-42	61		N/71	COL	HACKEN+. TRANS. ANAL TBC. NO DATA	60058
IN	DIFF ELASTIC	EXPT-PROG	2.0 6		NCSAC-42	10		N/71	ANL	COX. NO DATA GIVEN.	59998
IN	POLARIZATION	EXPT-PROG	2.0 6		NCSAC-42	10		N/71	ANL	COX. NO DATA GIVEN	59980
SN	DIFF ELASTIC	EXPT-PROG	2.0 6		NCSAC-42	10		N/71	ANL	COX. NO DATA GIVEN.	59997
SN	DIFF ELASTIC	EXPT-PROG	7.6 6		NCSAC-42	256		N/71	ABD	HOLLANDSWORTH+. 2-15DEG. TO BE DONE	60388
SN	POLARIZATION	EXPT-PROG	2.0 6		NCSAC-42	10		N/71	ANL	COX. NO DATA GIVEN	59979
SN 116	RESON PARAMS	EXPT-PROG	1.5 2		NCSAC-42	43		N/71	BNL	CHRIEN+. WG FOR 2 GAMMA ES. CFD TH	60112
SN 116	SPECT NGAMMA	EXPT-PROG	1	2	NCSAC-42	43		N/71	BNL	CHRIEN+. P-WAVE CAPT.DATA 148EV RES	59918
SN 117	SPECT NGAMMA	EXPT-PROG	THR		NCSAC-42	28		N/71	ANL	BOLLINGER+. 8.3-MEV BROAD MAXIMUM	59934
SN 117	SPECT NGAMMA	EXPT-PROG	NDG		NCSAC-42	43		N/71	BNL	CHRIEN+. S-WAVE CAPTURE. NO DATA GVN	60110
SN 118	RESON PARAMS	EXPT-PROG	4.6 1		NCSAC-42	43		N/71	BNL	CHRIEN+. WG FOR 2 GAMMA ES. CFD TH	60111
SN 118	SPECT NGAMMA	EXPT-PROG	1	2	NCSAC-42	43		N/71	BNL	CHRIEN+. P-WAVE CAPT.DATA 46EV RESON	59919
SN 119	SPECT NGAMMA	EXPT-PROG	THR		NCSAC-42	28		N/71	ANL	BOLLINGER+. 8.3-MEV BROAD MAXIMUM	59933
SN 120	TOTAL XSECT	EXPT-PROG		5.0 5	NCSAC-42	183		N/71	ORL	HARVEY+. NO DATA GIVEN. TRANSMISSION	60253
SN 120	RESON PARAMS	EXPT-PROG	NDG		NCSAC-42	183		N/71	ORL	HARVEY+. TRANS. ANAL TBC. NO DATA	60312

ELEMENT S A	QUANTITY	TYPE	ENERGY MIN	ENERGY MAX	DOCUMENTATION REF	VOL	PAGE	DATE	LAB	COMMENTS	SERIAL NO.
SN 122	RESON PARAMS	EXPT-PROG	1.1 2	2.6 2	NCSAC-42	48		N/71	BNL	CHRIEN+. J FOR 2RESON FROM CAPT SPEC	60104
SN 122	SPECT NGAMMA	EXPT-PROG	2		NCSAC-42	48		N/71	BNL	CHRIEN+. RESON CAPTURE. SOME DATA	60105
SN 124	RESON PARAMS	EXPT-PROG	6.2 1		NCSAC-42	43		N/71	BNL	CHRIEN+. WG FOR 2 GAMMA ES. CFD TH	60113
SN 124	SPECT NGAMMA	EXPT-PROG	1	2	NCSAC-42	43		N/71	BNL	CHRIEN+. P-WAVE CAPT.DATA 62EV RESON	59920
SB	DIFF ELASTIC	EXPT-PROG	2.0 6		NCSAC-42	10		N/71	ANL	COX. NO DATA GIVEN.	59996
SB	POLARIZATION	EXPT-PROG	2.0 6		NCSAC-42	10		N/71	ANL	COX. NO DATA GIVEN	59978
SB 121	N,GAMMA	EXPT-PROG	PILE		NCSAC-42	5		N/71	MTR	HARHER+. ACT. CFRMF INTEGRAL MEAST	59949
SB 123	N,GAMMA	EXPT-PROG	PILE		NCSAC-42	5		N/71	MTR	HARHER+. ACT. CFRMF INTEGRAL MEAST	59950
TE 122	N,GAMMA	EXPT-PROG	3.0 3	5.0 5	NCSAC-42	185		N/71	ORL	MACKLIN+. ORELA. ANAL TBC. NO DATA	60328
TE 123	N,GAMMA	EXPT-PROG	3.0 3	5.0 5	NCSAC-42	185		N/71	ORL	MACKLIN+. ORELA. ANAL TBC. NO DATA	60327
TE 124	N,GAMMA	EXPT-PROG	3.0 3	5.0 5	NCSAC-42	185		N/71	ORL	MACKLIN+. ORELA. ANAL TBC. NO DATA	60326
TE 125	N,GAMMA	EXPT-PROG	3.0 3	5.0 5	NCSAC-42	185		N/71	ORL	MACKLIN+. ORELA. ANAL TBC. NO DATA	60325
TE 126	N,GAMMA	EXPT-PROG	3.0 3	5.0 5	NCSAC-42	185		N/71	ORL	MACKLIN+. ORELA. ANAL TBC. NO DATA	60324
TE 130	N,GAMMA	EXPT-PROG	3.0 3	5.0 5	NCSAC-42	185		N/71	ORL	MACKLIN+. ORELA. ANAL TBC. NO DATA	60323
I 127	N,GAMMA	EXPT-PROG	PILE		NCSAC-42	5		N/71	MTR	HARHER+. ACT. CFRMF INTEGRAL MEAST	59951
CE 140	TOTAL XSECT	EXPT-PROG	NDG		NCSAC-42	61		N/71	COL	HACKEN+. TRANS. ANAL TBC. NO DATA	60055
ND 148	N,GAMMA	EXPT-PROG	PILE		NCSAC-42	5		N/71	MTR	HARHER+. ACT. CFRMF INTEGRAL MEAST	59952
ND 150	N,GAMMA	EXPT-PROG	PILE		NCSAC-42	5		N/71	MTR	HARHER+. ACT. CFRMF INTEGRAL MEAST	59953
SM 152	RES INT ABS	EXPT-PROG	4.1-1	UP	NCSAC-42	61		N/71	COL	HACKEN+. VALUE GIVEN	60086
SM 154	RES INT ABS	EXPT-PROG	4.1-1	UP	NCSAC-42	61		N/71	COL	HACKEN+. VALUE GIVEN	60085
EU 151	RES INT ABS	EXPT-PROG	4.1-1	UP	NCSAC-42	61		N/71	COL	HACKEN+. VALUE GIVEN	60084
EU 151	RES INT ABS	EXPT-PROG	5.0-1	UP	NCSAC-42	61		N/71	COL	HACKEN+. VALUE GIVEN	60219
EU 153	RES INT ABS	EXPT-PROG	4.1-1	UP	NCSAC-42	61		N/71	COL	HACKEN+. VALUE GIVEN	60083
EU 153	RES INT ABS	EXPT-PROG	5.0-1	UP	NCSAC-42	61		N/71	COL	HACKEN+. VALUE GIVEN	60218
GD 154	RESON PARAMS	EXPT-PROG	NDG		NCSAC-42	61		N/71	COL	HACKEN+. TRANS. AVG WG GIVEN	59916
GD 154	STRNTH FNCTN	EXPT-PROG	NDG		NCSAC-42	61		N/71	COL	HACKEN+. TRANS. SO GIVEN	60023
GD 154	RES INT ABS	EXPT-PROG	4.1-1	UP	NCSAC-42	61		N/71	COL	HACKEN+. VALUE GIVEN	60082
GD 158	TOTAL XSECT	EXPT-PROG	NDG		NCSAC-42	61		N/71	COL	HACKEN+. TRANS. ANAL TBC. NO DATA	60048
GD 158	RESON PARAMS	EXPT-PROG	NDG		NCSAC-42	61		N/71	COL	HACKEN+. TRANS. AVG WG GIVEN	59917
GD 158	STRNTH FNCTN	EXPT-PROG	NDG		NCSAC-42	61		N/71	COL	HACKEN+. TRANS. SO GIVEN	60228
GD 158	RES INT ABS	EXPT-PROG	4.1-1	UP	NCSAC-42	61		N/71	COL	HACKEN+. VALUE GIVEN	60081
GD 160	TOTAL XSECT	EXPT-PROG	NDG		NCSAC-42	61		N/71	COL	HACKEN+. TRANS. ANAL TBC. NO DATA	60047
GD 160	RESON PARAMS	EXPT-PROG	NDG		NCSAC-42	61		N/71	COL	HACKEN+. TRANS. AVG WG GIVEN	59915
GD 160	STRNTH FNCTN	EXPT-PROG	NDG		NCSAC-42	61		N/71	COL	HACKEN+. TRANS. SO GIVEN	60227
GD 160	RES INT ABS	EXPT-PROG	4.1-1	UP	NCSAC-42	61		N/71	COL	HACKEN+. VALUE GIVEN	60080
DY 160	TOTAL XSECT	EXPT-PROG	NDG		NCSAC-42	61		N/71	COL	HACKEN+. TRANS. ANAL TBC. NO DATA	60054
DY 160	RESON PARAMS	EXPT-PROG	NDG		NCSAC-42	61		N/71	COL	HACKEN+. TRANS. ANAL TBC. NO DATA	60226
DY 161	TOTAL XSECT	EXPT-PROG	NDG		NCSAC-42	61		N/71	COL	HACKEN+. TRANS. ANAL TBC. NO DATA	60053
DY 161	RESON PARAMS	EXPT-PROG	NDG		NCSAC-42	61		N/71	COL	HACKEN+. TRANS. ANAL TBC. NO DATA	60223
DY 162	TOTAL XSECT	EXPT-PROG	NDG		NCSAC-42	61		N/71	COL	HACKEN+. TRANS. ANAL TBC. NO DATA	60052
DY 162	RESON PARAMS	EXPT-PROG	NDG		NCSAC-42	61		N/71	COL	HACKEN+. TRANS. ANAL TBC. NO DATA	60225
DY 163	TOTAL XSECT	EXPT-PROG	NDG		NCSAC-42	61		N/71	COL	HACKEN+. TRANS. ANAL TBC. NO DATA	60051
DY 163	RESON PARAMS	EXPT-PROG	NDG		NCSAC-42	61		N/71	COL	HACKEN+. TRANS. ANAL TBC. NO DATA	60222
DY 164	TOTAL XSECT	EXPT-PROG	NDG		NCSAC-42	61		N/71	COL	HACKEN+. TRANS. ANAL TBC. NO DATA	60050
DY 164	RESON PARAMS	EXPT-PROG	NDG		NCSAC-42	61		N/71	COL	HACKEN+. TRANS. ANAL TBC. NO DATA	60224
ER 166	RES INT ABS	EXPT-PROG	4.1-1	UP	NCSAC-42	61		N/71	COL	HACKEN+. VALUE GIVEN	60079
ER 167	RESON PARAMS	EXPT-PROG	NDG		NCSAC-42	43		N/71	BNL	CHRIEN+. FROM CAPT SPECT. NO DATA	60114
ER 167	RES INT ABS	EXPT-PROG	4.1-1	UP	NCSAC-42	61		N/71	COL	HACKEN+. VALUE GIVEN	60078

ELEMENT S A	QUANTITY	TYPE	ENERGY MIN	ENERGY MAX	DOCUMENTATION REF VOL PAGE	DATE	LAB	COMMENTS	SERIAL NO.
ER 167	SPECT NGAMMA	EXPT-PROG	NDG		NCSAC-42 43	N/71	BNL	CHRIEN+. GEILI). TOF SPECTRUM SHOWN	60115
ER 168	RES INT ABS	EXPT-PROG	4.1-1	UP	NCSAC-42 61	N/71	COL	HACKEN+. VALUE GIVEN	60077
ER 170	RES INT ABS	EXPT-PROG	4.1-1	UP	NCSAC-42 61	N/71	COL	HACKEN+. VALUE GIVEN	60076
TM 169	TOTAL XSECT	EXPT-PROG	NDG		NCSAC-42 61	N/71	COL	HACKEN+. TRANS. ANAL TBC. NO DATA	60087
TM 169	RESON PARAMS	EXPT-PROG	3.9 0	7.2 2	NCSAC-42 33	N/71	BNL	CHRIEN+. ORELA. J FOR 68 RESON.	60124
TM 169	RESON PARAMS	EXPT-PROG	NDG		NCSAC-42 189	N/71	ORL	CHRIEN+. WN/WG CORRELATIONS. NO DATA	60301
TM 169	SPECT NGAMMA	EXPT-PROG			NCSAC-42 33	N/71	BNL	CHRIEN+. ORELA. GAMMA SPECTRA SHOWN	60125
YB 168	RES INT ABS	EXPT-PROG	4.1-1	UP	NCSAC-42 61	N/71	COL	HACKEN+. VALUE GIVEN	60075
YB 170	RES INT ABS	EXPT-PROG	4.1-1	UP	NCSAC-42 61	N/71	COL	HACKEN+. VALUE GIVEN	60074
YB 171	RES INT ABS	EXPT-PROG	4.1-1	UP	NCSAC-42 61	N/71	COL	HACKEN+. VALUE GIVEN	60073
YB 172	RES INT ABS	EXPT-PROG	4.1-1	UP	NCSAC-42 61	N/71	COL	HACKEN+. VALUE GIVEN	60072
YB 174	RES INT ABS	EXPT-PROG	4.1-1	UP	NCSAC-42 61	N/71	COL	HACKEN+. VALUE GIVEN	60071
YB 176	RES INT ABS	EXPT-PROG	4.1-1	UP	NCSAC-42 61	N/71	COL	HACKEN+. VALUE GIVEN	60070
LU 175	RESON PARAMS	EXPT-PROG	NDG		NCSAC-42 61	N/71	COL	HACKEN+. TRANS. PRELIM VALUES AVAILB	60024
LU 175	RES INT ABS	EXPT-PROG	4.1-1	UP	NCSAC-42 61	N/71	COL	HACKEN+. VALUE GIVEN	60069
TA 181	TOTAL XSECT	EXPT-PROG	NDG		NCSAC-42 61	N/71	COL	HACKEN+. TRANS. ANAL TBC. NO DATA	60066
TA 181	DIFF ELASTIC	EXPT-PROG	2.0 6		NCSAC-42 10	N/71	ANL	COX. NO DATA GIVEN.	59995
TA 181	POLARIZATION	EXPT-PROG	2.0 6		NCSAC-42 10	N/71	ANL	COX. NO DATA GIVEN	59977
TA 181	NONEL GAMMAS	EXPT-PROG	1.0 6	1.5 7	NCSAC-42 195	N/71	ORL	MORGAN+. NAI DET. GAM SPECT. NO DATA	60416
W	DIFF ELASTIC	EXPT-PROG	2.0 6		NCSAC-42 10	N/71	ANL	COX. NO DATA GIVEN.	59994
W	DIFF ELASTIC	EXPT-PROG	7.6 6		NCSAC-42 256	N/71	ABD	HOLLANDSWORTH+. 2-15DEG. TO BE DONE	60387
W	POLARIZATION	EXPT-PROG	2.0 6		NCSAC-42 10	N/71	ANL	COX. NO DATA GIVEN	59976
W 182	STRNTH FNCTN	EXPT-PROG	3	5	NCSAC-42 221	N/71	RPI	BLOCK+. S1 VALUE GIVEN	60395
W 182	RES INT ABS	EXPT-PROG	4.1-1	UP	NCSAC-42 61	N/71	COL	HACKEN+. VALUE GIVEN	60068
W 183	RESON PARAMS	EXPT-PROG	NDG		NCSAC-42 61	N/71	COL	HACKEN+. TRANS. FINAL VALUES AVAILBL	60025
W 183	RES INT ABS	EXPT-PROG	4.1-1	UP	NCSAC-42 61	N/71	COL	HACKEN+. VALUE GIVEN	60067
W 184	STRNTH FNCTN	EXPT-PROG	3	5	NCSAC-42 221	N/71	RPI	BLOCK+. S1 VALUE GIVEN	60394
W 184	RES INT ABS	EXPT-PROG	4.1-1	UP	NCSAC-42 61	N/71	COL	HACKEN+. VALUE GIVEN	60221
W 186	STRNTH FNCTN	EXPT-PROG	3	5	NCSAC-42 221	N/71	RPI	BLOCK+. S1 VALUE GIVEN	60393
W 186	RES INT ABS	EXPT-PROG	4.1-1	UP	NCSAC-42 61	N/71	COL	HACKEN+. VALUE GIVEN	60220
RE 187	SPECT NGAMMA	EXPT-PROG	THR		NCSAC-42 163	N/71	LAS	SHERA+. RE188 LVLS GIVEN	60156
AU 197	TOTAL XSECT	EXPT-PROG	NDG		NCSAC-42 61	N/71	COL	HACKEN+. TRANS. ANAL TBC. NO DATA	60065
AU 197	DIFF ELASTIC	EXPT-PROG	2.0 6		NCSAC-42 10	N/71	ANL	COX. CURVE.	59993
AU 197	POLARIZATION	EXPT-PROG	2.0 6		NCSAC-42 10	N/71	ANL	COX. CURVE	59972
AU 197	SPECT NGAMMA	EXPT-PROG	THR	2	NCSAC-42 29	N/71	ANL	BOLLINGER+. THERMAL+AVG RES SPEC.NDG	59929
AU 197	SPECT NGAMMA	EXPT-PROG	THR	4.9 0	NCSAC-42 57	N/71	BNL	KANE. E+I FOR 2 NEUT ES TABULATED	60101
TL	TOTAL XSECT	EXPT-PROG	NDG		NCSAC-42 61	N/71	COL	HACKEN+. TRANS. ANAL TBC. NO DATA	60064
TL 203	TOTAL XSECT	EXPT-PROG	NDG		NCSAC-42 61	N/71	COL	HACKEN+. TRANS. ANAL TBC. NO DATA	60057
TL 203	TOTAL XSECT	EXPT-PROG		1.0 4	NCSAC-42 183	N/71	ORL	HARVEY+. NO DATA GIVEN. TRANSMISSION	60254
TL 203	RESON PARAMS	EXPT-PROG	NDG		NCSAC-42 183	N/71	ORL	HARVEY+. TRANS. ANAL TBC. NO DATA	60311
TL 205	TOTAL XSECT	EXPT-PROG	NDG		NCSAC-42 61	N/71	COL	HACKEN+. TRANS. ANAL TBC. NO DATA	60056
TL 205	TOTAL XSECT	EXPT-PROG		1.0 4	NCSAC-42 183	N/71	ORL	HARVEY+. NO DATA GIVEN. TRANSMISSION	60255
TL 205	RESON PARAMS	EXPT-PROG	NDG		NCSAC-42 183	N/71	ORL	HARVEY+. TRANS. ANAL TBC. NO DATA	60310
TL 205	SPECT NGAMMA	EXPT-PROG	THR	7.0 4	NCSAC-42 187	N/71	ORL	EARLE+. 5.5-MEV GAMMA ANOMALY. CURVE	60302
PB	EVALUATION	EVAL-PROG	NDG		NCSAC-42 210	N/71	ORL	KINNEY+. NO DATA GIVEN	60410
PB	TOTAL XSECT	EXPT-PROG	5.0 5	6	NCSAC-42 172	N/71	NBS	SCHRACK. INTERMEDIATE STRUCT.NDG.TBP	60294
PB	DIFF ELASTIC	EXPT-PROG	2.0 6		NCSAC-42 10	N/71	ANL	COX. NO DATA GIVEN.	59992
PB	DIFF ELASTIC	EXPT-PROG	7.6 6	9.0 6	NCSAC-42 256	N/71	ABD	HOLLANDSWORTH+. 4ES.3.5-15DEG CURVS	60380

ELEMENT S A	QUANTITY	TYPE	ENERGY MIN	ENERGY MAX	DOCUMENTATION REF VOL PAGE	DATE	LAB	COMMENTS	SERIAL NO.
PB	POLARIZATION	EXPT-PROG	2.0 6		NCSAC-42 10	N/71	ANL	COX. NO DATA GIVEN	59975
PB 204	TOTAL XSECT	EXPT-PROG		1.0 4	NCSAC-42 183	N/71	ORL	HARVEY+. NO DATA GIVEN. TRANSMISSION	60256
PB 204	RESON PARAMS	EXPT-PROG	NDG		NCSAC-42 183	N/71	ORL	HARVEY+. TRANS. ANAL TBC. NC DATA	60309
PB 206	TOTAL XSECT	EXPT-PROG		1.0 4	NCSAC-42 183	N/71	ORL	HARVEY+. NO DATA GIVEN. TRANSMISSION	60257
PB 206	RESON PARAMS	EXPT-PROG	NDG		NCSAC-42 183	N/71	ORL	HARVEY+. TRANS. ANAL TBC. NC DATA	60308
PB 206	NONEL GAMMAS	EXPT-PROG	4.9 6	8.0 6	NCSAC-42 194	N/71	ORL	DICKENS. GE(LI) DET. GAMMA SPECTRA	60230
PB 206	DIFF INELAST	EXPT-PROG	5.5 6	8.5 6	NCSAC-42 191	N/71	ORL	PEREY+. 500KEV STEPS. NO DATA GIVEN	60262
PB 207	TOTAL XSECT	EXPT-PROG	4.0 4		NCSAC-42 127	N/71	LRL	PHILLIPS+. TRANS. CURVE.	60192
PB 207	TOTAL XSECT	EXPT-PROG		1.0 4	NCSAC-42 183	N/71	ORL	HARVEY+. NO DATA GIVEN. TRANSMISSION	60258
PB 207	RESON PARAMS	EXPT-PROG	NDG		NCSAC-42 183	N/71	ORL	HARVEY+. TRANS. ANAL TBC. NC DATA	60307
PB 207	NONEL GAMMAS	EXPT-PROG	4.9 6	8.0 6	NCSAC-42 194	N/71	ORL	DICKENS. GE(LI) DET. GAMMA SPECTRA	60435
PB 207	DIFF INELAST	EXPT-PROG	5.5 6	8.5 6	NCSAC-42 191	N/71	ORL	PEREY+. 500KEV STEPS. NO DATA GIVEN	60263
PB 208	DIFF ELASTIC	EXPT-PROG	5.5 6	8.5 6	NCSAC-42 191	N/71	ORL	PEREY+. ANG. DIST. 3ES. NO DATA GIVN	60232
PB 208	NONEL GAMMAS	EXPT-PROG	4.9 6	8.0 6	NCSAC-42 194	N/71	ORL	DICKENS. GE(LI) DET, GAMMA SPECTRA	60229
PB 208	DIFF INELAST	EXPT-PROG	5.5 6	8.5 6	NCSAC-42 191	N/71	ORL	PEREY+. ANG. DIST. 3ES. NO DATA GIVN	60236
PB 208	DIFF INELAST	EXPT-PROG	5.5 6	8.5 6	NCSAC-42 191	N/71	ORL	PEREY+. 500KEV STEPS. NO DATA GIVEN	60264
PB 208	INELST GAMMA	EXPT-PROG	NDG		NCSAC-42 182	N/71	TNC	NELLIS+. NO DATA GIVEN. TBP PR	60341
BI 209	TOTAL XSECT	EXPT-PROG		5.0 5	NCSAC-42 183	N/71	ORL	HARVEY+. NO DATA GIVEN. TRANSMISSION	60259
BI 209	RESON PARAMS	EXPT-PROG	NDG		NCSAC-42 183	N/71	ORL	HARVEY+. TRANS. ANAL TBC. NC DATA	60306
BI 209	NONEL GAMMAS	EXPT-PROG	6.0 6		NCSAC-42 195	N/71	ORL	DICKENS+. NO DATA GIVEN	60426
TH 232	TOTAL XSECT	EXPT-PROG	1.0 1	4.0 3	NCSAC-42 84	N/71	COL	RAHN+. RESON PARAMS ONLY GIVEN	60028
TH 232	TOTAL XSECT	EXPT-PROG	NDG		NCSAC-42 61	N/71	COL	HACKEN+. TRANS. ANAL TBC. NC DATA	60061
TH 232	RESON PARAMS	EXPT-PROG	2.2 1	4.0 3	NCSAC-42 84	N/71	COL	RAHN+. WN+WG.ALSO P-T+WIGNER DISTS	60027
U	TOTAL XSECT	EXPT-PROG	NDG		NCSAC-42 61	N/71	COL	HACKEN+. TRANS. ANAL TBC. NO DATA	60063
U 233	RESON PARAMS	EXPT-PROG	NDG		NCSAC-42 153	N/71	LAS	KEYWORTH+. J AND K TO BE MEASD.ORELA	60169
U 233	RESON PARAMS	EXPT-PROG	NDG		NCSAC-42 100	N/71	COL	FELVINCI+. ANAL TBC. NO DATA GIVEN	60201
U 233	SCATTERING	EVAL-PROG	2.5-2		NCSAC-42 29	N/71	ANL	DE VOLPI. ADJUSTED VALUE GIVEN	60134
U 233	FISSION	EVAL-PROG	2.5-2		NCSAC-42 29	N/71	ANL	DE VOLPI. ADJUSTED VALUE GIVEN	60139
U 233	FISSION	EXPT-PROG	1.0 3	1.5 7	NCSAC-42 130	N/71	LRL	BOWMAN+. TO BE DONE	60191
U 233	FISSION	EXPT-PROG	NDG		NCSAC-42 100	N/71	COL	FELVINCI+. ANAL TBC. NO DATA GIVEN	60202
U 233	ETA	EVAL-PROG	2.5-2		NCSAC-42 29	N/71	ANL	DE VOLPI. ADJUSTED VALUE GIVEN	60136
U 233	ALPHA	EVAL-PROG	2.5-2		NCSAC-42 29	N/71	ANL	DE VOLPI. ADJUSTED VALUE GIVEN	60137
U 233	NU	EVAL-PROG	2.5-2		NCSAC-42 29	N/71	ANL	DE VOLPI. ADJUSTED VALUE GIVEN	60135
U 233	NU	EXPT-PROG	1.0 3	1.5 7	NCSAC-42 130	N/71	LRL	BOWMAN+. TO BE DONE	60184
U 233	NU	EXPT-PROG	NDG		NCSAC-42 219	N/71	RPI	REED+. TO BE COMPLETED. NO DATA GIVN	60364
U 233	ABSORPTION	EVAL-PROG	2.5-2		NCSAC-42 29	N/71	ANL	DE VOLPI. ADJUSTED VALUE GIVEN	60140
U 233	N,GAMMA	EVAL-PROG	2.5-2		NCSAC-42 29	N/71	ANL	DE VOLPI. ADJUSTED VALUE GIVEN	60138
U 235	EVALUATION	EVAL-PROG	NDG		NCSAC-42 171	N/71	LAS	HUNTER+. NO DATA GIVEN	60343
U 235	EVALUATION	EVAL-PROG	NDG		NCSAC-42 170	N/71	LAS	HUNTER+. GAM PROD SIGS. NO CATA GIVN	60348
U 235	RESON PARAMS	EVAL-PROG	1.0 0	8.2 1	NCSAC-42 3	N/71	MTR	SMITH,J.R.+. FOR ENDF/B 3. NO DATA	59924
U 235	RESON PARAMS	EXPT-PROG	2.9-1	3.2 1	NCSAC-42 48	N/71	BNL	CHRIEN+. J PI FOR 7 RESON FROM CAPT	60102
U 235	RESON PARAMS	EXPT-PROG	NDG		NCSAC-42 153	N/71	LAS	KEYWORTH+. J AND K TO BE MEASD.ORELA	60168
U 235	RESON PARAMS	EXPT-PROG	1.1 0	4.5 1	NCSAC-42 98	N/71	COL	FELVINCI+. WT SIGO*WF FOR 7C RESON	60217
U 235	SCATTERING	EVAL-PROG	2.5-2		NCSAC-42 29	N/71	ANL	DE VOLPI. ADJUSTED VALUE GIVEN	60127
U 235	NONEL GAMMAS	EVAL-PROG	NDG		NCSAC-42 170	N/71	LAS	HUNTER+. GAM PROD SIGS. NO DATA GIVN	60345
U 235	FISSION	EXPT-PROG	NDG		NCSAC-42 1	N/71	MTR	SIMPSON+. LINAC. HIGH ALFA CENS. NDG	59926
U 235	FISSION	EXPT-PROG	2.0 6	3.0 6	NCSAC-42 17	N/71	ANL	POENITZ+. RATIO TO U238NF. CURV.TBP	59937
U 235	FISSION	EXPT-PROG	3.0 4		NCSAC-42 15	N/71	ANL	MEADOWS+. U236 ISOMER CONTRIBUTION	59964

ELEMENT S	A	QUANTITY	TYPE	ENERGY MIN	ENERGY MAX	DOCUMENTATION REF	VOL	PAGE	DATE	LAB	COMMENTS	SERIAL NO.
U	235	FISSION	EXPT-PROG	5.5 5	6.4 5	NCSAC-42	16		N/71	ANL	POENITZ. ABSOL VALUES AT 2ES GIVEN	59965
U	235	FISSION	EVAL-PROG	2.5-2		NCSAC-42	29		N/71	ANL	DE VOLPI. ADJUSTED VALUE GIVEN	60132
U	235	FISSION	EXPT-PROG	NDG		NCSAC-42	160		N/71	LAS	SMITH+. ABSOL MEAST TO BE DONE	60158
U	235	FISSION	EXPT-PROG	1.0 3	1.5 7	NCSAC-42	130		N/71	LRL	BOWMAN+. TO BE DONE	60190
U	235	FISSION	EXPT-PROG	5.0-1	1.0 3	NCSAC-42	98		N/71	COL	FELVINCI+. SIG INTEGRAL 15INTERVALS	60216
U	235	FISSION	EXPT-PROG	FISS		NCSAC-42	175		N/71	NBS	GRUNDL. RATIO U235/U238 AVG SIGS GVN	60293
U	235	FISSION	EXPT-PROG	1.0 4	1.0 5	NCSAC-42	199		N/71	ORL	GWIN+. ORELA. PRELIM CURV SHOWN	60428
U	235	FISSION	EXPT-PROG	1.0 4	3.0 5	NCSAC-42	199		N/71	ORL	GWIN+. ORELA. CURV PU239/U235 RATIO	60429
U	235	FISSION	EXPT-PROG		6.0 1	NCSAC-42	195		N/71	ORL	DE SAUSSURE+. MULTILVL ANAL RPI DATA	60434
U	235	ETA	EVAL-PROG	2.5-2		NCSAC-42	29		N/71	ANL	DE VOLPI. ADJUSTED VALUE GIVEN	60129
U	235	ALPHA	EVAL-PROG	2.5-2		NCSAC-42	29		N/71	ANL	DE VOLPI. ADJUSTED VALUE GIVEN	60130
U	235	ALPHA	EXPT-PROG	2.0-2	4.0 5	NCSAC-42	199		N/71	ORL	GWIN+. ORELA. CURVE. CFD OTHERS	60431
U	235	NU	EVAL-PROG	2.5-2		NCSAC-42	29		N/71	ANL	DE VOLPI. ADJUSTED VALUE GIVEN	60128
U	235	NU	EXPT-PROG	1.0 3	1.5 7	NCSAC-42	130		N/71	LRL	BOWMAN+. TO BE DONE	60183
U	235	NU	EXPT-PROG	NDG		NCSAC-42	219		N/71	RPI	REED+. TO BE COMPLETED. NO DATA GIVN	60365
U	235	SPECT FISS N	EXPT-PROG	NDG		NCSAC-42	15		N/71	ANL	SMITH. NO DATA. SEE NSE 44,439(1971)	59940
U	235	SPECT FISS G	EXPT-PROG	THR		NCSAC-42	190		N/71	ORL	PLEASONTON+. AVERAGE VALUES GIVEN	60242
U	235	FISS PROD GS	EXPT-PROG	1.9 6		NCSAC-42	142		N/71	LOK	IMHOF+. 4MIN TO 24HR. ANAL TBC. NDG	60174
U	235	FISS PROD GS	EXPT-PROG	THR		NCSAC-42	117		N/71	GA	SUND+. GE(LI). ISOMERIC GAMMA ES GVN	60197
U	235	ABSORPTION	EVAL-PROG	2.5-2		NCSAC-42	29		N/71	ANL	DE VOLPI. ADJUSTED VALUE GIVEN	60133
U	235	N,GAMMA	EVAL-PROG	2.5-2		NCSAC-42	29		N/71	ANL	DE VOLPI. ADJUSTED VALUE GIVEN	60131
U	235	N,GAMMA	EXPT-PROG		6.0 1	NCSAC-42	195		N/71	ORL	DE SAUSSURE+. MULTILVL ANAL RPI DATA	60433
U	235	SPECT NGAMMA	EXPT-PROG	4.8-1	3.2 1	NCSAC-42	48		N/71	BNL	CHRIEN+. RESON CAPTURE SPECTRA SHOWN	60103
U	236	FISSION	EXPT-PROG	5.0 5	6.0 6	NCSAC-42	206		N/71	ORL	ROSLER+. ORELA. CURV. HIGH RESOL.TBC	60414
U	238	EVALUATION	EVAL-PROG	NDG		NCSAC-42	171		N/71	LAS	HUNTER+. NO DATA GIVEN	60342
U	238	TOTAL XSECT	EXPT-PROG	NDG		NCSAC-42	61		N/71	COL	HACKEN+. TRANS. ANAL TBC. NO DATA	60049
U	238	TOTAL XSECT	EXPT-PROG	1.0 0	3.0 3	NCSAC-42	71		N/71	COL	RAHN+. ANAL OF 1970 DATA. NDG	60204
U	238	RESON PARAMS	EXPT-PROG	THR		NCSAC-42	28		N/71	ANL	BOLLINGER+. PARTIAL WG. NO DATA. TBP	59935
U	238	RESON PARAMS	EXPT-PROG	6.7 0	3.0 3	NCSAC-42	71		N/71	COL	RAHN+. PARAMS,ALSO P-T+WIGNER DISTS	60203
U	238	DIFF ELASTIC	EXPT-PROG	1.5 6	3.0 6	NCSAC-42	8		N/71	ANL	GUENTHER+. 20-160DEG. TBC. NO DATA	59954
U	238	DIFF INELAST	EXPT-PROG	1.5 6	3.0 6	NCSAC-42	8		N/71	ANL	GUENTHER+. 20-160DEG. TBC. NO DATA	59966
U	238	FISSION	EXPT-PROG	2.0 6	3.0 6	NCSAC-42	17		N/71	ANL	POENITZ+. RATIO TO U235NF. CURV.TBP	59938
U	238	FISSION	EXPT-PROG	1.0 3	1.5 7	NCSAC-42	130		N/71	LRL	BOWMAN+. TO BE DONE	60189
U	238	FISSION	EXPT-PROG	FISS		NCSAC-42	175		N/71	NBS	GRUNDL. RATIO U235/U238 AVG SIGS GVN	60292
U	238	NU	EXPT-PROG	1.0 3	1.5 7	NCSAC-42	130		N/71	LRL	BOWMAN+. TO BE DONE	60102
U	238	FISS PROD GS	EXPT-PROG	1.9 6		NCSAC-42	142		N/71	LOK	IMHOF+. 4MIN TO 24HR. ANAL TBC. NDG	60173
U	238	SPECT NGAMMA	EXPT-PROG	THR		NCSAC-42	28		N/71	ANL	BOLLINGER+. NO DATA GIVEN. TBP	59936
U	238	SPECT NGAMMA	EXPT-PROG	THR		NCSAC-42	168		N/71	LAS	JURNEY. GAMMA PRODUCTION SIGS GIVEN	60155
NP	237	RESON PARAMS	EXPT-PROG	NDG		NCSAC-42	153		N/71	LAS	KEYWORTH+. J AND K TO BE MEASD.ORELA	60167
PU	238	RESON PARAMS	EXPT-PROG	1.9 1	5.0 2	NCSAC-42	150		N/71	LAS	SILBERT+. FINAL VALUES WN WF 49 ES	60177
PU	238	STRNTH FNCTN	EXPT-PROG	1.9 1	5.0 2	NCSAC-42	150		N/71	LAS	SILBERT+. SO VALUE GIVEN	60176
PU	238	FISSION	EXPT-PROG	1.0 3	1.5 7	NCSAC-42	130		N/71	LRL	BOWMAN+. TO BE DONE	60185
PU	238	NU	EXPT-PROG	1.0 3	1.5 7	NCSAC-42	130		N/71	LRL	BOWMAN+. TO BE DONE	60178
PU	239	EVALUATION	EVAL-PROG	NDG		NCSAC-42	171		N/71	LAS	HUNTER+. NO DATA GIVEN	60344
PU	239	EVALUATION	EVAL-PROG	NDG		NCSAC-42	170		N/71	LAS	HUNTER+. GAM PROD SIGS. NO DATA GIVN	60350
PU	239	TOTAL XSECT	EVAL-PROG	1.0 0	3.0 2	NCSAC-42	4		N/71	MTR	SIMPSON+. FOR ENDF/B 3. NO DATA GIVN	59923
PU	239	TOTAL XSECT	EXPT-PROG	6.5 5	1.5 6	NCSAC-42	9		N/71	ANL	SMITH+. 2.5-KEV RESOL. NO DATA GIVEN	59962
PU	239	DIFF ELASTIC	EXPT-PROG	3.0 5	1.5 6	NCSAC-42	9		N/71	ANL	SMITH+. NO DATA GVN. RESULTS AVAILBL	59963

ELEMENT S A	QUANTITY	TYPE	ENERGY MIN	ENERGY MAX	DOCUMENTATION REF VOL PAGE	DATE	LAB	COMMENTS	SERIAL NO.
PU 239	NONEL GAMMAS	EVAL-PROG	NDG		NCSAC-42 170	N/71	LAS	HUNTER+. GAM PROD SIGS. NO DATA GIVN	60347
PU 239	FISSION	EVAL-PROG	1.0 0	3.0 2	NCSAC-42 4	N/71	MTR	SIMPSON+. FOR ENDF/B 3. NO DATA GIVN	59922
PU 239	FISSION	EVAL-PROG	2.5-2		NCSAC-42 29	N/71	ANL	DE VOLPI. ADJUSTED VALUE GIVEN	60122
PU 239	FISSION	EXPT-PROG	1.0 3	1.5 7	NCSAC-42 130	N/71	LRL	BOWMAN+. TO BE DONE	60188
PU 239	FISSION	EXPT-PROG	1.0 4	3.0 5	NCSAC-42 199	N/71	ORL	GWIN+. ORELA. CURV PU239/U235 RATIO	60430
PU 239	ETA	EVAL-PROG	2.5-2		NCSAC-42 29	N/71	ANL	DE VOLPI. ADJUSTED VALUE GIVEN	60119
PU 239	ALPHA	EVAL-PROG	2.5-2		NCSAC-42 29	N/71	ANL	DE VOLPI. ADJUSTED VALUE GIVEN	60120
PU 239	ALPHA	EXPT-PROG	2.0-2	4.0 5	NCSAC-42 199	N/71	ORL	GWIN+. ORELA. CURVE. CFD OTHERS	60432
PU 239	NU	EVAL-PROG	2.5-2		NCSAC-42 29	N/71	ANL	DE VOLPI. ADJUSTED VALUE GIVEN	60118
PU 239	NU	EXPT-PROG	1.0 3	1.5 7	NCSAC-42 130	N/71	LRL	BOWMAN+. TO BE DONE	60181
PU 239	SPECT FISS N	EXPT-PROG	NDG		NCSAC-42 15	N/71	ANL	SMITH. NO DATA. SEE NSE 44,439(1971)	59939
PU 239	FISS PROD GS	EXPT-PROG	1.9 6		NCSAC-42 142	N/71	LOK	IMHOF+. 4MIN TO 24HR. ANAL TBC. NDG	60172
PU 239	FISS PROD GS	EXPT-PROG	THR		NCSAC-42 117	N/71	GA	SUND+. GE(LI). ISOMERIC GAMMA ES GVN	60196
PU 239	ABSORPTION	EVAL-PROG	2.5-2		NCSAC-42 29	N/71	ANL	DE VOLPI. ADJUSTED VALUE GIVEN	60123
PU 239	N,GAMMA	EVAL-PROG	1.0 0	3.0 2	NCSAC-42 4	N/71	MTR	SIMPSON+. FOR ENDF/B 3. NO DATA GIVN	60022
PU 239	N,GAMMA	EVAL-PROG	2.5-2		NCSAC-42 29	N/71	ANL	DE VOLPI. ADJUSTED VALUE GIVEN	60121
PU 240	EVALUATION	EVAL-PROG	NDG		NCSAC-42 170	N/71	LAS	HUNTER+. GAM PROD SIGS. NO DATA GIVN	60349
PU 240	TOTAL XSECT	EXPT-PROG	1.0 5	1.5 6	NCSAC-42 9	N/71	ANL	SMITH+. 25KEV STEPS. NDG. TBP NSE	60018
PU 240	TOTAL XSECT	EXPT-PROG	1	3	NCSAC-42 213	N/71	RPI	HOCKENBURY+. TRANS. NO DATA GIVEN	60409
PU 240	RESON PARAMS	EXPT-PROG	2.0 1	5.0 2	NCSAC-42 213	N/71	RPI	HOCKENBURY+. AVG D,WN,AND WG GIVEN	60376
PU 240	STRNTH FNCTN	EXPT-PROG	2.0 1	5.0 2	NCSAC-42 213	N/71	RPI	HOCKENBURY+. SO VALUE GIVEN	60375
PU 240	DIFF ELASTIC	EXPT-PROG	3.0 5	1.5 6	NCSAC-42 9	N/71	ANL	SMITH+. NO DATA GIVEN TBP NSE	60017
PU 240	NONEL GAMMAS	EVAL-PROG	NDG		NCSAC-42 170	N/71	LAS	HUNTER+. GAM PROD SIGS. NO DATA GIVN	60346
PU 240	DIFF INELAST	EXPT-PROG	3.0 5	1.5 6	NCSAC-42 9	N/71	ANL	SMITH+. NO DATA GIVEN. TBP NSE	60016
PU 240	FISSION	EXPT-PROG	1.0 3	1.5 7	NCSAC-42 130	N/71	LRL	BOWMAN+. TO BE DONE	60187
PU 240	NU	EXPT-PROG	1.0 3	1.5 7	NCSAC-42 130	N/71	LRL	BOWMAN+. TO BE DONE	60180
PU 240	N,GAMMA	EXPT-PROG	1	3	NCSAC-42 213	N/71	RPI	HOCKENBURY+. NO DATA GIVEN	60408
PU 241	FISSION	EXPT-PROG	1.0 3	1.5 7	NCSAC-42 130	N/71	LRL	BOWMAN+. TO BE DONE	60186
PU 241	NU	EXPT-PROG	1.0 3	1.5 7	NCSAC-42 130	N/71	LRL	BOWMAN+. TO BE DONE	60179
PU 242	TOTAL XSECT	EXPT-PROG	1.5 1	3.0 4	NCSAC-42 1	N/71	MTR	SIMPSON+. ORELA. TRANS. 77DEGK. NDG.	59928
PU 242	TOTAL XSECT	EXPT-PROG	6.0 2	5.0 4	NCSAC-42 121	N/71	LRL	AUCHAMPAUGH+. TRANS. ANAL TBC,NDG	60195
PU 242	RESON PARAMS	EVAL-PROG		3.9 2	NCSAC-42 3	N/71	MTR	YOUNG+. FOR ENDF/B 3. NO DATA GIVEN	59925
PU 242	RESON PARAMS	EXPT-PROG	1	3	NCSAC-42 1	N/71	MTR	SIMPSON+. ORELA. TRANS. 77DEGK.D GVN	59927
PU 242	SPECT NGAMMA	EXPT-PROG	2.7 0		NCSAC-42 57	N/71	BNL	KANE. 2.66EV RESON. NO DATA GIVEN	60100
AM 242	FISSION	EXPT-PROG	1.0-2	1.4 7	NCSAC-42 135	N/71	LRL	BROWNE+. TO BE DONE. AM242M	60175
CM 243	FISSION	EXPT-PROG	1.0-2	1.4 7	NCSAC-42 135	N/71	LRL	BROWNE+. TO BE DONE.	59910
CM 244	TOTAL XSECT	EVAL-PROG	THR	5.0 2	NCSAC-42 4	N/71	MTR	BERRETH+. FOR ENDF/B 3. NO DATA GIVN	60021
CM 244	FISSION	EVAL-PROG	THR	5.0 2	NCSAC-42 4	N/71	MTR	BERRETH+. FOR ENDF/B 3. NO DATA GIVN	60019
CM 244	N,GAMMA	EVAL-PROG	THR	5.0 2	NCSAC-42 4	N/71	MTR	BERRETH+. FOR ENDF/B 3. NO DATA GIVN	60020
CM 245	FISSION	EXPT-PROG	1.0-2	1.4 7	NCSAC-42 135	N/71	LRL	BROWNE+. TO BE DONE.	59911
CM 247	FISSION	EXPT-PROG	1.0-2	1.4 7	NCSAC-42 135	N/71	LRL	BROWNE+. TO BE DONE.	59912
BK 249	FISSION	EXPT-PROG	1.0-2	1.4 7	NCSAC-42 135	N/71	LRL	BROWNE+. TO BE DONE.	59913
CF 249	FISSION	EXPT-PROG	1.0-2	1.4 7	NCSAC-42 135	N/71	LRL	BROWNE+. TO BE DONE.	59914
CF 252	NU	EVAL-PROG	2.5-2		NCSAC-42 29	N/71	ANL	DE VOLPI. ADJUSTED VALUE GIVEN	60126
CF 253	FISSION	EXPT-PROG	THR		NCSAC-42 123	N/71	LRL	WILD+. TO BE COMPLETED. NO DATA GIVN	60194

AEROJET NUCLEAR COMPANY

A. CROSS SECTIONS

1. Total Neutron Cross Section of ^{242}Pu Below 10 keV Measured at Liquid Nitrogen Temperatures (F. B. Simpson, O. D. Simpson, and H. G. Miller, ANC; J. A. Harvey and N. Hill, ORNL)

A liquid nitrogen cryostat was adopted to our radioactive sample changer installed on the Oak Ridge Electron Linear Accelerator (ORELA). This facility enables us to make cross section measurements at liquid nitrogen temperatures which reduces the Doppler effect and makes possible measurements at higher neutron energies with good energy resolution. The total neutron cross section of ^{242}Pu has been measured from 15.0 - 30,000 eV using the ORELA.

Transmission data were taken on three different metal samples at liquid nitrogen temperature (77°K) having inverse thicknesses of 41.19, 175.5 and 763.9 barns/atoms. The metal samples were made at Los Alamos and were originally prepared for thermal cross section measurements on the Materials Testing Reactor (MTR) fast chopper. The measurements were made at the 80 meter flight path with a 28 nsec accelerator burst width. Figure A-1 is a plot of the observed neutron levels as a function of neutron energy. From these data the average level spacing, below 1,000 eV, is approximately 16.3 eV. The experiment worked exceedingly well and preliminary studies of the raw data indicate that we will be able to analyze resonances below 6-10 keV. Extending the resolved energy region above 400 eV, as reported in the ENDF/B Version II, to 6-10 keV should be of great interest to the LMFBR Program. The average parameters obtained from these new data will predict better cross sections for the unresolved resonance region. (Pertinent to Request 479, Priority I, Wash. 1144)

2. Evaluation of a Gas Scintillation Counter for Measuring Fission Cross Sections in High Alpha Environment, (F. B. Simpson, and L. G. Miller, ANC; C. D. Bowman and J. Brown, LRL)

In order to make final tests on the gas scintillation counter, fission cross section measurements were made on ^{235}U using the Lawrence Radiation Laboratory (LRL) Electron Linear Accelerator with and without a ^{244}Cm foil in the chamber. The ^{244}Cm foil simulated an alpha background of 10^9 α/min. These results showed that with the use of this fast scintillation fission chamber in the coincidence mode that the large alpha pulse rate could be rejected in the presence of a few fission pulses. It demonstrated that this type of system is capable of producing high resolution time-of-flight data up to 14 MeV without any interference from the accelerator-gamma-flash. (Pertinent to Request 506, Priority I, Wash. 1144)

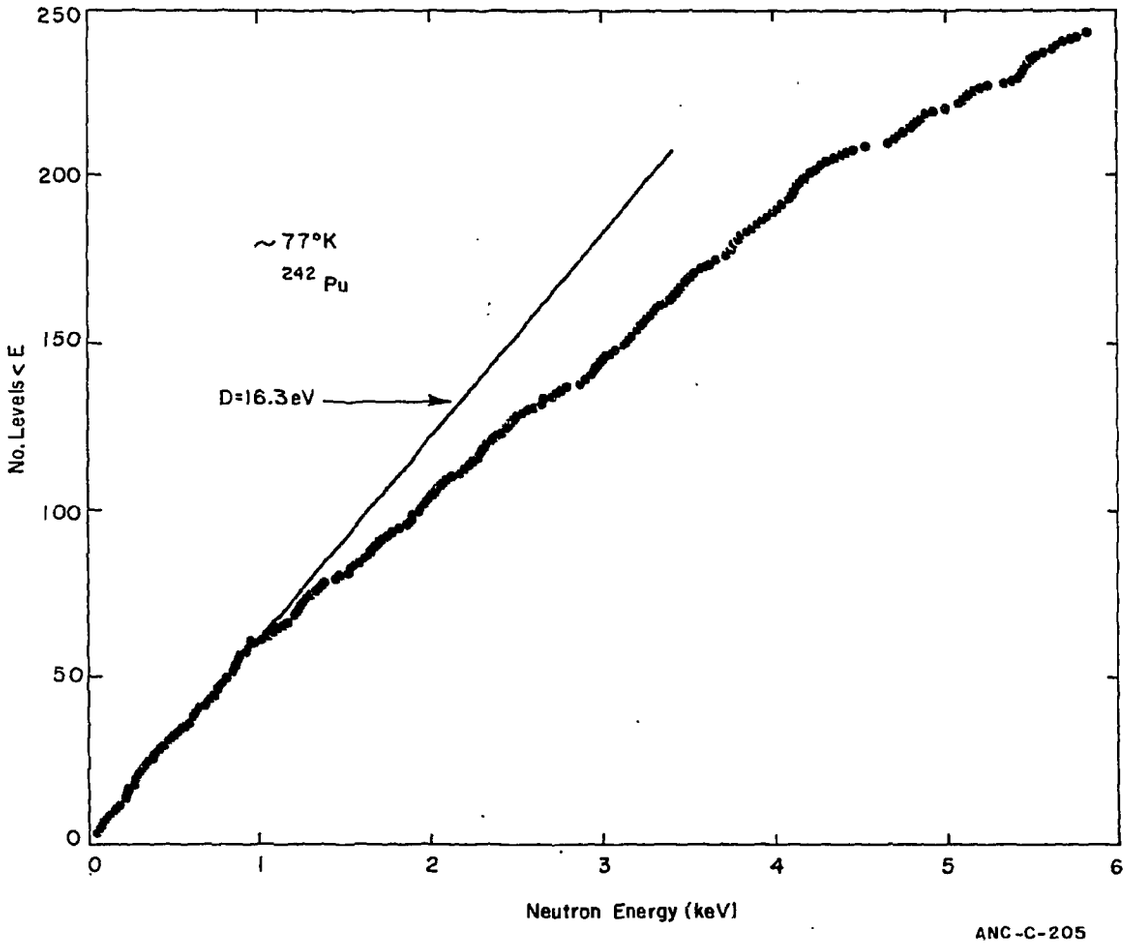

Figure A-1 The number of resonances below energy E (keV) as a function of energy for ^{242}Pu.

B. CROSS SECTIONS EVALUATIONS

1. ^{242}Pu Resonance Parameters for ENDF/B-III (T. E. Young and R. A. Grimesey)

A new evaluation for ^{242}Pu in the resolved resonance range and thermal energy region has been computed and submitted to BNL for Version III of ENDF/B. Resolved resonance parameters for resonances below 390 eV and all thermal energy cross sections were revised. No changes were made in the cross section values above 390 eV. (Pertinent to Request 479, Priority I, WAsh. 1144)

2. ^{235}U Resonance Parameters for ENDF/B-III (J. R. Smith and R. C. Young)

The resolved resonance files for ^{235}U were revised for Version III of ENDF/B. ^{235}U represents probably the most challenging task in all neutron resonance analysis. This is due not only to the close spacing and assymmetry of the resonances, but also to the fact that ^{235}U is the most used nuclear fuel, and there are vast quantities of data from many experiments to be examined. From the many sets of data available, the following were selected for fitting:

a. Simultaneous fission and capture measurements by deSaussure, et al. [1]

b. Total cross section measurements of Michaudon. [2]

c. Fission cross sections of Blons, et al. [3]

d. Fission cross sections measured by Cao. [4]

---

1. G. deSaussure, et al., "Simultaneous Measurements of the Neutron Fission and Capture Cross Sections for ^{235}U for Incident Neutron Energies from 0.4 eV to 3 keV," AEC Report ORNL-TM-1804 (1967).

2. A Michaudon, "Contribution a l'Etude par des Methods du Temps de Vol de l'Interaction des Neutrons Lents Ave. l'U-235," Report CEA-R2552 (1964).

3. J. Blons, H. Derrien, and A. Michaudon, "Measurements and Analysis of the Fission Cross Sections of ^{233}U and ^{235}U for Neutron Energies Below 30 keV," CONF-710301, Vol. 2, p. 829 (1971).

4. M. G. Cao, et al., "Fission Cross-Section Measurement on ^{235}U," J. Nucl. Energy 22, 211 (1968).

These data were fitted using the Automated Cross Sections Analysis Program (ACSAP).[5] Single-level parameters plus smooth files were obtained in the energy region 1-82 eV. Generally speaking, the new parameters have total widths comparable to those of Michaudon and alpha values given by the deSaussure data. (Pertinent to Requests 381, 387, and 593, Priorities II, II, and I, Wash. 1144)

3. Evaluation of the ^{239}Pu Cross Sections in the Resonance Region for ENDF/B-III, (O. D. Simpson and F. B. Simpson)

An extensive evaluation of ^{239}Pu in the resolved resonance region has been completed and covers the energy region from 1-300 eV. This evaluation is an improvement over the Version II data file for the resolved resonance region. Four different sets of experimental data were selected for the evaluation. Derrien's totals[6] and Blons' [7] fission data measured at Saclay and Gwin's fission and capture data [8] measured at Rensselaer Polytechnic Institute. The data were evaluated using the "Automated Cross Sections Analysis Program" ACSAP.[5] (Pertinent to Requests 442, 447, and 449, Priority I, Wash. 1144)

4. ENDF/B Version III Evaluation of the Resolved Resonance and Thermal Energy Cross Sections of ^{244}Cm, (J. R. Berreth and R. A. Grimesey)

A new evaluation of the resonance and thermal cross sections of ^{244}Cm below 500 eV has been made for Version III of ENDF/B based on new

---

5. N. H. Marshall, et al., "An Automated Cross Section Analyses Program (ACSAP)" The Third Neutron Cross Section Technology Conference, Knoxville, Tennessee, March 1971.

6. H. Derrien, et al., "Sections Efficaces Totale et de Fission du ^{239}Pu," Proc. of IAEA Symp. on Nucl. Data Microscopic Cross Sections and Other Data Basic for Reactors, Paris, Oct. 17-21, 1966, Vol. II, IAEA, Vienna (1967) p. 195.

7. J. Blons, et al., "Nuclear Data for Reactors I," IAEA Vienna (1970) 513.

8. R. Gwin, et al., "Measurements of the Neutron Fission and Absorption Cross Sections of ^{239}Pu over the Energy Region 0.02 eV to 30 keV, Part II," ORNL-4707, July 1971.

measurements[9,10,11] both at low energies and in the resolved resonance region. These measurements bring up to date the low energy evaluation of ^{244}Cm based on direct low energy measurements and new and additional determinations of resonance parameters. Low energy resonances up to and including 85.8 eV are a composite of three sets of data, Cote, et al.[9], M. S. Moore, et al.,[10] and J. R. Berreth and F. B. Simspon[11]. The data of Berreth and Cote are total neutron cross sections. The Moore data are capture and fission cross section measurements. (Pertinent to Requests 499 and 503, Priority II, Wash. 1144).

C. INTEGRAL CROSS SECTION MEASUREMENTS IN THE CFRMF (V. D. Harker and J. J. Scoville)

Relative capture cross section integrals for a variety of materials have been measured in the Coupled Fast Reactivity Measurement Facility at Idaho. The spectral measurements and calculations are reported in earlier NCSAC reports[12] along with earlier activation and reactivity measurements. Listed in Table C-1 are the activation measurements completed since the last meeting. The calculated values are derived from semi-empirical cross section calculations of Cook [13] and Benzi [14] by Schenter [15]. An electromagnetic mass spearator is on order and performance checks are now being completed at the manufacturer's plant. Once this separator is operational at our facility, capture cross sections of non-activation type materials will also be measured.

---

9. R. E. Cote, et al., "Total Neutron Cross Section of ^{244}Cm," Phys. Rev. Vol. 134, No. 6B, pp. 1281-1284 (June 22, 1964).

10. M. S. Moore and G. A. Keyworth, "Analysis of the Fission and Capture Cross Sections of the Curium Isotopes," Phys. Rev. C, Vol. 3, No. 4 pp. 1656-1667 (April 1971).

11. J. R. Berreth and F. B. Simpson, "Total Neutron Cross Sections of the Cm Isotopes from 0.01 to 30 eV," (to be published).

12. R. E. Chrien, "Reports to the AEC Nuclear Cross Sections Advisory Committee," Dec. 1, 1970, BNL-50276 (T-603), NCSAC-33 and May 1, 1971, BNL-50298 NCSAC-38.

13. J. L. Cook, private communication to M. K. Drake (evaluated data made available by JLC to NNSCS, January 1971).

14. V. Benzi and G. Reffo, CCDN-NW/10, ENEA Neutron Data Computation Centre (December 1969) p. 6

15. R. E. Schenter, WADCO Corp., (private communication).

Table C-1

$\bar{\sigma}$ (barns)

	CFRMF (Exp.) $\bar{\sigma}$ = 0.5	Cook (calc.)	Benzi (Cook-E<1 keV) (calc.)
^{87}Rb	0.0171 ± 0.0012	0.0226	0.0237
^{102}Ru	0.1125 ± 0.0085	0.137	0.192
^{104}Ru	0.106 ± 0.006	0.0789	0.0897
^{121}Sb	0.350 ± 0.028		
^{123}Sb	0.186 ± 0.025		
^{127}I	0.342 ± 0.026	0.341	0.386
^{148}Nd	0.126 ± 0.012		
^{150}Nd	0.12 ± 0.03		

ARGONNE NATIONAL LABORATORY

A. CHARGED PARTICLE PHYSICS

1. Enhanced Reaction Cross Sections of Possible CTR Interest: $^9Be + p$[1] (A. J. Elwyn, J. E. Monahan, and J. P. Schiffer)

It has been suggested[2] that the discovery of a low-energy nuclear resonance reaction yielding energetic charged particles might be important in the development of a "clean" controlled thermonuclear reactor. Many reactions of potential interest have not been measured at low bombarding energies. It seems appropriate, therefore, to consider what predictions about possible resonance enhancement can be made by combining present-day resonance reaction theory with the available data.

We have estimated the maximum possible enhancement from the ratio of the resonant value of the reaction cross section to the corresponding "black nucleus" (i.e. average) value. The major requirement for a significant enhancement at low energy (say, 50—500 keV) is that a resonance with a large (very nearly single-particle) reduced width in the entrance channel should exist near zero binding energy. With the assumption of a single-particle entrance channel reduced width and for a total reaction width of 100 keV, the enhancement is of the order of 100 at the resonance energy and decreases by a factor of two within one half-width for an $\ell=0$ resonance. (For the case of $\ell=1$ resonances, the enhancement is reduced approximately in the ratio $3P_{\ell=1}/P_{\ell=0}$, where P_ℓ is the entrance-channel penetrability for relative angular momentum ℓ).

A survey of the known levels of light nuclei indicates that the $p + {}^9Be$ reaction is a quite favorable case. An $\ell=0$ resonance in ^{10}B at excitation energy 6.88 MeV ($E_p \approx 330$ keV) has a nearly single-particle reduced width in the incident-proton channel and a total width $\Gamma \approx 100$ keV. Although the cross sections for the reactions $^9Be(p, d)^8Be \rightarrow 2\,^4He$ ($Q = 0.56$ MeV) and $^9Be(p, \alpha)^6Li$ ($Q = 2.13$ MeV) have not been measured below 250 keV proton energy, we can predict

---

[1] A letter with this title will appear in the journal, Nuclear Fusion.

[2] J. R. McNally, Jr., ORNL Report, ORNL-TM-3233, Rev. (1971).

the low-energy behavior of these cross sections using the measured values for the parameters that describe the resonance at 330 keV. At about 100 keV the estimated cross section is enhanced by a factor of 2 over the "black nucleus" value and has a magnitude of ~2 mb. Very probably these reactions receive no significant contribution from other resonances at energies below 250 keV since the s-wave levels in ^{10}B at 6.88 and 7.43 MeV account for most of the s-wave single particle strength; this situation should however be investigated further. Another possible source of additional low-energy enhancement lies in the fact that ^{9}Be has the most loosely bound neutron of any known stable nucleus. This means that the wave function of this neutron will extend to considerably larger radii than in other nuclei and a direct pick-up process may dominate the reaction at proton energies well below the barrier. The importance of this process remains to be determined experimentally.

2. Study of ^{236}U with the $^{235}U(d,p)^{236}U$ Reaction (K. Katori and J. R. Erskine)

Two-quasiparticle states in ^{236}U have been studied with the split-pole spectrograph at ANL. Angular distributions were measured at six different angles for the deuteron energy of 12 MeV. A number of previously unknown states have been found. These data have been interpreted within the framework of the single-particle rotational model in order to identify the two-quasiparticle states. Two series of states starting at 1050 ± 20 and 1187 ± 20 keV are assigned as the $K=4^-$ and 3^- bands, respectively, of the $(\frac{1}{2}+[631] + \frac{7}{2}-[743])$ Nilsson orbital both by the $I(I+1)$ rule for band energies and by the relative yields in the (d, p) reaction. Band mixing between these two bands has an important role in the determination.

B. FAST NEUTRON PHYSICS

1. Neutron Scattering

a. Fast Neutron Elastic and Inelastic Neutron Scattering in the Energy Range 1.5—3.0 MeV (P. Guenther and A. B. Smith)

A program of measurements using the new time-of-flight facility, described below, is making good progress. Differential scattering cross sections have been determined at 16—20 angles

between 20—160 degrees at incident energy intervals of ~100 keV from 1.5—3.0 MeV. The elements now under study are: ^{238}U, V, Fe, Ti, Co, C, Nb and (to a lesser extent) Ni. The results are expressed as cross sections, as yet uncorrected for such perturbations as multiple scattering.

(Req. No. NCSAC-35; 99, 97, 84, 32, 205, 203, 204, 412, 413, 414)

b. Total and Elastic Scattering Neutron Cross Sections of ^{239}Pu (A. B. Smith, P. Guenther and J. F. Whalen)

Elastic neutron scattering cross sections of ^{239}Pu were measured at $\lesssim$ 50 keV intervals from 0.3 to 1.5 MeV. Total neutron cross sections were measured from 0.65 to 1.5 MeV at intervals of $\lesssim$ 5 keV and with resolutions of ~2.5 keV. The experimental results were compared with the predictions of spherical- and deformed-optical models, with other measured values and with representative evaluated data. A draft of this work is available on request.

(Req. No. NCSAC-35; 444)

c. Fast Neutron Total and Scattering Cross Sections of ^{240}Pu (A. B. Smith, P. Lambropoulos and J. F. Whalen)

This work is formally completed with a manuscript accepted for publication in Nuclear Science and Engineering. The abstract follows.

Experimental fast neutron total cross sections and elastic- and inelastic-scattering cross sections of ^{240}Pu are reported. The total cross sections are measured from neutron energies of 0.1 to 1.5 MeV in increments of ~25 keV. The scattering cross sections are measured at $\lesssim$ 50 keV intervals from incident neutron energies of 0.3 to 1.5 MeV. The inelastic neutron excitation cross sections of states at 42 ± 5, 140 ± 10, 300 ± 20, 600 ± 20 and 900 ± 50 keV are measured. The experimental results are discussed in the context of the optical, compound-nucleus and direct-reaction nuclear models including the effects of resonance width fluctuations and the fission process. The measured results are compared with the corresponding quantities in the evaluated nuclear data file ENDF/B.

(Req. No. NCSAC-35; 463)

d. Palladium Fast Neutron Total and Scattering Cross Sections (A. B. Smith, P. Lambropoulos, P. Guenther and J. F. Whalen)

The neutron total and scattering cross sections of elemental palladium were experimentally studied. Total cross sections were measured from 0.1 to 1.5 MeV with resolutions of ~2 keV and elastic and inelastic scattering cross sections were determined from incident neutron energies of 0.3 to 1.5 MeV. The inelastic neutron excitation of states at 320 ± 50, 390 ± 20, 440 ± 20, 500 ± 30, 570 ± 20, 830 ± 20 and 940 ± 25 keV was prominently observed. In addition, the excitation of states at 650 ± 25, 720 ± 25, 760 ± 25 and 1010 ± 50 keV was qualitatively and/or tentatively observed. An optical potential deduced from detailed comparisons of calculated and measured fast neutron cross sections was descriptive of the present experimental results, previously reported high energy cross sections and of the minimum in the $\ell = 0$ strength function in the region of $A \sim 105$. A full report of this work is given in ANL-7869.

e. Polarization in the Elastic Scattering of 2 MeV Neutrons from Intermediate Weight Nuclei (S. A. Cox)

At present data have been taken at 2.000 MeV for 10 elements: Al, V, Ti, Co, Cu, Zn, Se, Y, Zr, Nb, Mo, Cd, Ag, In, Sn, Sb, Ta, W, Au and Pb. It is hoped and expected that the analysis of the data for these and other elements at 2.00 MeV and higher energies will result in an improved optical-model parameter set for neutron interaction calculations. Representative results are shown in Fig. B-1 for differential cross sections (b/sr) and polarizations.

2. Neutron Total and Reaction Cross Sections

a. Measurement of (n, p) Cross sections for Titanium, Nickel and Iron by Activation Methods (J. W. Meadows and D. L. Smith)

Cross sections for the $^{47}Ti(n,p)^{47}Sc$ ($Q = +0.22$ MeV), $^{58}Ni(n,p)^{58}Co$ ($Q = +2.26$ MeV) and $^{56}Fe(n,p)^{56}Mn$ ($Q = -2.90$ MeV) reactions have been determined by measuring the activity induced in samples of titanium, nickel and iron irradiated by fast neutrons. The relative activities of the neutron irradiated samples were measured by detecting the following gamma rays with both lithium-drifted

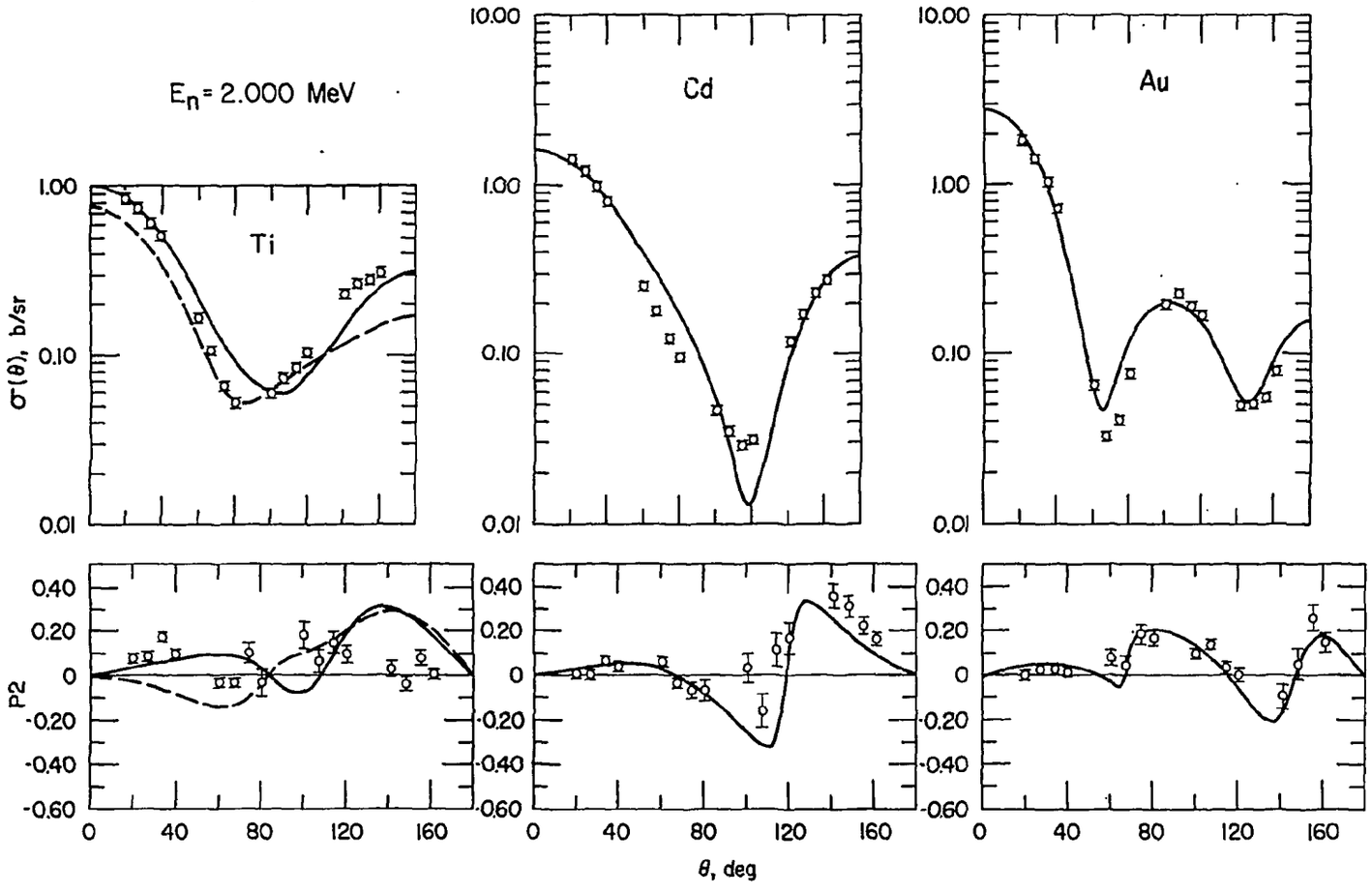
E_n = 2.000 MeV
Ti
Cd
Au
σ(θ), b/sr
P2
θ, deg
1.00
0.10
0.01
10.00
0.40
0.20
0
-0.20
-0.40
-0.60
0
40
80
120
160

Figure B-1

germanium and sodium iodide scintillation detectors:

^{47}Sc:	0.16 MeV gamma ray (3.4 day half life)
^{58}Co:	0.51 and 0.81 MeV gamma rays (71 day half life)
^{56}Mn:	0.84 MeV gamma ray (2.58 hour half life)

Fig. B-2 summarizes the results of this work. Box data symbols represent measurements made with a lithium-drifted germanium detector while cross data symbols correspond to measurements made with a sodium iodide scintillation detector. Corrections for geometric effects and for second-group neutrons from the $^{7}Li(p, n)^{7}Be^{*}$ reaction have been applied to this data, however no corrections for finite sample thicknesses have been determined as yet. These corrections will be small because the neutron transmission of all the samples exceed 95 percent.

(Req. No. NCSAC-35; 48)

b. Total Cross Section Measurements Using TOF Methods on the FNG (J. F. Whalen and A. B. Smith).

An experimental set up for total cross section measurements on the FNG has been designed and put into operation. The new set up was tested by measuring σ_T for carbon over the prominent resonance at 2.08 MeV. The results are shown in Fig. B-3: two sets of data are displayed to demonstrate the long-term stability of the apparatus by passing over the resonance twice in opposite directions. The resonance peak is not as high as other reported measurements[1] (4.2 barns) compared to 5.1 barns) as a result of the target thickness of ≈ 5 keV or about $\frac{1}{2}$ the resonance width. The region immediately on either side of the resonance follows the ENDF values extremely well.[2]

---

[1] S. Cierjacks, "Measurements and Analysis of the Total Neutron Cross Section of Carbon from 0.5 to 30 MeV," Proc. Conference on Neutron Standards and Flux Normalization, October 21-23, 1970, Argonne, Illinois.

[2] Evaluated Neutron Data File-B, National Neutron Cross Section Center, Brookhaven National Laboratory (1970).

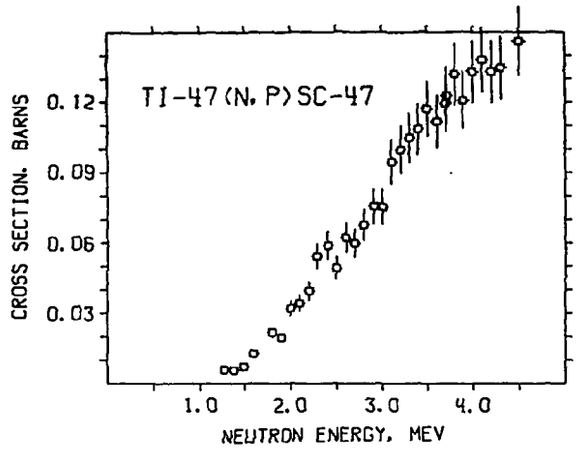
TI-47(N, P)SC-47
CROSS SECTION, BARNS
0.12
0.09
0.06
0.03
1.0
2.0
3.0
4.0
NEUTRON ENERGY, MEV

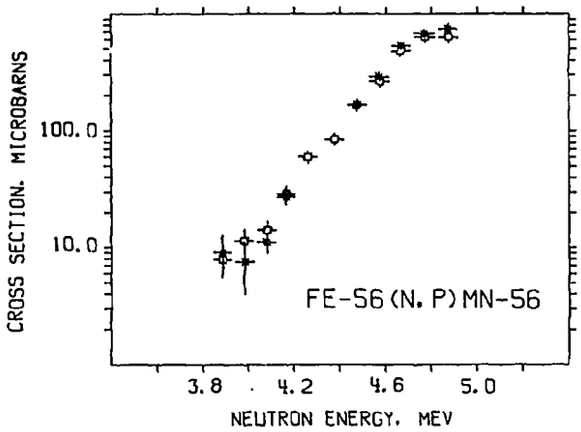
FE-56(N, P)MN-56
CROSS SECTION, MICROBARNS
100.0
10.0
3.8
4.2
4.6
5.0
NEUTRON ENERGY, MEV

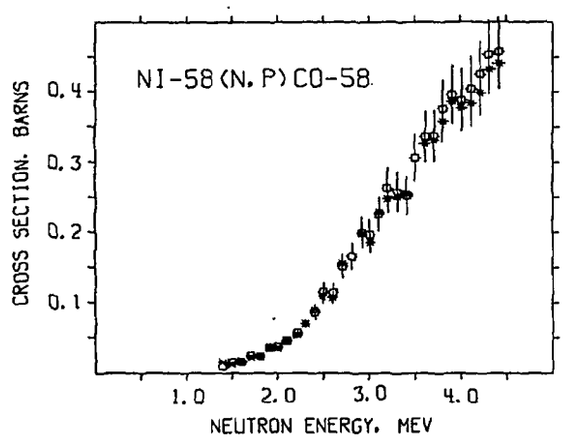
NI-58(N, P)CO-58
CROSS SECTION, BARNS
0.4
0.3
0.2
0.1
1.0
2.0
3.0
4.0
NEUTRON ENERGY, MEV

Fig. B-2

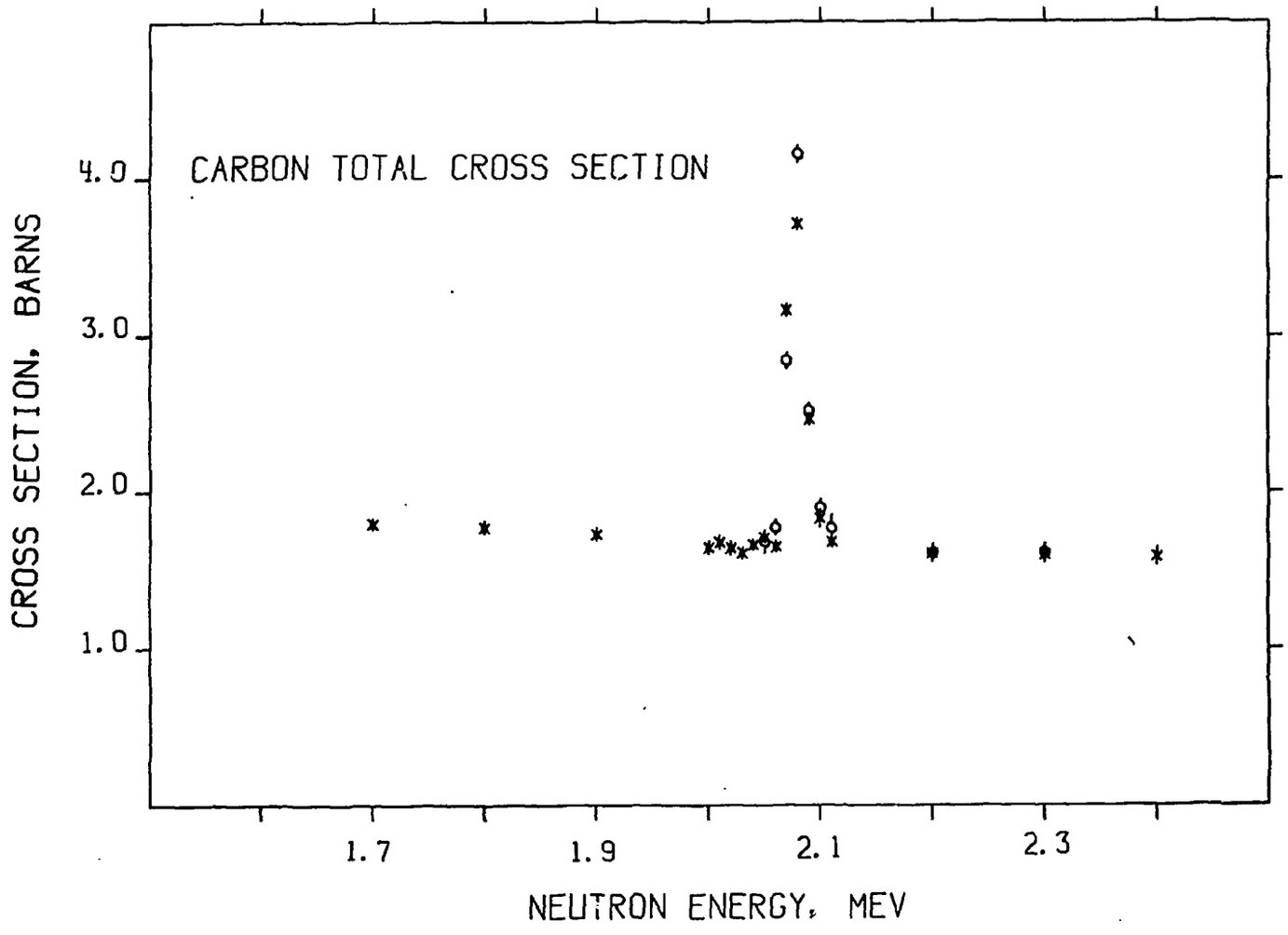
CARBON TOTAL CROSS SECTION
CROSS SECTION, BARNS
4.0
3.0
2.0
1.0
1.7
1.9
2.1
2.3
NEUTRON ENERGY, MEV

Figure B-3

3. Fission Cross Sections and Properties

a. Spontaneously Fissioning Isomer of ^{236}U (J. W. Meadows and W. P. Poenitz)

The existence of an isomeric state in ^{236}U which decays by spontaneous fission with a half-life of 85–115 nsec has been proposed by Pilcher and Brooks.[1] From the figure given in that report, at least 1% of the apparent total ^{235}U fission events induced by 30-keV incident neutrons are due to such a spontaneously fissioning isomer of ^{236}U. This amount would be of practical importance in absolute and relative fission cross-section experiments, fission neutron-spectrum measurements, and other fission studies that use the time-of-flight method for background suppression and spectroscopic purposes. Therefore, direct search for this isomer has been carried out using a fast-ionization-fission chamber with a time resolution of about 3 nsec. The measurement was made at an incident neutron energy of 30 keV using the kinematic collimation of the neutron beam close to the threshold energy of the $^{7}Li(p,n)^{7}Be$ reaction. The general room background was measured by positioning the fission counter outside the neutron beam. From a total of 3.7×10^4 observed fission events the total relative number of events outside the prompt peak was about ~0.12%, approximately 75% of which were attributed to the measured room background. Thus, the contribution to observed ^{235}U neutron-induced fission of a possible spontaneously fissioning isomeric state in ^{236}U is less than 3×10^{-2} %. This is one to two orders of magnitude lower than indicated by the work of Pilcher and Brooks[1] and too small to significantly affect fission cross-section measurements using time-of-flight techniques.

b. Note on the Prompt-Fission-Neutron Spectra of Uranium-235 and Plutonium-239 (A. B. Smith)

This is a summary of completed work formally published in Nuclear Science and Engineering 44, 439 (1971). The reader is referred to this reference for explicit experimental results and conclusions.

(Req. No. NCSAC-35; 396)

---

[1] J. V. Pilcher and F. D. Brooks, "Spontaneously Fissioning Isomers of Uranium-236 and -239," Annual Report of Southern Universities Nuclear Institute-SUNI-14, Faure, Republic of South Africa (1970).

c. Measurements of the ^{235}U Fission Cross Section at 552 keV and 644 keV (W. P. Poenitz)

The fast fission cross section of ^{235}U has been repeatedly measured in the past in many different laboratories. It appears that as time passes the results reflect a downward trend of this cross section. New absolute experimental values obtained at this laboratory are:

σ_f (552 keV) = 1.085 ± 0.043 barn
σ_f (644 keV) = 1.066 ± 0.042 barn.

The uncertainties were determined by statistical error evaluation using statistical quantities only and then adding systematic uncertainties in a straightforward summation. The present values are in agreement with recent preliminary values by the author,[1] measurements by Gorlove et al.[2] and Szabo et al.[3] The values are lower by 7–8 % than the smooth curve given by Davey[4] which is based on the measurements by White.[5]

---

[1] W. P. Poenitz, "Measurements of the ^{235}U Fission Cross Section in the keV Energy Range," Second Conference Neutron Cross Sections and Technology, Washington, D. C. 1968, NBS Sp. Public. 299, Vol. I, 503 (1968), Conf. 680307.

[2] G. V. Gorlove, B. M. Goshberg, V. M. Morozov, G. A. Ostroshehenko and V. A. Shigin, "The Fission Cross-Sections of ^{233}U and ^{235}U for Neutrons Having Energies between 3 and 800 keV," J. Nucl. Energy, 12, 79 (1960).

[3] I. Szabo, J. P. Marquette, E. Fort and J. L. Leroy, "Mesure Absolue de la Section Efficace de Fission," Proc. IAEA Conference on Nuclear Data for Reactors, Helsinki, 1970, CN-26/69.

[4] W. G. Davey, "An Analysis of the Fission Cross Sections of ^{232}Th, ^{233}U, ^{234}U, ^{235}U, ^{236}U, ^{237}Np, ^{238}U, ^{239}Pu, ^{240}Pu, ^{241}Pu and ^{242}Pu from 1 keV to 10 MeV," Nucl. Sci. Eng. 26, 149 (1966), and W. G. Davey, "Selected Fission Cross Sections for ^{232}Th, ^{233}U, ^{234}U, ^{235}U, ^{236}U, ^{237}Np, ^{238}U, ^{239}Pu, ^{240}Pu, ^{241}Pu and ^{242}Pu," Nucl. Sci. Eng. 32, 35 (1968).

[5] P. H. White, "Measurements of the ^{235}U Neutron Fission Cross Section in the Energy Range 0.04–14 MeV," J. Nucl. Eng. A/B 19, 325 (1965).

d. The Fission Cross Section Ratio of U-238 to U-235 from 2—3 Mev (W. P. Poenitz and R. J. Armani)

Measurements of $\sigma_f(^{238}U)/\sigma_f(^{235}U)$ were primarily carried out in the "plateau"-range near 2.5 MeV. Gas scintillation counters and the time-of-flight technique for background suppression were used. Four different methods were employed for mass assignment. The measured values shown in Fig. B-4 were slightly higher than those presently used in reactor evaluations. The present values agree very well with previous results by Jarvis[1] and White and Warner.[2] A paper will be submitted to the Journal of Nuclear Energy.

(Req. No. NCSAC-35; 417)

4. (p, n) Cross Section and Polarizations

a. Relative Yields of the Neutron Groups from the $^7Li(p,n)^7Be$, $^{7*}Be$ Reactions (J. W. Meadows)

The $^7Li(p,n)^7Be$ reaction is a convenient and widely used source of neutrons. Below proton energies of 2.38 MeV the reaction goes only to the ^7Be ground state and the neutrons are monoenergetic in the center of mass system. Above 2.38 MeV the reaction can also go to the first excited state of ^7Be and yield a second neutron group. However the third neutron group does not appear until 7.07 MeV so the reaction is still useful for monoenergetic experiments providing the relative intensities of the first and second groups are known.

The relative yields of the two neutron groups were measured by time-of-flight methods. Fig. B-5 shows the relative yields of these neutron groups (I_2/I_1) at 3°, 15° and 50°. The error associated with each data point above 3.6 MeV is 5% and is largely due to the counting statistics and the background subtraction. The differential cross sections for total neutron yield were also deduced.

---

[1] G. A. Jarvis, USAEC Report LA-1571, Los Alamos Scientific Laboratory (1953).

[2] P. H. White and G. P. Warner, J. Nucl. Energy 21, 671 (1967).

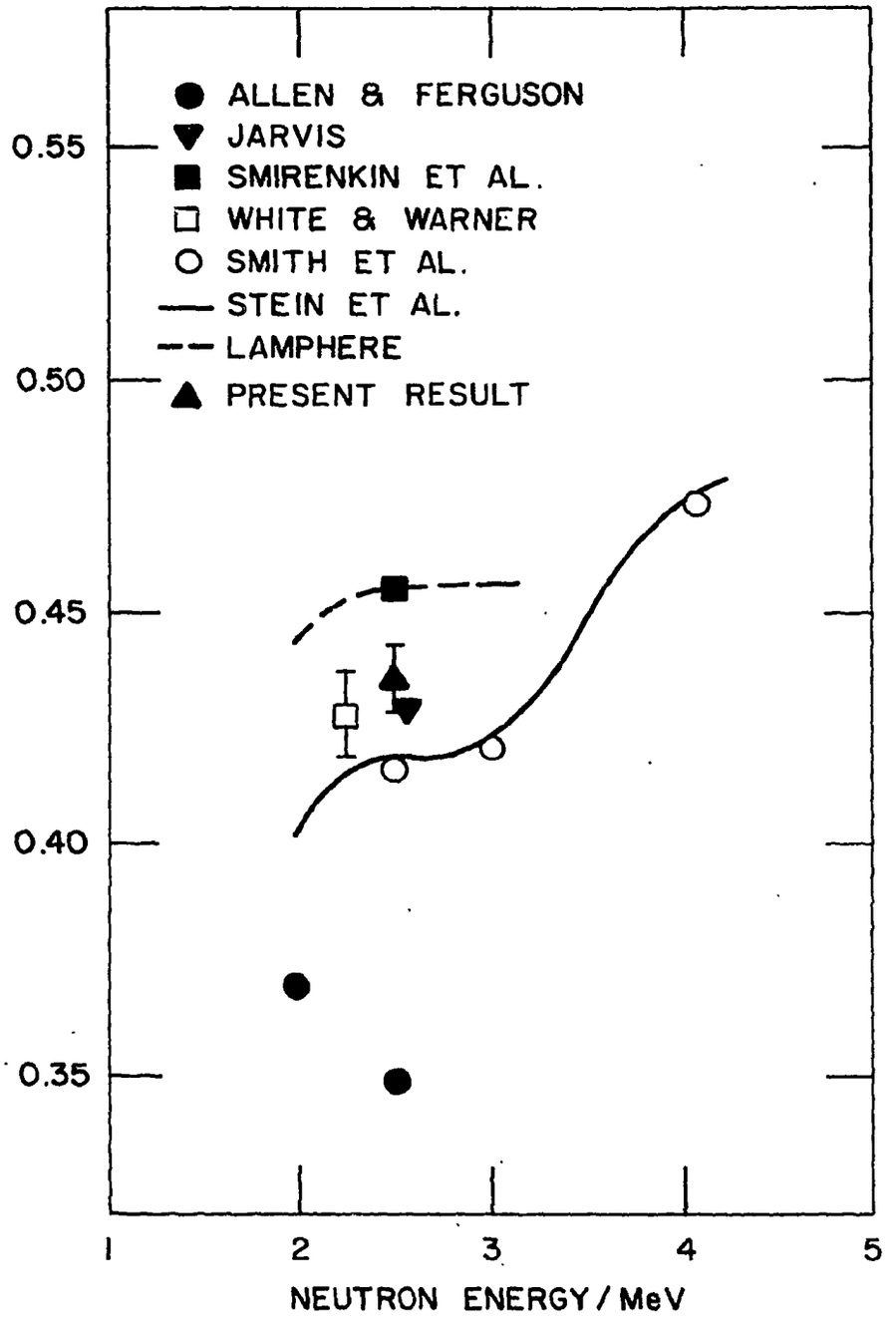
ALLEN & FERGUSON
JARVIS
SMIRENKIN ET AL.
WHITE & WARNER
SMITH ET AL.
STEIN ET AL.
LAMPHERE
PRESENT RESULT
0.55
0.50
0.45
0.40
0.35
1
2
3
4
5
NEUTRON ENERGY / MeV

Figure B-4

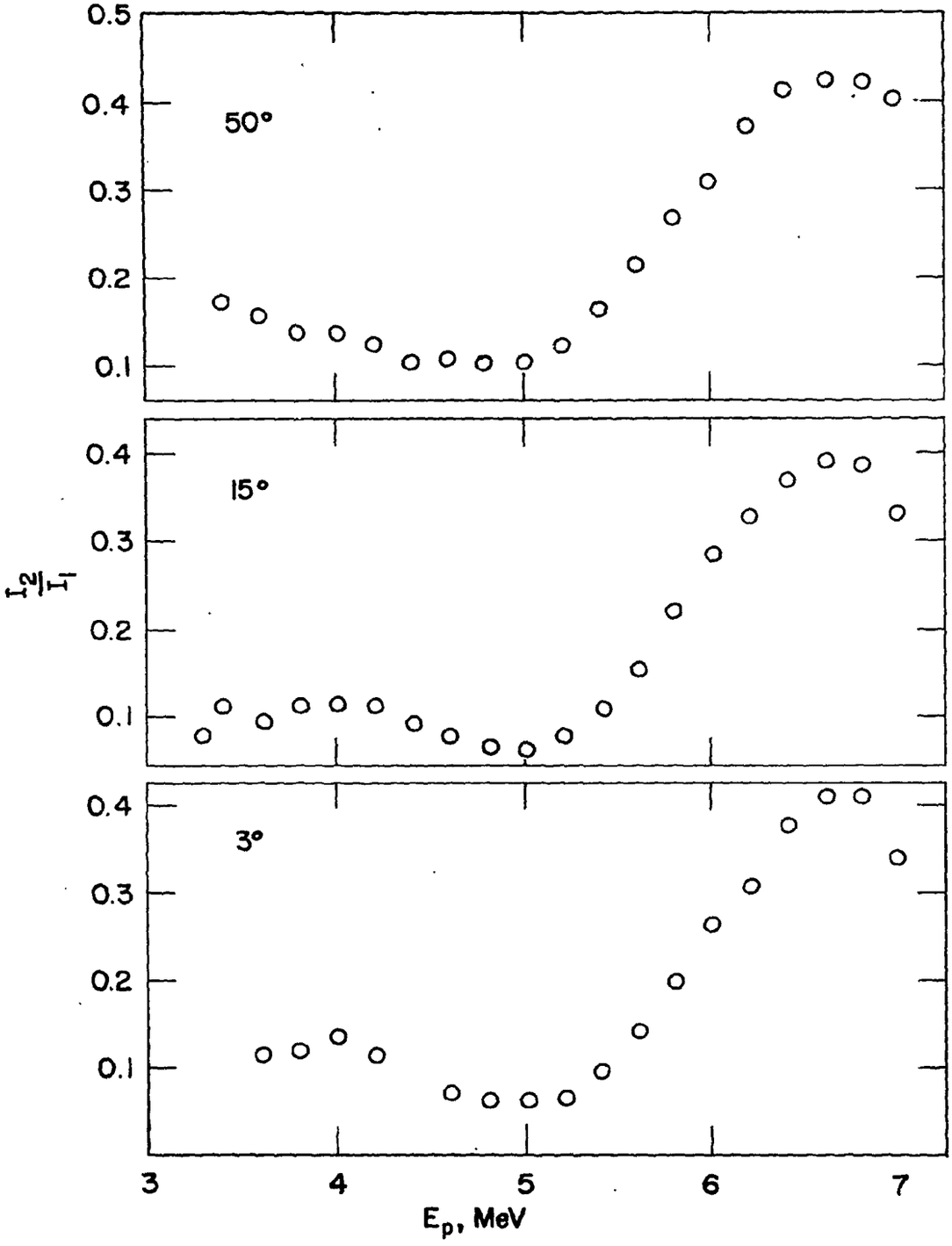

Figure B-5

b. Polarization and Angular Distributions of Neutrons in (p, n) Reactions (A. J. Elwyn, F. T. Kuchnir, F. P. Mooring, J. Lemming, E. Sexton, R. W. Finlay, W. G. Stoppenhagen, and R. E. Benensen)

A high-pressure He gas scintillator has been utilized as an analyzer of neutron polarization in (p, n) reactions initiated by protons accelerated in the ANL Dynamitron. Neutrons from the reaction of interest are incident on the gas cell. He recoils are detected in fast coincidence with scattered neutrons detected in either stilbene or plastic scintillators. The side detectors are positioned either at an angle of 60° or 90° relative to the He cell. In the (p, n) studies to be mentioned the neutron energies vary from about 0.5—1.5 MeV. There are few if any previous reports of the use of these techniques (i.e. He cells) at such low neutron energies.

The pulsed source of the Dynamitron and time-of-flight techniques have been utilized to measure the angular distributions of the neutrons in a number of these reactions. The neutrons were detected at four angles simultaneously with stilbene scintillators employing pulse-shape discrimination circuitry. The neutron's time-of-flight is measured relative to a signal generated by the proton beam pulse at a pick-off near the target.

1. The $^{51}V(p,n)^{51}Cr$ and $^{55}Mn(p,n)^{55}Fe$ Reactions: Measurements of the neutron polarization and differential cross section have been made at a number of angles at various proton energies corresponding to the excitation of isobaric analog resonances in the compound nuclei ^{52}Cr (at E_p = 2.21 and 2.335 MeV) and ^{56}Fe (at about 1.544, 1.686 and 1.778 MeV). In most cases the polarization is quite small ($\leq$ 10%); however, in the region of the IAS in ^{52}Cr, the values are somewhat larger and show an approximate sin θ dependence with angle. Preliminary observation indicates that the unpolarized angular distributions are symmetric about 90°. The significance of all of these results with respect to interference effects in these singly isospin-forbidden reactions is being investigated.

2. The $^{18}O(p,n)^{18}F$ Reaction: Both polarization and differential cross sections of neutrons corresponding to ^{18}F in its ground state have been measured at 18 proton energies between 3.035 and 3.475 MeV at 6 or 7 reaction angles. These energies encompass between 5 or 6 resonances corresponding to states in ^{19}F at excitation

energies around 11 MeV. At some energies in this region polarization values of near 50% are observed. In addition, angular distributions have been obtained at 12 more energies from 3.5 to 3.9 MeV. All these data will be utilized to determine if possible the spins and parities of the observed resonances.

5. Facilities

a. Improved Fast Neutron Time-of-Flight System (A. B. Smith)

An improved fast neutron time-of-flight system for scattering studies has been designed, constructed, and made operational. An impression of the scope of this new system can be gained from the illustration of Fig. B-6. Neutrons scattered from the samples are concurrently observed in 10 detectors placed at flight paths defined by the collimator system. The range of scattering angles is -125 to +160 degrees and the flight paths are variable from 2 to 7 meters. The ten detectors are connected to a special interface system feeding into a devoted on-line computer which handles data acquisition and preliminary processing. Interestingly, this computer is neither large nor particularly modern yet has proven ample for the purpose and has demonstrated a very good degree of reliability.

Initial performance of the system has been very encouraging with a number of measurements completed with scattered neutron resolutions of about 0.5 nsec/M. An entire angular distribution, inclusive of elastic events and prominent inelastic groups, can be obtained in the order of an hour with a very good signal-to-background ratio. The system might be unique in both the quality of the data and in overall efficiency.

b. A Large Liquid Scintillation Detector (W. P. Poenitz)

A 1300 ℓ liquid-scintillator has been assembled at the ANL Fast Neutron Generator for time-of-flight measurements of fast neutron capture cross sections.

Twelve phototubes of the type 57AVP have been chosen. They view the scintillation light in the liquid (a self-made mixture of Pseudo-cumene, P-Terphenyl and POPOP, with Trimethylborate

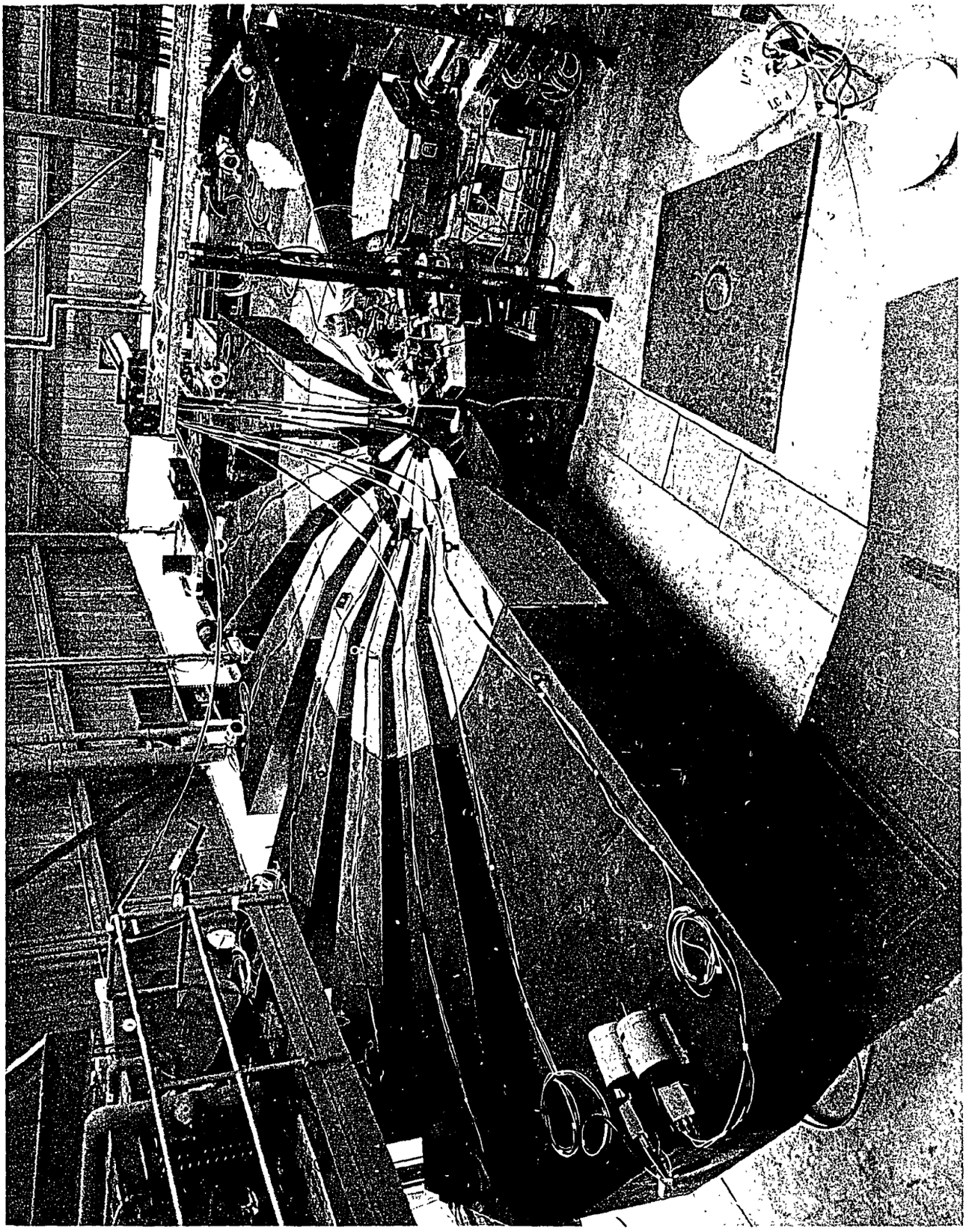

Figure B-6

added for the repression of capture γ-rays from hydrogen) through quartz-windows.

The energy resolution was measured and found to be about 26% for ^{60}Co and 52% for ^{137}Cs. The time resolution was measured in a "real experimental set-up" with a flight-path of 3 m. A FWHM of 3 nsec was found for the γ-peak which includes the time-uncertainty of the source pulse. This is in reasonably good agreement with measurements using a Cf-fission source in the center of the tank.

First measurements will be carried out for the ^{238}U and ^{232}Th capture cross sections in the 200—1500 keV energy range.

C. PHOTONUCLEAR PHYSICS

1. Intermediate Structure in the M1 Radiative Excitation of Resonances in ^{57}Fe (H. E. Jackson and E. N. Strait)

Earlier high resolution measurements of the photoneutron cross section of ^{57}Fe near threshold reported in NCSAC 38 have been extended to 800 keV. The photoneutron spectrum observed at 90° is shown in Fig. C-1. Spins of resonances have been assigned on the

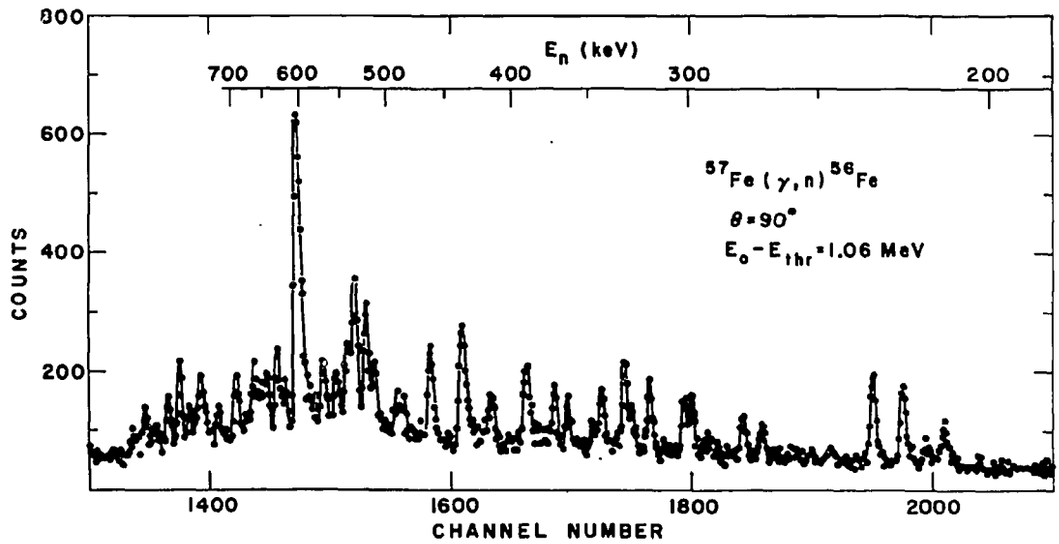

Figure C-1

basis of angular distributions of resonance groups for emission angles of 90° and 135°. Parity assignments where possible are based on a comparison of data with total neutron cross sections of the daughter nucleus. Angular momentum assignments and the corresponding observed intensity ratios are given in Table C-1. No assignments were attempted for an unresolved structure of resonances between 515 and 556 keV because of uncertainty in the resonance backgrounds. One important feature of the data: the integrated M1 strength although consistent with prediction is anomalously concentrated in a few of the many resonances in the p-wave neutron channel, a very intense $J^{\pi} = \frac{3}{2}^{-}$ doublet at 224 and 235 keV and a single $J^{\pi} = \frac{1}{2}^{-}$ resonance at 606 keV with a value of $\Gamma_{\gamma 0}$ over 40 times the value of $\overline{\Gamma}_{\gamma 0}$ observed for $\frac{1}{2}^{-}$ resonances below 300 keV. Such intermediate structure can be attributed to the presence of a strong two-quasiparticle doorway excitation consisting of a $(f_{5/2})(f_{7/2})^{-1}$ particle-hole coupled to the ^{57}Fe ground state.

2. Photoneutron Resonances from $^{29}Si(\gamma, n)^{28}Si$ (H. E. Jackson and R. E. Toohey)

Photoneutron resonance yields and angular distributions have been measured in the reaction $^{29}Si(\gamma, n)$ for neutron energies of 10 keV to 1.4 MeV. Agreement between resonance energies observed in $^{29}Si(\gamma, n)$ and $^{28}Si(n, n)^{28}Si$ is good. One discrepancy is observed. A very strong asymmetric shape observed for the photoneutron resonance at 761 keV suggests an unresolved doublet and the isotropic distribution for this group indicates $J = \frac{1}{2}$. However, the corresponding peak cross section in the $^{28}Si(n, n)$ reaction would indicate $J = \frac{3}{2}$. An isotropic group observed at 1.093 MeV is believed to correspond to the isobaric analogue of the $J^{\pi} = \frac{1}{2}^{+}$ first excited state of ^{29}Al. Analysis of the data is continuing.

3. $^{208}Pb(\gamma, n)^{207}Pb$ and the Giant M1 Resonance (R. E. Toohey and H. E. Jackson)

In a recent letter the Livermore group[1] presented evidence for a intense concentration of M1 radiative strength in group of five photoneutron resonances in the reaction $^{208}Pb(\gamma, n)^{207}Pb$. The observed

---

[1] C. D. Bowman, et al. Phys. Rev. Letters 25, 1302 (1970).

TABLE C-1. Angular momentum assignments for resonances in the reaction $^{57}Fe(\gamma, n)$.

E_n (keV)	$\frac{d\sigma(90^o)/d\Omega}{d\sigma(135^o)/d\Omega}$	J^π	E_n (keV)	$\frac{d\sigma(90^o)/d\Omega}{d\sigma(135^o)/d\Omega}$	J^π
26.7	s-wave	$\frac{1}{2}^+$	303	0.94 ± 0.10	$\frac{1}{2}$
32.9	1.10 ± 0.08	$\frac{1}{2}^-$	319	1.46 ± 0.17	$\frac{3}{2}$
56.9	1.08 ± 0.09	$\frac{1}{2}^-$	328	1.18 ± 0.16	—
70.2	s-wave, other	$\frac{1}{2}^+$, ?	331	1.17 ± 0.09	—
118.4	s-wave	$\frac{1}{2}^+$	345	0.97 ± 0.10	$\frac{1}{2}^-$
125.1	s-wave	$\frac{1}{2}^+$	353	0.81 ± 0.20	$\frac{1}{2}^-$
136	s-wave	$\frac{1}{2}^+$	364	1.24 ± 0.20	—
163	s-wave	$\frac{1}{2}^+$	372	1.88 ± 0.30	$\frac{3}{2}$
181	1.05 ± 0.09	$\frac{1}{2}^+$	389	0.92 ± 0.07	$\frac{1}{2}$
212	1.00 ± 0.03	$\frac{1}{2}^+$	415	1.41 ± 0.17	$\frac{3}{2}$
	1.00 ± 0.11		437	1.39 ± 0.08	$\frac{3}{2}$
217	0.90 ± 0.10	$\frac{1}{2}^-$	462	1.28 ± 0.11	$\frac{3}{2}$
	1.53 ± 0.32		493	0.89 ± .09	$\frac{1}{2}^-$
224	1.32 ± 0.04	$\frac{3}{2}^-$	515	* * *	—
	1.37 ± 0.10		524	* * *	—
233	1.43 ± 0.04	$\frac{3}{2}^-$	537	* * *	—
	1.43 ± 0.10		547	* * *	—
270	1.36 ± 0.09	$\frac{3}{2}^-$	556	* * *	—
	1.25 ± 0.25		571	1.44 ± 0.11	$\frac{3}{2}$
277	0.99 ± 0.07	$\frac{1}{2}^-$	605	1.05 ± 0.03	$\frac{1}{2}^-$
	1.09 ± 0.15		617	0.98 ± 0.09	$\frac{1}{2}$
299	0.97 ± 0.11	$\frac{1}{2}^-$	631	0.80 ± 0.06	$\frac{1}{2}$

1+ resonances exhaust the entire M1 strength for ^{208}Pb. Because of the importance of this result and the surprisingly large anisotropies observed for the 1^+ levels we have repeated the measurement with improved energy resolution and a target of 99.1% ^{208}Pb. The photoneutron spectra observed at 90° and 135° are shown in Fig. C-2. The analysis of data is not complete. Discrepancies with the Livermore data for the strength of $P_2(\cos\theta)$ terms in the photoneutron angular distributions and in the magnitude of the integrated M1 strength do exist, but in general the new data give strong support to conclusions of Bowman et al. regarding the presence the giant M1 resonance.

4. Ground State M1 and E1 Radiation Widths in ^{119}Sn (E. N. Strait and H. E. Jackson)

The threshold photoneutron spectra from an enriched target of ^{119}Sn are currently under study at the ANL photoneutron facility. Photoneutron transitions are limited to the ground state of ^{118}Sn. Spins of 24 excited states in ^{119}Sn associated with resolved peaks and $E_n < 30$ keV, were assigned on the basis of yields measured at 90° and 135°. Five peaks have been identified as s-wave neutron transitions by comparison with transmission data on ^{118}Sn. If the reduced width for the corresponding M1 transitions, K_{M1} is approximated by $\Sigma\Gamma_{\gamma 0}/\Delta E\, E^3$, we obtain the value .003 for $\frac{1}{2}^+$ resonances. This value is much lower than those observed in ^{118}Sn at higher excitation energies.

5. Facilities, Extended Model 12 Electron-Gun Life (G. Mavrogenes)

On the assumption that the current accelerated in the ANL electron Linac when the gun-grid is not being driven by the pulser (dark current) originates from active cathode material deposited on the grid, a procedure has been developed to clean it by electron bombardment from the cathode. In the initial application of the clean-up procedure the emissivity of the cathode was down by 50% and the dark current by a factor of 20 at completion of the operation. However, after one weeks operation the gun recovered its normal operating condition without any increase in the dark current.

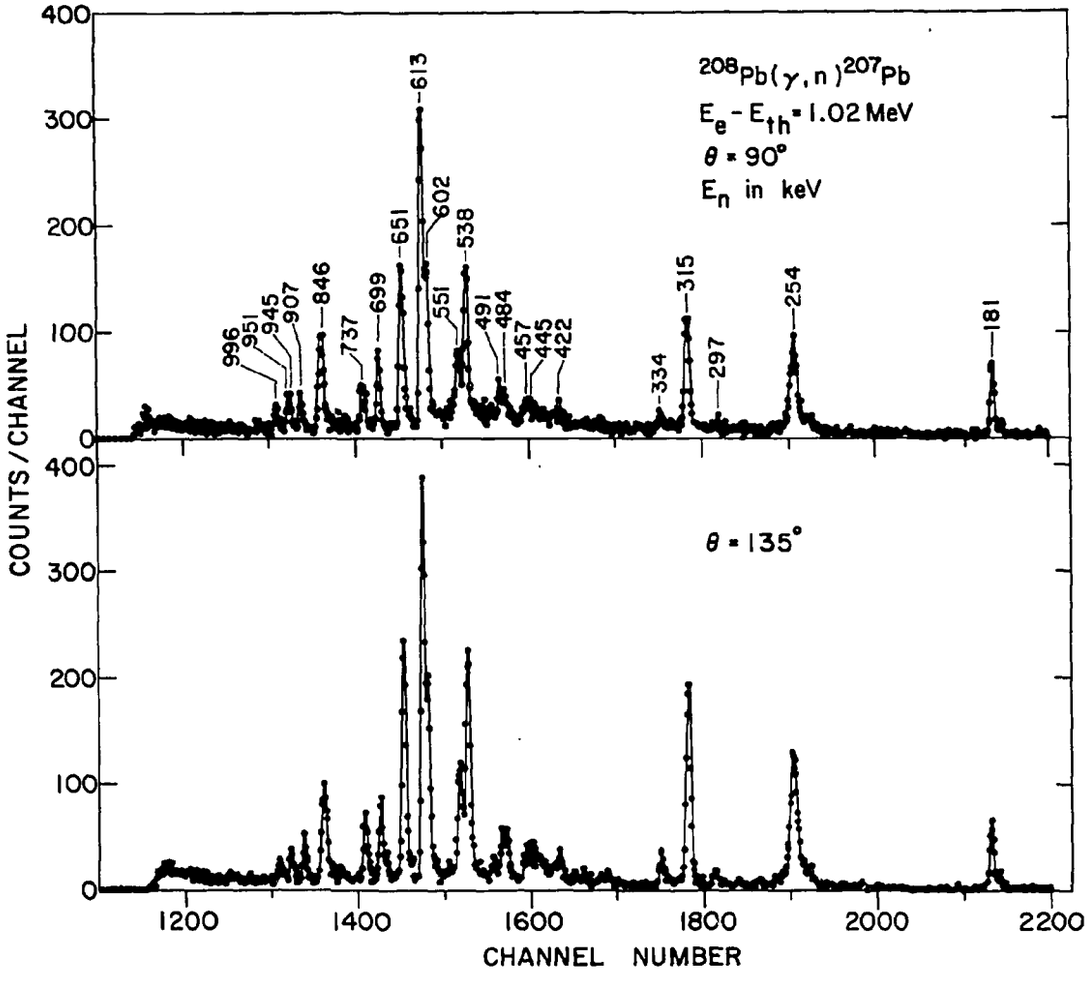
$^{208}Pb(\gamma,n)^{207}Pb$
$E_e - E_{th} = 1.02$ MeV
$\theta = 90°$
E_n in keV
$\theta = 135°$
996
951
945
907
846
737
699
651
613
602
538
551
491
484
457
445
422
334
315
297
254
181
COUNTS / CHANNEL
CHANNEL NUMBER
0
100
200
300
400
1200
1400
1600
1800
2000
2200

Figure C-2

D. REACTOR NEUTRON PHYSICS

1. The Reaction $^{238}U(n, \gamma)^{239}U$ (L. M. Bollinger and G. E. Thomas)

The study of the reaction $^{238}U(n, \gamma)^{239}U$ has been completed, and a paper on the results obtained is about to be submitted for publication. The results for low-energy states of ^{239}U were outlined in the last report to the NCSAC. Since then, the effort has been devoted to a study of absolute values of partial radiation widths. A technique for measuring accurate values of absolute intensities (branching ratios) of thermal-neutron-capture γ rays has been developed; intensities that are accurate to 5—10% may be measured with ease by relating an unknown intensity to the well-known intensities of lines in ^{13}C, ^{15}N, or ^{208}Pb. The average intensities obtained in this way for primary transitions in ^{239}U are generally consistent with those reported for resonance capture. Five E2 transitions are observed, and their average intensity is much stronger than is expected on the basis of what has been reported for E2 transitions in other nuclides.

2. The Equivalence of Thermal-Neutron-Capture and Resonance-Capture γ-ray Intensities (L. M. Bollinger)

It has been shown that, under the statistical model, the average intensity of thermal-neutron-capture γ-ray transitions to many final states is (except for trivial energy-dependent effects) equal to the average intensity of transitions from many initial states to a single final state. Thus, the intensities of thermal-neutron-capture γ rays provide a measure of the average widths of radiative transitions following resonance capture. This idea has been implicit in various previous publications but there appears to be no published mathematical justification.

3. The Reactions $^{117, 119}Sn(n, \gamma)^{118, 120}Sn$ (L. M. Bollinger and G. E. Thomas)

The reactions $^{117, 119}Sn(n, \gamma)^{118, 120}Sn$ have been studied by the average-resonance-capture method. Transitions to positive-parity states exhibit a broad maximum at a γ-ray energy of about 8.3 MeV. In principal, this could be caused by either E1, M1, or E2 transitions. The data themselves allow one to rule out E1 transitions,

whose widths for ^{118}Sn are found to be in good agreement with what is expected on the assumption that they result from the tail of the well-known E1 giant resonance at much higher energy. The E2 possibility is ruled out on the basis of the small widths reported for other nuclides. Thus, the observed intensity peak at ~8.3 MeV is attributed to M1 radiation. Various efforts to extend our understanding of the characteristics of the giant-resonance-like structure for M1 radiation are in progress.

4. $^{93}Nb(n,\gamma)^{94}Nb$, $^{103}Rh(n,\gamma)^{104}Rh$, and $^{197}Au(n,\gamma)^{198}Au$ (L. M. Bollinger, G. D. Loper, Jr., and G. E. Thomas)

Studies of the above reactions are in progress. Both thermal-neutron-capture and average-resonance-capture spectra are being measured.

5. Incoherent Scattering Cross Section of ^{169}Tm (G. H. Lander and T. O. Brun)

The very large hyperfine field that is present in thulium metal polarizes the spin of the Tm nuclei at low temperature. The effect of nuclear polarization was not observed in a polarized neutron experiment done at 1.6 K, where the polarization in the metal is approximately 1%. From this negative result the conclusion can be drawn that the spin-incoherent cross section of ^{169}Tm is less than 0.8 barns.

6. 2200 m/s Fission Cross-Sections (A. De Volpi)

An independent review of the 2200 m/s fission cross-sections has culminated in recent issuance of an Argonne National Laboratory report ANL-7830 (June, 1971), "Discrepancies and Possible Adjustments in the 2200-m/s Fission Parameters." Table D-1 is a summary of revisions considered reasonable by the author. The primary and most defensible modifications are for ^{235}U with a fission cross-section 1% higher and a neutron yield 1% lower than recommended by the IAEA. Significant deficiencies in some ^{239}Pu and ^{233}U parameters lead to certain improved-accuracy experiments recommended for clarification: ^{233}U and ^{234}U decay constants, ν_t ($^{239}Pu/^{252}Cf$), ν_t (^{252}Cf) (from NPL), η (^{233}U and ^{235}U), and 2200 m/s scattering. Table D-2 contains a summary of estimated accuracies of the fission parameters.

TABLE D-1 Revised Values for 2200-m/s Constants

	^{233}U				^{235}U		^{239}Pu		
	Experiment	Adjustment A[a]	Adjustment B[a]	Adjustment C[b]	Experiment	Adjusted	Experiment	Adjustment A[c]	Adjustment B[c]
σ_a	575.6 ± 1.6 (0%)[d]	582.5 ± 1.8 (+0.85%)	578.0 (+0.07%)	575.6 (-0.35%)	680.5 ± 2.7 (+0.15%)	683.0 ± 1.9 (+0.66%)	1012.1 ± 6.2 (0%)	1021.6 (+0.86%)	1013.4 ± 4.6 (+0.13%)
σ_f	539.3 ± 4.8 (+1.6%)	537.9 ± 1.9 (+1.4%)	536.5 (+1.1%)	531.9 (+0.25%)	587.4 ± 2.5 (+1.0%)	585.7 ± 1.8 (+0.95%)	742.5 ± 2.8 (+0.26%)	742.5 (+0.26%)	742.5 ± 3.1 (+0.26%)
σ_γ	50.6 ± 3.2 (0%)	44.6 ± 0.9 (-5%)	41.5 (-13%)	43.7 (-7.6%)	- -	97.3 ± 1.1 (-1.0%)	275.5 ± 7.8 (0%)	279.1 (+2.9%)	270.9 ± 2.6 (-1.7%)
α	0.0900 ± 0.0004 (0%)	0.0830 ± 0.0018 (-6.6%)	0.0773 (-14%)	0.0822 (-7.7%)	0.1691 ± 0.0021 (-0.59%)	0.1661 ± 0.0021 (-2.0%)	0.3598 (0%)	0.376 (+2.8%)	0.365 ± 0.004 (+1.4%)
η	2.278 ± 0.008 (-0.44%)	2.265 ± 0.006 (-0.86%)	2.278 (-0.29%)	2.284 (0%)	2.067 ± 0.009 (-0.48%)	2.058 ± 0.006 (-0.68%)	2.100 ± 0.009 (-0.48%)	2.091 (-0.84%)	2.091 ± 0.007 (-0.84%)
ν_t	2.464 ± 0.005 (-1.0%)	2.453 ± 0.007 (-1.4%)	2.454 (-1.3%)	2.472 (-0.6%)	2.393 ± 0.008 (-1.2%)	2.400 ± 0.007 (-0.92%)	2.854 ± 0.008 (-1.0%)	2.877 (-0.10%)	2.854 ± 0.007 (-0.91%)
σ_s[e]	10.5 (+24%)	3.5 (-59%)	8.1 (-4.9%)	10.5 (+24%)	14.3 ± 0.5 (-7.0%)	13.6 ± 1.5 (-5.0%)			

$\nu_t(^{252}Cf)$ = 3.731 ± 0.008 (Experiment) (-0.35%)
= 3.735 ± 0.008 (Adjusted) (-0.94%)

$\sigma_f(^{239}Pu)/(^{235}U)$ = 1.2633 ± 0.0081 (Experiment) (-1.5%)
= 1.2677 ± 0.0081 (Adjusted) (-0.8%)

$\tau_{1/2}(^{233}U)$ = 1.554 ± 0.003 x 10^5 years (Adjustment A) (-2.5%)
= 1.562 ± 0.003 x 10^5 years (Adjustment B) (-2.0%)
$\tau_{1/2}(^{234}U)$ = 2.444 ± 0.005 x 10^5 years (Experiment) (-1.8%)

$\nu_t(^{235}U)/(^{252}Cf)$ = 0.6414 ± 0.0018 (Experiment) (0%)
= 0.6426 ± 0.0015 (Adjusted) (0%)
$\nu_t(^{239}Pu)/(^{252}Cf)$ = 0.7648 ± 0.0062 (Experiment) (0%)
= 0.7703 ± 0.0022 (Adjustment A) (+0.85%)

$\nu_t(^{235}U)\sigma_f(^{235}U)$ = 1405.6 (Experiment) (-0.01%)
= 1405.7 (Adjusted) (-0.01%)
$\eta(^{235}U)\sigma_a(^{235}U)$ = 1406.6 (Experiment) (+0.06%)
= 1405.6 (Adjusted) (-0.01%)

$\nu_t(^{233}U)\sigma_f(^{233}U)$ = 1328.8 (Experiment) (+0.71%)
= 1319.5 (Adjustment A) (0%)
= 1316.6 (Adjustment B) (-0.22%)
$\eta(^{233}U)\sigma_a(^{233}U)$ = 1311.2 (Experiment) (-0.63%)
= 1319.4 (Adjustment A) (0%)
= 1316.7 (Adjustment B) (-0.21%)

$\nu_t(^{239}Pu)\sigma_f(^{239}Pu)$ = 2119.1 (Experiment) (-0.81%)
= 2136.2 (Adjustment A) (+0.02%)
= 2119.1 (Adjustment B) (-0.81%)
$\eta(^{239}Pu)\sigma_a(^{239}Pu)$ = 2125.4 (Experiment) (-0.51%)
= 2136.2 (Adjustment A) (+0.02%)
= 2119.0 (Adjustment B) (-0.81%)

	Other Values
$\eta(^{239}Pu)\sigma_a(^{239}Pu)/\eta(^{235}U)\sigma_a(^{235}U)$ = 1.5110 (Experiment) (+0.15%) = 1.5197 (Adjustment A) (+0.03%) = 1.5075 (Adjustment B) (-0.76%)	1.509 ± 0.023 (Magnuson[53])
$(\eta - 1)(^{239}Pu)\sigma_a(^{239}Pu)/(\eta - 1)(^{235}U)\sigma_a(^{235}U)$ = 1.5333 (Experiment) (+3.6%) = 1.5424 (Adjustment A) (-0.09%) = 1.5300 (Adjustment B) (-0.90%)	
$\eta(^{239}Pu)/\eta(^{235}U)$ = 1.0160 (Experiment) (+0.13%) = 1.0160 (Adjustment A) (-0.16%) = 1.0160 (Adjustment B) (-0.16%)	1.017 (Vidal et al.[69])
$\eta(^{233}U)/\eta(^{235}U)$ = 1.1021 (Experiment) (-0.05%) = 1.1006 (Adjustment A) (-0.17%) = 1.1069 (Adjustment B) (+0.40%)	1.081 ± 0.005 (Vidal et al.[69])
$\eta(^{233}U)\sigma_a(^{233}U)/\eta(^{235}U)\sigma_a(^{235}U)$ = 0.9322 (Experiment) (-0.19%) = 0.9386 (Adjustment A) (0%) = 0.9367 (Adjustment B) (-0.20%)	0.934 ± 0.014 (Magnuson[53])

[a]For ^{233}U Adjustment A, $\nu_t(^{233}U)\sigma_f(^{233}U)$ = 1319.5 (as Hanna et al.[42]); for Adjustment B, the product is 1316.6.
[b]For $\nu_t(^{233}U)\sigma_f(^{233}U)$ = 1314.8.
[c]For ^{239}Pu Adjustment A, $\nu_t(^{239}Pu)\sigma_f(^{239}Pu)$ = 2136.2 (as Hanna et al.[42]); for Adjustment B, the product is 2119.1.
[d]In parentheses are percentage differences comparing Hanna et al.[42] input-experimental and output-adjusted data. (The experiment averages derived in this report are compared with IAEA experimental averages; the adjusted output is compared with the IAEA LSF.)
[e]Rolled metal.

TABLE D-2. Estimated Accuracies[a] of the Fission Parameters

	^{233}U	^{235}U	^{239}Pu		^{233}U	^{235}U	^{239}Pu
σ_a	±0.4%	±0.3%	±0.8%	η	±0.6%	±0.3%	±0.4%
σ_f	±0.4%	±0.4%	±0.4%	ν	±0.5%	±0.3%	±0.8%
σ_γ	±10%	±1.3%	±3%	σ_s	±20%	±11%	-
α	±7%	±1.3%	±3%				

[a]67% confidence level.

E. NUCLEAR THEORY AND ANALYSIS

1. Differential Cross Sections for the Reactions $^{10}B(n,\alpha_0)^7Li$ and $^{10}B(n,\alpha_1)^7Li(0.48)$ Calculated from R-Matrix Parameters

(S. L. Hausladen, R. O. Lane and J. E. Monahan)

A manuscript with the following abstract has been submitted for publication in the Phys. Rev.:

Differential cross sections for alpha-particles to the ground and first-excited states of ^7Li in the reaction $^{10}B(n,\alpha)^7Li$ have been calculated from R-matrix parameters that fit neutron elastic scattering, neutron polarization, and $^{10}B(n,\alpha)^7Li$ reaction data. It should be noted that a measurement of these alpha-particle angular distributions could resolve some of the ambiguities that remain in the interpretation of the $^{10}B(n,\alpha)^7Li$ reaction for neutron energies below 1 MeV.

2. Analysis of the kth-Order Energy-Level Spacing Distributions (M. L. Mehta and N. Rosenzweig)

Bohigos and Flores[1] have shown that the kth-order energy-level spacing distributions for the conventional theory based on Wigner's Gaussian orthogonal ensemble (GOE) are substantially different from those of the rather simple examples of a "two-body random-matrix ensemble" (TBRE) introduced by French and Wong and Bohigos and Flores. We have analyzed the most recent Columbia neutron-capture data[1] for ^{166}Er, ^{168}Er, ^{170}Er, ^{182}W, ^{184}W, ^{186}W, ^{238}U and ^{232}Th. The quality of the data was judged by means of the Dyson-Mehta Δ statistic. We find that the data of highest quality are in much better agreement with the predictions of the GOE than with results obtained by the TBRE studied to date.

3. Analysis of the Distribution of the Spacings Between Nuclear Energy Levels (James E. Monahan and Norbert Rosenzweig)

The statistic $\Lambda(n)$, previously defined for the purpose of comparing empirical distributions of energy-level spacings with theoretical distributions, has been applied to the recently published series of neutron-capture levels observed in the even-A erbium isotopes. When the empirical values of $\Lambda(n)$ in the energy range of the highest experimental resolution are averaged over all possible sets of n successive spacings, the resulting value $\Lambda^*(n)$ is found to decrease sharply with increasing values of n. This decrease is consistent with that of the expectation value $\langle\Lambda(n)\rangle$ calculated for Wigner's Gaussian orthogonal ensemble of real symmetric matrices.

---

[1] Proc. International Conference on Statistical Properties of Nuclei, Albany, New York, August 23—27, 1971.

BROOKHAVEN NATIONAL LABORATORY

A. NEUTRON PHYSICS

1. Fast Chopper (R. E. Chrien, O. A. Wasson,* G. W. Cole, R. G. Graves,** S. F. Mughabghab,† and M. R. Bhat†)

a) Instrumental Developments

A new pulse height analysis system has been installed, including an analog-to-ditial converter with a 100 MHz digitizing rate, and hardware gain and zero stabilization. A precision dual pulser, designed by the BNL instrumentation division, is used as a stabilizing reference. This system provides the good stability necessary for high resolution capture γ-ray measurements over periods of several weeks. A pile-up rejection circuit, designed by V. Radeka of the BNL instrumentation division, has also been incorporated into the system. Shifting of counts from the 2-escape peak to the continuum at high instantaneous counting rates is largely eliminated.

An additional dual 4096 channel analog-to-digital converter has been interfaced to the fast chopper SDS 910 computer. A second pulse height analysis measurement, such as testing of GeLi detectors, can be carried out independently from the capture γ-ray experiment. This facility is also used for (n,α) measurements described below.

The SDS 910 data accumulation programs have been revised to accommodate the expanded experimental capacity of the system. In addition, the total dead-time per capture γ-ray event (electronic and computer contributions) has been reduced to 200 μsec from 650 μsec.

b) Experimental

1. Correlation studies near the 4s giant resonance: Thulium (with G. G. Slaughter, ORNL)

---

* On leave from BNL at Oak Ridge National Laboratory.

** Present address: Texas A&M University, College Station, Texas.

† Department of Applied Science, BNL.

Several years ago the BNL chopper group reported[1] the presence of correlations between the neutron widths and radiative widths for Tm-169(n,γ)Tm-170. The work was based on 9 J=1 resonances and 15 final states. Later work at BNL and Argonne extended this set to include the 153 eV resonance; the correlation became more firmly established thereby. The result was nonetheless surprising; on the basis of any direct reaction mechanism, the correlations predicted would be much smaller than those actually observed.

Recently the Harwell group reported[2] that the 153 eV resonance should be assigned J=0, rather than J=1. This result has been verified by recent experiments carried on by the BNL group at ORELA. With improved time-of-flight resolution it has been possible 1) to establish the spins of a number of resonances up to 700 eV and 2) to measure the high energy primary γ-ray spectra of many of these resonances and recalculate the correlation coefficients.

To determine the spins, the method of low energy γ-rays was used. The intensities of γ-rays depopulating the following states in Tm-170 were recorded: 149 keV (0^-), 166 (2^-), 181 (2^-), 204 (2^-), 220 (2^-), 237 (1^-), 243 (3^-) and 311 (3^-). We examine intensity ratios of γ-rays representing de-excitation from these levels, such as $3^-/1^-$ or $2^-/0^-$. For each such pair the higher spin component should be sensitive to resonance spin while the lower spin component should be insensitive. For the ratios of 4 such pairs, two ($3^-/1^-$) and two ($2^-/0^-$), normalized to the value of the 204 keV (2^-)/149 keV (0^-) ratio, the graph of Fig. A-1 can be constructed. The resonances fall into 2 groups as expected, and these correlate exactly with measured spins. The 153 eV resonance is clearly spin 0. Table I lists the spin assignments.

The time-of-flight curve of Fig. A-2 demonstrates the resolution improvement over the previous chopper experiment. The correlation coefficient previously obtained for the average over 9 resonances and 15 final states was rendered significant by the first resonance at 3.9 eV, a resonance characterized by strong transitions and a high reduced width. In the present experiment additional resonance spectra were included up to 283 eV. The value obtained for the average coefficient of correlation between Γ_n^o and $\Gamma_{\gamma i}$,

$$\langle \rho_i \rangle = +0.046 \pm 0.06, \quad \begin{cases} 24 \text{ resonances} \\ 15 \text{ final states} \end{cases}$$

---

[1] Beer, Lone, Chrien, Wasson, Bhat and Muether, Phys. Rev. Letters 20, 340 (1968). Lone, Chrien, Wasson, Beer, Bhat and Muether, Phys. Rev. 174, 1512 (1968).

[2] B. Thomas, Intl. Conf. on Statistical Properties of Nuclei, Albany, 1971 (in press).

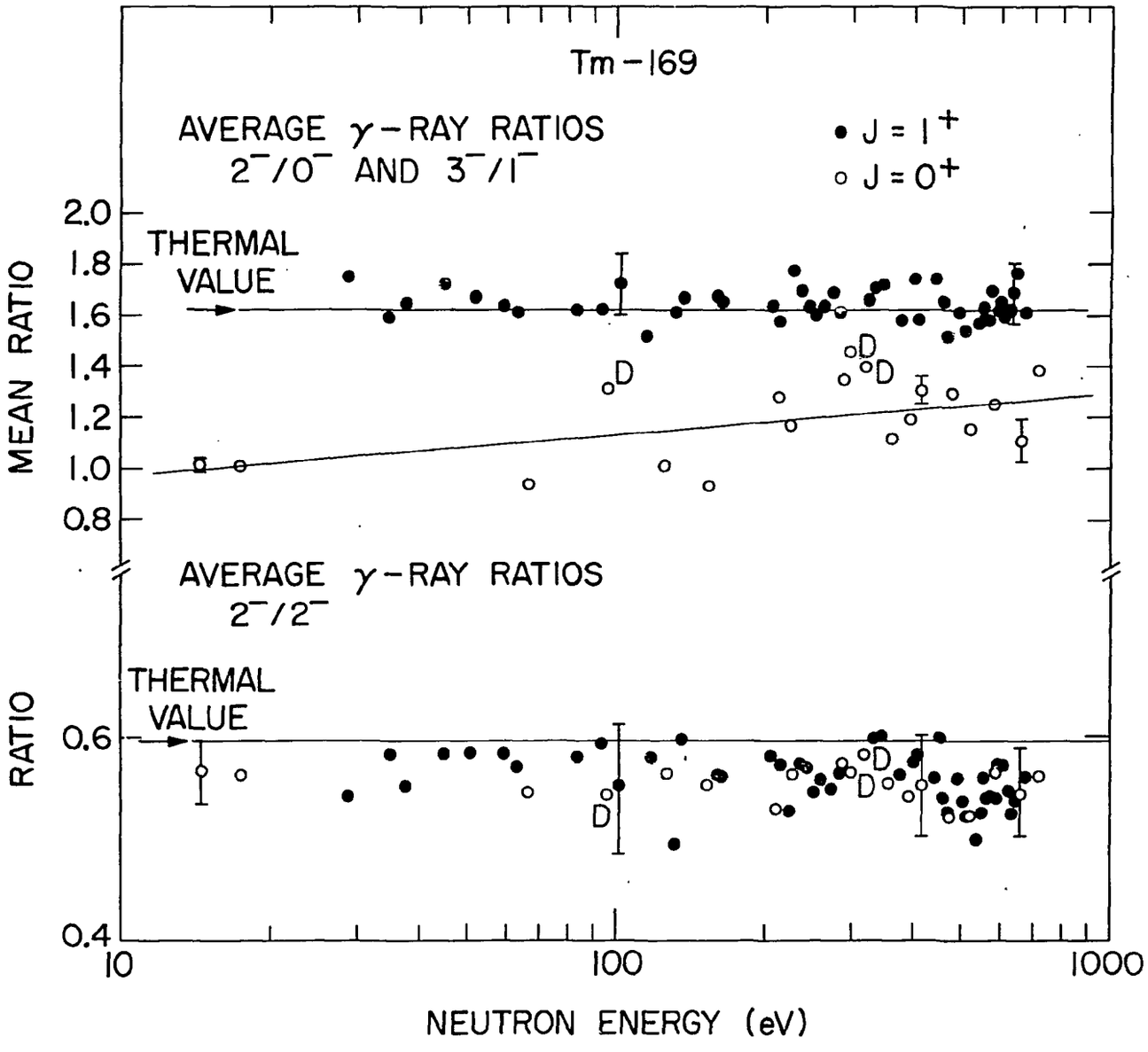
Tm-169
AVERAGE γ-RAY RATIOS
2⁻/0⁻ AND 3⁻/1⁻
• J = 1⁺
○ J = 0⁺
THERMAL VALUE
MEAN RATIO
2.0
1.8
1.6
1.4
1.2
1.0
0.8
D
AVERAGE γ-RAY RATIOS
2⁻/2⁻
THERMAL VALUE
RATIO
0.6
0.4
10
100
1000
NEUTRON ENERGY (eV)

Figure A-1

TABLE A-1

$Tm^{169}(n,\gamma)$ Spin Assignments

E_n(eV)	J
3.9	1
14.5	0
17.5	0
28.8	1
34.9	1
37.6	1
45.0	1
50.8	1
59.3	1
63.2	1
66.2	0
83.6	1
94.2	1 } incompletely resolved
95.7	(0) } incompletely resolved
101.9	1
115.6	1
125.3	0
132.3	1
136.1	1
153.8	0
160.7	1
164.5	1
207.9	1
210.2	(doublet, 1 and 0)
214.1	1
224.4	0
228.4	1

Table A-1 (Cont.)

E_n(eV)	J
238.8	1
243.8	1
251.6	1
260.6	1
274.2	1
283.8	1
289	(doublet, 1 and 0)
297.2	1
319.9	(doublet, 1 and 0)
325.1	1
333.6	1
346.8	1
358.2	0
378.1	1
391	0
400.5	1
409.2	1
416.2	(doublet, 1 and 0)
441.4	1
455.4	1
459.9	1
469	1
472.8	0
493.3	1
512.9	1
520.2	0
542.8	1
550.4	1
557.4	1

Table A-1 (Cont.)

E_n(eV)	J
565.9	1
573.9	1
586.7	0
592.4	1
599.8	1
607.8	1
626.3	1
631.8	1
643	1
659.5	0
676.1	1
716	1

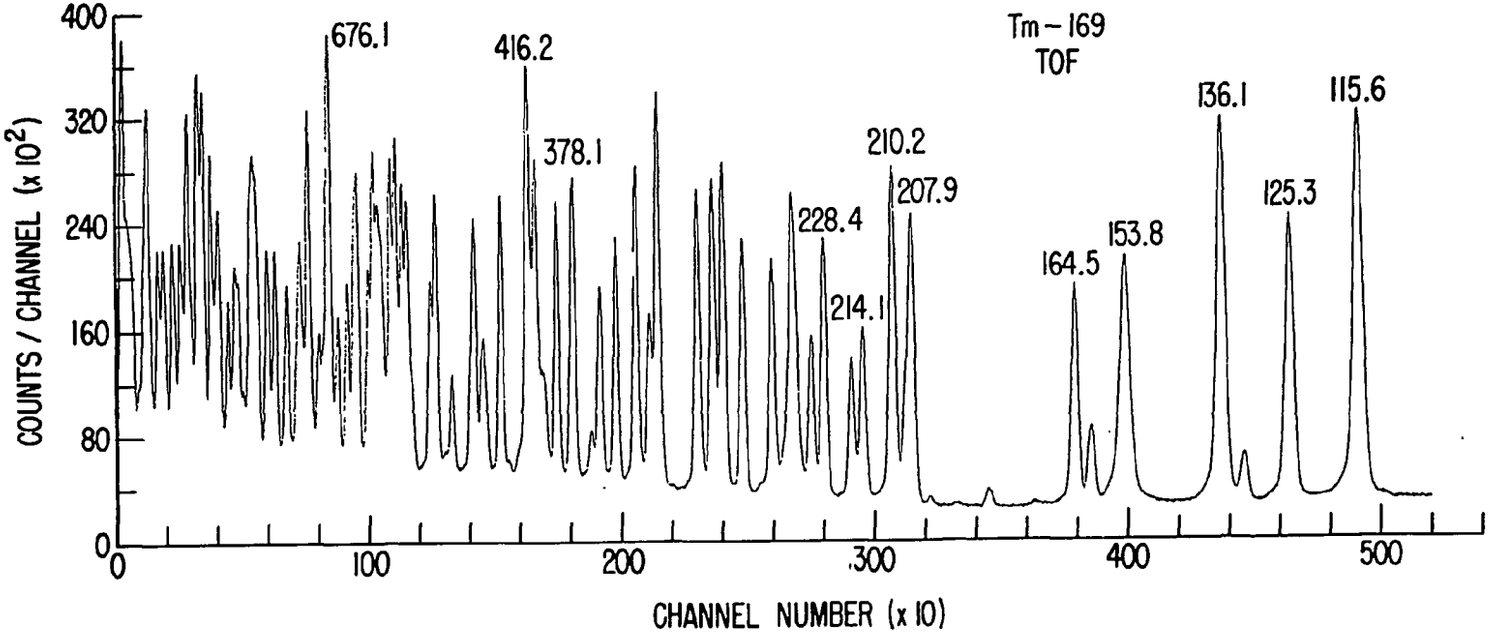
Tm-169
TOF
676.1
416.2
378.1
228.4
214.1
210.2
207.9
164.5
153.8
136.1
125.3
115.6
COUNTS / CHANNEL (x 10²)
400
320
240
160
80
0
0
100
200
300
400
500
CHANNEL NUMBER (x 10)

Figure A-2

has decreased to the point where it is no longer significantly different from zero. Hence there is no convincing evidence for non-statistical effects in Tm-169.

Similar correlations have also been reported for Dy-163[3] and Yb-173.[4] The number of resonances examined for each of these cases will be increased in planned experiments at ORELA.

2. $Mo^{92}(n,\gamma)$ and $Mo^{98}(n,\gamma)$ Studies (with G. G. Slaughter, ORNL)

The valence neutron model[5] has proved extremely successful in predicting radiative widths in Mo-92 and Mo-98, especially for resonances with large neutron reduced widths. Earlier this year, studies at the fast chopper were carried out[6] on both these isotopes, and in the case of Mo-98, angular distribution studies of the emitted capture γ-rays showed that the Mo-98 resonance at 818 eV was a $3/2^-$ resonance. This demonstration was crucial in the quantitative verification of the model.

The chopper work has recently been extended to higher neutron energies using the ORELA linac and 10-meter flight path station. In June work on Mo-98 was completed up to a neutron energy of 4842 eV. The time-of-flight spectrum, taken with a nominal resolution of 2.5 ns/m, is shown in Fig. A-3. The unusual concentration of p-wave strength from 1000 eV to 400 eV is quite evident in the time spectra. Above 1 keV the resonances have much smaller reduced neutron widths and statistical processes are expected to dominate the capture reaction.

Table A-2 summarizes the photon intensities deduced from this experiment, and also lists the relative intensities expected on the basis of the valence model. Spin assignments have been made on the basis of the high energy transitions observed; where doubtful these are shown in parentheses. Inspection of the table indicates that, overall the $p \rightarrow s$ transitions are in better agreement with the model than are the $p \rightarrow d$ transitions.

---

3. S. F. Mughabghab, R. E. Chrien and O. A. Wasson, Phys. Rev. Letters 25, 1670 (1970).

4 Mughabghab, Wasson, Cole, Chrien and Bhat, Bull. Am. Phys. Soc. II 16, 496 (1971).

5 A. M. Lane and J. E. Lynn, Nucl. Phys. 17, 586 (1960). J. E. Lynn, The Theory of Neutron Resonance Reaction, (Clarendon Press, Oxford), p. 330 (1968).

6 Mughabghab, Chrien, Wasson, Cole and Bhat, Phys. Rev. Letters 26, 1118 (1971).

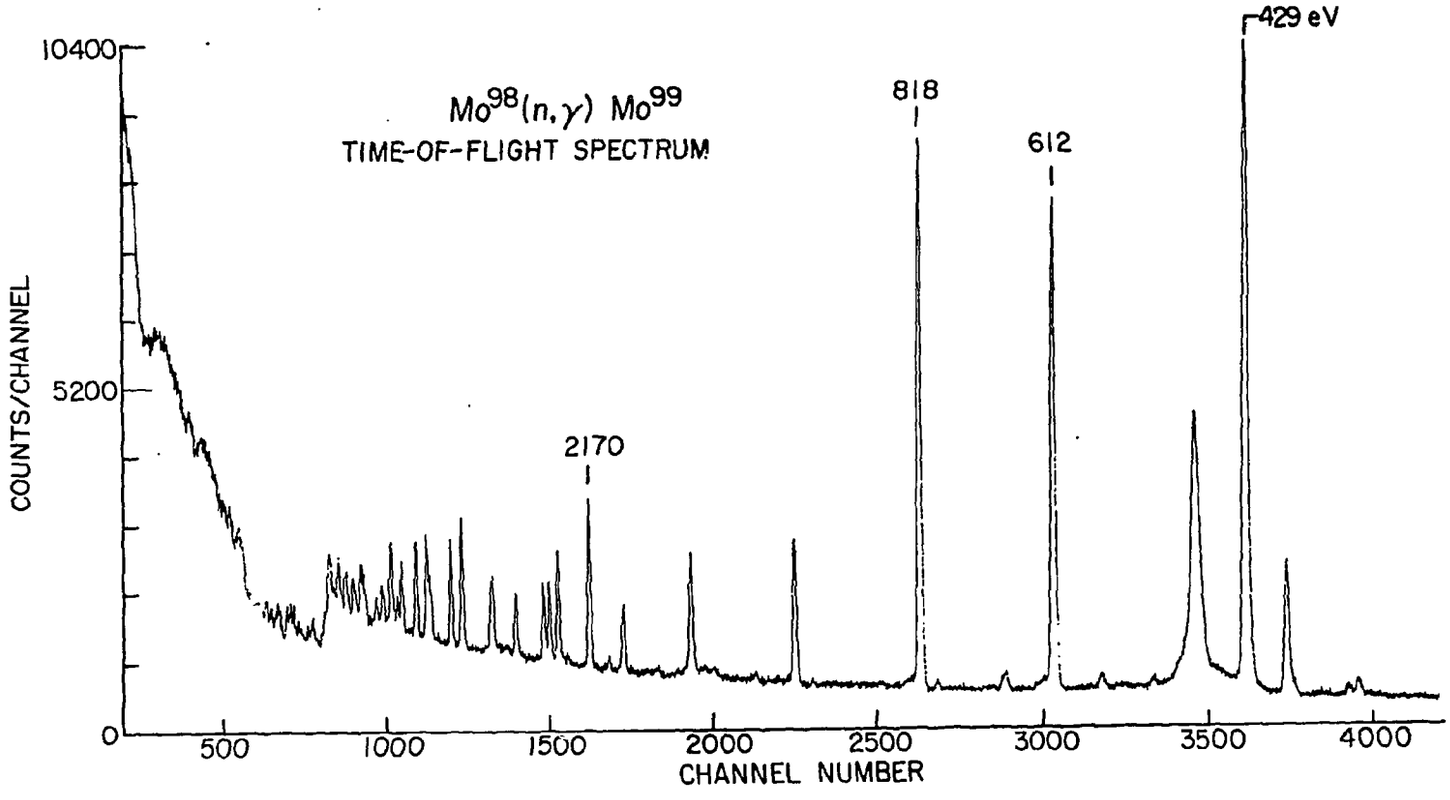
$Mo^{98}(n,\gamma)\ Mo^{99}$
TIME-OF-FLIGHT SPECTRUM
429 eV
818
612
2170
10400
5200
0
COUNTS/CHANNEL
500
1000
1500
2000
2500
3000
3500
4000
CHANNEL NUMBER

Figure A-3

E_n (eV)	ℓ_j	I_γ (a) 1/2+ℓ=0 5926.9	5/2+ℓ=2 5829.4	3/2+ℓ=2 5575.9	1/2+ℓ=0 5400.9	3/2+ℓ=2 5379.1	5/2+ℓ=2 5310.9	$\gamma^2_{\lambda n}$ (b) (eV)
12	p 3/2	24.9± 1.5	3.4± 1.2	12.4± 1.5		31.1± 1.8		122.6
401	p 3/2	23.8± 5.2	66.1± 9.3	23.5± 5.4	0 ± 4.4	6.5± 4.6	22.5± 5.2	35.0
429	p 1/2	210.0± 5.0	0 ± 1.8	144.0± 3.0	20.3± 2.0	91.8± 2.5	0 ± 1.5	1326.1
467	s 1/2	14.6± 2.8	0 ± 1.6	43.5± 2.6				
612	p 1/2	204.0± 5.0	2.0± 2.2	119.0± 4.0	8.5± 2.3	57.1± 3.0	0 ± 2.0	755.3
818	p 3/2	125.0± 4.0	0 ± 2.0	15.2± 2.2	0 ± 2.2	5.9± 2.3	6.7± 2.2	601.9
1122	p 3/2	28.2± 5.4	0 ± 6.1	26.2± 6.1		4.8± 5.4	41.8± 6.8	52.0
1528	s 1/2	20.1± 6.5	0 ± 5.6	47.6±13.3	33.4± 7.7	9.0± 6.4	0 ± 6.4	
1920	p 3/2	4.0± 8.7	0 ±11.0	15.1± 9.5	30.1±11.9	0 ±12.0	49.9±12.7	24.4
2170	p 1/2	51.9± 7.3	4.4± 5.5	0 ± 5.5	18.6± 6.2	38.0± 7.3	8.4± 5.8	[248]
2460		34.4± 9.5	0 ± 8.1	57.9±11.0	6.6± 9.5	11.7±10.3	11.7±10.3	
2546	s 1/2	13.6±11.0						
2623	p(3/2)	50.6±12.5	17.1± 9.3	6.2±10.9		71.7±14.8		
2950	p(1/2)	143.0±21.0		71.2±16.8	46.6±18.1			[58]
3260	p(1/2)	97.7±15.8		0 ±12.6				[47]
3290	s(1/2)	48.9±22.4						
3792	p(1/2)	178.0±12.6	0 ± 7.8			16.5± 8.3	12.1± 8.3	
4013	p 3/2	21.6± 9.9	113.7±14.0	29.7± 9.3			35.6± 9.9	[385]
4471	s 1/2							
4571	p(1/2)	149.0±33.0		3.3± 9.9	108.2±15.2		7.3± 9.9	309.3
4842	p 3/2	69.4±13.6	82.3±12.9	17.2±10.0				269.4
Valence Model								
	p 1/2	1.0	0.0	0.14	0.05	0.47	0.0	
	p 3/2	1.0	0.27	0.02	0.06	0.05	0.02	

(a) = photons/1000 captures
(b) = $g\Gamma_n$ from ref.
[ ] = assuming Γ_γ = 150 meV

TABLE A-2. Mo-98 γ-Ray Intensities (Normalized to 429 and 612 eV resonances, in BNL work)

Experiments on the Mo-92 sample, of approximately 200 grams, have just been completed. About 300 hours of beam time at a repetition rate of 800/sec and an average power of 26-28 kW in a 30 ns burst have been recorded. The data have been obtained with a 37 cc detector and the analysis is now under way.

3. Search for non-statistical effects in resonance neutron capture in $Er^{167}(n,\gamma)Er^{168}$

The usual statistical treatment of radiative neutron capture assumes that all decay widths of the nuclear states above the neutron binding energy are statistically independent. This assumption is violated in the product nuclei Yb^{174} and Dy^{164} for which significant correlations are observed[3,4] between partial radiative widths and reduced neutron widths of the resonances. These results motivated us to investigate the neighboring target nucleus Er^{167}. Using the fast chopper facility at Brookhaven, the γ-ray spectra from 16 resolved resonances were obtained with a 50 cc Ge(Li) detector. Fig. A-4 shows the time-of-flight spectrum. The spins of the resonances were determined using both the high and low energy γ rays. The relative intensities of 9 γ rays with energies exceeding 5800 keV were analyzed for each resonance. In Fig. A-5 the high energy region of the γ-ray spectrum is shown. The 6228 keV γ-ray peak was consistently wider in most resonances which suggests that this peak contains more than one component as was proposed by Bollinger and Thomas.[7] The correlation coefficient between each γ ray and the reduced neutron width of the corresponding resonance was determined for both groups of resonance spins. No statistically significant departures from zero correlation are observed for either spin group. In particular γ ray widths feeding the 2 neutron quasi-particle states at 1094 and 1542 keV which are formed from a superposition of the Nilsson orbitals 7/2+[633] and 1/2-[521], show no correlation. These states would be expected to show correlations if valency neutron transitions were important. This lack of correlation suggests that radiative neutron capture in Er^{167} is in accord with the predictions of the statistical model.

4. Further tests of the valency neutron model in S- and P-wave neutron capture

Measurements of radiative capture in P-wave resonances of $Sn^{116,118,124}$, and in S-wave resonances of Sn^{117} and $Mo^{92,96,98,100}$ have been made at the HFBR Fast Chopper in order to provide further experimental tests of the valence neutron model.[5] Predictions of the model have also been compared with the (γ,n) data of Jackson and Strait[8] near the 3-S giant resonance.

---

[7] L. M. Bollinger and G. E. Thomas, Phys. Rev. C2, 1951 (1970).

[8] H. E. Jackson and E. N. Strait, private communication.

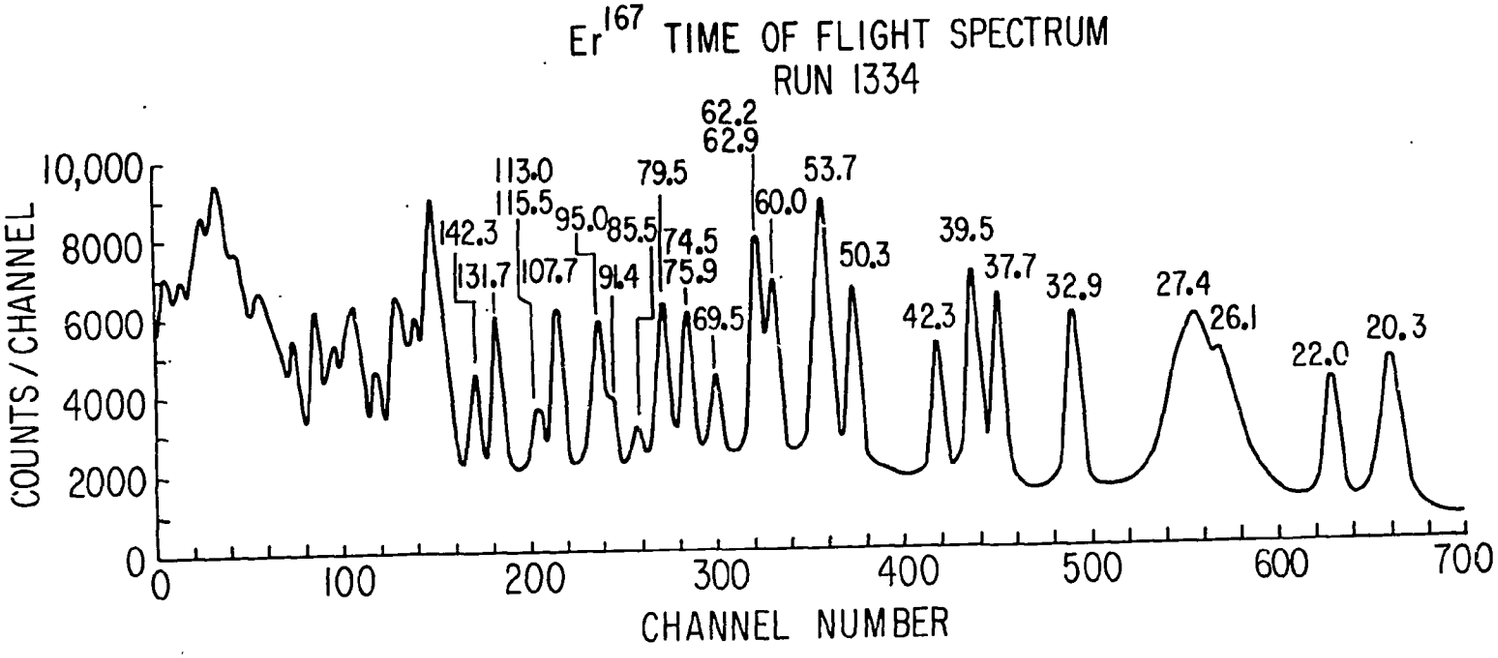
Er167 TIME OF FLIGHT SPECTRUM
RUN 1334
COUNTS / CHANNEL
CHANNEL NUMBER
10,000
8000
6000
4000
2000
0
0
100
200
300
400
500
600
700
142.3
131.7
113.0
115.5
107.7
95.0
91.4
85.5
79.5
74.5
75.9
69.5
62.2
62.9
60.0
53.7
50.3
42.3
39.5
37.7
32.9
27.4
26.1
22.0
20.3

Figure A-4

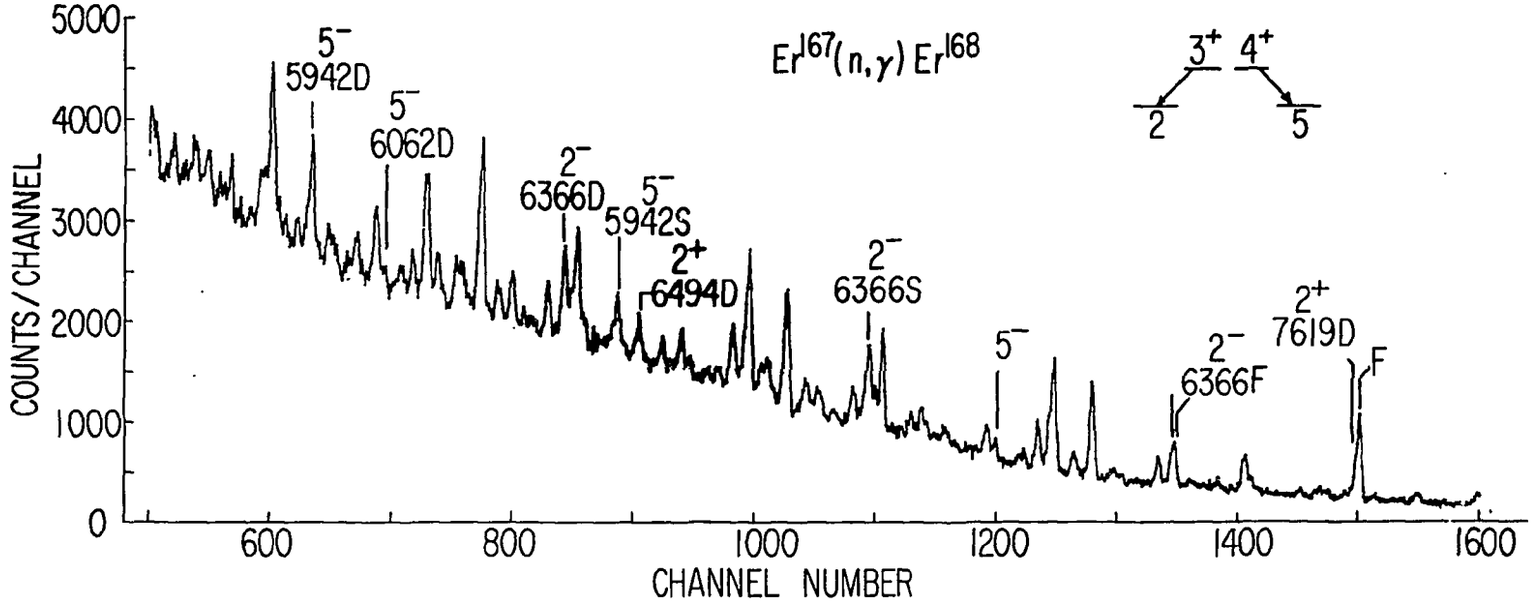
Er167(n,γ) Er168
3+ 4+
2 5
5−
5942D
5−
6062D
2−
6366D
5−
5942S
2+
6494D
2−
6366S
5−
2−
6366F
2+
7619D
F
COUNTS/CHANNEL
5000
4000
3000
2000
1000
0
600
800
1000
1200
1400
1600
CHANNEL NUMBER

Figure A-5

For the tin isotopes, partial radiative widths were determined by a calibration using the 7914 keV transition in the 11.9 eV resonance of Pt^{195}. This transition was assumed to have a width of 80 meV. The spin of the 148 eV P-wave resonance in Sn^{116} was determined to be 3/2 by angular correlation measurements carried out at the Fast Chopper. The spins of the other resonances are known. Table A-3 compares the measured radiative widths with theoretical values computed using the valence model. The measured widths were extracted using the resonance parameters of Julien[9] and BNL-325[10]; both results are included in the table.

In the case of Sn^{118} the ratio of γ-ray intensities does not agree with the model. In Sn^{124} (transitions p 1/2 → d 3/2 and p 1/2 → s 1/2) the agreement is better. Reasonable agreement is also obtained for Sn^{116} (p 3/2 → s 1/2).

One of the least understood problems in neutron capture investigations is M-1 strengths, particularly in the region near A=100. In the case of Sn^{117}, an M-1 transition at 8095 keV with a partial radiative width of 10.0 meV is observed in the 38.8 eV S-wave resonance ($J^{\pi} = 1^{+}$). However, M-1 transitions from an $\ell = 0$ initial state to an $\ell = 2$ final state are forbidden in the valence neutron model. The Fast Chopper measurements in the S-wave resonances of the molybdenum isotopes show some additional deviations from the model. Following capture in the 3170 eV resonance of Mo^{92} the partial width feeding the first excited state of Mo^{93} (E_x = 941.5 keV, s 1/2) is 68.8 meV. In the 467 eV S-wave resonance of Mo^{98} + n, the ground state of Mo^{99} (s 1/2) has a partial radiative width of 4 ± 1 meV. Calculations in the framework of the valence neutron model show that single particle effects cannot account for these values.

In order to test the validity of the valence neutron model near the 3-S giant resonance, calculations of ground state radiative widths $\Gamma_{\gamma 0}$ have been carried out for resonances in the compound nuclei Cr^{52}, Ni^{60} and Fe^{56}. These values are compared in Table A-4 with the results derived from the (γ,n) measurements of Jackson and Strait.[8] In each nucleus good agreement is found for the first resonance, but for higher energy resonances theory and experiment do not agree.

---

[9] Julien et al., Nucl. Phys. A132, 129 (1969).

[10] M. D. Goldberg et al., BNL-325, 2nd Ed. Supp. No. 2 (1966).

Table A-3

P-Wave Resonances in Tin*

Sn-124 E_R = 62 eV				Sn-116 148 eV				Sn-118 46 eV			
E_γ(keV)	Ref.10	Ref.9	Theory	E_γ(keV)	Ref.10	Ref.9	Theory	E_γ(keV)	Ref.10	Ref.9	Theory
5701	56.0	137.0	61.0	6949	37.0	11.0	10.0	6484	20.0		8.3
5512	25.0	61.0	42.0	6791	~0	~0	0.7	6461	33.0		0.9

* widths in meV

Table A-4

Comparison of Measured and Predicted Values of $\Gamma_{\gamma 0}$**

Cr 52			Ni 60			Fe 56		
E_R(keV)	Ref. 8	Valency Model	E_R(keV)	Ref. 8	Valency Model	E_R(keV)	Ref. 8	Valency Model
50.2	0.179	0.198	12.47	0.367	0.390	27.9	0.112	0.127
97.1	1.275	0.635	28.64	---	0.077	74.0	0.082	0.021
123.2	0.930	0.040	43.08	0.018	0.006	83.7	---	0.046
141.4	---	0.506	65.13	---	0.025	123.5	0.119	0.006
239.4	1.315	0.052	86.8	---	0.018	130.0	0.105	0.018
285.4	---	0.029	98.1	0.102	0.045	141.0	0.068	0.081
331.1	0.184	0.296	107.8	0.209	0.030	169.0	0.066	0.022
			156.4	---	0.018	188.0	0.423	0.096
			162.1	0.166	0.051	220.0	0.683	0.037
			186.5	0.062	0.227			
			198.0	0.557	0.114			

** widths in eV

5. Spin assignments in $Sn^{122}(n,\gamma)$ from angular distribution measurements

The $Sn^{122}(n,\gamma)$ reaction has been studied at the 48m flight path of the Fast Chopper facility. Assuming an energy of 24 keV for the first excited state in Sn^{123}, a neutron binding energy of 5948 ± 2 keV is obtained. The 5924 keV γ-ray (d 3/2 final state) and the 5798 keV γ-ray (s 1/2 final state) were observed at reaction angles of 90° and 135°. The anisotropy of these transitions in the 106.9 eV resonance identifies it as a P-wave resonance with spin 3/2. The same two transitions show an isotropic distribution in the 259.9 eV resonance. The parity of this resonance is uncertain; if it is a P-wave resonance, however, its spin is 1/2.

6. Resonance spin assignments and identification of capture γ-rays in $U^{235}(n,\gamma)$

The spins of seven resonances in the reaction $U^{235}(n,\gamma)U^{236}$ have been determined and a partial level scheme has been constructed for U^{236} on the basis of extensive experiments carried out at the Fast Chopper. Resonance capture γ-rays and prompt fission γ-rays were separated from γ-rays due to delayed decay of fission products and natural target activity by comparison of spectra obtained on-resonance and off-resonance. Further distinction between capture and prompt fission γ-rays was made in measurements using a 4π neutron detector operated in coincidence with a GeLi detector. The coincidence resolving time was 140 nsec. The apparatus for detection of fission events has been described in previous NCSAC reports.

Fig. A-6 shows the time-of-flight spectrum of the low energy resonances, obtained at the 22 m flight path. Resonances up to 33 eV were studied in data obtained at 48 m. Fig. A-7 shows an on-resonance spectrum, together with an off-resonance spectrum which should contain only delayed fission γ-rays and γ-rays due to target activity. These spectra were obtained with a 40 cc GeLi detector. Peaks 8 and 10 are due to capture in Al and Fe, while peak 22 is a delayed fission γ-ray. Peak A is the known 6396 keV capture line. For the high energy γ-ray spectra, the coincidence spectra obtained using the fission detector showed no discrete lines; the continuous spectrum obtained indicates that the prompt fission γ-rays are highly Doppler shifted. It is therefore certain that no high energy prompt fission lines have been wrongly assigned as capture γ-rays.

Transitions of 6396, 5588, 5546, 5487, 5417 and 5292 keV are assigned as capture γ-rays; they populate final states in U^{236} at excitations of 149, 957, 999, 1058, 1128 and 1253 keV. Fig. A-8 shows the high energy γ-ray spectrum of the 12.39 eV resonance. On the basis of the occurrence of the 5588 keV γ-ray, which populates a 2^{+} final state in

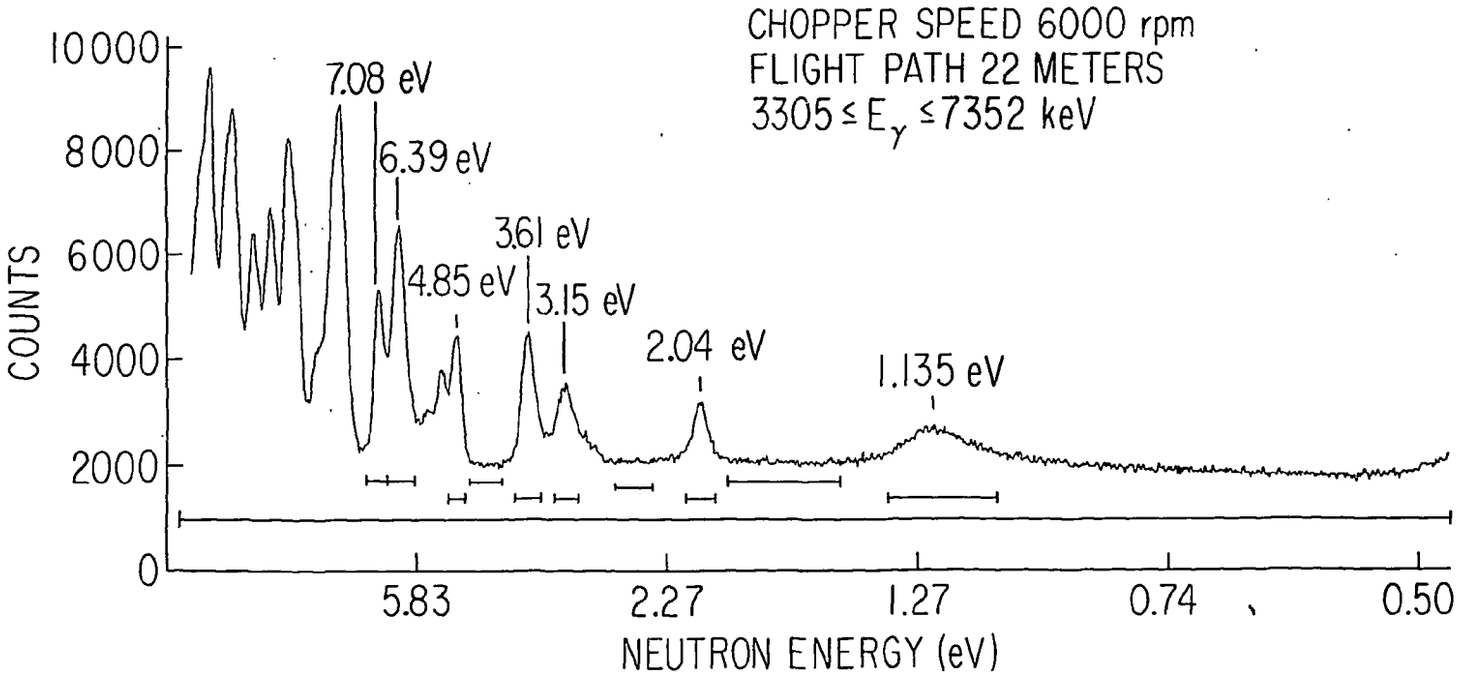

TIME-OF-FLIGHT SPECTRUM SHOWING 7 RESOLVED LOW ENERGY RESONANCES IN U-235.

Figure A-6

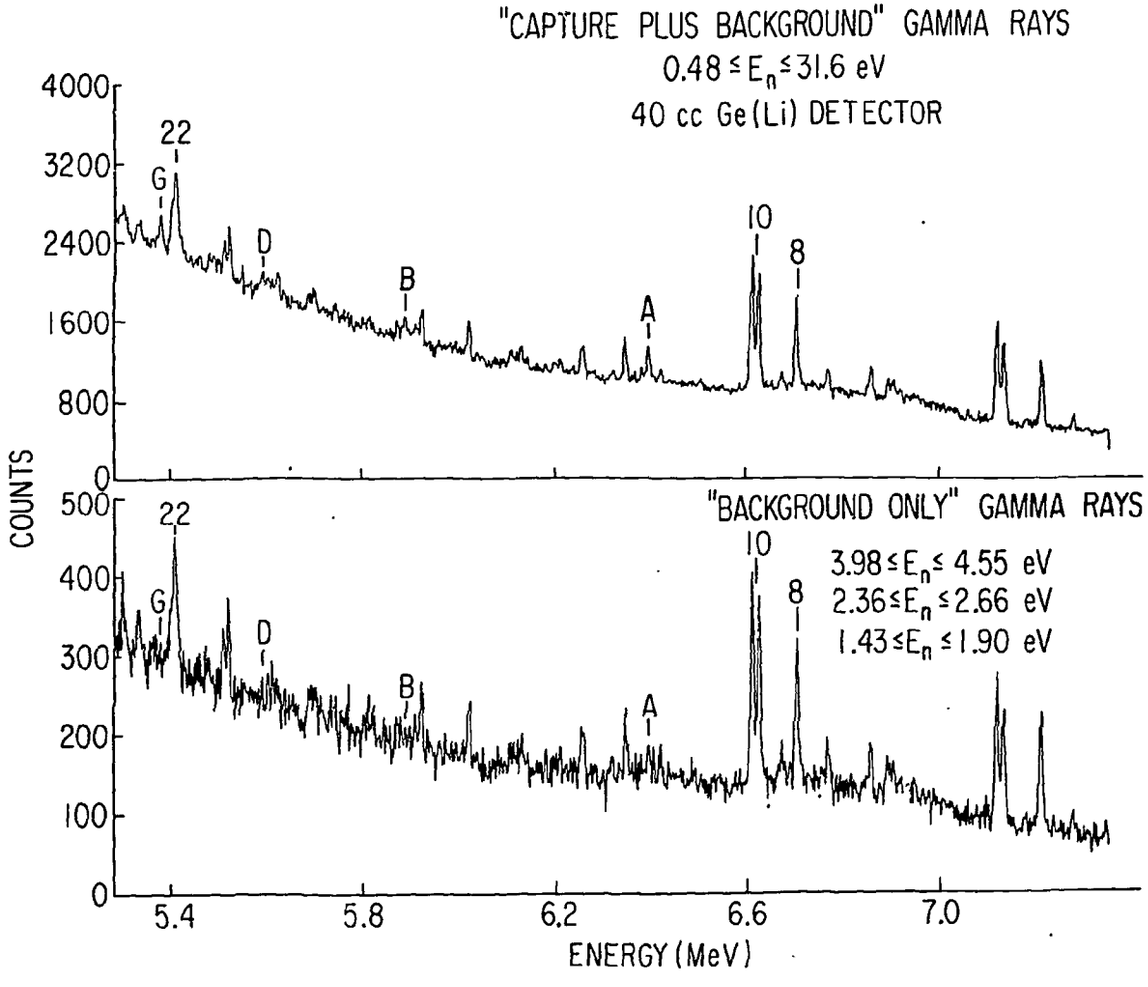

COMPARISON OF "CAPTURE + BACKGROUND" AND "BACKGROUND ONLY" SPECTRA.

Figure A-7

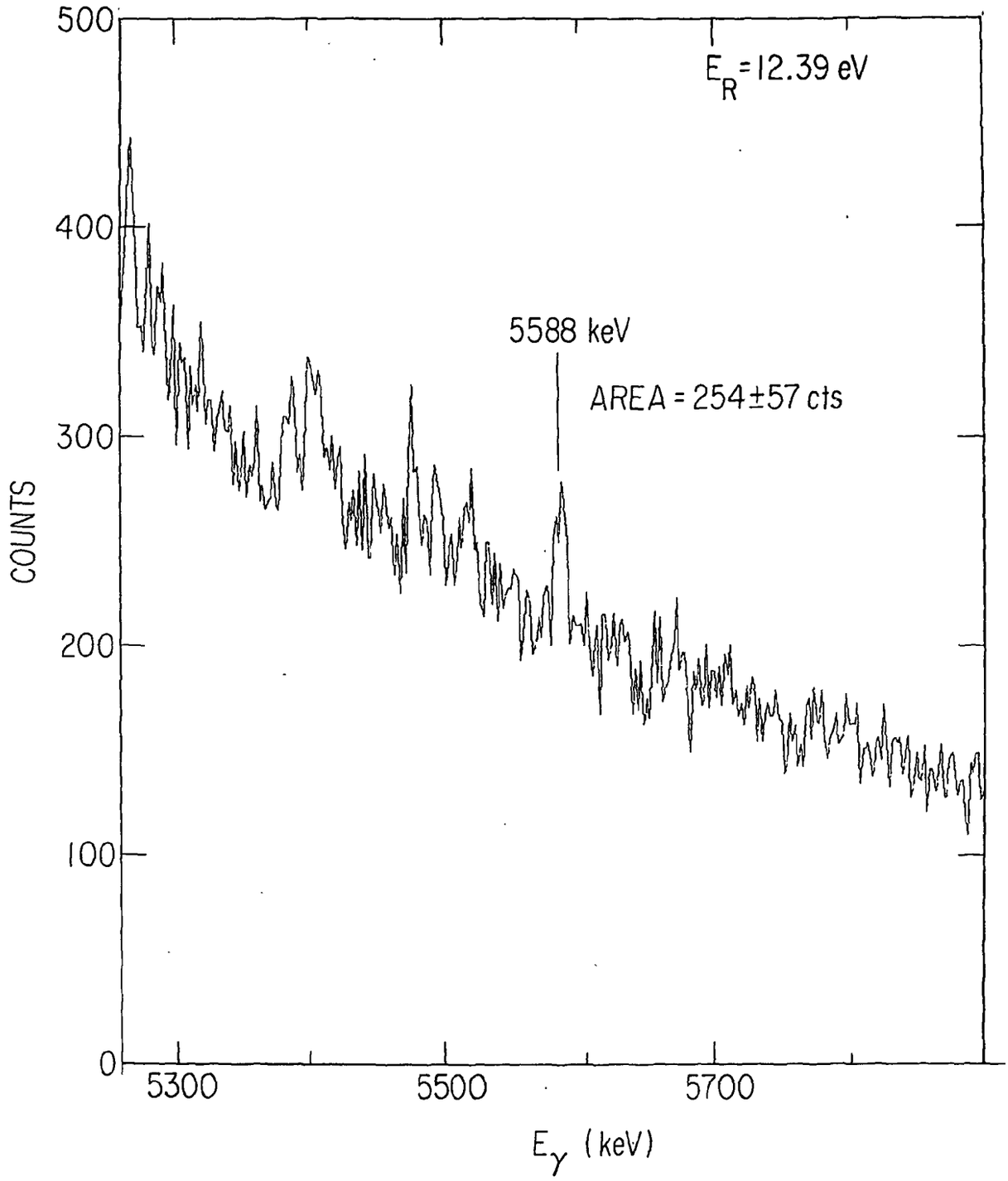

GAMMA RAY SPECTRUM FOR 12.39 eV RESONANCE.

Figure A-8

U^{236}, the resonances at 2.040, 6.39, 12.39, 14.53 and 32.05 eV are assigned as 3^-. The 3^- assignment for 2.040 eV resonance together with the work of Schermer et al.[11] gives assignments of 3^- and 4^- for the resonances at 0.290 and 1.14 eV, respectively.

Using recommended resonance parameters the above six 3^- resonances have an average fission width of 34 ± 23 compared with 48 ± 12 eV for all 51 3^- and 4^- resonances. Assuming that the distribution of fission widths for the 3^- resonances is chi-squared with two degrees of freedom and the distribution of fission widths for both the 3^- and the 4^- resonances is chi-squared with four degrees of freedom, then for the six resonances we have determined to be 3^- and the 51 resonances with recommended fission widths,

$$\langle \Gamma_f(J^\pi = 3^-)\rangle = (0.58\ ^{+0.48}_{-0.37})\ \langle \Gamma_f(J^\pi = 4^-)\rangle.$$

This is inconsistent with Lynn's prediction[12]

$$\langle \Gamma_f(J^\pi = 3^-)\rangle \approx 2\langle \Gamma_f(J^\pi = 4^-)\rangle$$

based on the Bohr theory[13] of fission using the presently known properties of the transition states.

Fig. A-9 shows a level scheme for U^{236} constructed on the basis of the high energy and low energy γ-rays observed in this work. The levels not populated by high energy γ-rays seen in this work were taken from reference 14. On the basis of level systematics in even uranium isotopes, we propose that the 1128 keV level in U^{236} is most likely the 5^+ member of the K^π, $J^\pi = 2^+$, 2^+ γ-vibrational band.

---

[11] Schermer, Passell, Brunhart, Reynolds, Sailor and Shore, Phys. Rev. 167, 1121 (1968).

[12] J. E. Lynn, Proc. Conf. on Nuclear Data for Reactors, Paris (I.A.E.A., Vienna), 89 (1967).

[13] A. Bohr, Proc. Intl. Conf. on Peaceful Uses of Atomic Energy, Geneva, Vol. 2, 151 (1955).

[14] W. Kane. Phys. Rev. Letters 25, 953 (1970). C. M. Lederer, J. M. Hollander and I. Perlman, Table of Isotopes, 6th Ed., J. Wiley, New York (1968).

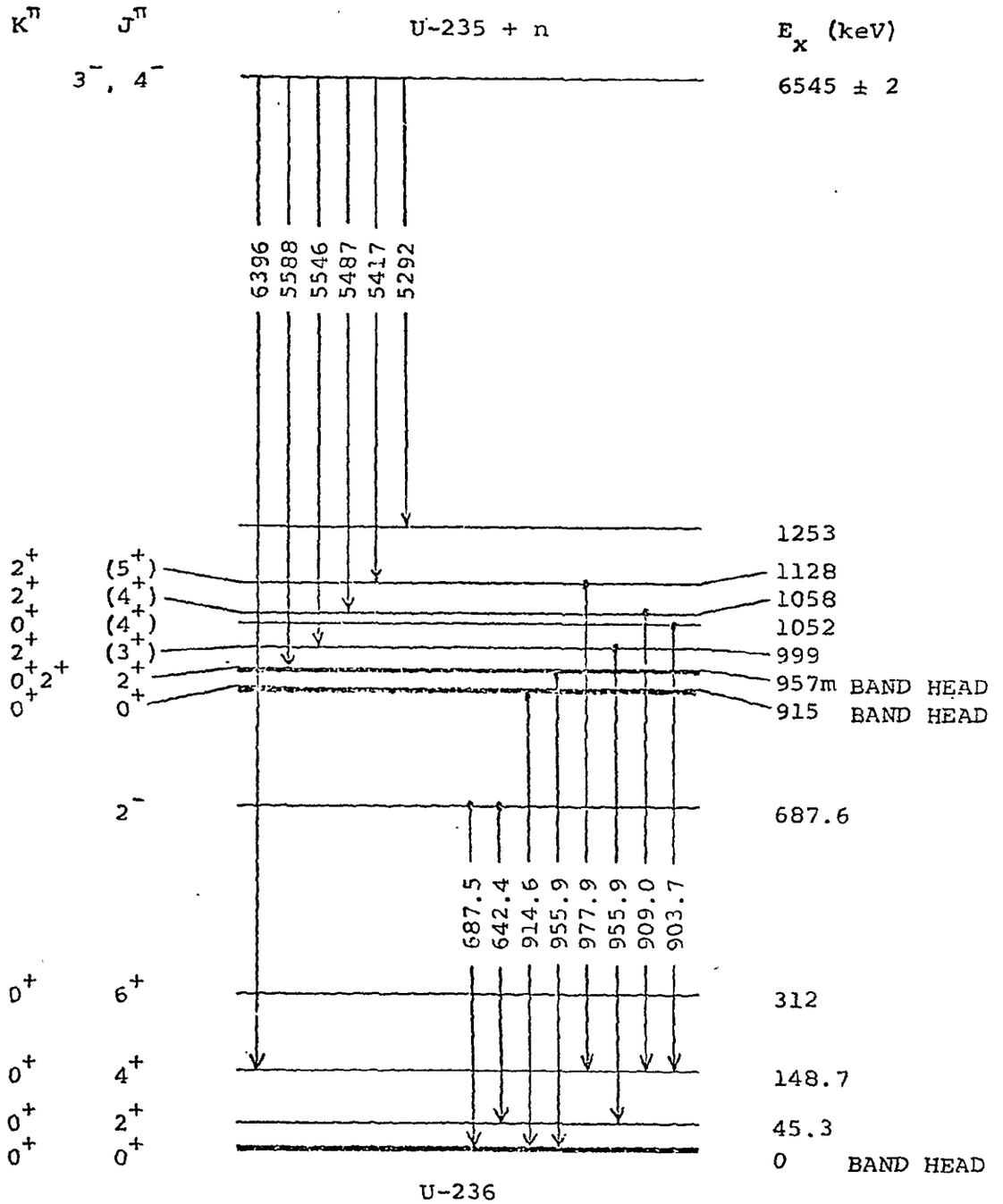

Figure A-9 LEVEL DIAGRAM OF U-236.

7. Determination of Boron density profiles in solids by the $B^{10}(n,\alpha)$ reaction. G. W. Cole, with J. F. Ziegler* and J. E. E. Baglin**

The distribution of impurities in semiconductors has been a problem of considerable interest in the study of semiconductor devices. Even in the case of single impurities diffused into semiconductors, the profiles obtained differ from the expected complementary error function at concentrations of 10^{19} cm^{-3} or greater (ref. 15, and references therein). When two impurities are diffused into the semiconductor, diffusion profiles have normally been calculated by superposition of the distributions. Hu and Schmidt[15] attempted a more complete calculation of profiles resulting from sequential diffusion processes, including the electrical interaction between the two impurities. They find that the second diffusant can be expected to cause a significant rearrangement in the initial impurity profile.

Understanding of the diffusion process in semiconductors has been hampered by the lack of any reliable technique for measuring the profiles of the impurities. Experiments carried out at the B-beam of the H-1 beam port of HFBR have for the first time yielded an accurate determination of boron density profiles in silicon. The high cross section of the $B^{10}(n,\alpha)$ reaction (3700 b at thermal) is exploited. A one inch diameter beam of $\sim 5 \times 10^8$ cm^{-2}-sec^{-1} thermal neutrons irradiates a thin silicon wafer containing boron and other impurities; a silicon surface barrier detector detects the α-particles and the Li^7 nuclei produced in the $B^{10}(n,\alpha)$ reaction. The energy of a detected particle is a direct indication of the depth at which it was produced in the silicon. Branching to the 479 keV state of Li^7 accounts for 94% of the reaction, and the 1470 keV α-particles thus produced are the most suitable for analysis. The energy loss of a 1470 keV α-particle in silicon is ~ 250 keV $-\mu^{-1}$; the experimental resolution of 20 keV therefore implies an approximate depth resolution of 8×10^{-6} cm in the density profile.

Initial tests in October were made using a silicon wafer which had been ion-implanted with separated B^{10} at an energy of 500 keV. The concentration of B^{10} was 5×10^{15} cm^{-2}. This run demonstrated the feasibility of the technique.

Measurements have just been completed on a series of silicon targets produced under varying conditions. While no analysis of

---

* IBM Thomas J. Watson Research Center, Yorktown Heights, N.Y.

** Iowa State University, Ames, Iowa.

15 S. M. Hu and S. Schmidt, J. Applied Phys. 39, 4272 (1968).

the results has been completed, visual inspection of the raw data allows two conclusions:

1) by comparison of boron-diffused wafers, one of which had been subjected to further high-temperature processing and one of which had not, it is clear that the later steps in processing cause boron near the surface of the silicon to diffuse out of the crystal.

2) by comparison of boron-diffused wafers, one of which had later been treated with a diffusion of arsenic (as in transistor fabrication), we observed for the first time a rearrangement of the boron due to the arsenic which was even larger than the effect predicted in ref. 15.

The measurement of such effects in sequential diffusion processes should lead to much improved understanding of semiconductor devices, and of diffusion processes in solids.

The H-1 beam port was made available through the cooperation of D. C. Rorer and H. L. Foote.

2. Nuclear Cryogenics

Magnetic moments of compound states corresponding to slow neutron cross section resonances (D. C. Rorer)

Slow neutron capture by heavy non-fissile nuclei leads to short-lived, highly excited compound states ($\tau \simeq 10^{-14}$ sec). The short lifetime precludes measurement of the magnetic moment of these compound states by the usual techniques of spin precession or perturbed angular correlations. We have attempted to measure the magnetic moment by observation of the shift in the resonance energy of the compound state in a magnetic field,

$$\Delta E = \mu H.$$

Straightforward neutron transmission measurements would not be able to detect this shift, since even for a field of 10^7 Oe and $\mu = 1$ nuclear magneton, $\Delta E = 3 \times 10^{-4}$ eV, which is too small to be seen above the total linewidth $\Gamma \simeq 0.1$ eV. However, as pointed out by Shapiro,[15] measurement of the transmission effect using polarized neutrons can lead to an observable result. The transmission effect is

$$\epsilon = \frac{T_P - T_A}{T_P + T_A}, \text{ where } T_{P(A)} =$$

the transmission with neutron spins parallel (anti-parallel) to the magnetic field, H. The transmission effect will show an asymmetric behavior as one sweeps through the resonance energy, with

$$\epsilon_{max} - \epsilon_{min} = 2.6 \times N\sigma_o \frac{\Delta E}{\Gamma}$$

This difference can very well approach the order of 1%.

Earlier measurements by our group[16] on Er^{168} indicated an unexpectedly large value of μ (= 5.9 μ_N) for the resonance at 0.584 eV. Erbium and dysprosium were chosen for these measurements because of their

---

[15] F. L. Shapiro, in Proceedings of the Panel on Research Applications of Nuclear Pulsed Systems (International Atomic Energy Agency, Vienna, 1967), p. 176.

[16] K. H. Beckurts and G. Brunhart, Phys. Rev. C, 1, 726 (1970).

large magnetic fields (5-7 x 10^6 Oe) at low temperatures and their relatively low-lying resonance energies (.584 and 1.71 eV). Several other rare earths may also be good candidates for the application of this method.

3. Nuclear Structure

a) The intensities of high energy gamma rays from neutron capture in Au^{197} (W. R. Kane)

The partial widths of individual high energy transitions from the capture of neutrons in Au^{197} with energies from thermal energy up to the 4.906 eV resonance have been remeasured. This work was stimulated by the publication of results from Saclay which were cited as evidence for direct capture in this nucleus. The measurements were carried out at the crystal diffraction monochromator at the Brookhaven HFBR. This equipment is well suited for this purpose, since for a target such as Au^{197}, the high energy capture gamma rays can be measured with the beam on, and then the decay gamma rays can be measured with the beam off, providing a reliable and accurate determination of the intensities of the capture gamma rays. While several transitions were found to exhibit an increase in intensity with decreasing neutron energy, this effect is not believed to be evidence for direct capture, but rather, it arises from the existence of a negative energy resonance, as proposed in earlier work of the Brookhaven Fast Chopper Group. The absolute intensities of the high energy capture gamma rays were found to be considerably higher ($\sim$ 35 percent) than previously assumed on the basis of thermal neutron capture data from the Kurchatov Institute. Since these gamma rays are frequently employed for comparison in determining gamma-ray intensities in other elements, the intensities of the highest energy transitions are given in Table A-5 for neutron capture at thermal energy and at 4.906 eV.

b) Gamma rays from resonance neutron capture in Pu^{242} (W. R. Kane)

While the thermal neutron capture cross section of Pu^{242} is moderate ($\sim$ 18b), a resonance at 2.66 eV has a very large cross section ($\sim$ 66,000 b). This property has been taken advantage of in studies of the level structure of Pu^{243} in the $Pu^{242}(n,\gamma)$ reaction. At the crystal diffraction monochromator at the HFBR Ge(Li) gamma-ray spectra have been obtained and Ge-Ge coincidence measurements made for neutron capture on this resonance. A preliminary analysis of the data has revealed the existence of 13 low spin levels in Pu^{243} below 1.2 MeV excitation energy. With the aid of existing results on the $Pu^{242}(d,p)Pu^{243}$ reaction it should be possible to characterize all single particle excitations in Pu^{243} up to an energy of several MeV.

Table A-5

Intensities of High Energy Capture Gamma Rays of Gold

E_γ (keV)	I(photons/1000 events)	
	Thermal Energy	4.906 eV
6513	17.2	15.6
6457	23.5	26.5
6320	36.1	28.2
6276	12.0	12.6
6264	2.5	1.5
6252	59.5	55.0
6165	1.8	0.2
6149, 6145	12.5	8.7
6106	5.9	9.8

c) Level structure of Tc^{100} from studies of the $Tc^{99}(n,\gamma)$ and $Mo^{100}(p,n)$ reaction (S. Cochavi and W. R. Kane)

The gamma rays from both thermal and resonance neutron capture in Tc^{99} have been investigated. In addition, this information has been supplemented in studies of the gamma rays from the $Mo^{100}(p,n)Tc^{100}$ reaction at the Brookhaven Tandem Van de Graaff accelerator. Detailed information on excited states of Tc^{100} has been accumulated.

d) Higher excited states of Hf^{179} and W^{183} (R. Casten and W. R. Kane)

Recent studies of the (d,p) reaction have yielded considerable new information and raised certain questions concerning energy levels in odd hafnium and tungsten isotopes with excitation energies between ~ 1 and ~ 2.5 MeV. Preliminary measurements on transitions excited in these nuclei by resonance neutron capture indicate that the properties of a number of energy levels in this region can be elucidated by neutron capture studies.

B. NATIONAL NEUTRON CROSS SECTION CENTER (S. Pearlstein, M. D. Goldberg, M. K. Drake, D. E. Cullen, R. R. Kinsey, T. J. Krieger, J. R. Stehn, M. R. Bhat, D. I. Garber, B. A. Magurno, V. May, S. F. Mughabghab, O. Ozer, A. Prince, H. Takahashi)

Procedures for correcting the computerized experimental data library, CSISRS, have been developed. New data are fairly well screened through its use of "Author proofs". Older data are presently being scanned for errors using graphical and other automated techniques that include a rough comparison of data with limits based on BNL-325 eye guides.

A preliminary third version of the Evaluated Nuclear Data File (ENDF/B-III) has been distributed to the Cross Section Evaluating Working Group. It contains 50% more evaluations than ENDF/B-II largely due to the inclusion of files for individual fission product nuclides. The new library also contains photon production and interaction data for several nuclides. The neutron data has been processed through a preliminary version of PSYCHE, a physics checking code. A review of these preliminary data and the approval of data for wide distribution will take place at a CSEWG meeting December 1-2, 1971.

A meeting of the heads of U. S. Centers active in compiling low energy physics data took place at Brookhaven National Laboratory on September 23-24, 1971. Represented were the Nuclear Data Project, Table

of Isotopes, Energy Levels of Light Nuclei, Chart of the Nuclides, Charged Particle Information Center, Photonuclear Data Center, Gamma Ray Spectrum Catalogue, and the National Neutron Cross Section Center. Plans are underway to exchange basic information among the Centers, develop a unified dialogue with Journals publishing nuclear data, and meet on a regular basis for the discussion of mutual problems.

The 7th 4-Center meeting took place at BNL October 25-27, 1971. There were two representatives from the USSR center at Obninsk, one from the IAEA center in Vienna, and two from the ENEA center at Saclay. Representatives from CINDA and the Nuclear Data Project were also present for part of the meeting. In addition to resolving operational problems connected with the exchange of experimental data, the group initiated an investigation of the adaptation of CINDA to also be an index to data available from the Centers as well as an index to the literature.

With the delivery of a random vector generator in August 1971, hardware was completed for the NNCSC interactive graphics system. The simultaneous display of experimental and evaluated data is now possible. Interactive tools similar to the AI-IBM SCORE system for the manipulation of data are being adapted or are under development.

COLUMBIA UNIVERSITY

I. NEUTRON SPECTROSCOPY

A. Neutron Resonance Cross Section Measurements (G. Hacken, F. Rahn, H. Liou, W. W. Havens, Jr., J. Rainwater, M. Slagowitz, S. Wynchank)

Since the last reporting period, the analysis of the data obtained from the 1968 series of experimental runs at the Nevis Cyclotron approached completion and attention has been focused on the analysis of the data from last year's experimental series. The 1970 data are at least as good as the 1968 data, with better equipment and improved operating conditions. The analysis is underway, but is not yet at the stage where many final results can be given. The measurements with our 200 meter and 40 meter detectors used several different sample thicknesses of each of the natural elements Na, Mg, Al, Cl (as CCl_4), K, Ca, Fe, Cu, Ne (gas), Se, Cd, Tm, Ta, Au, Tl, U, and Th. In addition, several thicknesses each of the following separated isotopes were studied: ^{110}Cd, ^{112}Cd, ^{114}Cd, ^{116}Cd, ^{203}Tl, ^{205}Tl, ^{140}Ce, ^{160}Dy, ^{161}Dy, ^{162}Dy, ^{163}Dy, ^{164}Dy, ^{238}U (depleted in ^{235}U), ^{158}Gd, and ^{160}Gd.

R matrix analysis for the lighter elements K, Ca, Cl, and Mg is being carried out by Mr. Singh at SUNY, Albany, as a Ph.D. thesis under the supervision of Prof. J. Garg. These elements can be analyzed to several hundred keV, with relatively large level spacings and Γ_n^0 values. Above ~10 keV, it is more difficult to unfold the sample and energy dependent background from our observed count histograms. Many additional measurements were made using "Standard Filter" methods to aid in this part of the analysis. The intensity and resolution of our spectrometer system is such that even for relatively poor samples our energy resolution is much better than other groups in the energy region below a few hundred keV.

The Nevis cyclotron modification program is nearing completion, with an initial test proton beam expected by the end of this year. After the modification program is complete, we expect to obtain ~550 MeV proton energy with a (time averaged) beam current of ~20μA. The system will have a 300 Hz repetition rate, with a new R.F. design and improved deflection of the protons into our Pb target. We expect that our new (time averaged) neutron intensity will increase by a factor of 20 by next year.

The work on the total cross section of natural iron at points of relative minima is complete and has been submitted for publication. Figure A-1 shows our new values, which represent our best experimental results to date. The knowledge of σ_T at the points presented in this figure is especially important, in that these energy regions represent

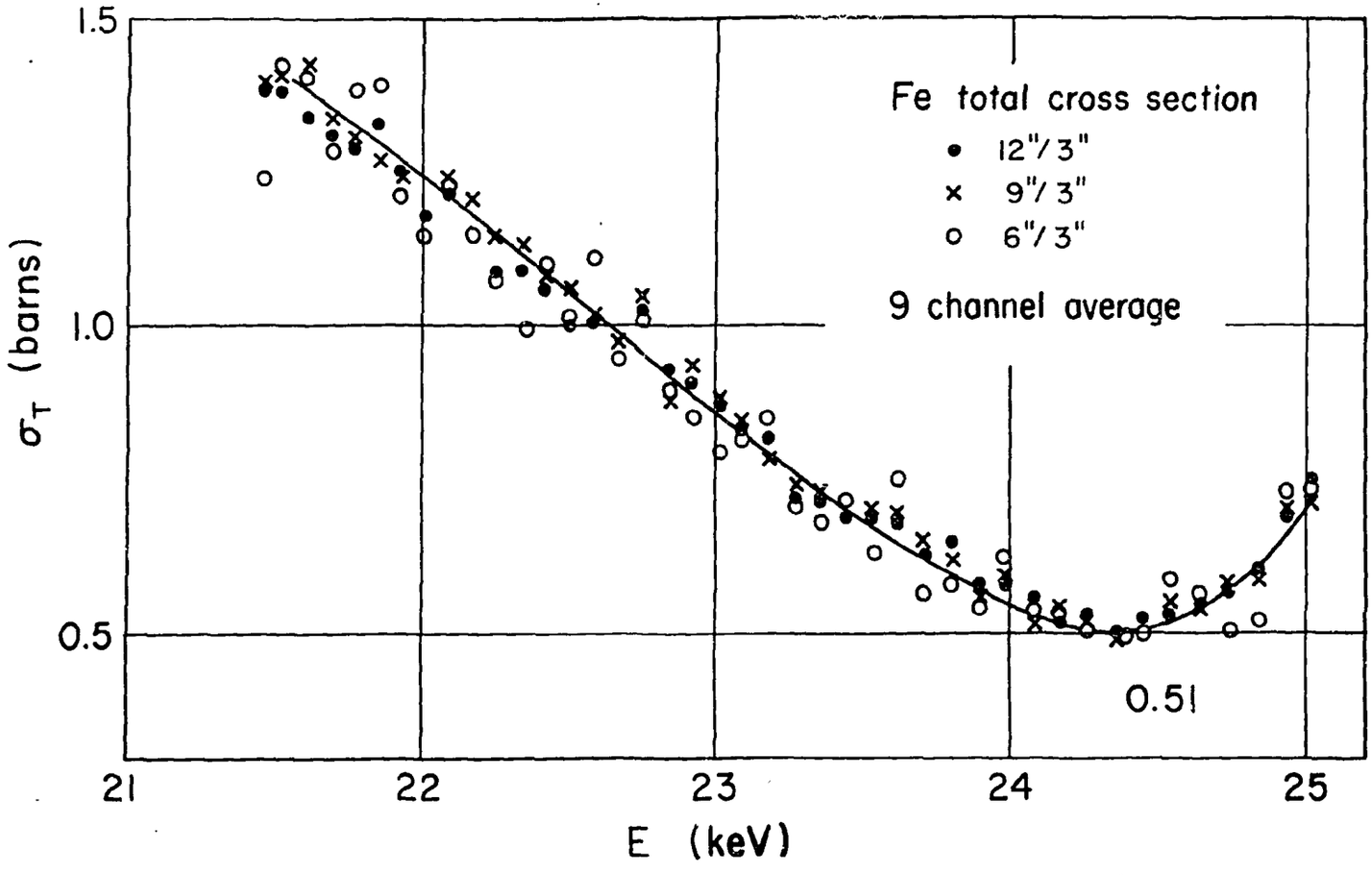

Figure A-1. The measured total neutron cross section for natural iron in selected energy regions. The σ_T shown in this figure is influenced by resolution effects (effective resolution of the experiment ≈ 0.6 nsec/meter). These resolution effects are greater where σ_T shows a rapid recovery from σ_{min} in terms of our timing channel widths.

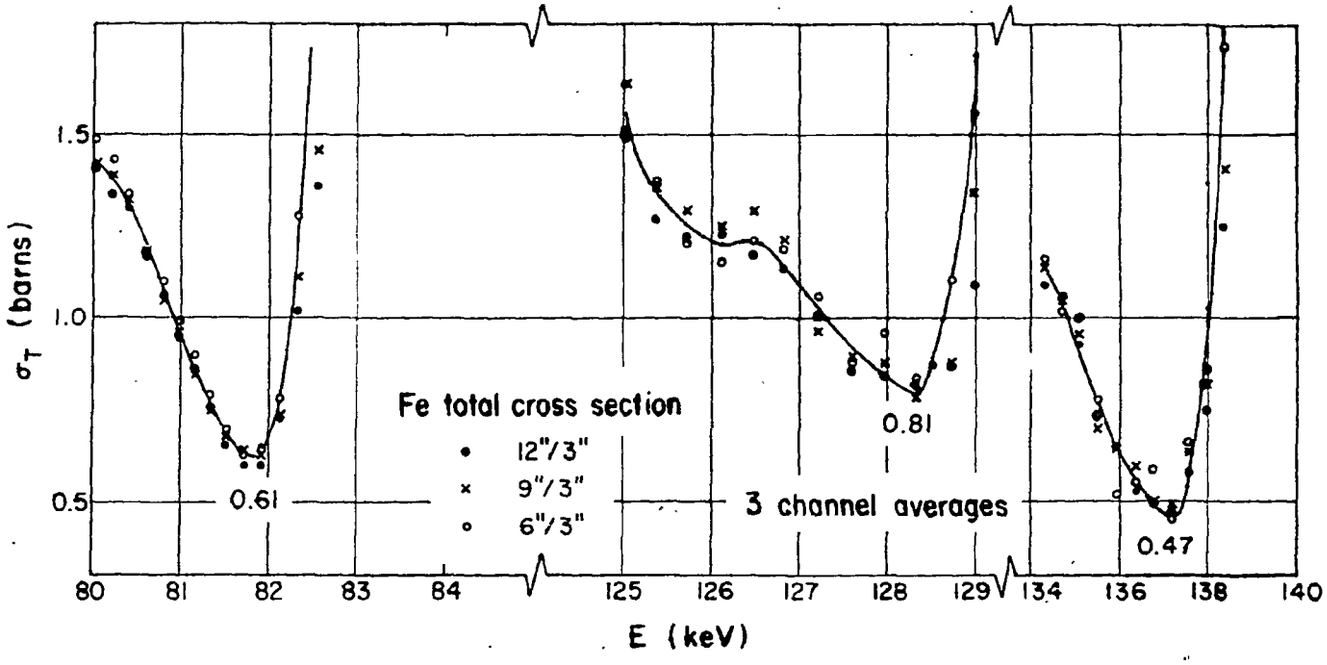

Figure A-1. The measured total neutron cross section for natural iron in selected energy regions. The σ_T *shown in this figure is influenced by resolution effects (effective resolution of the experiment* ≈ 0.6 nsec/meter). These resolution effects are greater where σ_T shows a rapid recovery from σ_{min} in terms of our timing channel widths.

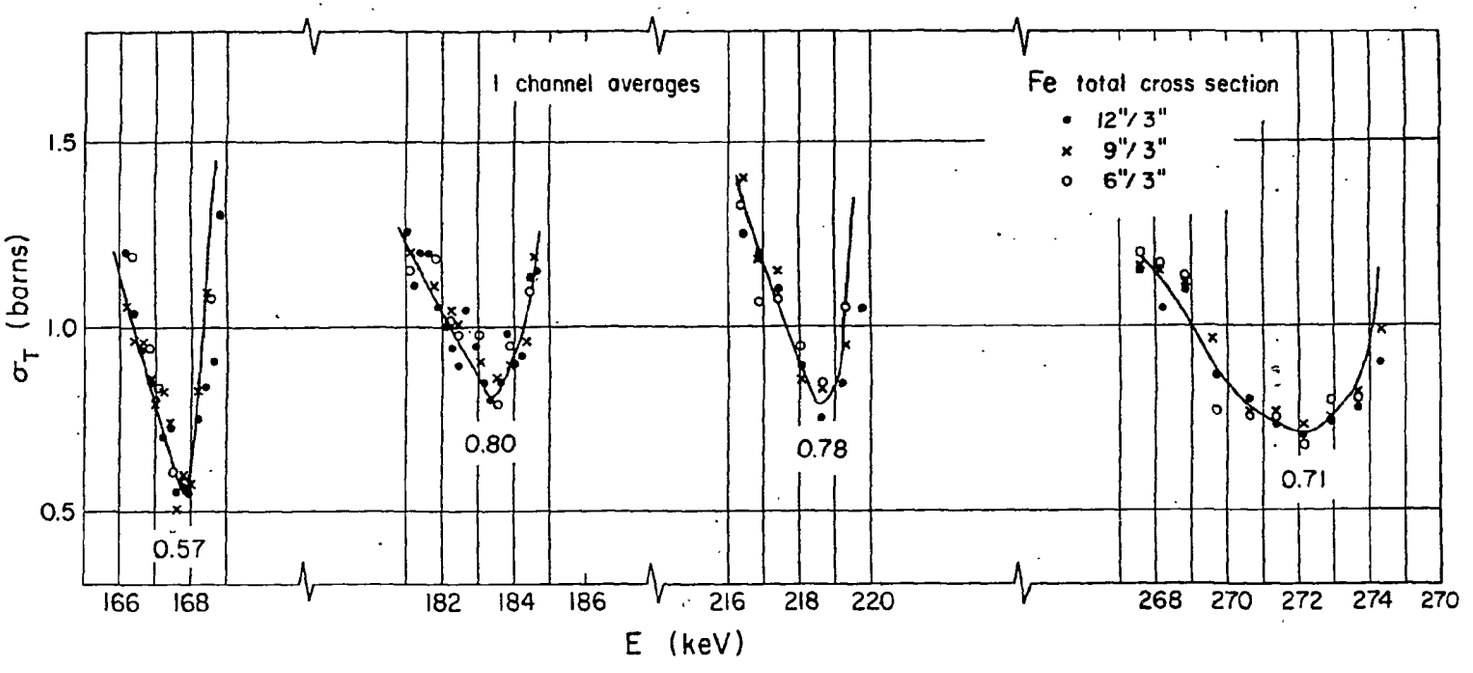

Figure A-1. The measured total neutron cross section for natural iron in selected energy regions. The σ_T shown in this fugure is influenced by resolution effects (effective resolution of the experiment ≈ 0.6 nsec/meter). These resolution effects are greater where σ_T shows a rapid recovery from σ_{min} in terms of our timing channel widths.

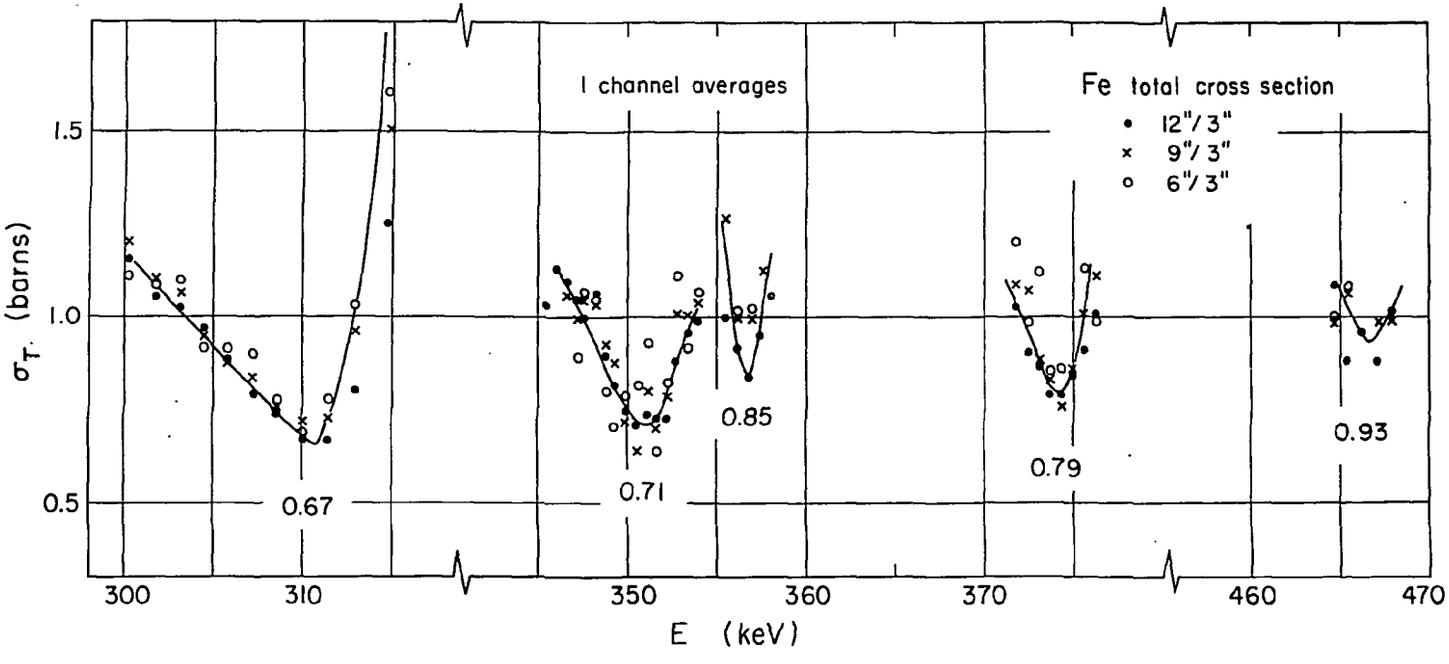

Figure A-1. The measured total neutron cross section for natural iron in selected energy regions. The σ_T shown in this figure is influenced by resolution effects (effective resolution of the experiment ≈ 0.6 nsec/meter). These resolution effects are greater where σ_T shows a rapid recovery from σ_{min} in terms of our timing channel widths.

"holes" in the total cross section which allow the transport and deep penetration of neutrons in several important applications, such as shielding and fast reactor design. Our results in Figure A-1 are lower than previous experimental results. The values of σ_T in this figure still do not represent our best experimental resolution, and we will redo our Fe measurements during our next experimental series.

From our 1968 high resolution data in the rare earth region 139<A<186, we have obtained final resonance parameters for ^{183}W, preliminary resonance parameters for ^{175}Lu, and these data are available on request. Preliminary results for the isotopes ^{154}Gd, ^{158}Gd, and ^{160}Gd. Gd results were obtained from the combined 1968 and 1970 sets of data on these isotopes. The analysis yielded values of the total radiation width $\langle\Gamma_\gamma\rangle$ in some favorable cases for the Lu and Gd isotopes. The average Γ_γ results are: $\langle\Gamma_\gamma\rangle$ = 100 meV (n=24) for ^{154}Gd, $\langle\Gamma_\gamma\rangle$ = 106 meV (n=27) for ^{158}Gd, $\langle\Gamma_\gamma\rangle$ = 129 meV (n=5) for ^{160}Gd, and $\langle\Gamma_\gamma\rangle$ = 60 meV (n=8) for ^{175}Lu.

We obtained s-wave strength function values of S = 1.4×10^{-4} for ^{154}Gd (n=41 from 0-1 keV); $S_0 = 1.4\times10^{-4}$ for ^{158}Gd (n=64 from 1-10 keV) and $S_0 = 1.5\times10^{-4}$ for ^{160}Gd (n=37 from 0-10 keV).

The transmission-cross section data processing is finished for the isotopes ^{160}Dy, ^{162}Dy, and ^{164}Dy and is nearly complete for ^{161}Dy and ^{163}Dy. The data is presently being evaluated for resonance energies and resonance parameters.

The resonance capture integrals for the rare earth isotopes measured during 1968: ^{152}Sm, ^{154}Sm, ^{151}Eu, ^{153}Eu, ^{154}Gd, ^{158}Gd, ^{160}Gd, ^{166}Er, ^{167}Er, ^{168}Er, ^{170}Er, ^{168}Yb, ^{170}Yb, ^{171}Yb, ^{172}Yb, ^{174}Yb, ^{176}Yb, ^{175}Lu, ^{182}W, ^{183}W, ^{184}W, and ^{186}W have been evaluated. These isotopes lie in the region of the periodic table that exhibits large nuclear deformation and the split "4S" giant resonance in the strength function. Their relatively high level density and fractionally large Γ_γ (compared to Γ) make these isotopes suitable for application as control poisons in nuclear reactors. Table A-1 shows our values of the resonance capture integral as well as $\langle\Gamma_\gamma\rangle$ as determined from our data.

Our results for ^{166}Er, ^{168}Er, ^{182}W, ^{184}W, ^{152}Sm and ^{172}Yb are particularly good test cases for statistical theories of short and long range order for nuclear level spacing. Except for ^{168}Er, we seem to have observed only s-wave resonances in these isotopes, and for ^{168}Er the p levels can be clearly separated out on the basis of their Γ_n^0.

The single population nearest neighbor level spacing distribution is believed to be of the simple form surmised by Wigner, to within experimental precision. All of the above isotopes give good fits to the Wigner shape, including ^{168}Er after p level removal. The Dyson-Mehta Δ statistic for the mean square deviation of the staircase plot

TABLE A-1

Isotope	Mass % in natural element	$I_c^{0.414}$ (barns)	$\langle\Gamma_\gamma\rangle$ meV*	other values of I_c (barns)
^{152}Sm	26.7	2644±604	65(9)	3100±200[a] , 3162±104[b] 2850±300[c] , 2920[f]
^{154}Sm	22.7	31±6	79(3)	
^{151}Eu	47.8	5729±650†	90.0(70)	3741[d] , <3000[e] , 3420[f]
^{153}Eu	52.2	1745±195†	94.8(44)	1833[d] , 1280±100[e]
^{154}Gd	2.1	179±17	100(24)	303[g]
^{158}Gd	24.9	60.5±6	106(27)	72[h]
^{160}Gd	21.9	6.9±1.0	129(5)	4.8[h]
^{166}Er	33.4	123±13	92.4(10)	56.5±11.3[g]
^{167}Er	22.9	4899±605	91(54)	
^{168}Er	27.1	35.6±7	85(2)	
^{170}Er	14.9	45±7		32.2[f]
^{168}Yb	0.1	34350±4500††		30,950[i]
^{170}Yb	3.0	212±20		326[i]
^{171}Yb	14.3	345±39	76.5(44)	313[i]
^{172}Yb	21.8	26.2±6	72(4)	18±7[g] , 23.5[i]
^{174}Yb	31.8	27.1±6	80(3)	33.8[i]
^{176}Yb	12.7	8±2	82(1)	7.6[i]
^{175}Lu	97.4	1158±280	60(8)	886[d]
^{182}W	26.4	592±60	75(2)	591[j]
^{183}W	14.4	371±42		387[j]
^{184}W	30.6	14.1±1.5		13.5[j] , 7.5±1.0[k], 14.9±1.6[l]
^{186}W	28.4	487±50	47(3)	345[f] , 551[j], 490±80[k] 441±22[l] , 318[m] , 450±36[n]

*followed by the number of levels from which $\langle\Gamma_\gamma\rangle$ was obtained.

†the resonance integrals in Eu are complicated by low energy resonances near our cut-off energy of 0.414 eV. We have obtained the value of $I_c^{0.5}$ = 3265 barns for ^{151}Eu and 1632 barns for ^{153}Eu.

††$I^{0.5}$ = 31,900 barns.

TABLE A-1 (CONTINUED)

a J. Walker, Can. J. of Phys. 39, 1184 (1961).

b M. Cabell, J. Inorg. Nucl. Chem. 24, 749 (1962).

c R. Tattersall, J. of Nucl. Energy A12, 32 (1960).

d J. Rogers, Trans. Am. Nucl. Soc. 10, 259 (1967).

e R. Tattersall, H. Rose, S. Pattenden, D. Jowitt, J. Nucl. Energy 12, 32 (1960).

f Report: "Certain Accounts on the Utilization of the THAI Research Reactor" Bangkok Conf. THAI-AEC-10 (1967).

g R. Dobrozemsky, A. Edlmair, F. Pichlmayer, F. Viehbock, "Pile Neutron Capture Cross Sections for Rare Earth Isotopes" EANDC ()R)-68 "L".

h S. Mughubghub and R. Chrien, Phys. Rev. 180, 1131 (1969).

i S. Mughubghub and R. Chrien, Phys. Rev. 174, 1400 (1968).

j G. Joanou, C. Stevens, "Neutron Cross Sections for the W Isotopes" GA report 5885 (1964).

k J. Scoville, Trans. Am, Nucl. Soc. 5, 377 (1962).

l C. Pierce, D. Shook, NSE 31, 431 (1968).

m J. Gillette, "Review of the Radioisotope Prog." ORNL-4013 (1965).

n L. Beller, D. Latham, J. Otter, "Measurement of the Resonance Integral in ^{186}W" NAA-SR-12500 (1967).

of the observed number of levels N versus E is predicted to have $\langle\Delta\rangle$ increase with the number of levels as $\ln(N)$, with $N \approx 20{,}000$ needed before $\langle\Delta\rangle = 1.00$. Earlier experimental values of Δ were all larger than the Dyson-Mehta prediction, mainly due to the partial inclusion of p-wave levels and/or missed s-wave. In all the present cases, as shown in Table A-2, we obtained good agreement with the D-M value of $\langle\Delta\rangle$ within the theoretical S.D. of 0.11. This agreement was also found for the low energy ends of the data for the odd A isotopes ^{183}W, ^{167}Er, ^{171}Yb, ^{173}Yb, where the two randomly mixed s level populations for $J=(I\pm1/2)$ are present. The short range order expected from Wigner's random matrix model leads to the prediction for the covariance of adjacent level spacings $Cov(S_i,S_{i+1}) \approx -0.27$.

Table A-2 shows that the experimental results are in good agreement with this prediction. In addition, we obtained the unexpected result for ^{166}Er, our best quality data, that there seems to be a definite negative correlation between adjacent level Γ_n^0 value, $Cov(\Gamma_{n\gamma}^0,\Gamma_{n\gamma+1}^0) = (-0.28\pm0.09)$. Also the Γ_n^0 values in ^{166}Er showed less fluctuation of the $\langle\Gamma_n^0\rangle$ values (averaged over regions having >10 levels) than that expected from an uncorrelated sequence of Γ_n^0 values. The observed set of Γ_n^0 values agreed with the Porter-Thomas theory.

When the values of Δ and $Var(\Delta)$ were calculated from Monte Carlo calculations using Wigner's statistical model, we obtained the expected, but previously undemonstrated, result that they were in agreement to within statistical fluctuations, with the Dyson-Mehta results, using Dyson's circular ensemble. This is shown in Table A-3. To convert the "semicircular" distribution to a more physically constant density eigenvalue distribution, we used the transformation $P_W(\varepsilon)d\varepsilon = P(y)dy$, where $P_W(\varepsilon)$ is Wigner's semicircular law and $P(y)$ is set equal to a constant. The resulting set of constant density eigenvalues was then used to evaluate the mean distribution of values of various parameters such as and $Cov(S_i,S_{i+1})$. In addition to the agreement of Δ with the Dyson-Mehta predictions, it was found that $Cov(S_i,S_{i+1}) \approx -0.27$ for matrices of large dimension (greater than 50×50). The eigenvalue behavior was also found to agree well with Dyson's F statistic, giving further confirmation of the equivalence of Dyson's circular ensemble and the random matrix model.

B. Cross Section and Resonance Parameters A<60 (U.N. Singh and J Garg, SUNY Albany; J. Rainwater, W.W. Havens, Jr., and S Wynchank, Columbia University)

High resolution total neutron cross section measurements for samples run during the 1970 experimental series (fluorine, magnesium, aluminum, sulfur, chlorine, potassium, and calcium) have been analyzed at SUNY by an R-matrix to fit the data. From the analysis it has been

Table A-2 Summary of Experimental Results for Even-Even Isotopes and Comparison with Theory

	Er^{166}	Er^{168}	W^{182}	W^{184}	Sm^{152}	Yb^{172}
N	109	50	41	30	70	55
E_{max}	4200	4700	2607	2621	3665	3900
Δ_{exp}	0.455	0.287	0.259	0.446	0.400	0.412
Δ_{th}^{C}	0.468	0.389	0.369	0.338	0.420	0.399
Δ_{th}^{UC}	2.052	0.985	0.822	0.625	1.346	1.073
$Cov(S_j, S_{j+1})$	-0.22 ±0.08	-0.29 ±0.14	-0.37 ±0.15	-0.28 ±0.18	-0.26 ±0.11	-0.24 ±0.13
$P_<^{C}$	0.590	0.180	0.103	0.705		0.610
$P_<^{UC}$	0.0004	0.0035	0.002	0.159	0.004	0.017

N = number of levels
E_{max} = upper limit of energy interval (in eV) containing the N levels

Table A-3

Predicted Behavior of $\langle\Delta\rangle$ and $\sqrt{Var(\Delta)}$ as a Function of the Number of Levels for Wigner's Random Matrix Model and Dyson's Circular Ensemble. It is seen that for these tests the predictions of the two models are indistinguishable.

Monte Carlo Random Matrix Calculations					Theoretical Predictions of the Circular Ensemble	
No. of Matrices Diagonalized	Matrix Dimension	Eigenvalues Used	$\bar{\Delta}$	$\sqrt{Var(\Delta)}$	$\langle\Delta\rangle$	$\sqrt{Var(\Delta)}$
78	21	13	0.257±0.011	0.098	0.253	0.11
78	31	23	0.324±0.012	0.106	0.311	0.11
78	41	33	0.364±0.014	0.124	0.347	0.11
78	50	42	0.372±0.011	0.098	0.372	0.11
62	81	77	0.424±0.012	0.094	0.433	0.11
† 900	120	109	0.470±0.003	0.093	0.468	0.11

Tabulated below are the average values of $Cov(S_i, S_{i+1})$ calculated using the average sample spacing $\bar{s}$ and the true average spacing $\langle s\rangle$. The difference between the values of $\overline{Cov(S_i, S_{i+1})}$ obtained using $\bar{s}$ and $\langle s\rangle$ (for the same number of levels) is much less than the difference (1/n) found in the uncorrelated case.

No. of Matrices Diagonalized	Matrix Dimension	Eigenvalues Used	$\overline{Cov(S_i, S_{i+1})}_{\bar{s}}$	$\overline{Cov(S_i, S_{i+1})}_{\langle s\rangle}$
78	21	15	-0.250±0.026	-0.236±0.026
78	31	25	-0.241±0.021	-0.233±0.021
78	41	35	-0.269±0.018	-0.266±0.018
78	50	44	-0.274±0.016	-0.272±0.016
62	81	77	-0.256±0.012	-0.256±0.012
† 900	120	109	-0.277±0.003	-0.276±0.003

† Calculated using Dyson's Brownian motion model.

possible to determine the energies and neutron widths of the observed levels and make their L- and J-value assignments. Table B-1 gives a summary of S_0 and S_1, the s and p wave strength functions for isotopes of these elements. Table B-2 gives the resonance parameters for the isotopes ^{19}F, ^{27}Al, ^{35}Cl, ^{37}Cl, ^{24}Mg, ^{25}Mg, ^{32}S, ^{40}Ca, ^{44}Ca, ^{39}K, and ^{41}K determined from the analysis. Values for <D>, the mean level spacing, are also given in these tables. Figure B-1 shows the R-matrix fit to Cl, F and Al with the isotopic assignments to the resonances. It is possible to determine Γ_γ for the strong levels by combining these measurements with the known thermal data on the coherent scattering and capture cross section.

C. Cross Section and Neutron Resonance Parameters of ^{238}U
(F. Rahn, H. Camarda, G. Hacken, W.W. Havens, Jr., H. Liou, J. Rainwater, M. Slagowitz, S. Wynchank)

The analysis of the ^{238}U data from the 1970 run is nearing completion. Preliminary total neutron cross section plots and resonance parameters appeared in our last progress report. Our work during this report period concentrated on the spin assignment of the observed levels. We have applied the following statistical tests in the s-population selection: Wigner distribution, Porter-Thomas distribution, Dyson-Mehta Δ statistic and $Cov(S_i,S_{i+1})$. In addition we used the F test, due to Dyson, for final level spin assignment. The F test (or F statistic) involves the evaluation at each resonance position E_i of a parameter F_i, defined as

$$F_i = \sum_{i \neq j} f(x_{ji}),$$

where $x_{ji} = (E_j-E_i)/L$, and $f(x) = \frac{1}{2}\,\ell n\{[1+(1-x^2)^{1/2}]/[1-(1-x^2)^{1/2}]\}$. The summation is taken over all resonances between (E_i-L) and (E_i+L), where $L = M\langle D\rangle$ is the largest interval characterized by a properly chosen integer M times the average level spacing D . Dyson finds that $\langle F_i\rangle = n-\ell n(n)-0.656$, with a standard deviation of $[\ell n(n)]^{1/2}$ where $n=\pi M$. If a spurious level is present $\langle F_i\rangle=n$ at this spurious level. Thus a large positive fluctuation occurs at a "spurious" level, while a low value of F_i results near a missed level.

The problem in ^{238}U is eliminating as p wave or spurious the large number of excess levels seen in the data. Nearly all s wave levels were observed. We tacitly assumed that the stronger levels were s wave and therefore the analysis concentrated on the assignment of the weaker levels. The Porter-Thomas distribution was used to determine the expected number of small resonances. Table C-1 presents our spin assignments for ^{238}U. Figure C-1 and C-2 show the comparison of our data with the theoretical Porter-Thomas and Wigner distributions. For this set of s wave energy levels, we obtain a $\Delta_{exp}=0.42$ (versus

TABLE B-1

Element	% abundance in natural (f) sample	Energy region investigated	number of resonances observed	$S_0 \times 10^4$	$S_1 \times 10^4$
$_9F^{19}$	100%	100 eV - 200 keV	3	--	(14.31±12.53)
$_{12}Mg^{24}$	78.7%	100 eV - 500 keV	3	--	(14.55±5.81)
$_{12}Mg^{25}$	10.13%	100 eV - 500 keV	1	--	1.05 (determined from one level)
$_{13}Al^{27}$	100%	100 eV - 225 keV	8	0.34 (determined from one level)	(10.13±5.81)
$_{16}S^{32}$	95.0%	100 eV - 400 keV	6	1.60 (determined from one level)	(0.58±0.44)
$_{17}Cl^{35}$	75.53%	100 eV - 200 keV	23	(0.08±0.07)	(1.65±0.54)
$_{17}Cl^{37}$	24.47%	100 eV - 200 keV	21	(0.12±0.09)	(2.87±1.05)
$_{19}K^{39}$	93.1%	100 eV - 200 keV	30	(0.37±0.23)	(2.70±0.82)
$_{19}K^{41}$	6.88%	100 eV - 200 keV	39	(0.12±0.06)	(4.52±1.17)
$_{20}Ca^{40}$	96.97%	100 eV - 300 keV	10	(3.12±2.37)	(0.33±0.20)
$_{20}Ca^{44}$	2.06%	100 eV - 300 keV	4	0.0212 (determined from one level)	(1.68±1.47)

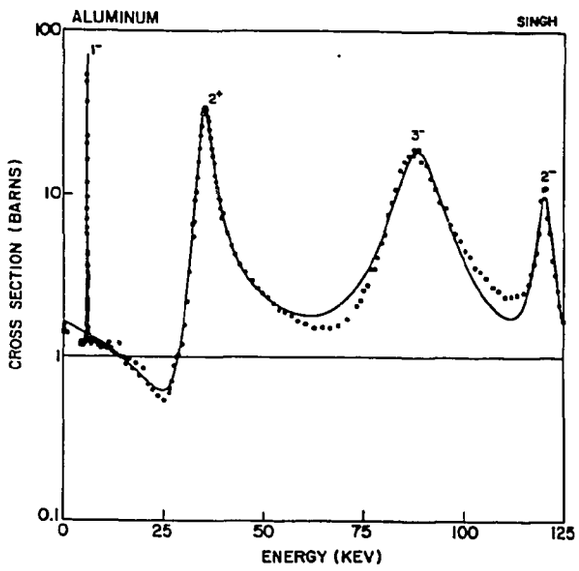

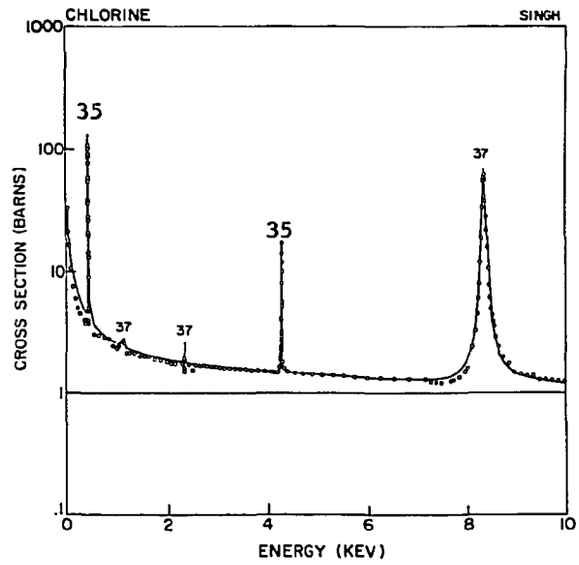

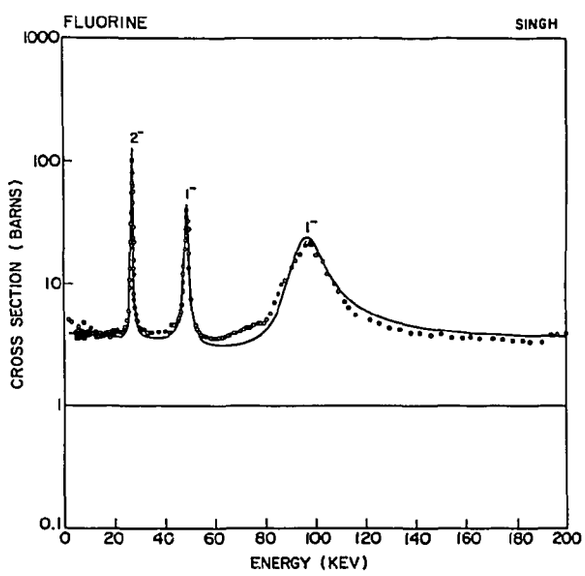

Figure B-1. The total neutron cross section of Al, Cl, and F, with isotopic assignments shown above the peaks, in the 0-200 keV region. The solid curve is an R-matrix fit to the data from the resonance parameters from Table B-2.

TABLE B-2

Resonance Parameters

E_0(keV)	ℓ	J^{Π}	Γ_n(keV)	Γ_n^1(eV)	Wigner limit Γ_W (ℓ=0)(keV)	Wigner limit Γ_W (ℓ=1)(keV)	Assumed Γ_γ
$I^{\Pi} = 1/2^+$	f = abundance in natural sample = 100%				element = $_9F^{19}$		
27.02±0.07	1	2^-	0.37	125.50	600	10.7	1.1
49.10±0.17	1	1^-	1.31	185.2	800	25.5	1.6
97.00±0.45	1	1^-	14.31	750.5	1130	79.4	
					$S_1 = (14.31 \pm 12.53)\times10^{-4}$		
$I^{\Pi} = 0^+$			f = 78.7%			$_{12}Mg^{24}$	
82.0±0.352	1	$3/2^-$	7.7		950	57.3	
265.6±1.978	1	$1/2^-$	88		1710	298	
430.0±4.035	1	$3/2^-$	26.65		2180	549	
					$S_1 = (14.55 \pm 12.74)\times10^{-4}$		
$I^{\Pi} = 5/2^+$			f = 10.13%			$_{12}Mg^{25}$	
20.0±0.046	1	3^-	0.6		460	7	
$I^{\Pi} = 0^+$			f = 95%			$_{16}S^{32}$	
30.35±0.083	1	$1/2^-$	0.04		520	13.7	
102.9±0.490	0	$1/2^+$	16.98		970	82	
202.2±1.322	1	$1/2^-$	1.98		1360	209	
275.5±2.054	1	$1/2^-$	1.87		1580	311	
288.7±2.238	1	$1/2^-$	2.06		1630	336	
377.4±3.326	0	$1/2^+$	6.745		1860	471	
$S_0 = 1.60\times10^{-4}$ (determined from 2 levels)					$S_1 = (0.58 \pm 0.44)\times10^{-4}$		

TABLE B-2 (CONTINUED)

E_0 (keV)	ℓ	J^{Π}	Γ_n (keV)	Wigner limit $\Gamma_W(\ell=0)$ (keV)	Wigner limit $\Gamma_W(\ell=1)$ (keV)
$I^{\Pi} = 0^+$		f = 96.97%			element $_{20}Ca^{40}$
20.427±0.023	1	$1/2^-$	0.008	410	9
88.84±0.175	1	$1/2^-$	0.171	840	76
132.0±0.308	0	$1/2^+$	3.535	1030	132
145.32±0.353	1	$1/2^-$	0.186	1070	149
169.380±0.440	0	$1/2^+$	2.351	1160	185
*211.5±0.606	1	$1/2^-$	0.337	1300	248
217.4±0.630	0	$1/2^+$	7.891	1310	256
*229.7±0.682	1	$1/2^-$	0.200	1350	275
244.0±0.745	0	$1/2^+$	30.305	1410	306
292.60±0.969	1	$1/2^-$	1.552	1520	374
*from BNL 325 Vol. I (1964)					
$S_0 = (3.12\pm2.37)\times10^{-4}$				$S_1 = (0.33\pm0.20)\times10^{-4}$	
$I^{\Pi} = 0^+$		f = 2.06%			$_{20}Ca^{44}$
10.834±0.0098	1	$3/2^-$	0.012	290	3.5
42.075±0.062	0	$3/2^+$	0.130	580	26
51.270±0.081	1	$3/2^-$	0.572	640	35
101.180±0.211	1	$3/2^-$	0.629	900	91
$S_0 = 0.0212\times10^{-4}$ (determined from one level)				$S_1 = (1.68\pm1.47)\times10^{-4}$	

TABLE B-2 (CONTINUED)

Al^{27} ($I^{\Pi} = 5/2^+$) f=100%

E_0(keV)	ℓ	J^{Π}	Γ_n(keV)
5.903±0.008	1	1^-	0.01
34.70±0.10	0	2^+	3.42
88.50±0.39	1	3^-	11.28
120.0±0.60	1	2^-	3.49
145.0±0.80	1	3^-	15.14
159.0±0.90	1	4^-	2.84
204.8±1.3	1	2^-	4.26
208.1±1.4	1	2^-	4.35

<D> = 28.1 keV, S_0=0.3397x10^{-4}
S_1 = (10.13±5.81) x 10^{-4}

Cl^{37} ($I^{\Pi} = 3/2^+$) f= 24.47%

E_0(keV)	ℓ	J^{Π}	Γ_n(eV)
1.101±0.0008	1	0^-	0.003
2.312±0.0014	1	0^-	0.012
8.317±0.007	1	3^-	73.1
25.24±0.03	0	1^+	138
27.36±0.034	1	0^-	506
27.727±0.035	1	0^-	65.8
27.820±0.035	1	0^-	75.2
29.172±0.037	1	0^-	35.0
33.9±0.046	1	0^-	315
34.33±0.047	1	0^-	57.6
46.600±0.071	0	2^+	350
51.570±0.082	1	0^-	184
54.920±0.089	0	2^+	166
56.670±0.093	1	0^-	190
62.043±0.106	1	0^-	330
62.726±0.107	1	2^-	275
66.850±0.117	1	1^-	185
68.260±0.121	1	2^-	450
90.323±0.180	0	2^+	304
93.120±0.188	1	2^-	807
141.0±0.339	1	2^-	739

<D>= 9.5 keV, S_0=(.12±0.09)x10^{-4}
S_1=(2.87±1.06)x10^{-4}

Cl^{35} ($I^{\Pi} = 3/2^+$) f= 75.53%

E_0(keV)	ℓ	J^{Π}	Γ_n(eV)
-0.185 (Γ_γ = 4.53 eV)	0	2^+	13.6
0.398±0.0005	1	0^-	0.3
4.249±0.002	1	0^-	1.7
14.797±0.015	0	1^+	45.5
16.350±0.017	1	0^-	26.4
17.131±0.018	1	1^-	29.9
25.680±0.031	1	0^-	185
26.630±0.033	1	1^-	150
44.190±0.066	1	0^-	110
55.430±0.090	1	0^-	307
57.800±0.096	1	1^-	147
101.160±0.211	1	0^-	725
103.480±0.218	1	1^-	468
113.471±0.248	1	2^-	582
127.700±0.294	1	0^-	669
133.798±0.314	0	1^+	814
136.550±0.323	1	1^-	688
139.250±0.333	1	0^-	1017
143.200±0.346	1	1^-	931
149.937±0.370	1	0^-	731
165.708±0.427	1	0^-	443
183.242±0.493	1	2^-	1503
188.390±0.513	1	1^-	824
190.769±0.522	1	0^-	940

<D>=8.7 keV, S_0=(0.08±0.07)x10^{-4}
S_1=(1.65±0.55)x10^{-4}

TABLE B-2 (CONTINUED)

K^{39} ($I^{\pi} = 3/2^+$) f= 93.10%

E_0(keV)	ℓ	J^{π}	Γ_n(eV)
-1.00 (Γ_γ=1eV)	0	1^+	45.5
9.38±0.008	1	2^-	46.2
25.540±0.031	1	2^-	113
42.600±0.063	0	2^+	554
46.009±0.070	1	1^-	84.4
57.850±0.096	0	2^+	865
59.940±0.101	1	1^-	137
68.805±0.122	1	1^-	2070
87.700±0.172	1	1^-	358
96.750±0.198	0	2^+	329
99.268±0.205	1	0^-	746
101.173±0.211	1	0^-	684
102.239±0.214	1	0^-	451
104.500±0.221	1	0^-	544
108.600±0.234	0	2^+	1255
116.240±0.257	1	0^-	913
118.62±0.265	1	0^-	682
121.300±0.273	1	0^-	836
127.300±0.293	1	0^-	771
132.700±0.310	1	1^-	687
135.000±0.318	1	1^-	459
136.690±0.324	1	0^-	1017
144.400±0.350	1	0^-	1288
145.820±355	1	0^-	1474
147.736±0.362	1	0^-	1673
149.110±0.367	1	0^-	526
154.320±0.385	1	1^-	1591
162.500±0.415	1	1^-	879
178.100±0.473	1	1^-	890
193.520±0.533	1	3^-	166
199.500±0.556	0	1^+	199

<D>= 6.7 keV,
S_0=(0.37±0.23)x10^{-4}
S_1=(2.71±0.82)x10^{-4}

K^{41} ($I^{\pi} = 3/2^+$) f= 6.88%

E_0(keV)	ℓ	J^{π}	Γ_n(eV)
1.111±0.0008	1	1^-	0.59
2.029±0.0012	1	2^-	3.82
3.205±0.002	1	0^-	1.74
3.278±0.002	1	1^-	2.86
4.038±0.003	1	0^-	0.64
5.536±0.004	0	1^+	118
8.461±0.007	1	0^-	7.2
12.148±0.011	1	1^-	10.9
12.615±0.012	1	3^-	12.6
13.340±0.013	1	1^-	11.9
14.291±0.014	1	1^-	17.5
15.026±0.015	1	0^-	34
15.947±0.016	1	2^-	25.5
16.585±0.017	0	1^+	81.8
16.710±0.017	1	2^-	48
16.785±0.017	1	1^-	52
16.840±0.018	1	1^-	57.6
20.299±0.023	1	1^-	69.1
24.740±0.030	0	1^+	143
24.950±0.030	1	3^-	81
27.651±0.035	1	1^-	99
32.200±0.043	1	1^-	65
32.510±0.043	1	1^-	52
33.350±0.045	1	3^-	136
33.808±0.045	1	1^-	42
37.085±0.052	1	1^-	60
37.55±0.053	1	3^-	117
38.045±0.054	1	1^-	116
38.250±0.054	0	1^+	310
38.582±0.055	1	3^-	170
44.645±0.067	1	2^-	41.6
52.152±0.083	1	3^-	137
54.620±0.089	1	3^-	262
55.789±0.091	1	2^-	43.5
79.890±0.151	1	3^-	437
81.20±0.154	1	3^-	647
90.621±0.180	1	1^-	318
91.524±0.183	1	1^-	284
93.100±0.187	0	2^+	355

<D>= 5.13 keV
S_0=(0.12±0.06)x10^{-4}
S_1 = (4.52±1.18)x10^{-4}

TABLE C-1

G Values of U^{238} Calculated with M = 12

E(eV)	$\sqrt{\Gamma_n^o}$ (meV)$^{\frac{1}{2}}$	G (Old)	G (New)
6.68	0.77	4.36*	0.90*
Q 10.20P	0.02	4.00*	
21.00	1.38	2.77*	0.83*
36.70	2.27	1.60*	0.54*
66.30	1.76	1.12*	0.44*
80.77	0.48	1.44*	0.40*
Q 90.00P	0.09	1.44*	
102.78	2.55	0.80*	0.15*
116.93	1.82	0.01*	-0.14*
145.80	0.26	-1.24*	-0.70*
165.54	0.52	-1.67*	-0.79*
190.34	3.30	-2.18*	-0.94*
208.65	1.97	-2.52*	-1.05*
237.40	1.34	-2.03	-1.04*
Q242.88P	0.10	-2.04	
Q263.94	0.12	-2.13	-0.70
273.74	1.23	-2.32	-0.63
291.11	0.95	-2.86	-0.98
311.12	0.24	-3.64	-1.37
347.92	2.10	-3.84	-1.68
376.92	0.24	-3.36	-1.18
397.56	0.55	-2.73	-0.54
410.23	0.97	-2.61	-0.45
434.19	0.63	-2.09	-0.41
Q454.17	0.14	-1.59	-0.03
463.31	0.49	-1.32	-0.01
478.70	0.37	-1.42	-0.46
Q488.89P	0.14	-1.60	
518.59	1.38	-1.80	-0.80
535.49	1.26	-1.18	-0.54
Q556.05	0.14	-0.84	-0.39
580.20	1.06	-0.05	-0.09
595.15	1.83	0.46	-0.08
619.94	1.07	1.90	0.32
Q623.53P	0.13	2.20	
628.67	0.40	1.79	0.20
661.18	2.12	1.16	-0.56
Q677.00P	0.14	1.73	
693.23	1.14	2.22	0.15
708.46	0.84	3.10	0.56
721.80	0.22	4.04	0.82
Q730.10P	0.17	4.99	
732.26	0.22	5.02	0.54
Q742.95P	0.14	3.94	
765.05	0.49	3.32	0.43
779.14	0.24	3.23	0.71
790.88	0.42	2.82	0.57
821.58	1.43	2.81	0.19

Table C-1 (Cont'd.)

E (eV)	$\sqrt{\Gamma_n^o}$ (meV)$^{\frac{1}{2}}$	G (Old)	G (New)
Q845.62P	0.14	4.90	
851.02	1.38	5.46	0.98
855.15	1.66	5.38	1.14
866.52	0.37	4.83	0.61
Q891.29P	0.17	5.08	
905.11	1.22	6.33	0.04
909.90P	0.17	6.53	
925.18	0.53	6.56	0.44
Q932.50P	0.10	6.84	
936.87	2.19	6.54	0.50
958.43	2.26	5.37	-0.00
991.78	3.32	6.65	0.18
1000.3P	0.20	7.29	
1011.2	0.24	7.91	0.87
1023.0	0.45	8.61	1.24
1029.1	0.32	8.86	1.10
Q1033.2P	0.14	8.61	
1053.9	1.52	7.66	0.05
1058.1P	0.14	8.62	
Q1070.5P	0.10	8.71	
Q1081.1P	0.14	8.10	
Q1094.8P	0.14	8.52	
1098.3	0.67	8.65	0.56
Q1102.3P	0.14	8.23	
1108.9	0.95	7.03	0.65
1131.4	0.24	4.69	1.09
1140.4	2.55	4.02	1.09
1167.5	1.53	2.44	1.15
1177.6	1.36	1.99	1.22
1195.0	1.63	0.80	1.09
1210.9	0.51	-0.26	0.77
1245.1	2.55	-1.10	0.56
1267.0	0.87	-0.91	0.96
1273.2	0.89	-1.05	0.81
1298.4	0.28	-2.32	0.33
1317.2	0.33	-3.00	0.42
1335.7	0.17	-3.20	0.23
1363.0N			-0.23
1393.0	1.92	-1.01	0.25
1405.1	1.43	0.59	0.62
Q1410.0P	0.17	1.09	
Q1417.0P	0.17	1.42	
1419.6	0.50	1.40	0.72
1427.7	0.89	0.35	0.45
1444.1	0.75	-0.93	-0.44
1473.8	1.43	-2.32	-1.43
1523.1	2.35	-1.04	-1.14
1532.0	0.22	-0.46	-0.95

Table C-1 (Cont'd.)

E(eV)	$\sqrt{\Gamma_n^o}$ (meV)$^{\frac{1}{2}}$	G (Old)	G (New)
Q1546.0P	0.14	0.24	
1550.0	0.17	0.23	-1.08
1565.0	0.22	-0.56	-1.25
1598.2	2.83	-1.19	-1.69
1622.9	1.45	-1.01	-1.38
1638.2	1.00	-0.46	-1.32
Q1645.4P	0.14	-0.32	
1662.1	2.00	-0.75	-1.69
1688.3	1.38	-0.72	-1.63
Q1700.7F	0.14	-0.34	
1709.4	1.16	-0.46	-1.35
1723.0	0.57	-1.05	-1.39
1744.0P	0.20	-2.06	
1755.8	1.22	-2.79	-1.36
1782.3	3.32	-3.50	-1.12
1797.7	0.22	-3.82	-0.74
1808.3	0.63	-4.56	-0.99
1845.6	0.56	-6.80	-1.23
1868.0N			0.10
1870.0N			0.06
1902.3	0.69	-7.93	-1.12
1917.1	0.71	-8.24	-1.15
1953.0N			-1.05
1968.7	3.61	-7.56	-0.58
1974.6	3.24	-7.45	-0.81
2023.6	2.12	-6.61	-0.76
2031.1	1.05	-6.29	-0.73
2070.0N			-0.55
2088.6	0.55	-3.29	0.25
2096.5	0.47	-2.79	0.22
2124.3	0.32	-1.54	0.12
2145.9	0.87	0.41	0.84
2152.8	1.95	1.00	0.74
2172.0P	0.22	1.77	
2186.0	2.79	2.57	0.70
Q2194.0F	0.22	3.12	
2201.4	1.55	3.03	0.92
2230.0	0.32	3.98	1.79
2235.7	0.32	4.41	1.92
Q2241.5F	0.17	4.31	
2259.1	1.17	4.45	2.10
2266.4	1.75	4.48	2.05
2281.3	1.52	4.23	1.24
2288.7P	0.22	4.07	
Q2302.0F	0.14	3.14	
231[illegible].9	0.55	2.41	0.87
2337.4	0.32	1.55	1.20
2352.0	1.14	1.43	1.72

Table C-1 (Cont'd)

E(eV)	$\sqrt{\Gamma_n^o}$ (meV)$^{\frac{1}{2}}$	G (Old)	G (New)
2356.0	1.14	1.21	1.63
2392.5	0.48	-1.16	0.55
2410.2	0.30	-1.26	0.56
2426.5	1.28	-1.37	0.51
2446.2	1.50	-1.76	0.38
2454.0	0.22	-2.11	0.10
2489.8	1.05	-3.85	-1.21
2520.7	0.45	-3.86	-1.19
2548.7	2.61	-2.99	-0.42
2559.3	2.07	-2.77	-0.23
2580.7	2.19	-2.45	-0.39
2598.7	3.32	-1.59	-0.57
Q2604.0F	0.22	-1.43	
2620.6	0.89	-1.98	-0.64
2631.6	0.14	-2.36	-0.85
2672.8	1.84	-2.84	-1.35
2695.6	0.67	-2.24	-1.07
2716.8	1.17	-1.39	-0.60
Q2730.0	0.22	-0.99	-0.32
2750.1	0.87	-0.62	-0.23*
2761.9	0.55	-0.53	-0.30*
2787.9	0.45	0.29*	-0.67*
Q2798.0P	0.22	0.83*	
2806.2	0.36	0.77*	-0.90*
2828.6	0.41	0.69*	-1.38*
Q2845.2F	0.22	1.01*	
2856.1	1.22	1.81*	-1.17*
2882.9	3.13	2.48*	-1.01*
2897.8	0.71	3.18*	-1.07*
Q2908.5P	0.22	3.48*	
2923.6P	0.28	3.65*	
2932.3	0.68	3.73*	-1.16*
2956.3	0.53	3.98*	-0.58*
2967.4	0.39	4.58*	-0.53*
Q2974.0F	0.22	4.75*	
2987.4	0.32	4.70*	-0.63*

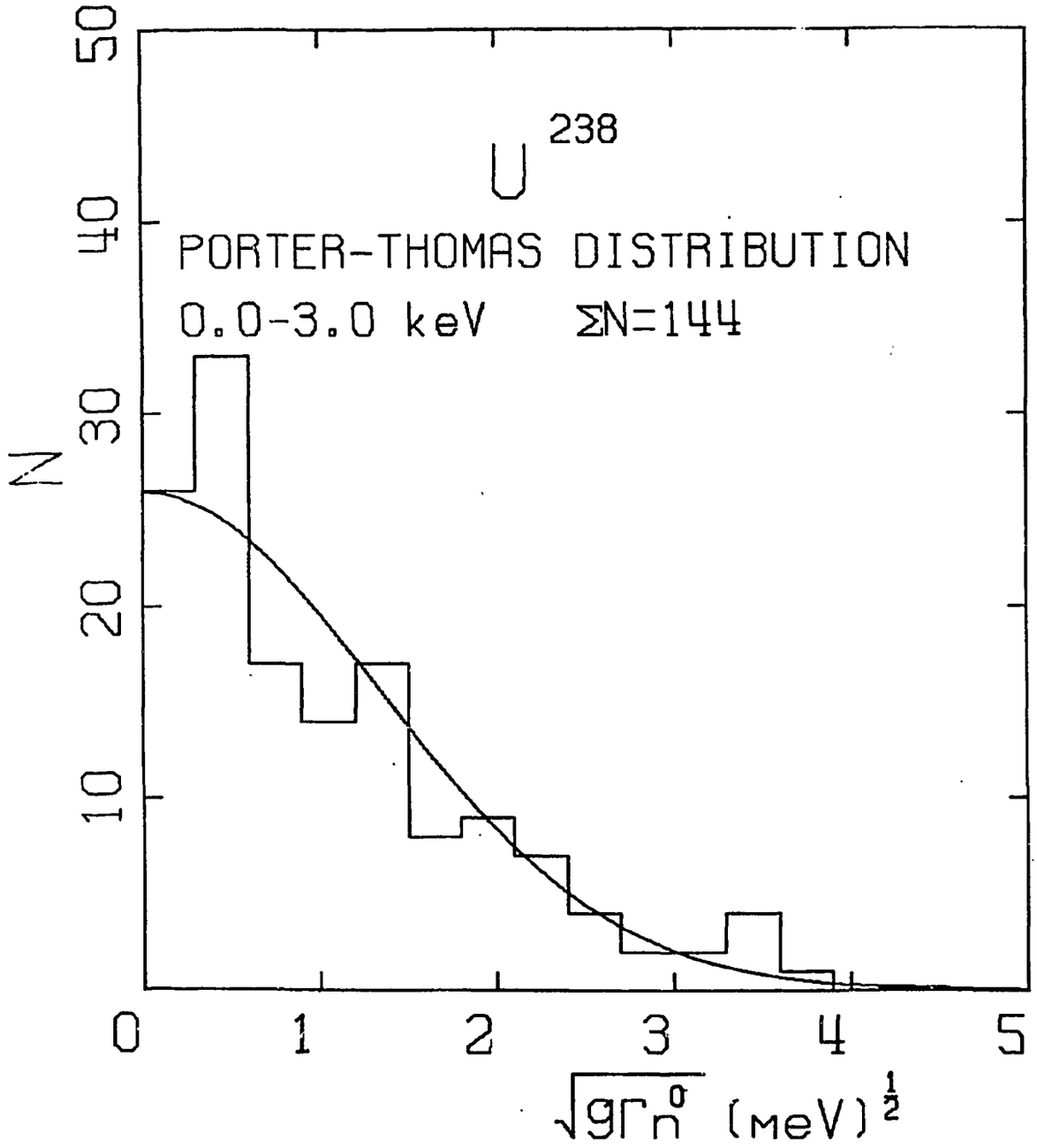

Figure C-1. Histogram of the reduced widths $\sqrt{\Gamma_n^0}$ for the selected $\ell=0$ population for ^{238}U. The Porter-Thomas theory is given by the smooth curve.

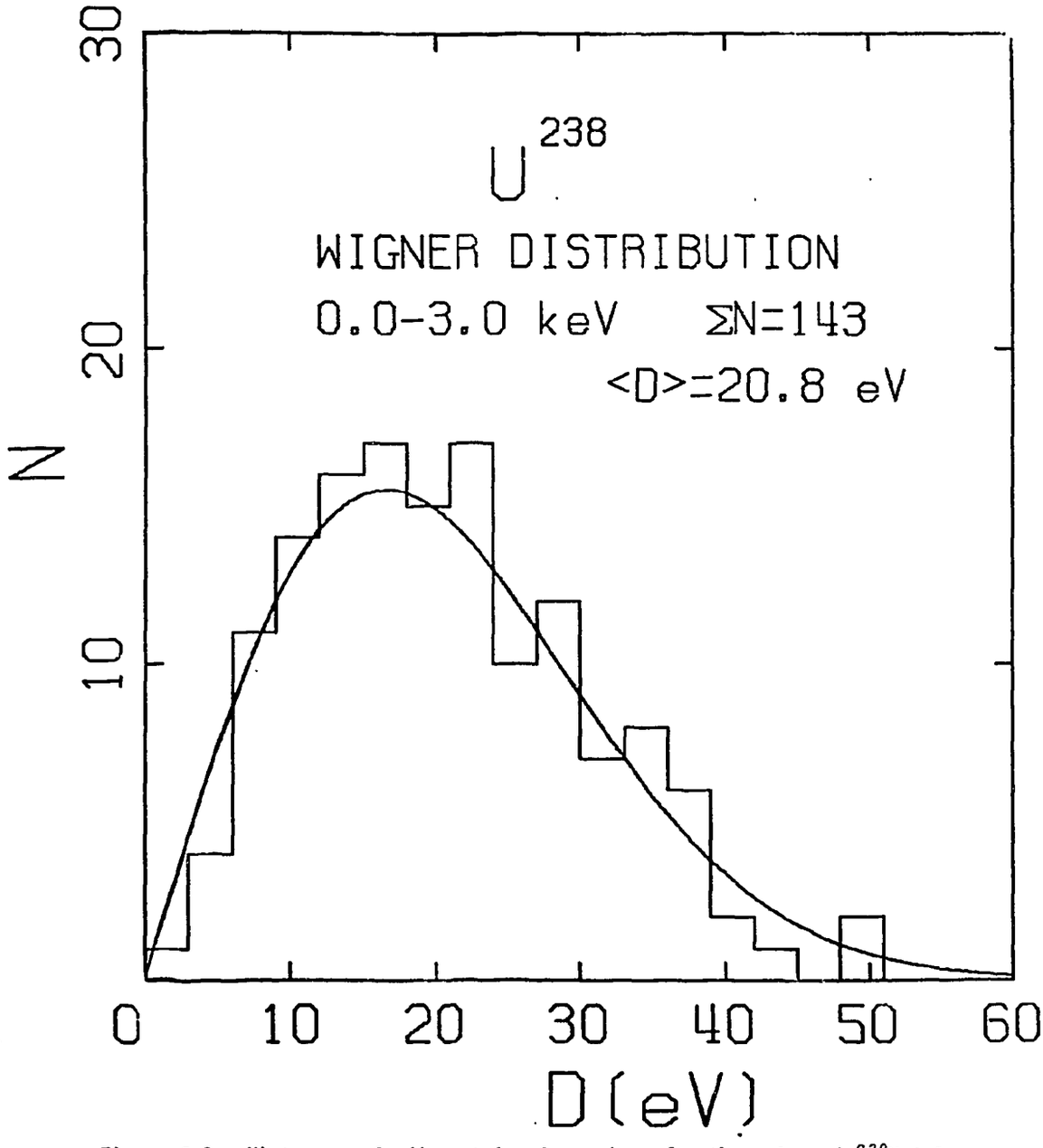

Figure C-2. Histogram of adjacent level spacings for the selected ^{238}U $\ell=0$ population. The smooth curve represents the Wigner distribution.

Δ_{DM}=0.49 0.11) and a $Cov(S_i,S_{i+1})$=-0.26±0.08 (versus an expected $Cov(S_i,S_{i+1})$≃-0.27). Our best choice for <D> is 20.8 eV.

D. Cross Section and Resonance Parameters of ^{232}Th (F. Rahn, G. Hacken, W.W. Havens, Jr., H. Liou, J. Rainwater, M. Slagowitz, S. Wynchank)

The preliminary transmission, self-indication and Moxon-Rae analysis of the data from the 1970 run has been completed. The ^{232}Th samples had thicknesses of (1/n) = 10.72, 31.9, 36.0, 191 and 885 barns/atom. The transmission measurements were carried out at 200 meters with a nominal resolution of 0.1 nsec/meter. The self-indication detector was at 40 meters and the Moxon-Rae measurements were carried out at 33 meters. A large number of reference samples such as Fe, Ta, Co, Cu, etc., were used as beam filters to help in the absolute normalization of the data. The sharp structure in the cross section of these reference samples determines the transmission of Th at the energies where the structure occurs in the reference samples, independent of the details of the background which is energy and sample dependent. The knowledge of the Th transmission at these points establishes T=0 and T=1, and allows a self-consistent determination of the (T,σ) values. Moxon-Rae measurements were performed simultaneously to give capture yields which could be related to the resonance parameters. Self-indication "D only" and "D+T" experiments were performed with a high efficiency plastic scintillation detector to give additional resonance information. There was good agreement between our "D only" and Moxon-Rae results.

The (T,σ) values of ^{232}Th were obtained by the transmission of the difference technique. A plot of the total neutron cross section appeared in our last progress report. We ran extra thick samples in the transmission measurement to accurately determine the total cross section between levels, where the cross section dips are due to potential-level interference.

To determine the resonance parameters, area analysis was mainly used and was supplemented by shape information. The area data gave a series of curves in the (Γ_n,Γ_γ) plane, and the intersection of these curves gave the value of the parameters Γ_n and Γ_γ. The shape fits used values of σ_T in the wings of the stronger, isolated resonances, in places where σ_T was not rapidly varying, so that resolution effects were relatively small. We then obtain a series of curves for R' versus Γ or Γ_n, where R' is the (local) potential scattering length. An example of this analysis is in Figures D-1 and D-2. The combination of the area results and the shape results determines our values of the resonance parameters.

Table D-1 lists the resonance parameters [E_0, $g\Gamma_n$ and Γ_γ] for 305 levels that we observed between 21 eV and 4 keV. In Figure D-3 we show the value of Γ_γ as a function of E for 84 levels up to 2400 eV. We found

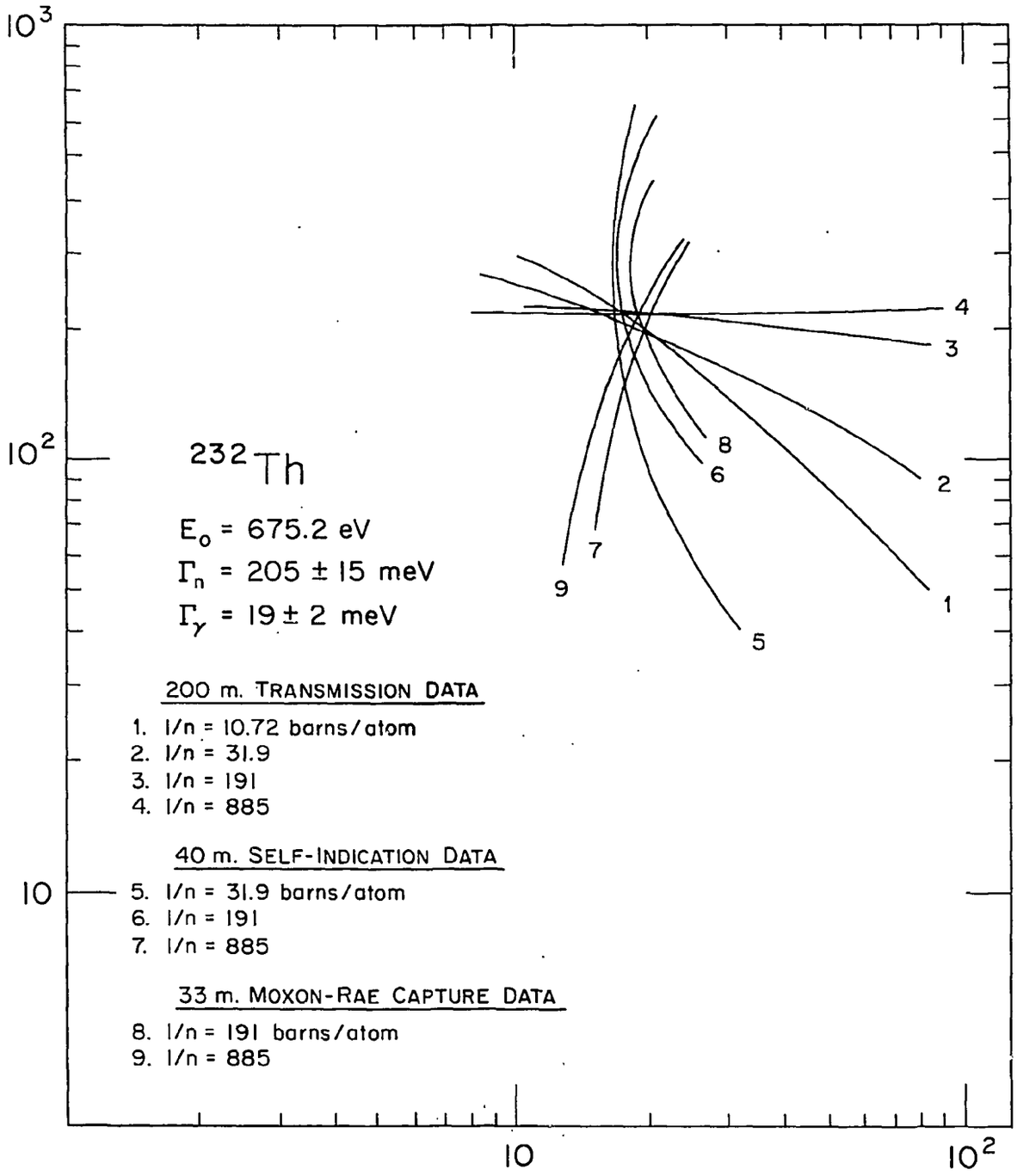

Fig. D-1

Example of the area analysis for the E_0= 675 eV level of ^{232}Th. The common intersection of the curves gives the values of the parameters Γ_n =205±15 meV and Γ_γ=19±2 meV.

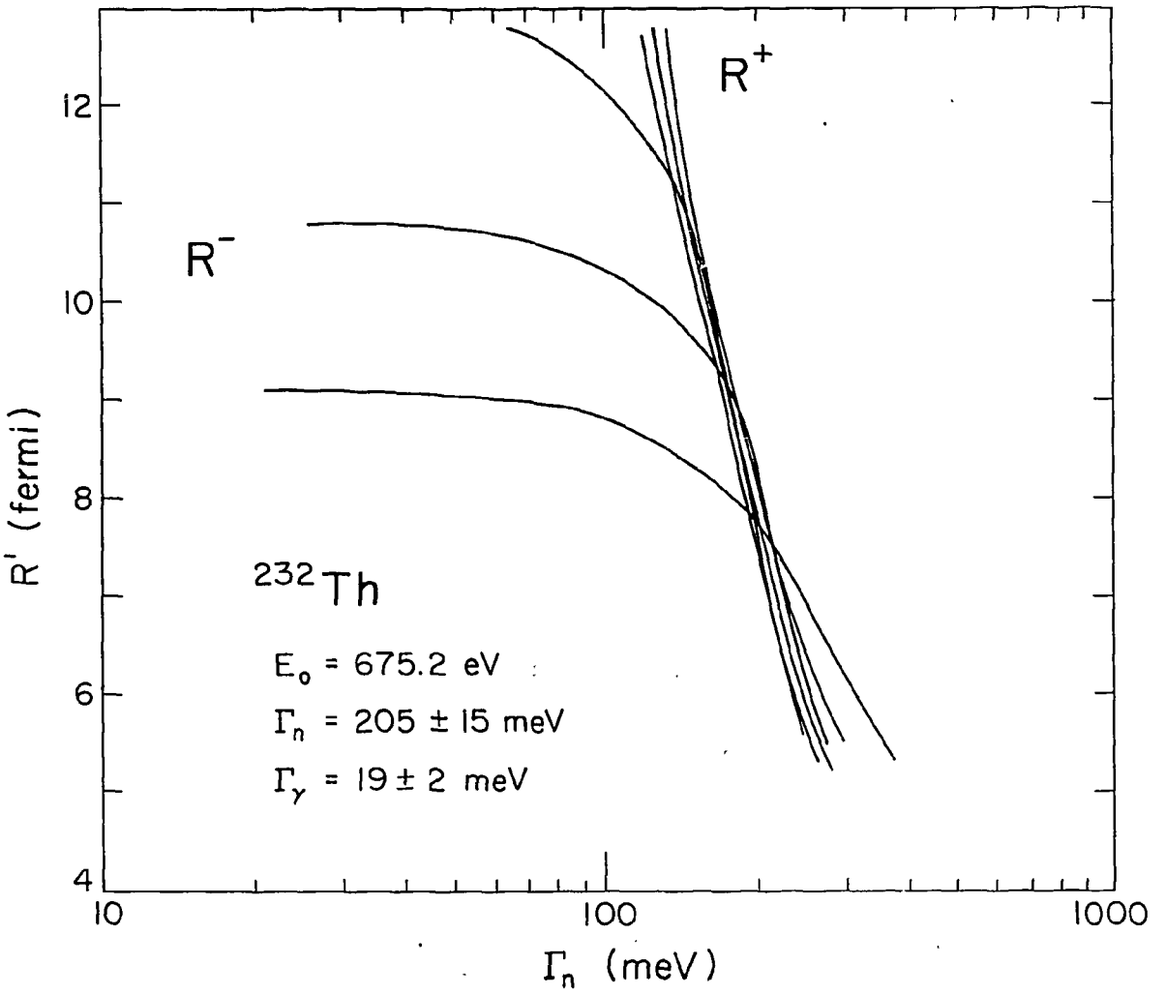

Fig. D-2

Example of the shape analysis for the E_0= 675 eV level in ^{232}Th. The series of curves are derived from the sum (R^+) and difference (R^-) of the cross section for points equidistant in energy from E_0. The cross section points are chosen in the wings of the resonance where the cross section is slowly varying and where resolution effects are less pronounced. The intersection of the points give further information on Γ_n = 205±15 meV and the (local) potential scattering radius R.

TABLE D-1

^{232}Th Resonance Parameters

E_0(eV)	ΔE	Γ_n^0(meV)	$\Delta\Gamma_n^0$	Γ_γ (meV)	$\Delta\Gamma_\gamma$
21.78	.02	.41	.02	20.	2.
23.43	.02	.67	.05	25.	2.
58.84	.07*	.001	.001		
59.48	.08	.51	.03	25.	2.
69.17	.10	5.29	.24	25.	2.
90.08	.08*	.001	.001		
112.93	.11	1.27	.09	20.	2.
120.78	.11	2.18	.14	22.	2.
128.21	.12*	.004	.001		
129.10	.13	.30	.02	18.	2.
145.72	.15*	.007	.002		
154.24	.16	.01	.002		
170.34	.19	4.98	.38	26.	2.
178.62	.21*	.004	.001		
192.57	.23	1.33	.07	17.	2.
196.13	.24	.005	.001		
199.30	.24	.89	.07	18.	2.
202.41	.25*	.002	.001		
210.87	.26*	.001	.001		
219.30	.28*	.001	.001		
221.16	.29	2.08	.13	22.	2.
242.23	.16*	.002	.001		
251.48	.18	2.02	.13	24.	2.
262.96	.19	1.48	.09	19.	2.
285.74	.21	1.77	.10	20.	2.
290.12	.21*	.002	.001		
302.30	.23*	.006	.002		
305.43	.24	1.49	.11	20.	2.
309.20	.24*	.003	.001		
321.47	.25*	.002	.001		
328.92	.26	4.19	.33	26.	2.
338.26	.27*	.003	.001		
341.83	.28	1.95	.11	19.	2.
361.47	.31*	.004	.002		
365.11	.31	1.47	.08	21.	2.
369.43	.31	1.30	.08	22.	2.
380.40	.33*	.006	.002		
391.53	.34	.006	.002		
400.86	.36	.52	.05	18.	2.
402.62	.36*	.004	.002		
411.62	.36	.007	.002		
420.92	.38	.02	.005		
454.1	.4	.05	.01		
462.3	.4	3.02	.23	22.	2.
476.3	.4	.01	.005		
488.6	.4	2.71	.18	18.	2.
510.31	.25	.17	.04		
528.46	.26	.52	.04	20.	3.
533.55	.27*	.010	.003		
535.45	.27*	.01	.003		
540.09	.28	.04	.004		
569.87	.30	1.21	.08	19.	2.
573.46	.30	.03	.01		
578.00	.30	.08	.02		
598.16	.32	.39	.04	19.	2.
617.84	.33	.18	.02		
656.41	.36	1.99	.16	20.	2.
660.66	.37*	.008	.004		
665.15	.38	.97	.06	18.	2.
675.22	.39	7.89	.58	19.	2.
687.3	.4	1.72	.15	23.	2.
700.9	.4	.64	.08	17.	4.
712.8	.4	.82	.11	19.	3.
740.9	.4	6.98	.55	23.	2.
764.7	.4	.03	.01		
771.7	.4*	.005	.003		
778.5	.4	.39	.03	26.	3.
804.1	.5	6.35	.46	20.	2.
820.9	.5	.03	.01		
836.6	.5	.04	.01		

*p levels or spurious

TABLE D-1 (CONTINUED)

E_0(eV)	ΔE	Γ_n^0(meV)	$\Delta\Gamma_n^0$	Γ_γ (meV)	$\Delta\Gamma_\gamma$
1640.35	.37	1.09	.12	25.	2.
1661.48	.37	2.80	.29	25.	4.
1677.73	.38	.61	.07		
1689.65	.38*	.04	.01		
1696.90	.38	.04	.01		
1704.97	.38	.06	.01		
1719.72	.39	.82	.07	17.	3.
1729.13	.39	.03	.01		
1740.2	.4	.14	.02		
1746.5	.4	.72	.07	23.	4.
1762.6	.4	2.43	.40	27.	4.
1767.1	.4*	.04	.02		
1785.4	.4	.05	.02		
1803.3	.4	2.00	.16	21.	3.
1811.9	.4	1.06	.14	20.	3.
1824.0	.4	1.94	.16	18.	3.
1848.6	.4	.13	.02		
1854.4	.4	1.04	.16	25.	3.
1861.9	.4	.95	.14	22.	3.
1897.1	.4*	.05	.02		
1899.9	.4	2.87	.32	29.	5.
1928.3	.4	.15	.02		
1931.1	.4	.22	.03		
1950.3	.4	2.88	.38	30.	4.
1971.2	.4	5.52	.52	25.	4.
1987.8	.4	.96	.11	18.	3.
2004.9	.4	.51	.07	22.	4.
2015.4	.4*	.02	.01		
2051.7	.5	.42	.07		
2055.5	.5*	.01	.01		
2061.9	.5	1.43	.18	17.	3.
2073.8	.5	.15	.04		
2079.0	.5	.20	.04		
2097.3	.5	.02	.01		
2116.9	.5	1.63	.13	20.	3.
2147.6	.5	1.92	.15	14.	4.
2158.5	.5*	.04	.01		
2162.9	.5	1.87	.15	26.	4.
2170.1	.5*	.06	.02		
2177.9	.5	1.59	.13	17.	3.
2196.9	.5	1.00	.11	17.	3.
2206.8	.5*	.04	.01		
2216.2	.5	.49	.04		
2222.0	.5	1.80	.19	27.	5.
2233.5	.5	.03	.01		
2270.9	.5	.59	.08		
2276.3	.6	.96	.10	24.	3.
2286.4	.6	5.44	.63	19.	5.
2307.2	.6*	.06	.02		
2320.9	.6	.09	.03		
2329.5	.6*	.04	.01		
2336.0	.6	2.28	.37	20.	4.
2344.4	.6	.09	.04		
2352.5	.6	.31	.06		
2353.7	.6	.29	.06		
2375.2	.6	2.42	.37	18.	3.
2382.8	.6	.04	.02		
2391.1	.6	.07	.02		
2418.5	.6	1.75	.18		
2427.4	.6*	.05	.04		
2434.6	.6*	.06	.04		
2439.8	.6	.21	.03		
2455.8	.6	3.53	.44		
2462.5	.6*	.07	.03		
2474.9	.6	.04	.02		
2491.8	.6	.13	.03		
2509.3	.6	6.29	.70		
2527.3	.6	.93	.12		
2557.1	.7	.07	.02		
2563.1	.7	6.12	.59		

*p levels or spurious

TABLE D-1 (CONTINUED)

E_0(eV)	ΔE	Γ_n^0(meV)	$\Delta\Gamma_n^0$	Γ_γ (meV)	$\Delta\Gamma_\gamma$
1640.35	.37	1.09	.12	25.	2.
1661.48	.37	2.80	.29	25.	4.
1677.73	.38	.61	.07		
1689.65	.38*	.04	.01		
1696.90	.38	.04	.01		
1704.97	.38	.06	.01		
1719.72	.39	.82	.07	17.	3.
1729.13	.39	.03	.01		
1740.2	.4	.14	.02		
1746.5	.4	.72	.07	23.	4.
1762.6	.4	2.43	.40	27.	4.
1767.1	.4*	.04	.02		
1785.4	.4	.05	.02		
1803.3	.4	2.00	.16	21.	3.
1811.9	.4	1.06	.14	20.	3.
1824.0	.4	1.94	.16	18.	3.
1848.6	.4	.13	.02		
1854.4	.4	1.04	.16	25.	3.
1861.9	.4	.95	.14	22.	3.
1897.1	.4*	.05	.02		
1899.9	.4	2.87	.32	29.	5.
1928.3	.4	.15	.02		
1931.1	.4	.22	.03		
1950.3	.4	2.88	.38	30.	4.
1971.2	.4	5.52	.52	25.	4.
1987.8	.4	.96	.11	18.	3.
2004.9	.4	.51	.07	22.	4.
2015.4	.4*	.02	.01		
2051.7	.5	.42	.07		
2055.5	.5*	.01	.01		
2061.9	.5	1.43	.18	17.	3.
2073.8	.5	.15	.04		
2079.0	.5	.20	.04		
2097.3	.5	.02	.01		
2116.9	.5	1.63	.13	20.	3.
2147.6	.5	1.92	.15	14.	4.
2158.5	.5*	.04	.01		
2162.9	.5	1.87	.15	26.	4.
2170.1	.5*	.06	.02		
2177.9	.5	1.59	.13	17.	3.
2196.9	.5	1.00	.11	17.	3.
2206.8	.5*	.04	.01		
2216.2	.5	.49	.04		
2222.0	.5	1.80	.19	27.	5.
2233.5	.5	.03	.01		
2270.9	.5	.59	.08		
2276.3	.6	.96	.10	24.	3.
2286.4	.6	5.44	.63	19.	5.
2307.2	.6*	.06	.02		
2320.9	.6	.09	.03		
2329.5	.6*	.04	.01		
2336.0	.6	2.28	.37	20.	4.
2344.4	.6	.09	.04		
2352.5	.6	.31	.06		
2353.7	.6	.29	.06		
2375.2	.6	2.42	.37	18.	3.
2382.8	.6	.04	.02		
2391.1	.6	.07	.02		
2418.5	.6	1.75	.18		
2427.4	.6*	.05	.04		
2434.6	.6*	.06	.04		
2439.8	.6	.21	.03		
2455.8	.6	3.53	.44		
2462.5	.6*	.07	.03		
2474.9	.6	.04	.02		
2491.8	.6	.13	.03		
2509.3	.6	6.29	.70		
2527.3	.6	.93	.12		
2557.1	.7	.07	.02		
2563.1	.7	6.12	.59		

*p levels or spurious

TABLE D-1 (CONTINUED)

E_0(eV)	ΔE	Γ_n^0(meV)	$\Delta\Gamma_n^0$	E_0(meV)	ΔE	Γ_n^0(meV)	$\Delta\Gamma_n^0$
2569.6	.7	1.18	.20	3039.7	.9	1.07	.09
2604.0	.7*	.03	.02	3050.2	.9	.09	.05
2612.5	.7	1.70	.20	3061.4	.9	.52	.05
2624.3	.7	.14	.04	3082.8	.9	.99	.11
2635.0	.7	3.12	.35	3103.6	.9	.03	.01
2655.5	.7	.09	.04	3109.2	.9	.39	.05
2663.4	.7	3.88	.39	3120.7	.9	.13	.04
2677.0	.7	.23	.04	3148.5	.9	3.30	.36
2688.4	.7	3.80	.39	3153.4	.9	3.47	.36
2713.0	.7	1.84	.23	3163.0	.9	.37	.07
2722.7	.7	.22	.04	3188.6	.9	1.33	.12
2733.2	.7	6.89	.57	3194.5	.9	.07	.05
2748.1	.7	.29	.06	3207.4	.9	1.59	.18
2773.6	.8	1.52	.25	3229.4	1.0	.30	.05
2792.9	.8	3.12	.36	3242.5	1.0	.25	.05
2803.4	.8*	.08	.02	3252.7	1.0	1.46	.14
2815.6	.8	.55	.08	3270.0	1.0	.45	.07
2832.9	.8	.70	.09	3295.7	1.0	7.11	.78
2838.7	.8	.03	.03	3307.2	1.0	.07	.07
2843.2	.8*	.03	.03	3317.6	1.0	.09	.05
2852.0	.8	3.93	.56	3331.8	1.0	.71	.10
2861.2	.8*	.15	.06	3342.9	1.0	2.94	.31
2870.4	.8*	.03	.01	3351.4	1.0	.31	.07
2883.9	.8	.08	.03	3383.5	1.0	1.20	.15
2895.9	.8	.04	.01	3409.5	1.0	.08	.03
2915.6	.8	.06	.02	3442.9	1.1	.34	.05
2932.0	.8*	.03	.02	3471.9	1.1	.31	.05
2948.6	.8	1.77	.18	3510.0	1.1	.08	.05
2956.5	.8	.81	.11	3521.8	1.1	1.79	.30
2966.2	.8	.26	.06	3544.2	1.1	.12	.05
2980.0	.8	.16	.04	3574.4	1.1	.28	.05
2988.0	.9	.68	.11	3594.4	1.1	.35	.07
3006.5	.9	.03	.01	3611.6	1.1	2.00	.25
3017.3	.9	.51	.05	3623.5	1.1	.20	.05
3027.3	.9	4.18	.45	3636.7	1.2	.13	.05

*p levels or spurious

TABLE D-1 (CONTINUED)

E_0(meV)	ΔE	Γ_n^0(meV)	$\Delta\Gamma_n^0$
3651.7	1.2	1.11	.13
3674.2	1.2	.20	.05
3692.7	1.2	.10	.07
3707.6	1.2	.08	.05
3716.0	1.2	.43	.07
3722.9	1.2	1.61	.33
3732.8	1.2	.79	.11
3745.2	1.2	.08	.05
3759.2	1.2	.13	.05
3786.4	1.2	.47	.08
3799.4	1.2	.08	.05
3820.5	1.2	.65	.10
3827.0	1.3	1.76	.27
3848.5	1.3	.19	.06
3868.8	1.3	1.05	.13
3883.4	1.3	.18	.05
3906.0	1.3	3.52	.48
3923.4	1.3	.14	.05
3931.5	1.3	.59	.10
3951.1	1.3	.16	.06
3961.4	1.3	.65	.10
3970.3	1.3	1.14	.14
3976.5	1.3	1.90	.27
3994.4	1.3	.57	.09
4007.6	1.4	.11	.06

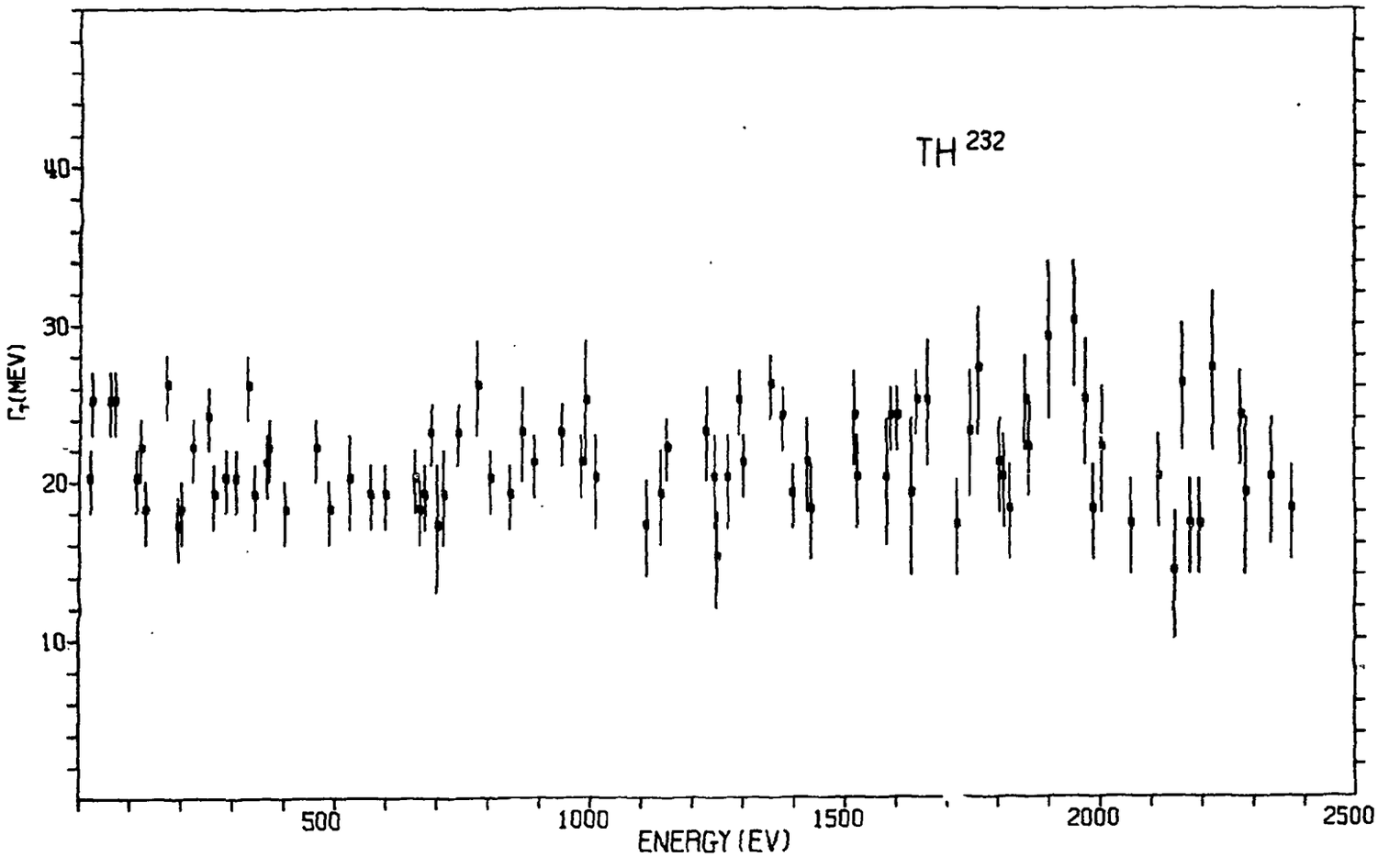

Figure D-3. The values of Γ_γ versus energy for 84 levels up to 2400 eV.

an average value of $\langle\Gamma_\gamma\rangle$ = [21.2±0.3 (statistical)±0.9 (systematic) meV] to be consistent with our data. We have assigned a systematic uncertainty of ±0.9 meV to account for the relative normalization of our data. We find no evidence for a quasiperiodic variation of Γ_γ with neutron energy. Figure D-4 shows the distribution of our Γ_γ values, with the histogram taken in intervals of 2 meV. The histogram can be suitably fit by a chi-squared function with 87 degrees of freedom, generated about a mean value of 21.2 meV. Our average value of 21.2 meV (0-2400 eV) compares with a value of $\langle\Gamma_\gamma\rangle$ = 20.5±3 meV obtained by Forman at Los Alamos, 20.9 meV obtained by Asghar (0-350 eV) and 21.6 meV (0-350 eV) obtained by Ribon at Saclay.

Our values of the total neutron width Γ_n in Table D-1 tend to be somewhat higher than the previous Columbia results of Garg et al. in the energy region above 1 keV. Figure D-5 shows $\Sigma g\Gamma_n^0$ versus E for ^{232}Th. The energy interval used in obtaining S_0 affords relatively complete level resolution. Our best choice of the strength function is $S_0=(0.84\pm0.08)\times10^{-4}$. Missing or spurious levels of small Γ_n have small effect on S_0. We are in good agreement with the recent Saclay results of Ribon [$S_0=(0.87\pm0.10)$] and Harwell results of Asghar (0.8±0.17) but are higher than the results of Garg (0.69±0.07).

By the application of the various statistical tests in a manner similar to ^{238}U (see section I.C), we attempted to assign spins to the observed resonances. We have indicated our spin assignments in Table D-1. The resulting s-wave population to 3 keV is in good agreement with all the statistical tests (Wigner distribution, Porter-Thomas distribution, Dyson-Mehta Δ, Cov(S_i,S_{i+1}), and F statistic). The stronger levels provided the framework for the choice of the weaker s-wave levels. The probability of another choice of the s-wave level population in ^{232}Th satisfying all the statistical tests is small. Figures D-6 and D-7 respectively show our comparison with the Porter-Thomas and Wigner distribution for our choice of the s-wave population in ^{232}Th.

E. Delayed Fission Following Gamma-Ray Emission in ^{235}U+n
(M. Derengowski, J. Felvinci, and E. Melkonian)

This experiment, which was performed in the spring of 1970 and which used the Nevis synchrocyclotron as a pulsed neutron source, has been described in previous reports to the NCSAC. The data have been analyzed and an isomeric fission state with a half-life of 7.0 2.2 nsec has been identified. This short-lived isomeric state has not been observed previously, although an isomeric state (or states) with half-lives ranging from 67 to 130 nsec has been reported. A longer lived state of at least 40 nsec is also required to fit our data, but the data are insensitive to the exact value.

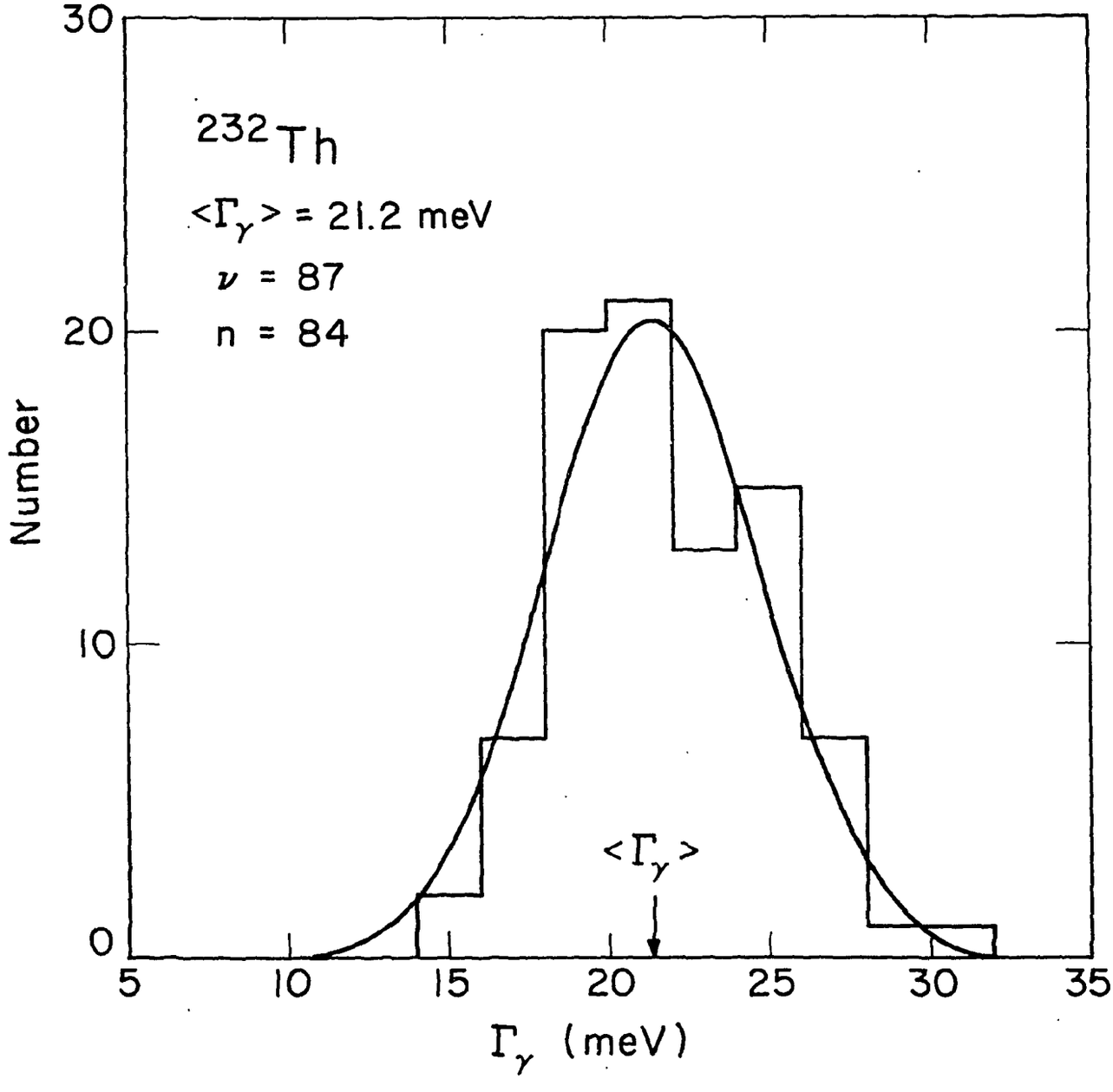

Figure D-4. The distribution of observed Γ_γ values in ^{232}Th taken in histogram intervals of 2 meV. The average $\langle\Gamma_\gamma\rangle$ is 21.2 meV. The curve is a chi-squared distribution with ν=87 degrees of freedom.

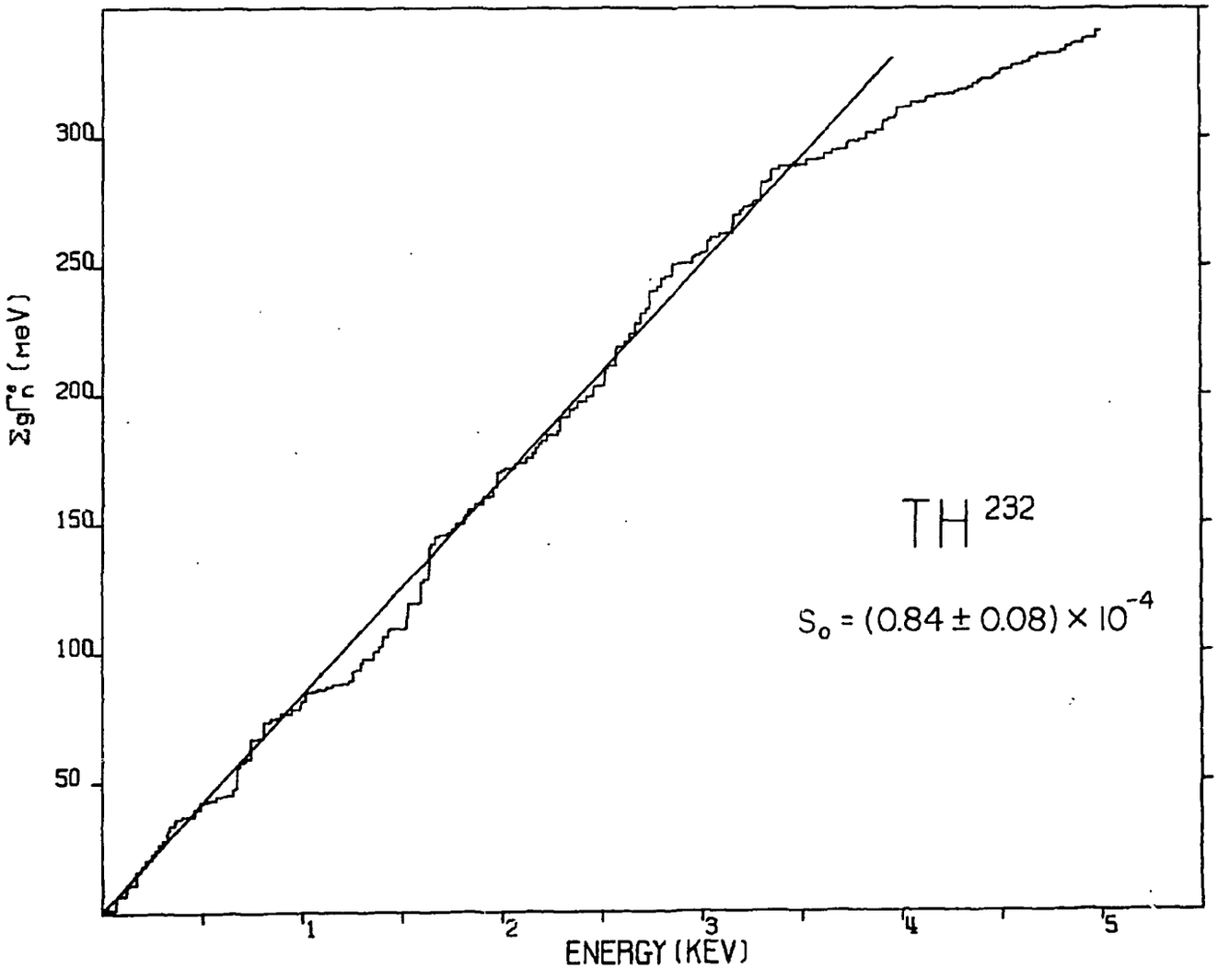

Figure D-5. The $\Sigma\Gamma_n^0$ versus E for ^{232}Th. The slope of the curve determines the s wave strength function. Our best choice is S_0=(0.84 0.08) 10^{-4}.

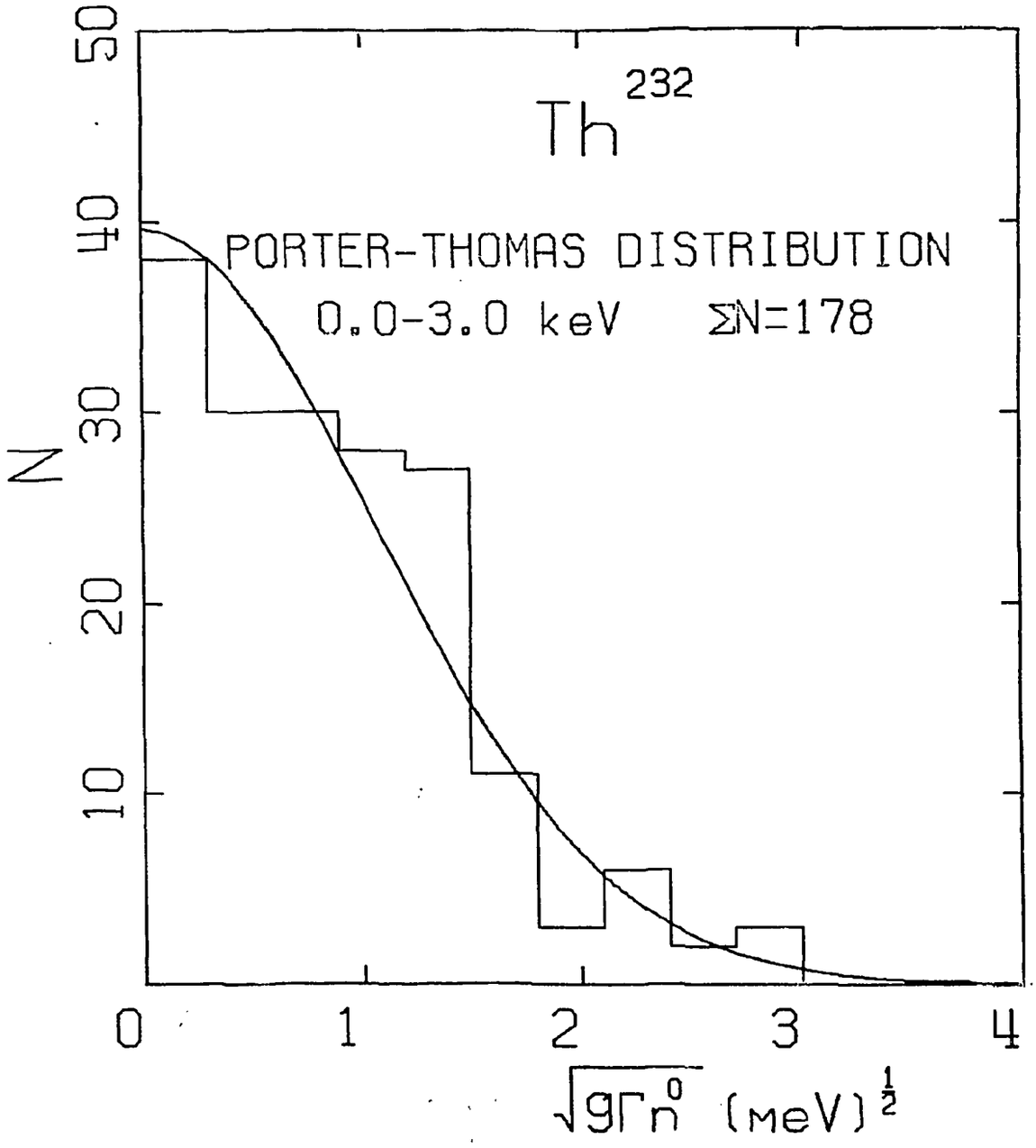

Figure D-6. Histogram of the reduced neutron widths $\sqrt{\Gamma_n^0}$ for our selection of the ℓ=0 population in ^{232}Th. The Porter-Thomas theory is represented by the smooth curve.

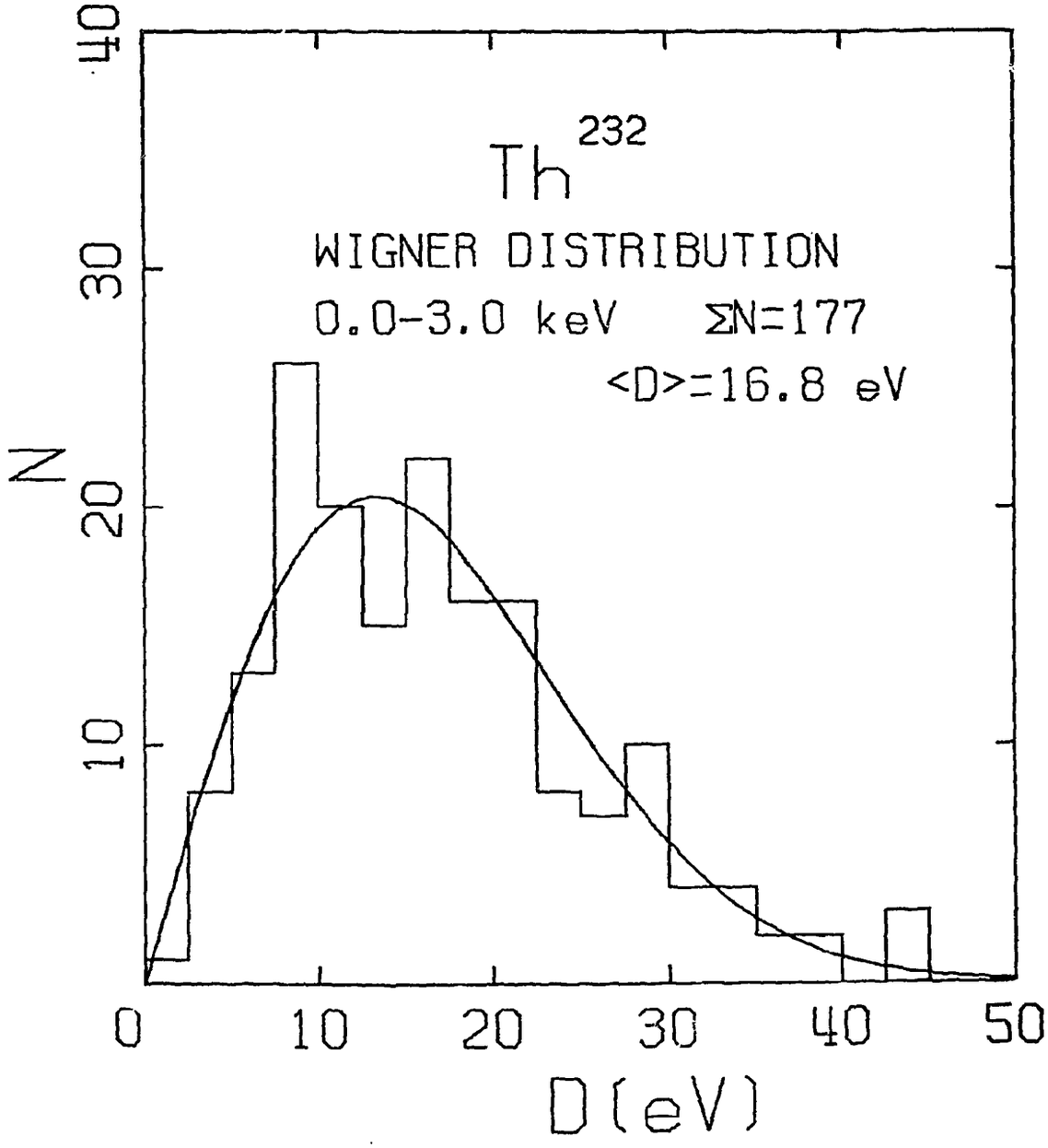

Figure D-7. Histogram of adjacent level spacings for the $\ell=0$ population in ^{232}Th. The Wigner distribution is given by the curve.

We estimate that at least 2% of all fissions go through the 7 nsec isomeric state. While this contribution is much higher than observed previously, it is consistent with the trend noted by others that the relative proportion of isomeric states increases with decreasing neutron energy. In our case, fissions were induced primarily by neutrons of a few eV, while other measurements were performed with neutrons in the keV and MeV ranges.

Figure E-1 shows the data used in this analysis together with the best fit curve obtained by a least squares fit using five functions, namely 1) a gaussian representing gammas associated with prompt fission and having a standard deviation of 3.0 nsec, corresponding to the time resolution; 2) a short lifetime exponential broadened by the gaussian resolution function, the actual lifetime being adjusted for best fit; 3) a similarly broadened long lifetime exponential arbitrarily set at 80 nsec; 4) a function representing the effect of detecting gamma rays produced by the capture or inelastic scattering of prompt fission neutrons; and 5) a constant background arising from chance coincidences. All but number 5 are shown in Figure E-2.

A paper is being submitted to Physical Review Letters.

F. Fission Cross Section of ^{235}U (J. Felvinci and E. Melkonian)

It is known that different sets of cross section data frequently differ by considerable amounts (up to 15%). This could be due to incorrect flux dependence, inadequate background corrections, and improper normalization. The peak cross sections in the major resonances are considerably different in the works of Michaudon et al.[1], Bowman et al.[2], Brown et al.[3], de Saussure et al.[4], and Brooks et al.[5]. We decided to undertake a critical examination of these discrepancies and of the possibility that experimental problems could cause them. This is quite important as possible differences in the width and height of the resonances will certainly affect the resonance parameters and thus the quantities calculated from them. Subtle effects due to selective pulse height discrimination in fission chambers or underestimating scattering

---

1. Michaudon, Derrier, Ribon, & Sanche, Nucl. Phys. 69, 545 (1965).
2. Bowman, Auchampough, Fultz, Moore, & Simpson, Conf. on Neutron Cross Sections & Technology, 1966, Washington DC, Vol. 2, p. 1004.
3. Brown, Berger, & Cramer, LA-3586, 1966.
4. de Saussure, Gwin, Weston, Ingle, Fullwood, & Hockenbury, ORNL TM-1804, 1967.
5. Brooks, Jolly, Schomberg, & Sowerby, AERE-M1670, 1966.

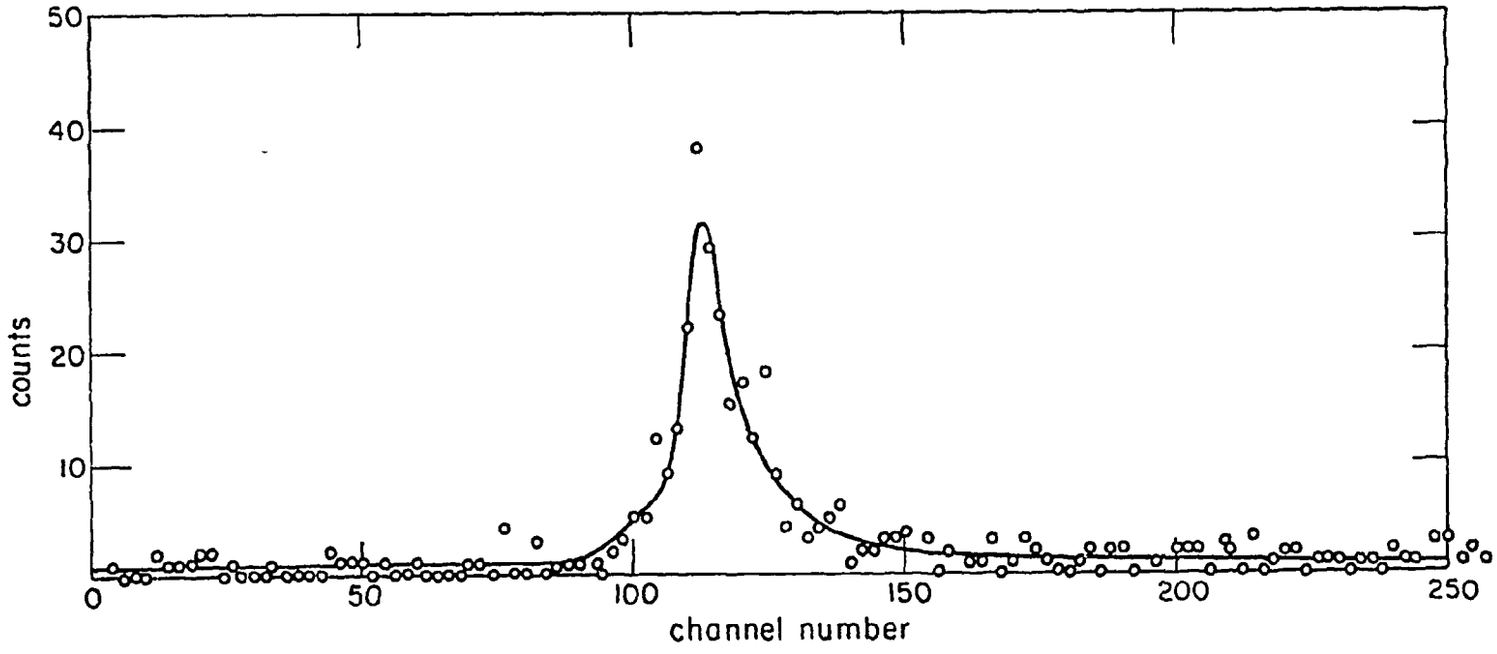

Figure E-1

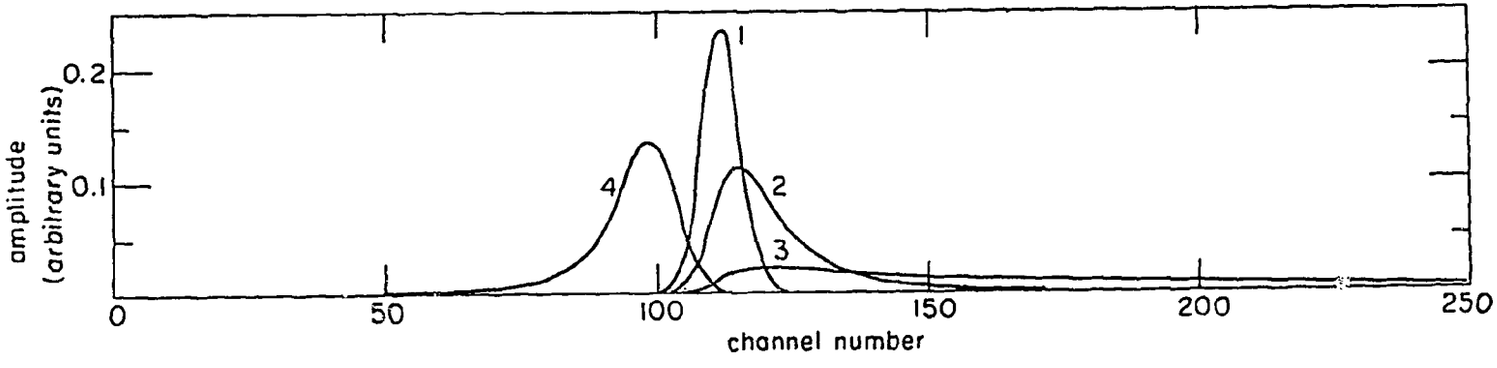

Figure E-2

contributions could all contribute to the discrepancies.

Areas for the resonances were calculated by means of shape analysis and are given in Table F-1. Comparison with some other existing sets of data is given. The analysis performed was of a single level nature and no multilevel fits were attempted at this time. It was noticed though that our data agreed rather well with other experimenters who applied single level analysis, but was rather different from equivalent multi-level values.

The errors given in Table F-1 include both statistical and fitting errors. Some results quoted in the literature appear not to include the errors due to fitting and thus are smaller than they should be.

Table F-2 shows a comparison between the fission integrals,

$$\int_{E_1}^{E_2} \sigma_f dE,$$

for our data and those of de Saussure et al.[6] Both sets are normalized to Deruytter's value of 237.1 eV b from 7.8 to 11.0 eV. These areas were calculated with the assumption that our flux varies as $\phi(t)dt=E^{0.60}dt$ from 1 eV to 10 keV. This variation was confirmed by other measurements during the same run and also by a Monte Carlo calculation performed to determine the flux emerging from the moderator. The background was taken to consist of two parts, one behaving as the flux and the other a constant.

Further work on the ^{235}U cross section is continuing; resonance integrals are going to be reported soon.

G. Fission Cross Section of ^{233}U (J. Felvinci & E. Melkonian)

Work on this isotope included the analysis of partial cross sections as reported in the earlier report and also in the Third Neutron Cross Section Technology Conference 1971. Work is continuing in this direction and also the analysis of the resonances is nearly complete and will be reported at the next meeting.

---

6. de Saussure et al., op. cit.

TABLE F-1

Resonance Parameters of ^{235}U

E(eV)*	Γ(mV)	Present Results $\sigma_0\Gamma_f$(eV b)	Michaudon[a] $\sigma_0\Gamma_f$(eV b)	Blons[b] $\sigma_0\Gamma_f$(eV b)	Cao[c] $\sigma_0\Gamma_f$(eV b)
1.13	140	14.5±0.4			
2.03	50	1.0±0.2	1.03±0.07		
2.92	150	1.2±0.3			
3.15	190	8.7±0.4	8.1±0.80		
3.61	100	9.6±0.3	8.65±0.90		
4.85	40	1.0±0.2	1.51±0.15		
5.52	300	3.4±0.5			
5.90	300	2.8±0.5			
6.20	200	9.3±0.6			
6.39	50	10.2±0.4	14±1.5		10.1±0.2
7.08	100	10.7±0.5	10±1		9.8±0.1
8.46	40	0.5±0.4			
8.79	150	115.0±1.4	105.5±5		109.9±0.8
9.30	200	18.8±0.8	17±4	20±2	19.9±0.4
9.70	70	1.9±0.4		3	
10.21	95	4.1±0.5	5±1	4.7±0.5	3.9±0.1
11.67	43	7.1±0.5	5.95±0.50	7.5±1	7.0±0.1
12.40	80	50.5±1.1	47±3	50.0±3	54.6±0.7
12.90	83	1.4±0.4	2.9±0.5	2.7±0.5	3.5±0.1
13.31	40	1.0±0.4	3.3±0.6	2.6±1	
13.73	40	2.3±0.6	2.4	3	1.6±0.5
14.03	500	38.1±1.6	27±5	31±6	
14.51	45	2.0±0.5	5±1	2.5±0.5	2.9±0.1

* ±0.02 eV (throughout Table F-1)

a. Michaudon et al., op. cit.

b. Blons, Derrier, Michaudon, Proc. of 3rd Conf. on Neutron Cross Sections & Technology, Knoxville 1971. Conf-710301, Vol. 2, p. 829.

c. Cao, Migneco, Theobald, Wartena, & Winter, Neutron Cross Sections & Technology, NBS-229, Washington DC 1968, p. 481.

TABLE F-1 (CONTINUED)

E(eV)	Γ(mV)	Present Results $\sigma_0\Gamma_f$(eV b)	Michaudon $\sigma_0\Gamma_f$(eV b)	Blons $\sigma_0\Gamma_f$(eV b)	Cao $\sigma_0\Gamma_f$(eV b)
15.42	80	8.0±0.6	10.5±1	10.0±1	11.4±0.2
16.09	55	7.9±0.6	10±1	8.7±1	9.8±0.2
16.69	138	12.8±0.8	13.6±1.5	14.2±1	15.2±0.3
17.06	40	0.6±0.4			
18.07	160	20.2±1.0	14.5±2.5	18.5±2	18.6±1.6
18.66	80	2.5±0.6			
18.97	80	8.4±0.9		2±0.5	
19.31	105	117.2±2.0	103±5	121.3±3	118.8±1.0
20.16	40	3.6±0.5	5±1.5	5.2±1	
20.63	90	6.7±0.7	4.35±0.3	6.3±0.5	6.9±0.2
21.07	70	34.0±1.0	29±1.5	34.6±1	34.7±0.4
22.54	40	0.5±0.5			
22.97	90	13.5±0.9	11.7±0.6	13.6±0.5	14.2±0.2
23.44	80	15.3±1.0	8±1	7.0±0.5	6.0±0.2
23.69	60	19.3±1.1	22±4	30±5	
24.32	200	12.3±1.5	8±1.5	7.0±1	
24.47	50	0.9±1.0		5	
24.89	600	18.8±2.0		8	
25.28	100	5.6±1.1		44	
25.59	250	22.0±1.4			
26.50	150	16.1±1.1		22.0±2	
26.83	100	2.6±0.8		4.6	
27.18	50	1.9±0.6	4±1.5	3.4±1	
27.83	110	18.3±1.1	16.5±1	22.4±2	17.8±0.1
28.37	70	3.4±0.7	5±1	5.6±0.5	5.8±0.1
29.67	73	2.0±0.6	3±0.6	3.55±0.5	3.3±0.1
30.63	200	6.2±1.1	4.6±0.9	6.5±1	6.0±0.2
30.87	60	5.8±0.9	6.2±0.7	7.7±0.6	7.1±0.2
32.09	130	40.7±1.6	36±4	45±2	41.8±0.3
33.54	80	28.2±1.4	24.5±3.7	28.2±2	27.1±0.7

TABLE F-1 (CONTINUED)

E(eV)	Γ(mV)	Present Results $\sigma_0\Gamma_f$(eV b)	Michaudon $\sigma_0\Gamma_f$(eV b)	Blons $\sigma_0\Gamma_f$(eV b)	Cao $\sigma_0\Gamma_f$(eV b)
34.40	130	43.4±1.8	33±5	39.0±2	37.3 0.6
34.85	110	26.6±2.0	15±5	24.4±2	25.5 1.2
35.21	170	105.1±2.9	102±20	124.0±4	118.3 2.0
35.77	250	7.3±1.5			
38.28	80	3.9±0.9	12±4	10.7±2	
39.45	95	40.0±1.7	41±4	47.4±1	47.3 0.3
39.88	40	3.2±1.0	6	6.7±0.5	
40.65	52	5.4±1.0	10	11.5±1	
41.30	120	4.6±1.4	8	7	
41.51	60	4.8±1.4	4	5.0	
41.91	90	10.7±1.3	19±2	13.3±1	10.5 0.2
42.28	40	3.2±1.0		7.1	
42.76	64	0.8±1.0	3±0.5	2.5±0.2	2.3 0.1
43.47	66	5.1±1.1	8	7.2±0.5	6.5 0.1
44.10	90	7.5±1.3	10±3	11.0	
44.66	220	18.8±1.9		21.0	
45.04	40	5.3±1.3		13.	

TABLE F-2

^{235}U Fission Integrals (normalized to Deruytter)

Energy Interval (eV)	de Saussure[a]	Our Results
0.50-0.70	13.47	13.2
0.70-1.0	17.05	17.1
1.0 - 1.8	29.19	28.2
1.8 - 5.0	50.70	45.2
5.0 - 7.4	62.30	61.6
7.4 - 10.0	219.6	221.2
10.0 - 15.0	216.3	216.5
15.0 - 20.5	316.3	329
20.5 - 33.0	447.8	481
33.0 - 41.0	497.1	514
41.0 - 60.0	918.4	970
60.0 - 100.0	975.5	1044
100.0 - 200.0	2097.4	2325
200.0 - 300.0	2085.3	2150
300.0 - 1000.0	8138.5	8560

a. de Saussure et al., op. cit.

GULF RADIATION TECHNOLOGY
A Division of Gulf Energy and Environmental Systems
San Diego, California

A. NEUTRON CROSS SECTIONS

1. Gamma-Ray Production Cross Sections for Discrete and Continuum Gamma-Rays from Fe and Aℓ (V. J. Orphan, C. G. Hoot, Joseph John and M. P. Fricke)

The analysis of (n, xγ) cross sections for Fe and Aℓ measured using an electron LINAC pulsed neutron source and an 80-cm^3 Ge(Li) detector has been completed.[1] These data span, continuously, the full neutron energy range $0.86 \leq E_n \leq 16.7$ MeV. Gamma-ray production cross sections have been determined for 13 principal gamma-rays from Fe(n, xγ) reactions and 9 principal gamma rays from ^{27}Aℓ(n, xγ) reactions using 20 neutron energy groups. Cross sections were determined for an additional 16 discrete gamma rays from Fe and 22 discrete gamma rays from Aℓ using 10 neutron energy groups to span the range 0.86 to 16.7 MeV. High-neutron-energy resolution (~ 10 keV at 1 MeV) results for some lines were obtained from the same data and have been illustrated in previous NCSAC contributions.

The gamma-ray spectra for the 10 neutron energy groups were also unfolded to obtain gamma-ray production cross sections for the sum of both discrete and continuum gamma rays. The latter are weak and/or broad, unresolved gamma rays which are not accounted for in an analysis for discrete gamma-ray peak areas. These summed results are grouped in ~ 240-keV-wide gamma-ray energy bins. As a test of the unfolding procedure the spectra for neutron energies less than ~ 5 MeV, where continuum gamma-rays are negligible, were also unfolded. Confidence in the unfolded data is enhanced by the reasonably good agreement obtained in this region between cross sections from the unfolded data and those from the discrete gamma-ray analysis. The gamma-ray production cross section for the sum of discrete and continuum gamma rays is given in Tables A-1 and A-2 for Fe and Aℓ, respectively.

---

[1] V. J. Orphan and C. G. Hoot, "Gamma-Ray Production Cross Sections for Iron and Aluminum," Gulf Radiation Technology Report Gulf-RT-A10743, June 21, 1971 (to be published).

Table A-1

GAMMA-RAY PRODUCTION CROSS SECTIONS (mb/sr) AT 125° FROM NEUTRON REACTIONS WITH NATURAL IRON (LINES + CONTINUUM)

Gamma-Ray Energy Interval (keV)	NEUTRON ENERGY INTERVAL (MeV)												
	0.86-1.02	1.02-1.32	1.32-1.72	1.72-2.14	2.14-2.56	2.56-3.06	3.06-4.10	4.10-5.15	5.15-6.15	6.15-7.71	7.71-9.78	9.78-12.56	12.56-16.74
469- 708									7.3	13.2	24.6	28.7	23.0
708- 946	37.8	47.8	62.7	68.2	85.0	82.6	92.2	91.2	113.1	96.7	91.2	84.0	62.7
946-1185							1.5	16.3	31.0	33.0	28.0	28.1	31.1
1185-1424			2.6	3.6	6.6	13.9	17.4	31.4	54.6	59.9	68.7	79.4	67.0
1424-1663								8.7	18.0	22.2	22.3	22.8	20.7
1663-1902						10.0	11.1	15.4	21.9	24.8	22.2	24.6	25.6
1902-2141							9.3	14.8	17.5	19.9	21.0	21.3	15.3
2141-2380							3.9	3.4	9.0	13.0	10.3	13.9	12.0
2380-2619							4.6	9.4	11.4	12.4	14.0	15.2	10.1
2619-2858							0.9	5.9	8.2	10.5	10.6	9.9	10.2
2858-3097								3.3	6.7	7.1	7.2	11.1	8.1
3097-3336								3.7	6.8	6.2	7.1	6.9	6.9
3336-3575							1.3	3.6	5.8	6.9	8.8	10.0	6.7
3575-3814							1.1	6.0	6.5	7.7	8.5	9.3	7.4
3814-4053								0.3	3.6	3.0	2.1	5.4	4.8
4053-4291								0.3	2.6	3.2	3.4	3.7	4.1
4291-4530											1.5	3.4	2.9
4530-4769									0.5	1.2	0.3	2.7	2.9
4769-5008									0.1	0.9	1.0	2.6	2.5
5008-5247										0.1	1.7	3.4	2.5
5247-5486										1.2	0.7	2.6	2.2
5486-5725										1.0	1.4	2.6	2.5
5725-5964										0.5	1.5	2.3	2.2
5964-6203												1.1	2.4
6203-6442											1.1	2.1	1.8
6442-6681											0.5	2.5	2.1
6681-6920											0.9	1.7	1.7
6920-7159												1.0	1.8
7159-7398											0.5	1.6	1.5
7398-7637											0.7	0.5	1.9
7637-7875											0.7	2.9	2.3
Total	37.8	47.8	65.3	71.8	91.6	106.5	143.3	213.7	324.6	344.6	362.5	407.3	348.9

Table A-2

GAMMA-RAY PRODUCTION CROSS SECTIONS (mb/sr) AT 125° FROM NEUTRON REACTIONS WITH ALUMINUM (LINES + CONTINUUM)

Gamma-Ray Energy Interval (keV)	NEUTRON ENERGY INTERVAL (MeV)												
	0.885-1.018	1.018-1.318	1.318-1.725	1.725-2.137	2.137-2.558	2.558-3.059	3.06-4.10	4.10-5.15	5.15-6.15	6.15-7.71	7.71-9.78	9.78-12.56	12.56-16.74
469- 708										2.0	4.8	9.4	6.7
708- 946	0.14	7.3	11.9	7.9	6.3	6.4	10.4	11.9	20.3	19.1	17.4	15.8	10.0
946-1185		7.8	11.5	14.2	13.7	14.3	16.8	17.1	19.5	21.9	19.2	18.0	15.7
1185-1424									4.8	4.5	5.4	6.7	3.1
1424-1663								0.5	3.4	4.8	3.9	6.4	7.4
1663-1902						3.5	6.0	6.1	5.2	5.1	5.6	6.1	14.2
1902-2141								0.1	4.1	4.8	5.4	6.5	8.8
2141-2380					5.9	11.9	15.7	15.0	20.8	21.9	20.7	21.9	15.4
2380-2619									4.1	6.9	8.0	7.6	7.5
2619-2858							1.8	2.7	1.8	2.4	2.7	3.8	4.3
2858-3097							7.3	13.3	12.3	14.3	12.2	12.2	9.0
3097-3336								0.6	5.0	7.9	8.0	8.2	6.7
3336-3575								0.5	1.5	2.2	2.5	2.9	3.1
3575-3814									0.7	1.7	2.2	2.6	1.5
3814-4053								1.0	2.0	2.1	3.1	4.1	3.2
4053-4291									1.6	2.6	2.7	3.3	3.6
4291-4530								0.8	0.7	0.9	1.8	2.0	1.8
4530-4769								1.1	2.2	2.2	2.2	2.4	1.8
4769-5008									0.9	1.6	2.0	2.2	1.7
5008-5247									0.5	1.5	2.5	2.6	2.0
5247-5486									0.3	1.7	2.2	2.6	2.1
5486-5725									0.08	1.0	1.5	1.9	1.8
5725-5964									0.06	1.1	1.6	1.7	1.2
5964-6203										0.5	1.0	1.4	0.8
6203-6442										0.4	1.2	1.3	1.0
6442-6681										0.2	1.6	2.6	1.6
6681-6920										0.1	0.8	1.5	1.7
6920-7159										0.05	0.6	1.0	1.1
7159-7398										0.09	0.6	1.0	0.6
7398-7637										0.09	0.7	1.6	1.0
7637-7875											0.7	1.8	1.4
Total	0.14	15.1	23.4	22.1	25.9	36.1	58.0	70.7	111.8	135.6	144.8	163.1	140.0

The present results have been compared with the gamma-ray production cross sections from the latest ENDF/B evaluations for Fe[2] and Aℓ.[3] The ENDF/B cross sections were prepared in the group structure of our experiment using the code LAPHANO.[4] The evaluated Aℓ data for three different neutron energy intervals are compared with the experimental results (including continuum contributions) in Figs. A-1 to A-3. At higher neutron energies the evaluated Aℓ gamma-ray production cross sections include contributions from particle decay to unknown levels which were obtained using a statistical-model treatment.[3] The agreement between the measured and evaluted total gamma-ray production cross sections (for all gamma-ray energies) is within ~ 15% over the full energy range ~ 7 to 17 MeV. At lower energies, where many of the gamma-ray transitions can be deduced from known level-excitation functions and gamma-ray branching ratios, the agreement with the evaluated gamma-ray data of MAT 4135[3] is excellent. For example, the total (n, xγ) cross sections in the group 4.10 - 5.15 MeV agree within ~ 1%.

The present experimental results for Fe are compared with the gamma-ray production cross section from MAT 1124[2] in Figs. A-4 and A-5 for the neutron intervals near 7 MeV and 15 MeV, respectively. As is evident in Figs. A-4 and A-5, the present experimental results are quite different from those obtained from the recent iron evaluation. Note that in the vicinity of 15 MeV the present results yield a total gamma-ray production cross section which is nearly a factor of two higher than the MAT 1124 data. This is likely due to the fact that the nuclear-model calculations made[2] for MAT 1124 neglected contributions from (n, n') to states above 9-MeV excitation energy.

The total gamma-ray production cross sections for Fe and Aℓ as a function of neutron energy are given in Fig. A-6. A smooth curve connects the present data points which represent the total gamma-ray

---

[2] S. K. Penny and W. E. Kinney, "A Re-Evaluation of Natural Iron Neutron and Gamma-Ray Production Cross Sections," Oak Ridge National Laboratory Report ORNL-4617 (April 1971).

[3] P. G. Young and D. G. Foster, ENDF/B Evaluation for Aluminum, MAT 4135, April 1971.

[4] D. J. Dudziak, Los Alamos Scientific Laboratory Report LA-4750-MS (to be published).

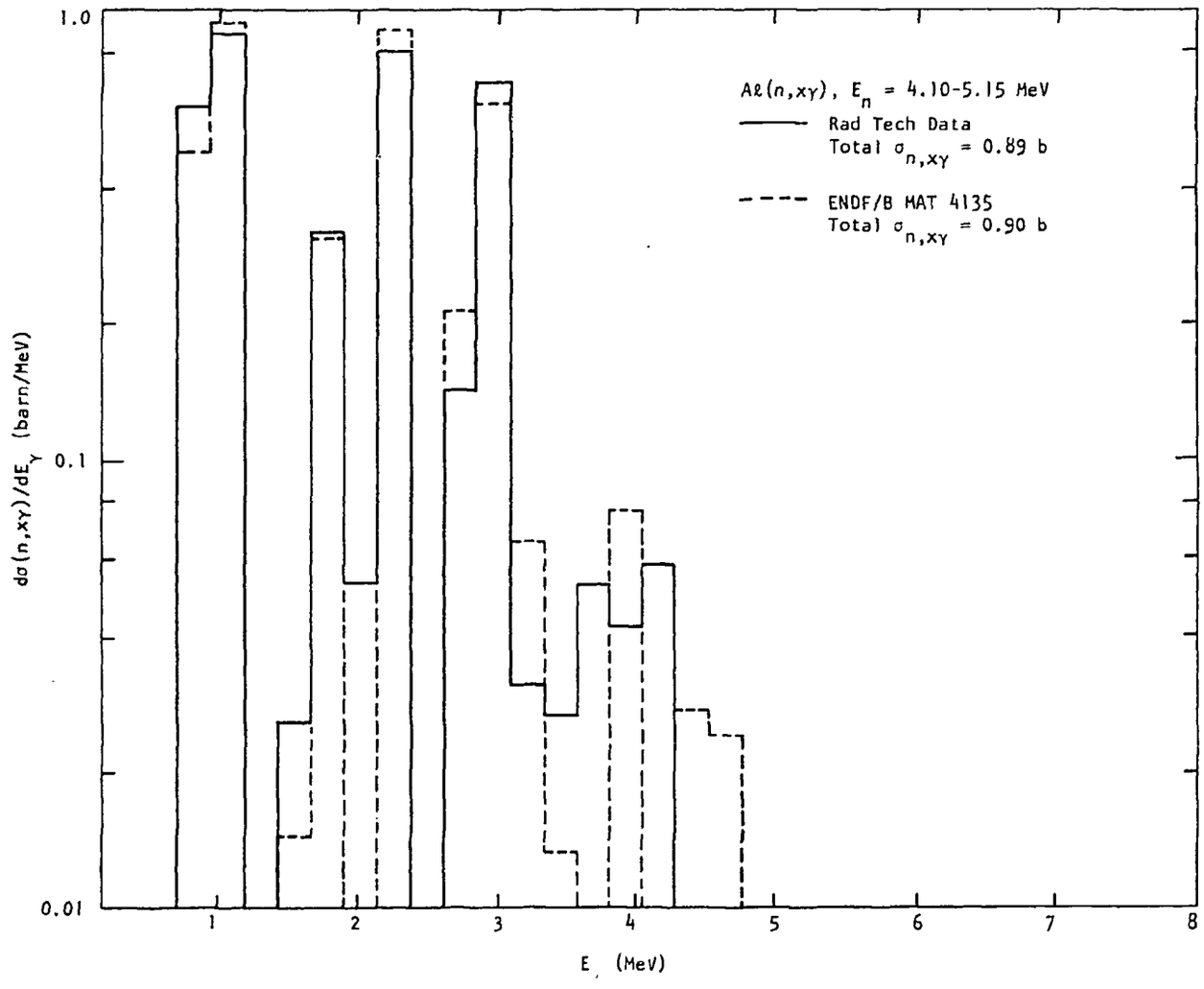

Fig. A-1.. Measured Aℓ(n, xγ) cross section versus data of MAT 4135

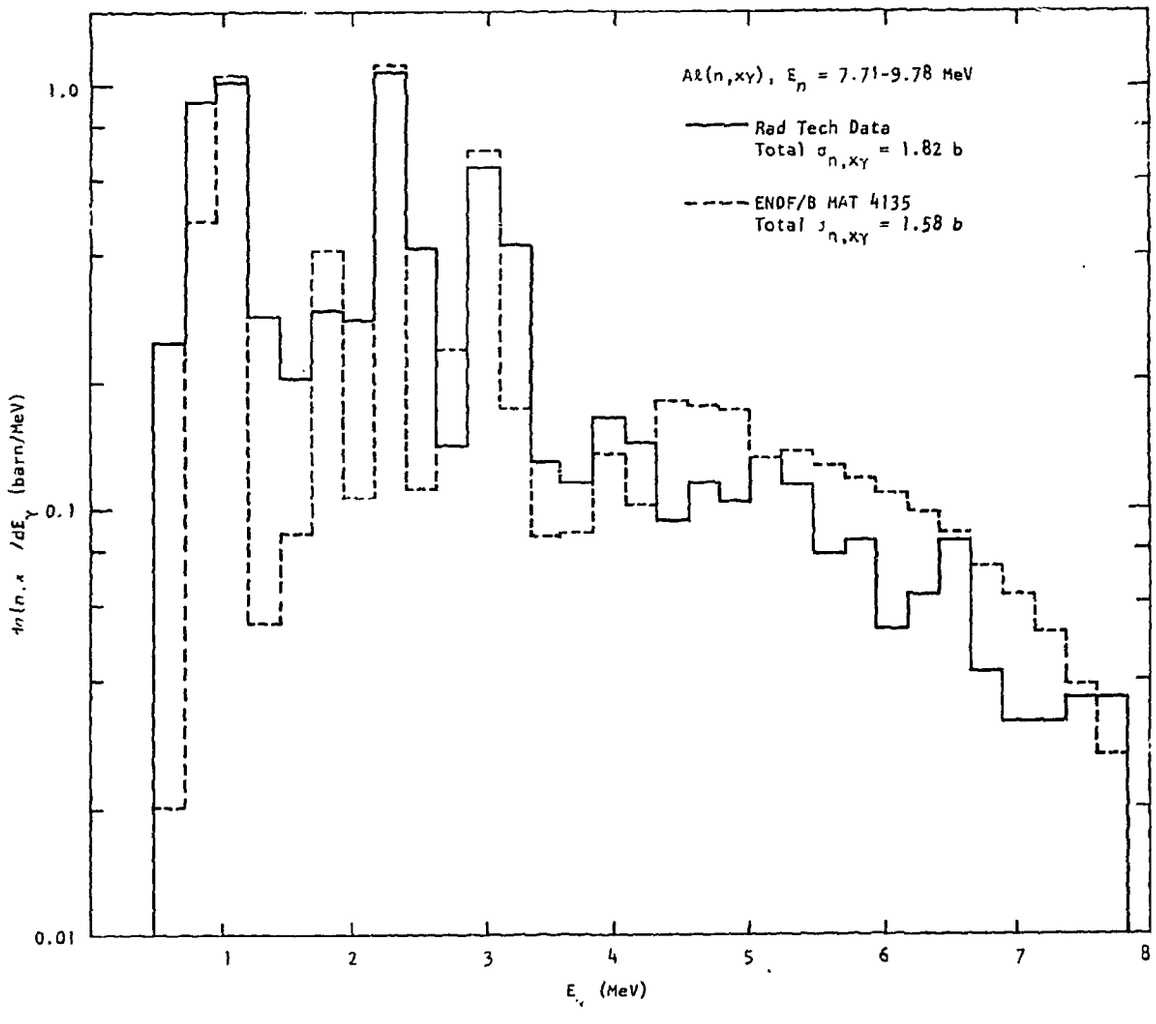

Fig. A-2. Measured Aℓ(n, xγ) cross section versus data of MAT 4135

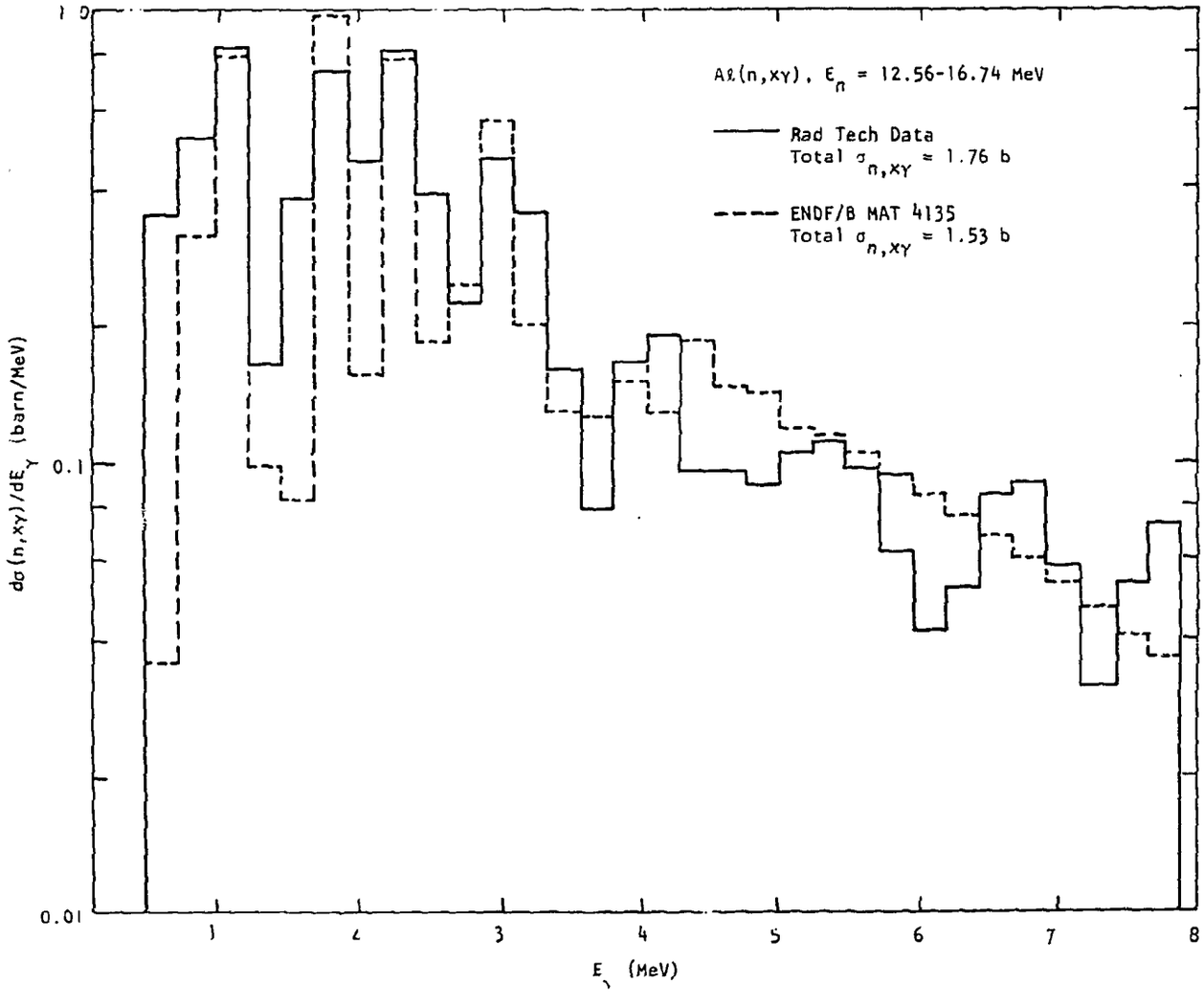

Fig. A-3. Measured Aℓ(n, xγ) cross section versus data of MAT 4135

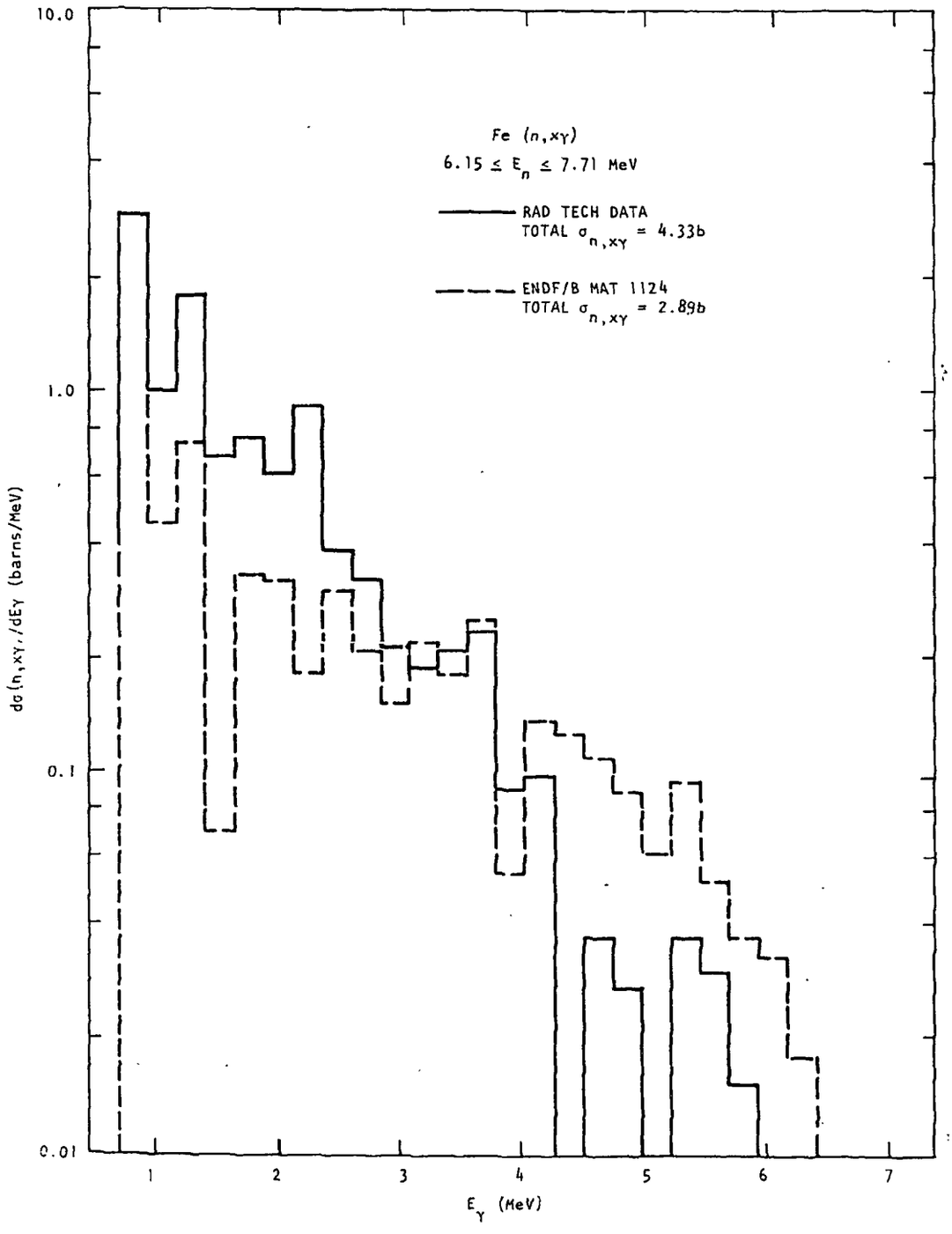

Fig. A-4. Measured and evaluated gamma-ray spectra from iron.

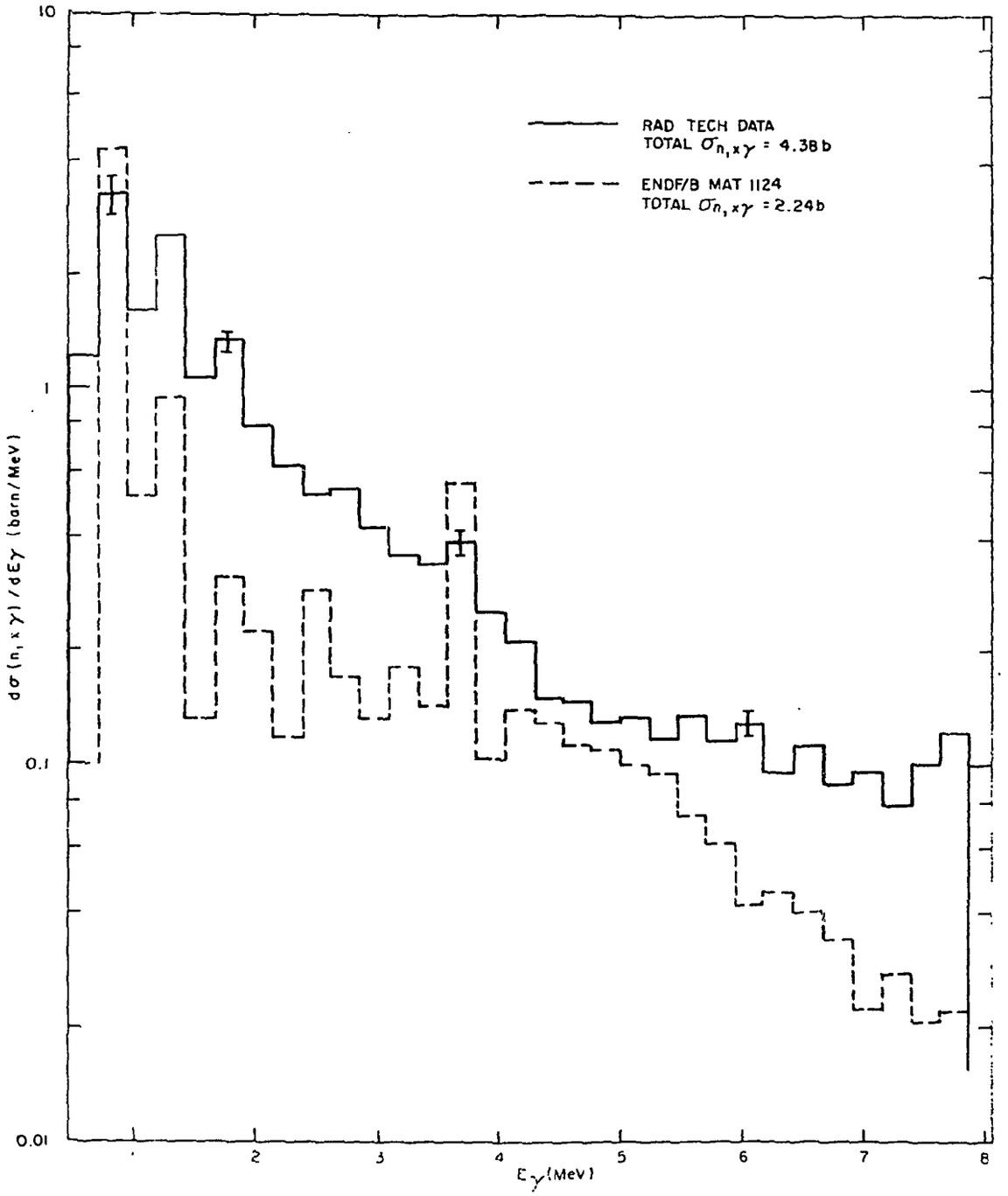

Fig. A-5. Measured and calculated gamma-ray spectrum from iron at a neutron energy near 15 MeV.

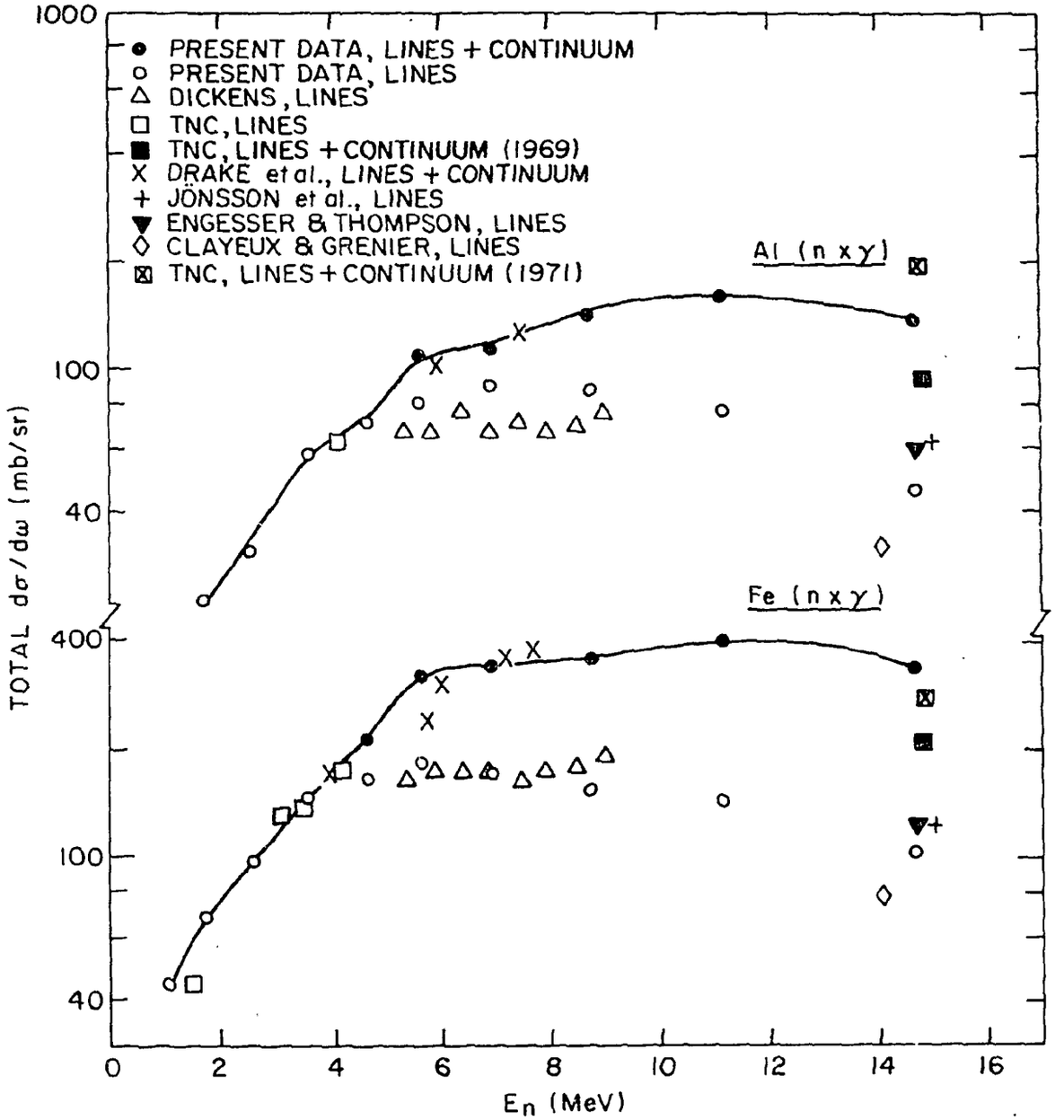

Fig. A-6. Present data (lines and total) compared to previous measurements. The cross sections shown are summed over all gamma-ray energies.

production cross section for discrete-plus-continuum (where present) gamma rays. Note that for both Fe and Aℓ the total gamma-ray production cross section obtained from the discrete-line cross sections is in good agreement with the discrete-line measurements of Dickens and Perey[5] and the results of Buchanan[6] (labeled TNC). In the vicinity of 15 MeV, the present discrete-line results for both Fe and Aℓ are lower than the data of Engesser and Thompson[7] and of Jönsson et al.[8] and Nyberg et al.[9] but are higher than the results of Clayeux and Greneir.[10] In addition, the present results for the sum of lines and continuum near 15 MeV are significantly higher (by a factor of 1.65 for Fe and 1.95 for Aℓ) than similar results reported in a 1969 TNC compilation.[6] However, a recent revision of the TNC compilation[11] contains new TNC results (labeled 1971 in Fig. A-6) which improve the agreement with the present data for Fe (the ratio of present value to the TNC value is 1.27) but which for Aℓ are more than a factor of two higher than the 1969 TNC values and only slightly improve the agreement with the present data (the ratio of the present value of the TNC value is 0.70).

---

[5] J. K. Dickens and F. G. Perey, ORNL-4592, Oak Ridge National Laboratory (September 1970).

[6] P. S. Buchanan, "A Compilation of Cross Sections and Angular Distributions of Gamma Rays Produced by Neutron Bombardment of Various Nuclei," Report No. ORO 2791-28, Texas Nuclear Corporation (1969).

[7] F. C. Engesser and W. E. Thompson, J. Nucl. Energy 21, 487 (1967).

[8] B. Jönsson et al., Arkiv für Fysik 39, 20 (1968) 295-311.

[9] K. Nyberg, B. Jönsson, and I. Bergqvist, private communication.

[10] G. Clayeux and G. Grenier, "Spectres de Renvoi des Gammas Produits par des Neutrons de 14.1 MeV," Report No. CEA-R-3807, CEN-Saclay (1969).

[11] P.S. Buchanan, D. O. Nellis, and W. E. Tucker, "A Compilation of Cross Sections and Angular Distributions of Gamma Rays Produced by Neutron Bombardment of Various Nuclei," Report No. ORO-2791-32, Texas Nuclear Corporation (1971).

For lower neutron energies, the present total gamma-ray production cross sections from the sum of both line and continuum gamma rays are in good agreement with the data of Drake et al.[12] obtained by unfolding NaI spectra. The inadvertent inclusion of "continuum" gamma rays in the low-resolution NaI measurements of Drake et al. may explain why such measurements of the cross sections for discrete lines are systematically higher than those reported from Ge(Li) measurements.[5] The present results show that the continuum contribution to the total gamma-ray production cross section near 15 MeV is approximately 70% for both Aℓ and Fe. These results demonstrate the great importance of including such continuum contributions in gamma-ray production cross sections used for radiation transport applications. (This work pertinent to request Nos. 63, 103, 104 and 105 in NCSAC-35.)

2. Measurements of the $^{10}B(n,\alpha)$ Cross Sections (S. Friesenhahn and A. Carlson)

The program to measure the $^{10}B(n,\alpha_0)^7Li$ and $^{10}B(n,\alpha_1\gamma)^7Li$ cross sections relative to the hydrogen scattering cross section has reached the detector testing stage. Flux measurements from 1 keV to 1 MeV using hydrogen and methane filled proportional counters have been made. A four-parameter computer based data-acquisition system is being used to measure the neutron time of flight, low-gain pulse height, high gain pulse height and rise time. The "low-gain" and "high-gain" pulse-height parameters allow the digitization of the pulse amplitude over a very wide dynamic range, thus allowing a large energy overlap between the hydrogen (low-energy) and methane (high-energy) data. The rise-time parameter is used for gamma ray discrimination.

Two very large ion chambers containing self-supporting films are in operation. Each of the two gridded ion chambers contain 11 plates, 10" x 10" in size. For one of the chambers the plates were formed using a newly developed technique which allows the dispersal of the active material (^{10}B) in the form of a colloid in a thin plastic substrate. The other chamber is identical except for the replacement of ^{10}B by C and will be used for background determinations. The ion chambers are currently undergoing time-of-flight checks using the four-parameter system to record time of flight, the pulse height from each side of the plates and the sum pulse height.

---

[12] D. M. Drake et al., Nucl. Sci. Eng. 40, 294 (1970).

An 80-cc Ge(Li) system is being used to observe the 478-keV gamma rays originating in a thin ^{10}B slab from the $^{10}B(n,\alpha\gamma)^{7}Li$ reaction and has achieved a 3.5-keV energy resolution under LINAC experimental conditions. The Ge(Li) data will be used in conjunction with the flux data to obtain the neutron energy dependence of the alpha particle branching ratio. (This work pertinent to request Nos. 28 and 29 in NCSAC-35.)

3. Measurement of Isomeric Gamma Rays from Fission for Times Less Than One Microsecond After Fission (R. E. Sund, V. V. Verbinski and H. Weber)

Measurements have been made on the delayed gamma rays from the thermal-neutron fission of ^{235}U and ^{239}Pu for times up to 1 μsec after fission. Fission events were detected with a surface barrier diode, and gamma rays were detected with a Ge(Li) detector.

The preliminary results for the energies, half-lives, and intensities of the observed, resolved gamma rays are shown in Tables A-3 and A-4. Many of the peaks were previously observed in the Livermore Cf results,[13] but a number of gamma rays observed in the present results for ^{235}U and ^{239}Pu, in particular, the photopeaks between the 614- and 1151-keV peaks, were not observed in the previous Cf data. These differences are likely due to the large differences in the mass-yield curves, as well as to the differences in the Z distribution for a given mass number. The integrated yield over all times for the peaks shown in Table A-3 for ^{235}U and Table A-4 for ^{239}Pu is ~ 0.13 and ~ 0.12 MeV/fission, respectively. The results in Tables A-3 and A-4 do not include peaks with multiple half-lives or gamma rays in the continuum. The delayed gamma-ray energy per fission in the peaks in this time region is significantly higher than observed in the Livermore Cf results for resolved lines, even without including the multiple half-life lines in the present results.

Data analysis is presently underway on the continuum of gamma rays. The peaks in the raw spectra are removed from the spectra, and then the corresponding Compton events are subtracted. The resulting

---

[13] W. John, F. W. Guy, and J. J. Wesolowski, Phys. Rev. C2, 1451 (1970).

Table A-3

PRELIMINARY RESULTS OF RESOLVED LINES FOR ^{235}U FISSION-PRODUCT ISOMERS

E (keV)	Half-Life (nsec)	±Δ (%)	Total Intensity (γ/Fission) (10^{-3})	±Δ (%)	E (keV)	Half-Life (nsec)	±Δ (%)	Total Intensity (γ/Fission) (10^{-3})	±Δ (%)
109.1	11.9	7	9.52	7	461.2	161.0	14	0.616	15
115.3	175.0	3	10.3	3	522.4	382.0	11	2.12	12
125.0	81.6	12	2.16	12	536.3	22.7	10	1.78	11
130.5	375.0	3	8.92	3	575.8	16.8	10	2.26	11
162.4	97.1	4	7.33	4	589.8	68.4	6	1.83	6
186.5	1166.0	12	1.73	12	614.2	17.3	3	19.4	3
191.7	115.0	10	2.32	10	619.6	96.1	3	1.87	3
217.4	94.4	10	3.60	10	648.7	165.0	17	1.46	18
228.8	16.9	4	1.39	4	746.7	132.0	37	0.93	38
276.1	78.5	10	6.69	10	770.4	2064.0	61	2.61	63
288.1	12.6	19	1.50	20	774.6	46.5	7	1.18	7
297.3	170.0	3	29.7	3	968.6	28.2	14	1.44	15
314.3	8.5	3	5.43	3	974.7	120.0	4	2.39	4
325.3	555.0	5	5.30	5	998.4	95.9	11	0.915	12
339.8	86.4	6	1.84	6	1025.3	20.5	6	2.11	6
352.3	21.8	2	32.6	2	1086.5	21.6	12	1.29	13
387.5	119.0	10	1.04	11	1103.4	113.0	5	4.52	5
400.1	8.0	3	5.75	3	1150.7	110.0	3	4.12	3
412.7	18.3	5	3.41	5	1180.8	612.0	10	5.35	11
415.7	24.5	4	2.39	4	1221.5	31.0	25	2.06	26
426.8	15.4	7	2.81	7	1279.8	169.0	3	23.5	3
433.0	1959.0	48	2.64	50	1313.9	3400.0	--	9.50	30
454.2	19.2	16	1.11	17					

(About 15 lines with multiple half-lives are not included.)

Table A-4

PRELIMINARY RESULTS OF RESOLVED LINES FOR ^{239}Pu FISSION-PRODUCT ISOMERS

E (keV)	Half-Life (nsec)	±Δ (%)	Total Intensity (γ/Fission) (10^{-3})	±Δ (%)	E (keV)	Half-Life (nsec)	±Δ (%)	Total Intensity (γ/Fission) (10^{-3})	±Δ (%)
109.4	10.7	10	7.89	10	454.2	15.5	17	1.25	17
115.3	175.0	5	8.94	5	461.4	90.0	60	0.75	62
125.0	79.2	14	3.44	14	535.5	28.9	9	1.61	9
153.8	143.0	10	2.10	10	576.2	19.8	16	1.47	16
186.1	1000.0	30	1.25	32	590.3	100.0	50	1.30	52
191.8	165.0	20	1.18	20	614.2	17.3	3	17.9	3
217.3	128.0	25	1.50	25	648.2	104.0	32	0.76	32
288.2	12.9	10	1.94	10	770.1	1047.0	35	2.54	35
297.2	183.0	5	22.6	.5	774.8	49.9	12	1.50	12
314.1	9.0	4	8.20	4	840.3	129.0	18	0.84	19
324.9	578.0	18	3.06	18	969.5	28.8	6	1.97	6
339.5	78.9	14	0.77	14	1025.9	20.9	5	1.46	5
343.2	674.0	36	1.08	37	1087.1	19.7	10	1.45	11
352.1	22.6	3	18.1	3	1103.7	111.0	4	6.17	4
387.2	115.0	3	2.95	3	1151.1	124.0	7	6.11	7
412.1	22.4	8	2.01	8	1180.8	499.0	13	3.06	13
415.4	20.2	10	2.12	10	1221.4	15.2	20	4.19	20
426.4	15.7	4	2.82	4	1279.8	179.0	4	17.7	4
432.3	1445.0	55	3.75	56	1313.4	3400.0	--	15.6	25
444.7	215.0	5	1.11	5					

(About 15 lines with multiple half-lives are not included.)

spectra are then unfolded with the FERDOR code.[14] The preliminary result for the 315 to 458 nsec time region is shown in Fig. A-7. Additional data analysis is presently underway.

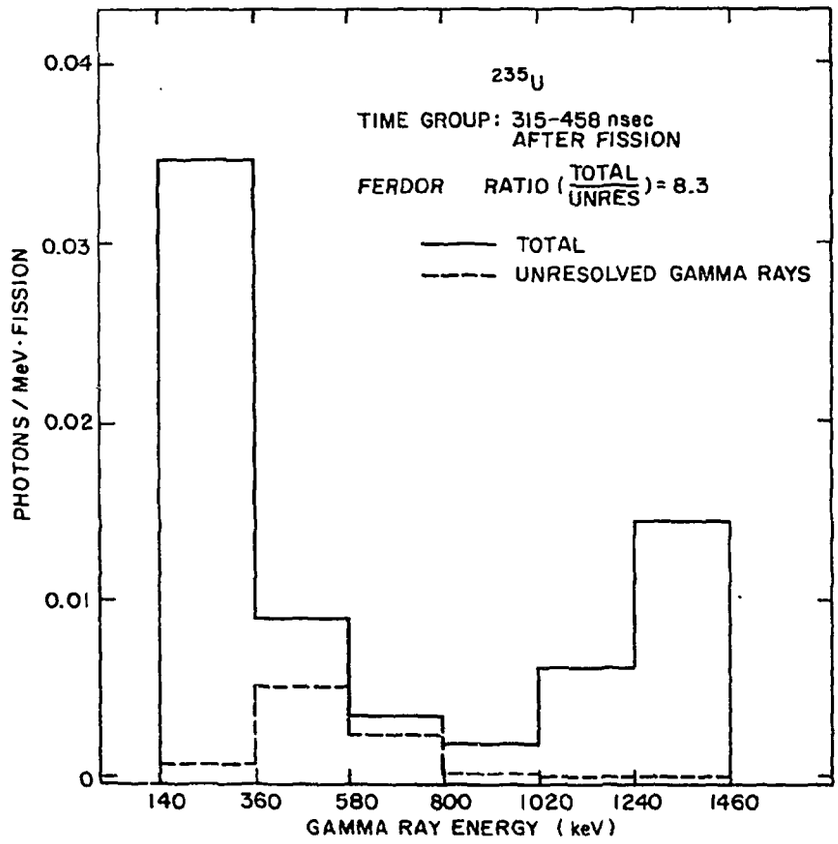

Fig. A-7. Preliminary results for the total of resolved and unresolved gamma rays (solid line) compared to the unresolved component alone (dashed line) obtained with FERDOR unfolding code. No data exist below our 140-keV cutoff.

[14] W. R. Burrus and V. V. Verbinski, Nucl. Instr. and Meth. 67, 181 (1969).

LAWRENCE RADIATION LABORATORY

A. NEUTRON PHYSICS

1. Search for γ-Ray Emission Preceding Isomeric Fission (J. C. Browne and C. D. Bowman) Relevant to Request 405

The time relationship between γ-rays and fission fragments was measured at the Livermore Electron Linac for neutrons ($E_n < 4eV$) captured on ^{235}U in an attempt to populate the 100-nsec fission isomer in ^{236}U. The results of this experiment are shown in Figure A-1. The main peak consists of coincidences between fission fragments and prompt fission γ-rays. The slope on the left corresponds to delayed γ-rays from the fission fragments. Pre-fission γ-rays would occur to the right of the peak. The inset in the figure shows the data averaged in 20 nsec intervals. The two dashed nearly-parallel curves represent ± one standard deviation from the curve that is expected from results of other experiments populating this fission isomer. An analysis of these data yields a limit of $\leq 8 \times 10^{-5}$ for the ratio of the rate of isomeric fission events with pre-fission γ-rays to the rate for prompt fission events for this neutron-energy range. This is a factor of 2.5 lower than the ratio expected from (d,pf) experiments and a factor of 8 lower than the ratio deduced from (n,γ) experiments with 2.2 MeV neutrons. Another experiment is planned in the neutron energy range of 1 eV to 100 eV which should be more sensitive than the measurement discussed above.

2. Neutron Total Cross Section Measurements of ^{242}Pu (G. F. Auchampaugh* and C. D. Bowman) Relevant to Request 489

Sub-barrier fission studies at Los Alamos on ^{242}Pu with high energy resolution have demonstrated the existence of a number of groups of resonances showing enhanced fission. We wish to complement that study with detailed information of the neutron widths of these levels. We have therefore carried out transmission measurements on ^{242}Pu with high resolution at the Livermore Electron Linac over the energy range from 50 keV to 600 eV. The ^{6}Li-glass neutron detector was located at the 250-meter neutron flight path. The accelerator operated at 720 pps with a 30 nsec wide beam pulse corresponding to an electron power of 10 KW. The resolution was determined at low energies by the doppler width; at higher energies a time resolution of 40 nsec was measured from the widths of the observed resonances. Measurements were completed on two 2-cm diameter samples; the thicker sample was four times the thickness of the other one. Analysis of the data is now underway.

---

* Los Alamos Scientific Lab., Los Alamos, New Mexico

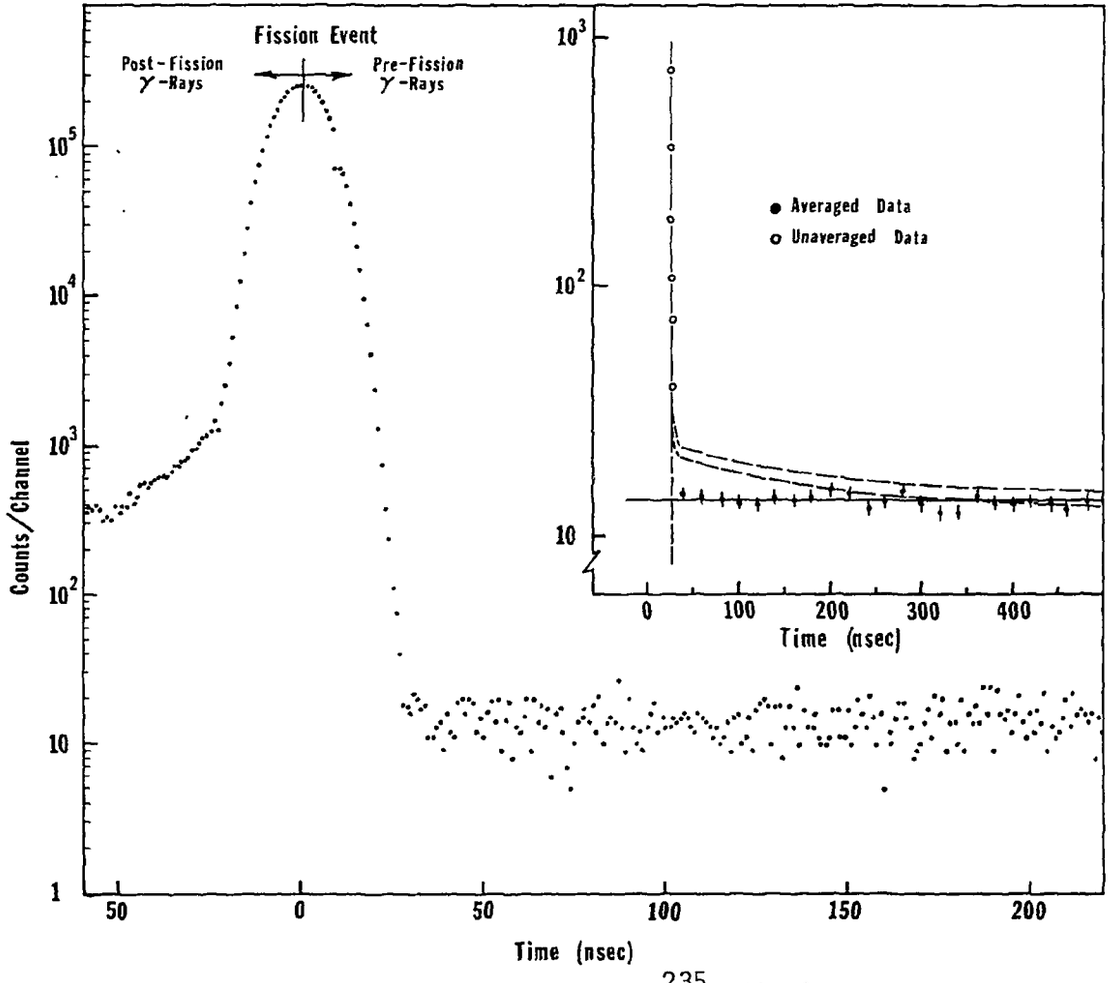

Fig. A-1. Time spectrum of γ-rays from ^{235}U fission.

3. Thermal-Neutron Cross-Sections of ^{257}Fm and ^{253}Cf (J. F. Wild and E. K. Hulet) Relevant to Request 537 and 541

We have measured the cross section of the 100.5-d isotope ^{257}Fm for the absorption of thermalized neutrons leading to either fission of the excited compound nucleus, ^{258}Fm, or the spontaneous-fission decay of its ground state.

Our measurements were carried out in a thermal column of the Livermore Pool-Type Reactor using mica foil as the fission-fragment detector and gold foil as the flux monitor. The cadmium ratio at our irradiation position in the thermal column is greater than 500.

We obtained a weighted-average value of 3060 ± 170 barns from eight individual measurements. Contributions to the number of fission tracks observed, in addition to background, were made by spontaneous-fission decay of ^{257}Fm; the data were corrected for these effects. The last three measurements were made with a ^{257}Fm target which had been specially purified from traces of natural uranium. The cross-section values obtained from this target were not significantly different from those from the first five experiments. It seems reasonable, therefore, to consider the level of uranium contamination in these targets insignificant insofar as the measurement of the ^{257}Fm cross section is concerned.

We have attempted to measure in a similar fashion the thermal-neutron-induced fission cross-section of 17.8-d ^{253}Cf. Our target, initially $\sim 2 \times 10^7$ atoms of ^{253}Cf, was separated from about 10^8 atoms of its parent, ^{257}Fm, after a growth period of about 90 days.

Due to the small amount of ^{253}Cf in our target, any amount of natural uranium contamination in excess of about 10^9 atoms would contribute significantly to the number of fissions observed. Again, even though our target was specially purified from uranium, we cannot rule out its presence and are currently continuing our bombardments on a weekly basis to determine if a uranium contribution appears after significant decay of the ^{253}Cf in the target. At this time we can say only that the cross-section value we have obtained is consistent with recent literature values.

4. The $^{130}Ba(n,\gamma)$ Cross Section and the Origin of ^{131}Xe on the Moon (B. L. Berman, with W. A. Kaiser*)

Studies of lunar rocks have revealed anomalously high concentrations of ^{131}Xe, which probably are associated with the cosmic ray

* University of California, Berkeley

flux at the lunar surface, the depth (or shielding) history of the lunar samples involved, and the abundance of barium in these samples. A hypothesis which could explain this anomaly is the existence of a large, nonthermal neutron-capture cross section for ^{130}Ba. The present experiment was undertaken in order to test this hypothesis.

The pulsed-neutron facility at the Livermore 100-MeV Electron Linear Accelerator served as the source of radiation. The spectrum and flux of neutrons were measured simultaneously with the sample irradiation, by the neutron time-of-flight technique, with a ^{235}U fission detector located at the end of a 250-m evacuated flight tube. The experimental neutron spectrum is shown in Figure A-2. The theoretical representation of Lingenfelter of the neutron spectrum at the lunar surface, normalized at 1 eV, also is shown, as the solid curve, in Figure A-2. One can see that the Linac neutron spectrum is a reasonably good representation of the lunar spectrum. The samples were irradiated for 34.7 hr at a power level of 8.6 kW and were located 0.83 m behind the source. Care was taken to keep the samples out of the intense bremsstrahlung beam to avoid photoactivation of the samples.

The samples consisted of about 2 g of chemically pure (p.a.) $BaCl_2 \cdot 2H_2O$, sealed in quartz ampoules. Two samples were irradiated on June 1-4, 1971, and a third served as a blank. One irradiated sample was melted in its quartz vessel on June 15, at $\sim 1000^{\circ}$ C (the melting point of $BaCl_2$ is 962° C) and analyzed on June 16. The other two samples were melted on October 13 and analyzed on October 14, after many half lives of the ^{131}Ba and ^{131}Cs activities (11.7 and 9.69 days, respectively). The samples were analyzed in a Pyrex-glass mass spectrometer with an all-metal sample system.

A typical spectrum from the June 16 analysis is shown in Figure A-3. The horizontal lines in Figure A-3 indicate the normal relative abundances of the various xenon isotopes. The large enhancement of ^{131}Xe must result almost entirely from the $^{130}Ba(n,\gamma)$ reaction; the amount of ^{131}Xe resulting from $^{132}Ba(\gamma,n)$ is negligible. This is measured by the small enhancement of ^{129}Xe resulting from $^{130}Ba(\gamma,n)$, since the abundances of ^{130}Ba and ^{132}Ba are nearly the same, as are the two integrated (γ,n) cross sections. Similarly, one can eliminate any significant contamination of the ^{131}Xe yield resulting from the ^{132}Ba $(n,2n)$ reaction.

The absolute ^{131}Xe enhancement was $30.4 \pm 0.4 \times 10^{-12}$ cc (STP)/g ^{nat}Ba, or $8.17 \pm 0.11 \times 10^{8}$ atoms/g ^{nat}Ba. Since there are 4.43×10^{18} atoms ^{130}Ba/g ^{nat}Ba, then $\int \sigma \phi dE = 1.84 \pm 0.02 \times 10^{-10}$. Using $\sigma_{capture} = 2\pi^2 \lambda^2 g < \frac{\Gamma_{n^0}}{D} > < \frac{\Gamma_\gamma}{\Gamma} > E^{1/2} = KE^{-1/2}$ with the best

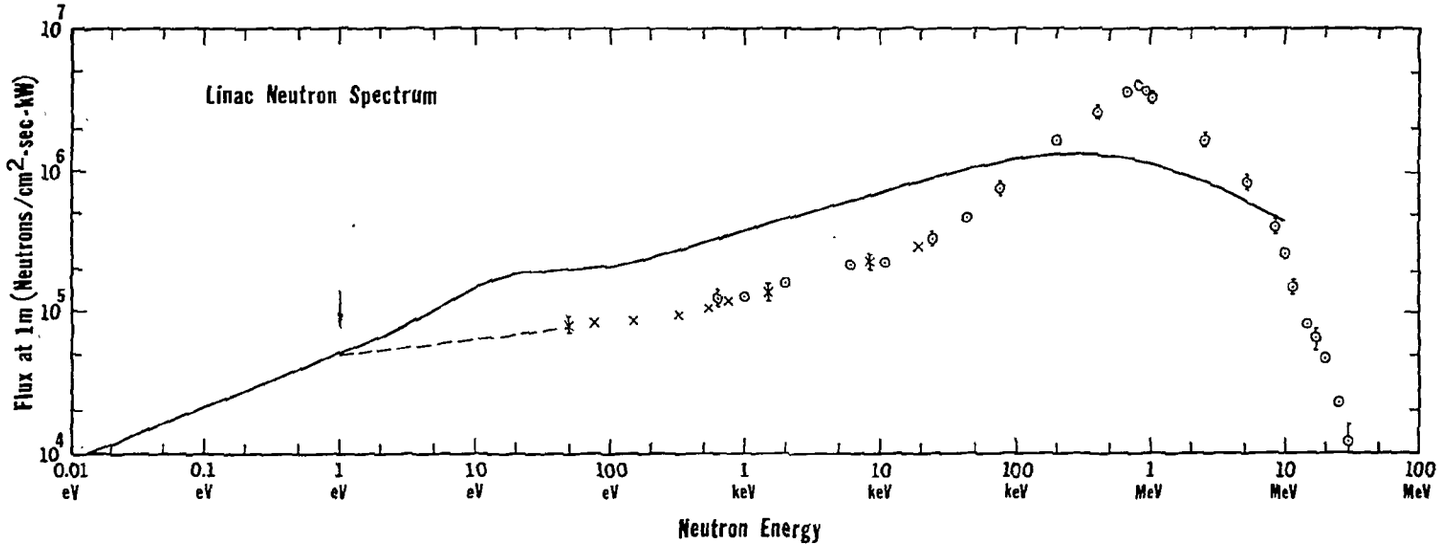

Fig. A-2. The spectrum of neutrons from the Linac. The circles are data taken with 30-nsec beam bursts, and the crosses with 3- sec beam bursts. The dashed line is an extrapolation down to 1 eV (arrow), where a theoretical spectrum (solid line) of neutrons at the lunar surface is normalized to the one used in the present experiment.

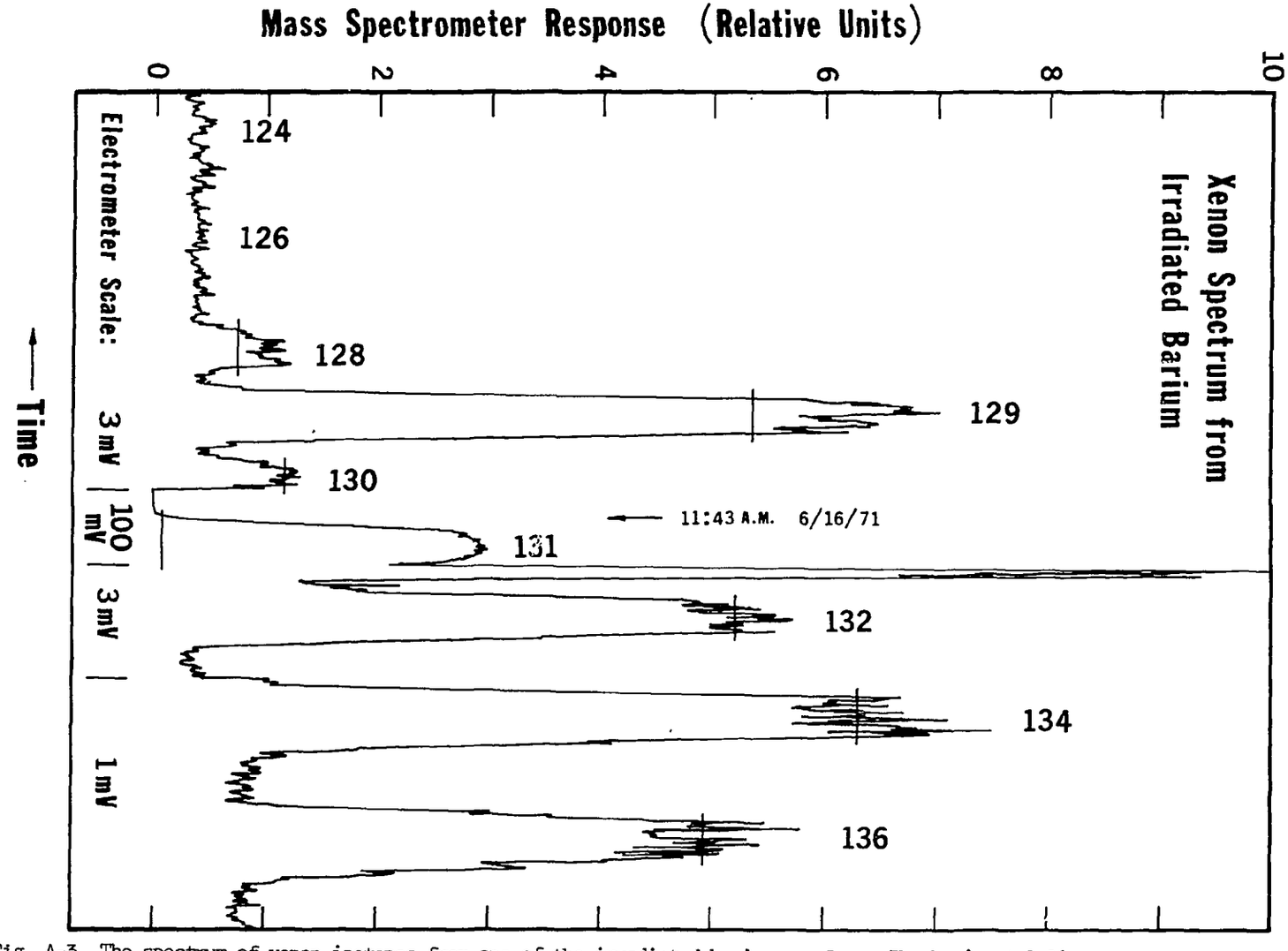

Fig. A-3. The spectrum of xenon isotopes from one of the irradiated barium samples. The horizontal lines indicate the normal relative isotopic abundances. Note the large enhancement of the ^{131}Xe, and the small enhancement of the ^{129}Xe (see text).

available data for the ^{130}Ba resonance parameters, we find K = 193 b-eV$^{1/2}$. The measured neutron flux, combined with this value for K, then yields $\int\sigma\phi dE = 3.5 \pm 0.7 \times 10^{-11}$, less than 20% of the measured ^{131}Xe yield.

We conclude that the anomalously high concentration of ^{131}Xe in lunar rocks probably can be explained by the neutron-capture cross section of ^{130}Ba, but that that cross section probably is dominated by one or more large resonances in the epithermal energy region. Clearly, a definitive microscopic measurement of the $^{130}Ba(n,\gamma)$ cross section is called for.

5. Neutron Total Cross Section for ^{207}Pb Near 40 keV (T. W. Phillips, B. L. Berman, and C. D. Bowman)

In a measurement of the threshold photoneutron cross section for ^{208}Pb[1] the prominent 1^- state at 40.8 keV was observed to be asymmetric, implying the existence of interference between resonant and a large amount of non-resonant capture for (s-wave) neutrons on ^{207}Pb. This asymmetry was confirmed subsequently by $^{208}Pb(\gamma,n)$ measurements at Toronto[2] and Argonne[3], but contradicted by a $^{207}Pb(n,\gamma)$ measurement at Oak Ridge[4]. The Toronto group[5] have suggested that the observed asymmetry in the (γ,n) results arises from a second resonance on the low-energy side of the 40.8-keV resonance.

In order to test this hypothesis, we have performed a high-resolution measurement of the neutron total cross section for ^{207}Pb. The pulsed-neutron facility at the Livermore 100-MeV Electron Linac was the source of radiation. The beam pulse width employed was 30 ns, the flight-path length was 250 m, and the neutron detector was a scaled-up version of a ^{235}U - plus - scintillator arrangement described previously[6]. The 0.477-kg ^{207}Pb sample was 0.935 cm thick. Measurements with natural lead and also with no transmission sample were performed as well.

The results are shown in Figure A-4. The peak at 38.1 keV (incident laboratory neutron energy) represents a 2^+ state, which emits p-wave neutrons, and thus does not interfere with the potential scattering as does the 41.4-keV state in question. Its width, then, is a measure of the experimental resolution function; area analysis yields $\Gamma_n = 20 \pm 3$ eV for g = 6/4. One can see at a glance that there is no evidence for a second peak on the low-energy side of the 41.4-keV resonance. This measurement sets an upper limit on the neutron width for such a peak to be 6 eV.

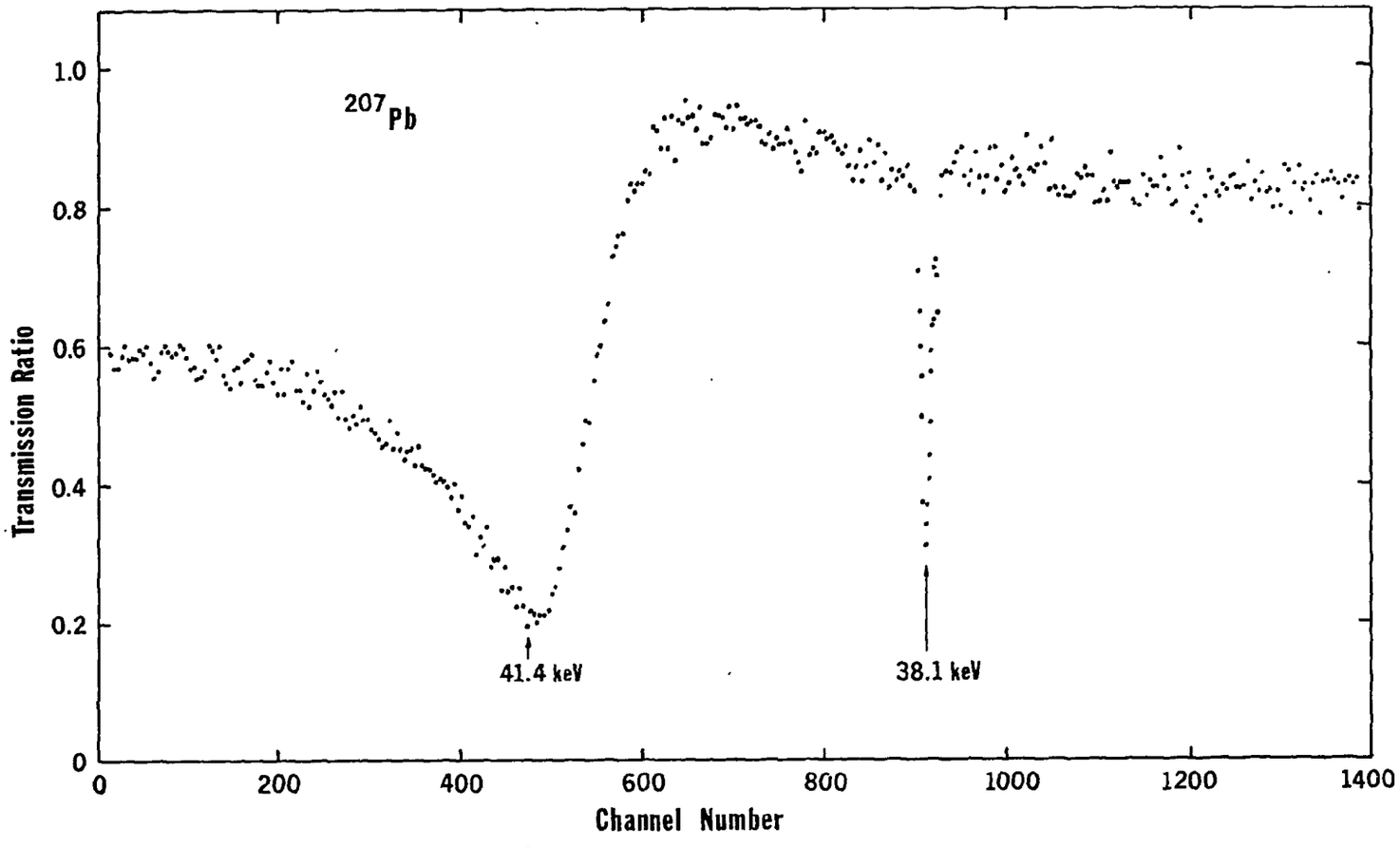

Fig. A-4. The transmission of ^{207}Pb in the 4 keV region. With the exception of the peak at 38.1 keV, the data are 4-channel averages.

[1] C. D. Bowman, R. J. Baglan, and B. L. Berman, Phys. Rev. Letters 23, 796 (1969).

[2] L. C. Haacke and K. G. McNeill, Bull. Am. Phys. Soc. 15, 482 (1970).

[3] H. E. Jackson, private communication.

[4] B. J. Allen and R. L. Macklin, Phys. Rev. Letters 25, 1675 (1970); B. J. Allen and R. L. Macklin, Proc. Conf. Neutron Cross Sections and Technology, 1971, p. 764.

[5] L. C. Haacke, B. J. Thomas, and K. G. McNeill, Bull. Am. Phys. Soc. 16, 65 (1971).

[6] R. L. Van Hemert, C. D. Bowman, R. J. Baglan, and B. L. Berman, Nucl. Instrum. Meth. 89, 263 (1970).

6. Nuclear Cross Section Calculations (D. G. Gardner, J. L. Brownlee, and A. Delucchi) Pertinent to all requests for cross sections on unstable targets

We are accumulating and developing computer programs for calculating excitation functions for essentially any neutron-induced reaction. These include statistical model programs for compound and precompound nucleus evaporation, a coupled-channels optical model program to compute transmission coefficients for nonspherical nuclei and cross sections for the direct excitation of inelastic levels, and various programs to compute isotope ratios following a gamma-ray cascade in the final nucleus. Our philosophy is that we wish to calculate concurrently all possible reactions that may occur, and to get them all right. This attitude is necessary because we are primarily interested in unstable target nuclei where confirming experimental data may never be available. If we cannot compute all competing reactions properly on stable nuclei where experimental data are available, then we will feel little confidence in our calculations for unstable nuclei.

a. Accomplishments and Status

In Radiochemistry Division of LLL we now have a number of codes for computing nuclear reaction cross sections. Most of these codes were obtained or developed during the past six months, and are not yet considered completely debugged. For several years we have used Moldauer's ABACUS-NEARREX code to compute (n,γ) cross sections. This code has now been replaced by a completely revised version of Dunford's COMNUC code, which was developed primarily at LLL over the past six months. It possesses many advantages over the NEARREX code, including a better fission channel, charged particle competition, and multiple

particle evaporation.

As supplementary programs we have improved versions of Dunford's CASCADE and FOURPLUS codes. The former code provides input to COMNUC for calculating reactions such as (n,γn'), (n,γp), and (n,γ fission). The FOURPLUS code is a coupled-channels program to be used in providing transmission coefficients for deformed nuclei, as well as direct inelastic excitation cross sections.

We have also obtained Uhl's code (called UHL here). This code permits up to four particles to be evaporated, and follows the gamma-ray cascade in the final nucleus. The code is operational, but we have not tested it thoroughly as yet.

We will continue the testing and debugging of our four new codes during the next Quarter. As time permits, a number of other codes will be developed and changes made in the existing codes. For example, UHL will now only accept transmission coefficients as a function of ℓ. We will modify the code so that a spin-orbit potential may be used. We will also modify UHL to follow more reaction sequences at one time. A new code, probably based on UHL, will be written to compute the precompound part of the cross section. Finally, we will complete a Monte Carlo gamma-ray cascade program, which was begun about one year ago. The latter will hopefully supply the best available estimates of isomer ratios.

B. PROGRAM FOR HIGH ACCURACY FISSION CROSS SECTIONS AND $\bar{\nu}$ MEASUREMENTS

Preparation is underway for the measurement of fission cross sections and $\bar{\nu}$ for ^{233}U, ^{235}, ^{238}, ^{239}Pu, ^{240}, ^{241} and possibly ^{238}Pu, in the energy range from 1 keV to 15 MeV with a goal for accuracy in σ of at least 2%. The measurements, which will be made at the Livermore Electron Linac, will make use of the linac's capability for carrying out measurements in the thermal neutron energy range. All cross sections will be normalized there, thus eliminating the need for absolute determination of flux mass, detector efficiency, solid angle, geometry etc. The non-thermally fissile isotopes will be normalized also at thermal energy by starting with a sample of high isotopic purity and adding an accurately known amount of a thermally fissile isotope of the same element.

Two groups will carry on these measurements; one carrying out an absolute measurement of the fission cross section of ^{235}U and the other measuring ratios of the other isotopes to ^{235}U. The results of both groups will then be combined to obtain absolute fission cross sections for all the isotopes. Brief descriptions of these two measurements and our proposed new technique for measuring $\bar{\nu}$ are given below.

1. Absolute Fission Cross-Section Measurements on ^{235}U from 1 kev to 15 MeV (J. B. Czirr, G. S. Sidhu and W. E. Farley) Relevant to Requests 388, 389, 390, 391

The primary problem in these measurements is the relative measurement of neutron flux from .01 eV to 15 MeV. In the region below 100 keV ^{6}Li glass will be used as the flux monitor. The principal problem in the use of ^{6}Li glass appears to be scattering in the glass itself or in the P.M. tube on which it is mounted. A 1 mm-thick piece of ^{6}Li glass detection 10 cm x 12.5 cm is viewed edge-on with two P.M. tubes located outside of the neutron beam as shown in Figure B-1. The pulse-height spectrum in Figure B-1 was taken with a Pu - Li neutron source. The shoulder on the left side of peak comes about from those reactions near the surface of the glass where one of the reaction particles leaves the glass before depositing all its energy. This detector might also be used to improve the ^{6}Li cross section in the keV region.

From 50 keV to 1.5 MeV we hope to use a proton-recoil proportional counter containing "germane" gas (GeH_4). This gas has the important advantage over methane that the Ge nucleus recoils with much less energy than the C nucleus does. Therefore, the recoil-proton plateau extends over a much wider range greatly reducing the uncertainties in the use of these detectors. In addition the stopping power is much larger so that the detector can be used over a wider range without serious problems from wall affects.

For the energy range from 1 to 15 MeV a recoil telescope is being designed which will take advantage of the intense well collimated, and parallel neutron beam from the linac. Its design will be somewhat simplified since absolute measurements are not necessary.

The fission detector is being designed primarily to eliminate the effects of angular distribution changes arising from the nuclear fission physics and from linear momentum carried by the incoming neutron. We hope to have the required detectors by June 1972 and final results by March 1973.

2. Ratios of Fission Cross Sections to ^{235}U Absolute Fission from 1 keV to 15 MeV (J. W. Behrens and C. D. Bowman) Pertinent to Requests 359, 360, 364, 417, 418, 435, 436, 450, 451, 464, 465, 474, 475

The main requirements for these experiments is a low background environment from .01 eV to 15 MeV, sufficient counting rate to obtain 1% counting statistics in the ratio, and a detector design which will eliminate the effect of changing angular distribution arising from nuclear fission physics and the momentum carried by the neutron. A

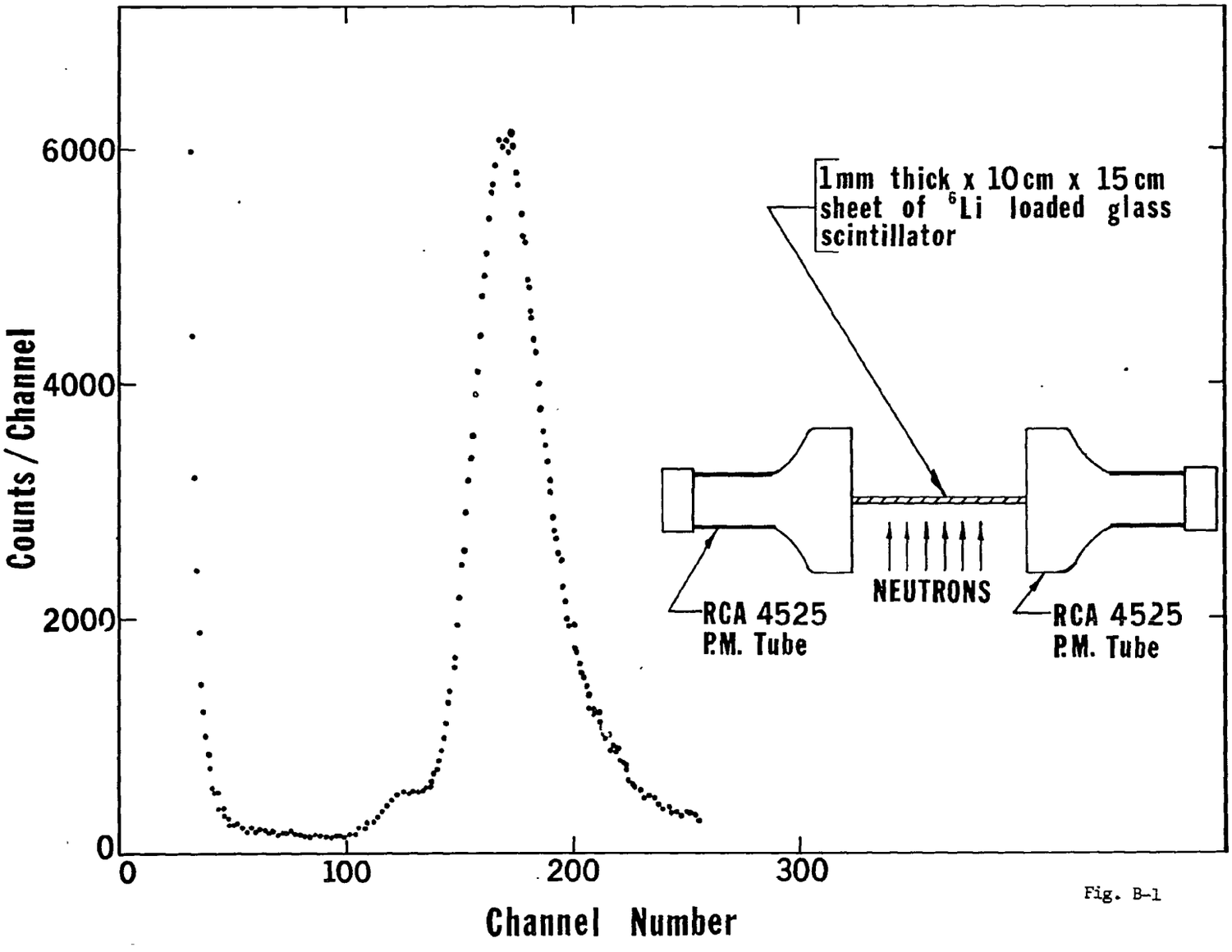
6000
4000
2000
0
Counts / Channel
0
100
200
300
Channel Number
1mm thick x 10cm x 15cm
sheet of ^{6}Li loaded glass
scintillator
NEUTRONS
RCA 4525
P.M. Tube
RCA 4525
P.M. Tube

Fig. B-1

number of possible arrangements based on gaseous ionization counters are being considered. Ionization counters have been developed which have rise times of less than 10 nsec. Four isotopes will be measured simultaneously in these measurements by stacking the relatively small detectors on the same neutron beam. One measurement therefore is planned for the uranium isotopes and another for the plutonium isotopes. The results of these ratio measurements will then be combined with the absolute ^{235}U fission measurements to obtain the final cross sections.

3. Fission ν Measurements (R. E. Howe and C. D. Bowman)

A neutron detector for use in $\bar{\nu}$ measurements with a white neutron source should have fast time response to permit time-of-flight measurements and should be insensitive to changes in the neutron spectrum. The technique in use at RPI achieves its insensitivity to the neutron spectrum by moderating the neutrons to relatively low energies before neutron detection. The neutron-detector time response is therefore quite long. Background from MeV neutrons must be allowed to decay away before measurements can be done and therefore the technique is restricted to low energies.

When the proton-recoil detector is used as a neutron detector in ν measurements, the time response is adequate, but the neutron detector usually has a bias level near 0.5 MeV. It has the disadvantage therefore that it is very sensitive to changes in the fission-neutron spectrum if such changes actually occur with neutron energy.

We are developing a new concept for $\bar{\nu}$ measurements which should possess both insensitivity to a changing neutron spectrum and fast time response. The detector is shown in Fig. B-2. The detector consists of a fission chamber situated inside of a spherical shell of ^{235}U which is in turn surrounded by concentric shells of ^{6}Li and Pb. The system has a criticality factor k = 0.8 and a decay time of 25 nsec. Two liquid scintillators with pulse-shape discrimination capability are located on the outside.

The neutrons from the fission interact with the ^{235}U, which has a nearly flat fission cross section over the range of the fission-neutron spectrum. Eventually neutrons from those subsequent fissions are detected by the liquid scintillators. However the energy of the detected neutrons is not correlated with the energy of the neutrons released in the primary fission event taking place in the fission chamber. Hence the ^{235}U assembly acts simply as a converter between the primary neutrons and the detected neutrons. The system is therefore insensitive to changes in the neutron spectrum and also has a fast time response. We believe that the concept will permit $\bar{\nu}$ studies from .01 eV to 15 MeV at the Livermore linac. We expect to begin measurements in January.

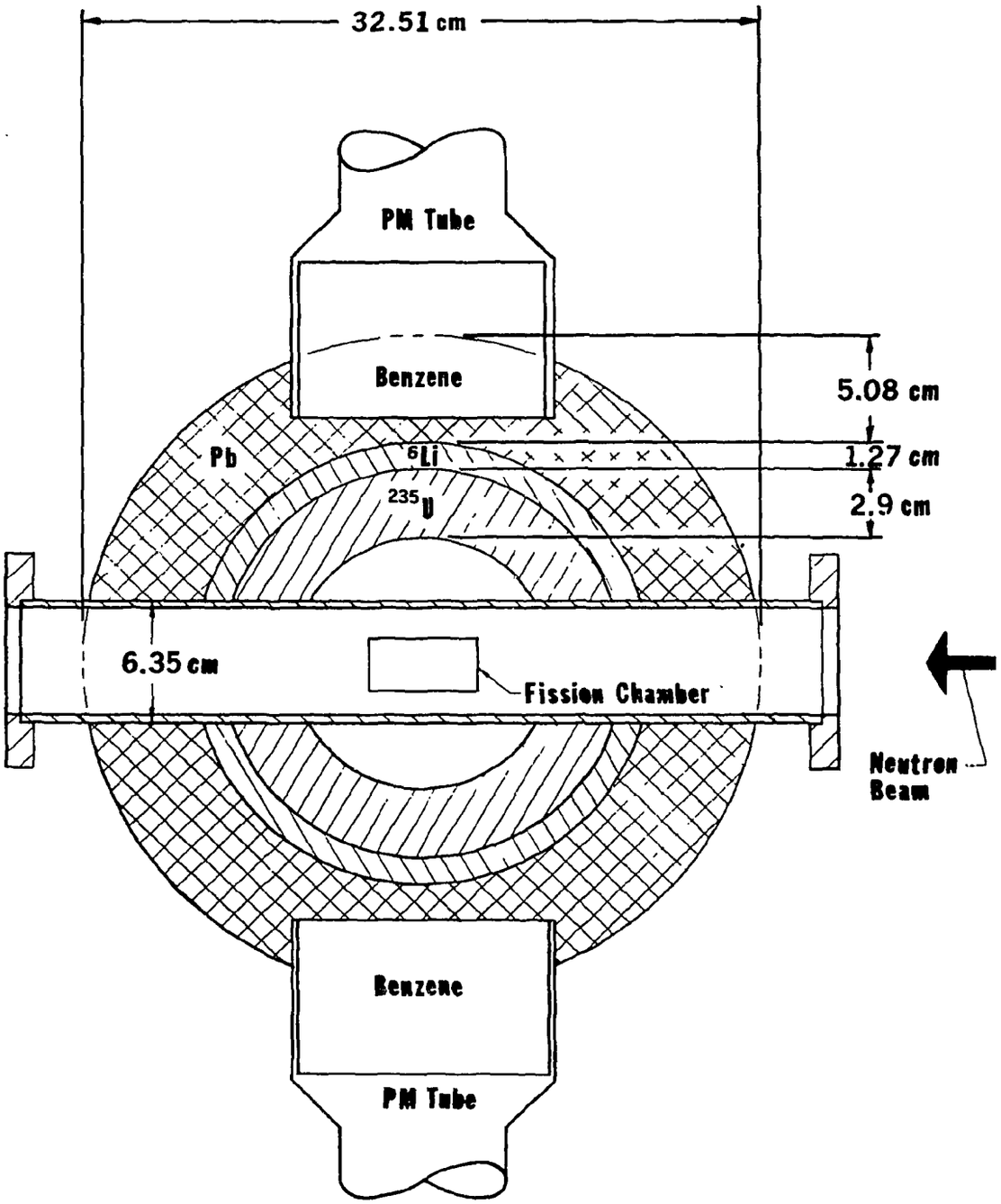

Fission $\bar{\nu}$ Assembly

Fig. B.2

C. FISSION CROSS SECTIONS ON THE TRANSPLUTONIUM ISOTOPES ^{242m}Am, ^{243}Cm, ^{245}Cm, ^{247}Cm, ^{249}Bk AND ^{249}Cf FROM .01 eV to 14 MeV (J. C. Browne, C. D. Bowman, and R. W. Hoff) Pertinent to Requests 499, 506, 515, 521, and 528

The intent of these measurements is to obtain data in the region below 20 eV, where no measurements have been made except for ^{242m}Am, and to obtain more accurate data than is presently available in the higher keV and MeV region. In the lower energy region the measurements will be made relative to ^{6}Li or ^{10}B and in the higher energy range relative to ^{235}U. A program of detector evaluation has been completed. We have selected a gaseous scintillation counter with a 2.5cm-diameter foil containing less than 1 mg of fissile material viewed with back-to-back P.M. tubes. The foils will be 1.25×10^{-4}-cm thick Al which permit both fragments to be detected. The technique for preparing and mounting these foils has been developed by J. Behrens of the linac staff. These detectors should permit efficient fission detection, fast time response, low γ-flash sensitivity and fast recovery, and adequate descrimination against α-particle activity. Four of the detectors will be stacked in one neutron beam; therefore two successful measurements will be required to complete our studies on all of these isotopes.

The ^{242m}Cm and the Cm isotopes will all require isotopic separation both to eliminate effects of the cross section of contaminent isotopes and to reduce the effects of spontaneous fission of the even-mass Cm isotopes. The separation will be carried out at LLL.

D. PHOTONUCLEAR CROSS-SECTION STUDIES

1. Photoneutron Spectra From Monochromatic Annihilation Radiation (T. W. Phillips, B. L. Berman and R. G. Johnson)*

Using the LLL 100 MeV linear accelerator in its short-pulsed, positron-acceleration mode, we have succeeded in observing the energy spectrum of photoneutrons produced by nearly monochromatic photons. These photons are made by the annihilation in flight of energy-selected positrons. The unanalyzed time spectrum of the events observed for a 470 g, 6"-dia water sample is shown in Fig. D-1. These events were observed with a neutron detector which consisted of three 5"-dia plastic scintillator disks 2" thick. Each disk is viewed by a pair of 5" photomultiplier tubes. A coincidence is required between each pair of phototubes for noise rejection. The data were obtained in a 4 hr run using a 10 ns wide, $\sim$24 MeV, positron beam pulsed at a rate of 720 s^{-1}. The average beam current was $\sim$1.5 nA. The ground-state neutron group due to the annihilation photons is clearly visible as a peak in the time spectrum. To extract information on the excited-state groups,

*Summer visitor from University of Toronto, Toronto, Ontario.

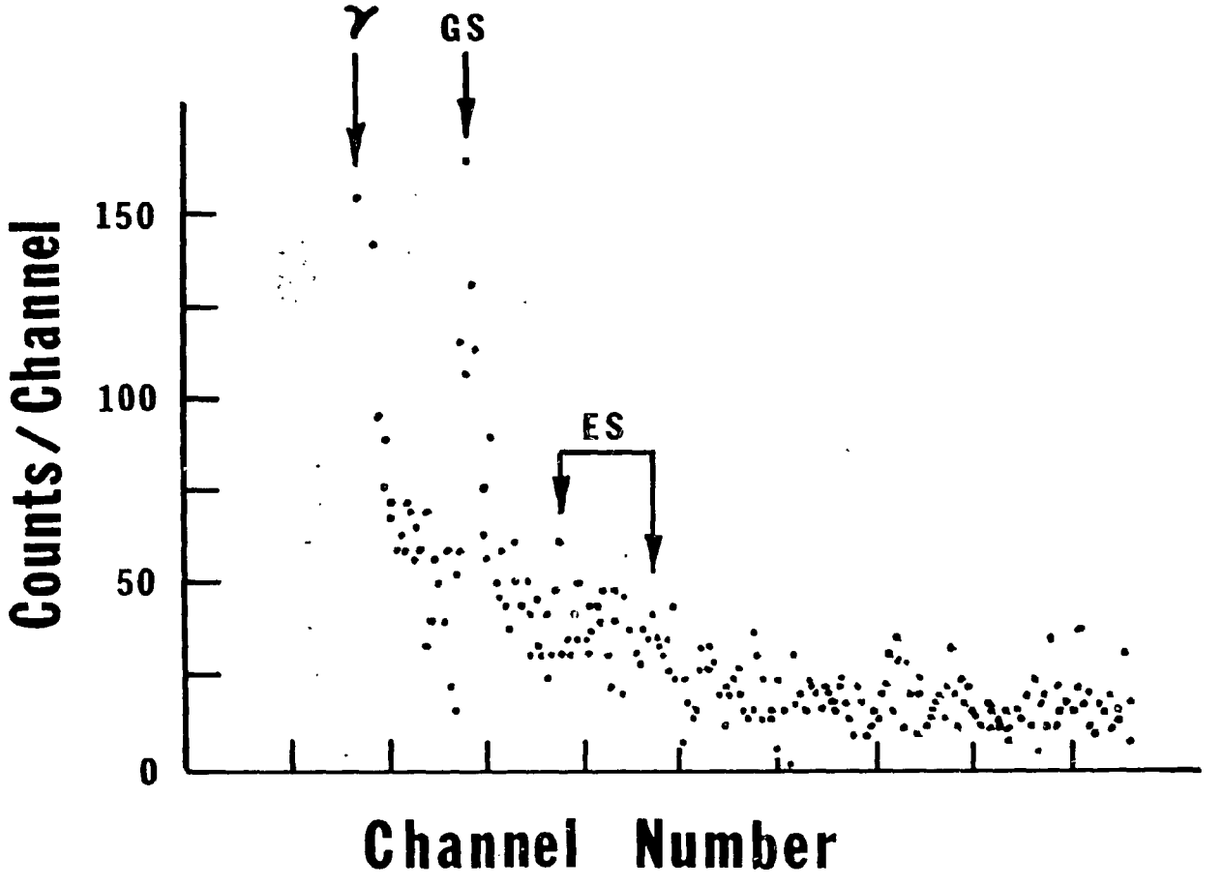

Fig. D-1. TIME-OF-FLIGHT DISTRIBUTION FOR ANNIHILATION PHOTONS

γ is the gamma flash from the photon beam. The channels corresponding to ground-and excited-state neutron decays from ^{16}O are indicated by GS and ES, respectively.

further running to obtain better statistics has been required. In addition, runs have been made with electrons instead of positrons to remove the background of events due to the positron bremsstrahlung. Analysis of this work is currently in progress.

2. Photoneutron Cross Sections for ^{58}Ni and ^{60}Ni (S. C. Fultz, R. A. Alvarez, P. Meyer and B. L. Berman)

We have measured the photoneutron cross sections of ^{58}Ni and ^{60}Ni in the giant resonance region using the nearly monoenergetic γ-rays from in-flight annihilation of positrons from the new Livermore 100 MeV electron linac. The annihilation-photon technique, as well as the neutron detector and electronics used for these measurements has been described previously in the literature.

Preliminary results are shown in Figs. D-2 and D-3, in which relevant thresholds are indicated by arrows. The photon energy resolution during these measurements was 1%. The measurements indicate that the cross section at the peak of the giant resonance is about three times as large for ^{60}Ni as for ^{58}Ni. The $(\gamma,2n)$ cross section in ^{60}Ni becomes an appreciable fraction of the total within 2 MeV of the threshold, whereas in ^{58}Ni it remains relatively small up to the highest energy measured. Our data agree qualitatively with previous results of Min and White,[1] shown as dashed curves, although our better resolution makes apparent the considerable structure in the ^{58}Ni cross section both near threshold and throughout the giant resonance region. Such pronounced structure does not seem to be present in ^{60}Ni.

Additional data on ^{58}Ni both at higher energies and with better resolution are being analyzed, and further measurements on ^{60}Ni at higher energies are planned.

3. Total Photon-Absorption Cross Section (B. L. Berman and T. W. Phillips)

In principle, the two most fundamental kinds of photonuclear experiments are measurements of total photon-absorption and photon-scattering cross sections. In practice, however, these are the most difficult, since conventional electron linear accelerators, by far the most powerful machines for producing intense photon beams, are low-duty-cycle devices. This implies that photon transmission and scattering experiments, which involve photon detection during the intense beam burst, are very difficult and have high backgrounds.

---

[1] K. Min and T. A. White, Phys. Rev. Letters 21, 1200 (1968).

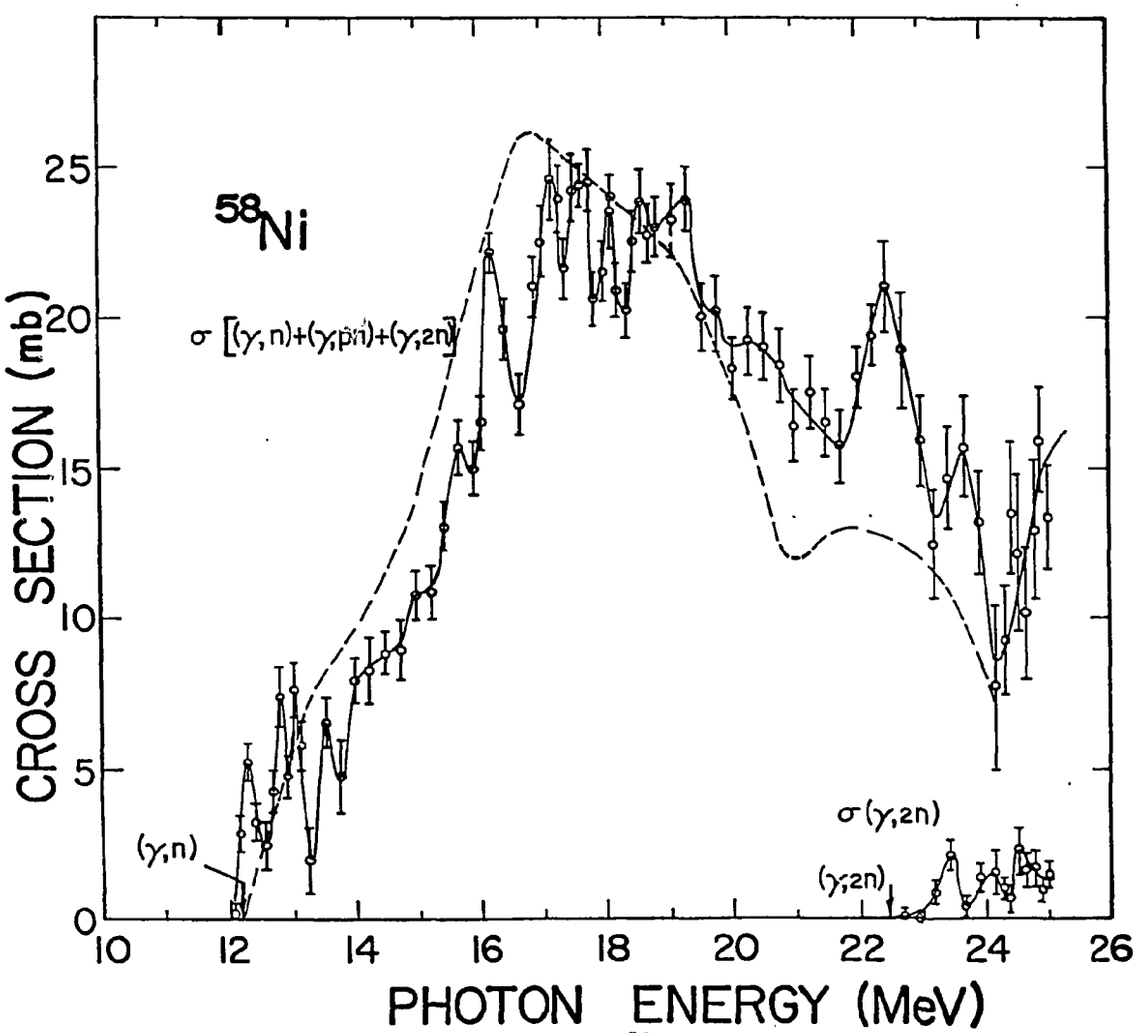

Fig. D-2. The photonuclear cross sections for ^{58}Ni. The dash line shows the results of Min and White.

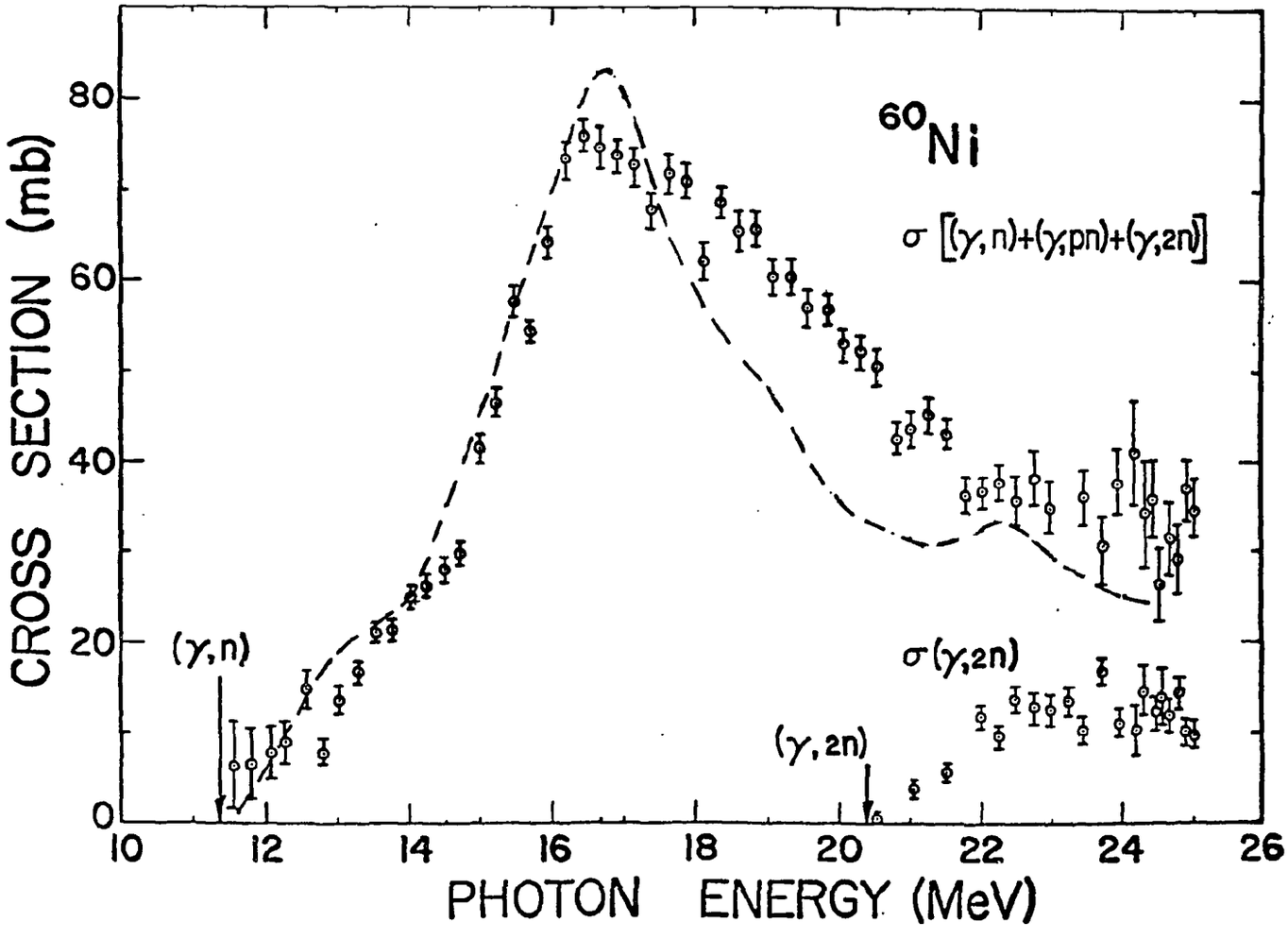

Fig. D-3. Photoneutron cross sections of ^{60}Ni. The dash line shows the results of Min and White.

A novel technique fashioned in response to this challenge makes use of the D(γ,n) reaction and neutron time of flight. A short burst of bremsstrahlung, having passed through the photon transmission sample, is allowed to strike a deuterium photon-to-neutron converter, viewed from afar by a fast neutron detector. The one-to-one correspondence between the energy of the neutron (detected between beam bursts) and the incident photon permits one to measure the total photon absorption cross section at all energies simultaneously from 2.2 MeV (the D(γ,n) threshold) to the bremsstrahlung end-point energy (which might be 100 MeV or more). The high resolution obtained by use of the time-of-flight technique is particularly valuable at the lower energies, especially below the particle thresholds. Photon scattering measurements can be done in a similar way. The feasibility of this method was first demonstrated at Yale.[1]

The first such measurement attempted at Livermore made use of ^{209}Bi as the transmission sample. The appearance of sharp transmission dips at several places in the D(γ,n) neutron time-of-flight spectrum corresponds to photon absorption by bound states in ^{209}Bi. Analysis of the data is proceeding, and further measurements are planned.

E. BI-LATERAL POSITION-SENSITIVE γ-RAY DETECTOR

Two identical position-sensitive γ-ray detectors are being constructed for bio-medical, neutron physics, and photonuclear physics studies. Each camera consists of a 1.25-cm thick by 38-cm diameter NaI crystal viewed from a small distance by 37 photomultiplier tubes which are 7.62 cm in diameter. By properly adding signals from neighboring P.M. tubes a resolution of about 0.5 cm can be achieved on the position of a γ-ray interaction in the NaI. The detector mounting will permit the detectors to be used separately or they may be arranged so as to face each other. The two detectors will be interfaced to the Livermore Linac Computer System which will provide drum storage and display for the x-and y-coordinate data from the detectors. The detectors were conceived originally primarily for medical studies using linac produced position activity, but other uses are now planned. Some of these used are given below.

1. Lung-Function Studies (P. Meyer, R. E. Yoder, E. Behrin and C. D. Bowman)

By using both detectors back-to-back and in coincidence one can detect the two annihilation γ-rays from positronium decay, and thus locate a line on which the positronium was located. By observing a large number of such lines and handling the data properly, one can take

---

[1] C.-P. Wu, F. W. K. Firk, and B. L. Berman, Nucl. Instrum. Meth. 79, 346 (1970).

pictures of the distribution of positron activity in a subject.

We are presently planning to use activated ozone ($^{15}O^{16}O_2$) which we can now produce with our linac to study the physiology of ozone. Experiments over a number of years seem to indicate that ozone does not travel directly to the lung from the air we breath. Rather the ozone is absorbed in the water on the nose, mouth and throat, then absorbed into the blood and carried by the blood to the lungs. It should be possible to confirm this very quickly and then move on to other aspects of ozone physiology.

2. Resonance Neutron Radiography (C. D. Bowman and E. Behrin)

By means of a relatively thin pad of ^{10}B placed over the outer surface of the NaI crystal, the detector can be made sensitive to keV and eV neutrons via the 0.478 MeV γ-ray from the $^{10}B(n,\alpha\gamma)$ reaction. Shadowgraphs of material placed between a small-size neutron source and the detector can therefore be obtained. By time-of-flight measurements one can select energies corresponding to strong neutron resonances in various materials and simultaneously measure the distribution of a number of different elements in the subject material. Other more basic studies with this technique are clearly possible also.

3. Photonuclear Physics (S. C. Fultz, T. W. Phillips and C. D. Bowman)

The kinematics of the positron annihilation-in-flight offer some interesting possibilities when combined with this detector. If a positron with known energy and direction annihilates in flight, a relationship exists between the two γ-rays; that is, if the position and therefore angle of one γ-ray is measured, the energy and angle of the sister γ-ray is also known. Thus a coincidence between a position-sensitive detector and some other detector such as a photo-fission detector determines the energy of the γ-ray which induced the fission event. A range of γ-ray energies therefore can be covered with the 38 cm diameter detectors without changing the positron energy. The resolution in γ-ray energy for a truly monenergetic positron is determined then by the position resolution of the detector and its distance from the annihilation target so that the γ-ray resolution can be improved simply by moving the detector further away. The possibilities for γ-ray cross-section studies appear to be numerous and we are now attempting to select the most promising one.

LOCKHEED PALO ALTO RESEARCH LABORATORY

A. NEUTRON PHYSICS

1. Gross-Fission-Product Gamma-Ray Spectroscopy (W. L. Imhof, L. F. Chase, Jr., R. A. Chalmers, F. J. Vaughn, and R. W. Nightingale)

An additional set of 40-min irradiations of ^{235}U, ^{238}U, and ^{239}Pu targets has been made with 1.9-MeV neutrons from the $T(p,n)^3He$ reaction. The resultant fission-product γ-ray spectra were observed from 4 minutes post-bombardment through the ensuing 24 hours. This brings the number of neutron energies at which measurements have been made to 12, 6, and 3 for ^{235}U, ^{239}Pu, and ^{238}U, respectively. Analysis of the fission-γ-ray data obtained during the various bombardments is proceeding.

2. Proton and Alpha Scattering from Aligned ^{165}Ho (T. R. Fisher, B. A. Watson,* S. L. Tabor,* and D. Parks*)

Data have been obtained on the elastic scattering of 5-10-MeV protons by aligned ^{165}Ho ($B_2/B_2(max) = -0.33$). The change in the scattering cross section for an aligned vs. an unaligned target is shown in Fig. A-1. The solid curve is the result of an adiabatic coupled-channels calculation using the value $\beta = 0.33$ for the nuclear deformation. This work has been published.[1] Preliminary data on alpha scattering from aligned holmium have also been obtained, and are in reasonable agreement with theoretical predictions.

3. Radiation-Damage Effects on Superconducting Microwave Cavities (T. R. Fisher and J. Ben Zvi*)

Construction of the microwave cavities and associated equipment for this experiment is in progress. X-band cavities will be irradiated with 3-MeV protons until a degradation of the Q of the cavities is observed. Annealing and recovery rates will be studied.

4. Deformation Effect in the $^{59}Co + n$ Total Cross Section (T. R. Fisher)

A dilution-refrigerator system designed for this experiment has been completed and is in the final stages of testing. The large Co single-crystal target will be operated at a temperature of 25 mK, corresponding to a nuclear alignment of 20%. The deformation effect, or change in cross section for an aligned vs. an unaligned target, will be studied for neutron energies from 0.3 to 15 MeV.

---

*Stanford University, Stanford, California.

[1] T. R. Fisher, S. L. Tabor, and B. A. Watson, Phys. Rev. Lett. 27, 1078 (1971).

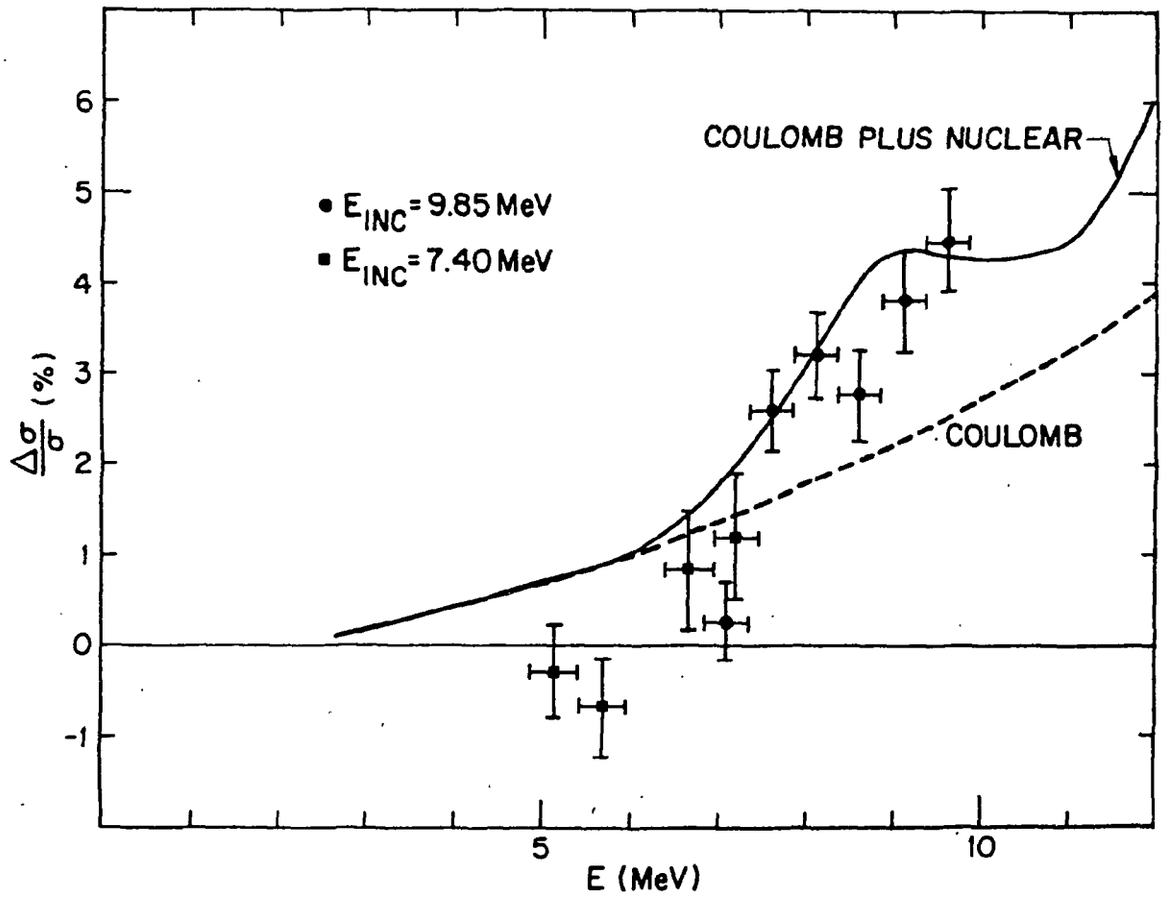

Figure A-1. The quantity $\frac{\Delta\sigma}{\sigma} = \frac{\sigma(\text{aligned}) - \sigma(\text{unaligned})}{\sigma}$ vs. energy for the elastic scattering of protons on ^{165}Ho. The nuclear alignment is -0.33. The solid curve is the result of an adiabatic coupled-channels calculation with β = 0.33. The dashed curve shows the effect of the coulomb potential alone.

5. Tensor Spin-Spin Potential in the $^{59}Co + n$ Reaction (T. R. Fisher)

Data on the spin-spin effect, σ_{SS}, in the $^{59}Co + n$ total cross section have been analyzed. It is shown that, by comparing the measurements of σ_{SS} in two suitably chosen geometries, it is possible to extract the strength of both the spherical and tensor spin-spin potentials. This work has been published.[2]

B. CHARGED-PARTICLE REACTIONS

1. β Decay in Mass-12 Nuclei and the Second-Class-Current Problem (J. A. Becker, R. A. Chalmers, L. F. Chase, Jr., R. W. Nightingale, R. E. McDonald, and D. H. Wilkinson*)

Intensities of the ^{12}B and ^{12}N β branches to the ^{12}C first-excited state relative to the ground state are being remeasured. The experimental apparatus has been revised to include a mechanical beam chopper and a gas stripper to produce $^{3}He^{++}$ beams for momentum analysis.

2. M1 γ decays and G-T β decays in the 2s-1d Shell (T. T. Bardin and J. A. Becker)

A comparison of M1 γ decays and the analogous β decays has led to estimates of the influence of the orbital contribution as well as the isoscalar contribution to $\Delta T = 0$ M1 γ decays. The multipole-mixing ratios of the radiations were found to agree with the quasi-rules governing electromagnetic transitions.

3. The ^{29}P 8.38-MeV Level (T. T. Bardin, J. A. Becker, and T. R. Fisher)

Analyses of the angular distributions of the γ rays from the ^{29}P 8.38-MeV level leads to alternative spins $J = 3/2$ or $5/2$ for this state, together with γ-ray multipole mixtures. Gamma-ray branches are also being obtained for this level.

4. Radiative Properties of the ^{48}Ti 2.420- and 3.224-MeV Levels (T. T. Bardin, J. A. Becker, and T. R. Fisher)

The p,p' reaction has been used to populate the ^{48}Ti 2.420- and 3.224-MeV levels. Lifetimes have been measured with the Doppler-shift technique. The γ-ray branching of the 3.224-MeV level has been remeasured using coincidence techniques.

---

*University of Oxford, Oxford, England.

[2] T. R. Fisher, Phys. Lett. 35B, 573 (1971).

5. Ge(Li)-Counter Efficiency Measurements (T. T. Bardin, J. A. Becker, and T. R. Fisher)

The $^{27}Al(p,\gamma)^{28}Si$ reaction has been used to obtain relative-efficiency measurements for the 31.6-cm^3 Ge(Li) counter employed in several of the experiments described above. Resonances at 992 and 1724 keV were used. Spectra were also collected with a Si counter.

6. The ^{18}O 6.86-MeV Level (T. T. Bardin, J. A. Becker, R. W. Nightingale, and E. K. Warburton*)

The ^{18}O 6.86-MeV level has been populated in the $^{19}F(t,\alpha)^{18}O$ reaction. Angular correlations of its decay radiations have been studied with a triple-coincidence technique in order to deduce the level spin.

7. A Mechanical Beam Chopper (R. E. McDonald).

A mechanical beam chopper which is installed in a standard High Voltage Engineering slit assembly has been used successfully for the study of millisecond activities. Readout is via optical sensors.

8. The ^{14}O Nucleus and the Mass-14 Triad (R. G. Hirko,** J. G. Pronko, and D. Slater**)

In order to expand on the intercomparison of the mass-14 triad members, more spectroscopic information is needed in regards to the excited states of the ^{14}O nucleus. The method of particle-particle angular correlations was used with the $^{12}C(He^3,n)^{14}O(p)^{13}N$ reaction to obtain the following preliminary spin assignments: [E_x(MeV),J]; 6.29, 2 or 3; 6.59, 2; 7.78, 2 or 3. Further analysis is presently being pursued.

9. A Study of ^{42}Ar using the ^{40}Ar (t,pγ)^{42}Ar Reaction (J. G. Pronko and R. E. McDonald)

Angular correlations of γ radiation have been measured in a collinear geometry, using both a Ge(Li) γ-ray counter and an array of NaI(Tℓ) counters. Data analyses to provide γ-ray branchings and level spins is in progress.

10. A Study of ^{32}Si with the ^{30}Si (t,pγ) Reaction (J. G. Pronko and (R. E. McDonald)

Measurements of lifetimes for states in ^{32}Si with $E_x < 6.4$ MeV have been done using the Doppler-shift attenuation method. Combined with the measurements of γ-ray branching, level spin, and γ-ray multipole mixing, these data provide a rather complete level scheme for ^{32}Si.

---

* Brookhaven National Laboratory, Upton, New York.

** Stanford University, Stanford, California.

LOS ALAMOS SCIENTIFIC LABORATORY

A. NEUTRON CROSS SECTIONS BY TIME-OF-FLIGHT

1. On the Observation of Neutron-Neutron Scattering at 14 MeV.

(L. Forman, A. D. Schelberg, J. H. Warren, K. Kohr and G. I. Bell)

The production of high energy neutrons (> 15 MeV) within a thermonuclear reaction region can be explained by two dominant processes. First, there is the possibility that 14-MeV neutrons can "upscatter" by means of neutron-neutron scattering. Second, energetic deuterons or tritons can be generated from collisions with 14-MeV neutrons, and then the kinematics of their D-T reactions results in the production of higher energy neutrons. Neutron spectra from two thermonuclear devices, which we shall designate as (D-T,1) (Bame, Hopkins, Felthauser, and Olson, private communication on the measurement of (D-T,1).) and (D-T,2), have been analyzed in this manner. Due to the poor signal-to-noise and the difficulty in accounting for gamma response of the neutron detectors, neither of these measurements can be considered as conclusive; however, because these measurements tend to support one another and both can be explained by theory, a reasonable argument for the observation of neutron-neutron scattering can be presented.

High energy deuterons and tritons are slowed down by interactions with electrons and ions in the mixture. The probability of the energetic particles reacting as they traverse a path length ΔX is $\Delta X N_T \sigma_{DT}$ or $\Delta X N_D \sigma_{TD}$, where N_D and N_T are the deuteron and triton densities respectively, and σ_{DT} and σ_{TD} are the cross sections for the D-T reactions as functions of the energy of the bombarding particles. The usual treatment (See, for example, C. Longmire, Elementary Plasma Physics, John Wiley and Sons, New York (1964)) for the energy loss cross section, σ_{PA}, of a particle P interacting with a target, A, gives

$$\sigma_{PA} = \frac{1}{N_A E_P} \left(\frac{dE}{dx}\right)_{PA} ; \qquad (1)$$

thus, if $N_D \simeq N_T$, the probability $P^{(D+T)}$ of both the deuterons and tritons reacting is:

$$P^{(D+T)}\Delta E = \frac{\Delta E}{E} \sigma_{DT} \frac{1}{2\sigma_{De} + \sigma_{DDR} + \sigma_{DTR}} + \frac{\Delta E}{E} \sigma_{TD} \frac{1}{2\sigma_{Te} + \sigma_{TDR} + \sigma_{TTR}} , \qquad (2)$$

where σ_{De} and σ_{Te}* are the energy loss cross sections to electrons, and σ_{DDR}, σ_{DTR}, σ_{TDR}, and σ_{TTR} are the Rutherford energy loss cross sections. The probability of neutron interaction to cause the in-flight deuterons and tritons is $[(3/4)RN_D\sigma_{nD}(14) + (3/4)RN_T\sigma_{nT}(14)]$ where $(3/4)R$ is the average distance travelled by a neutron born uniformly within the spherical volume $(4/3)\pi R^3$, and $\sigma_{nD}(14)$ and $\sigma_{nT}(14)$ are the 14-MeV neutron scattering cross sections. Since $\sigma_{nD}(14) \simeq \sigma_{nT}(14)$ to a first approximation, the probability of interaction is then proportional to $(N_D + N_T)R$.+

The probability of neutron-neutron scattering (P^{nn}) in a small volume can be shown to be:

$$P^{nn} \cong \frac{9}{16} \frac{R^2}{v_{14}} N_D N_T \langle\sigma v\rangle_{DT} F \sigma_{nn}(14) , \qquad (3)$$

where F is a number somewhat less than 1.0 which accounts for depletion of reactant particles and other secondary effects. The quantity v_{14} is the velocity of a 14-MeV neutron, $\langle\sigma v\rangle_{DT}$ is the Maxwellian average cross section times relative velocity which is a function of mixture ion temperature, and $\sigma_{nn}(14)$ is the neutron-neutron scattering cross section at 14 MeV. The shape of neutron energy spectrum shown in Figure A1 was derived using an isotropic distribution of colliding neutron velocities in the lab system, and an isotropic scattering distribution of scattered neutrons in the center of mass system. Since $[N_D N_T R^2]_{D-T,1} \sim 15\ [N_D N_T R^2]_{D-T,2}$ and $[(N_D+N_T)R]_{D-T,1} \sim 3.2\ [(N_D+N_T)R]_{D-T,2}$, then by normalizing the two curves at ~ 15 MeV (where the in-flight reactions are dominant) we would expect the n-n scatterings to differ by ~5; this is in some agreement with the data. Fig. A-2 shows the (D-T,1) spectrum corrected for neutron-neutron scattering as fitted with a spectrum derived from knock-on deuterons and tritons; this spectrum was derived by assuming isotropic D-T reactions in the lab system (N. Jarmie and J. D. Seagrave, LA-2014 (1956)) and that, since above 1.0 MeV σ_{DT} and σ_{TD} are very small, all deuterons and tritons slow down to 1 MeV before reacting. Since most cross sections in these energy regions are slowly varying with energy, we have ignored changes in the spectrum caused by attenuation between source and

*For electron temperatures less than 20 keV, the higher energy deuterons and tritons are slowed down primarily by electron collisions; we have chosen 10 keV for our calculations.

+At these mixture temperatures where energy loss to electrons is dominant, a more rigorous derivation gives the number of in-flight deuterons and tritons produced and then reacting with thermal ions as proportional to $N_D N_T R/(N_D + N_T)$ but this changes the following comparison of (D-T,1) and (D-T,2) by less than 25%.

detector. From the amplitude of the flux attributed to n-n scattering, relative to the 14-MeV peak, one can estimate the n-n scattering cross section. The present rough data and analysis are consistent with a $\sigma_{nn}(14)$ of a few tenths of a barn; although $\sigma_{nn}(14)$ values of a few barns or a few hundredths of a barn cannot be excluded.

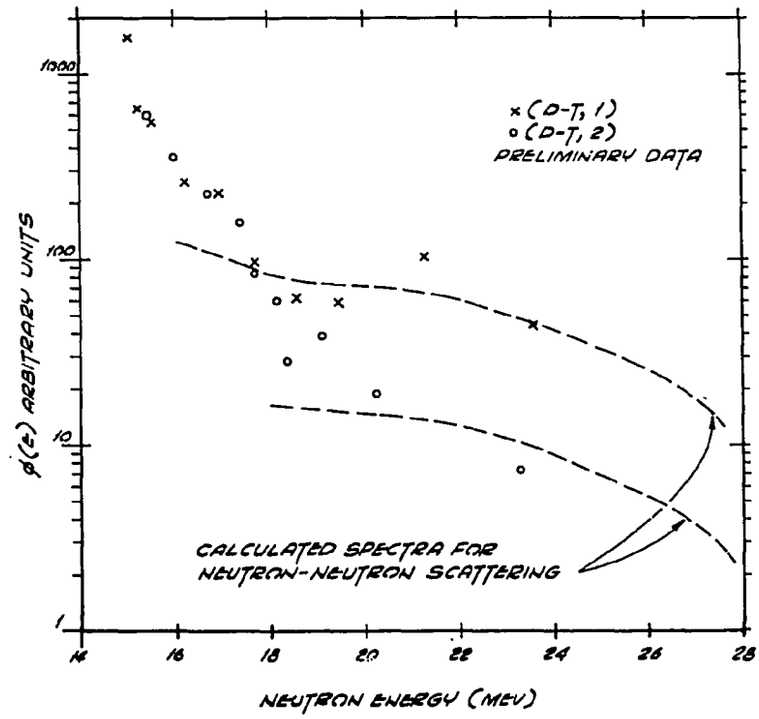

Fig. A-1. Neutron spectra from the (D-T,1) measurement of Bame et al and preliminary data of (D-T,2). The neutron-neutron scattered spectrum was derived assuming an isotropic distribution of colliding 14-Mev neutrons in the laboratory system and an isotropic scattering distribution of scattered neutrons in the center of mass system. A very rough estimate of the relative number of neutron-neutron scatters (see text) gives a factor of ~5 difference between the two devices when the spectra are normalized at 15 MeV. It is further clear that the (D-T,2) spectrum gives the maximum contribution of in-flight deuteron and triton generated fast neutrons which should be present in the (D-T,1) spectrum. The neutron-neutron cross section at 14-MeV was estimated at a few tenths barn.

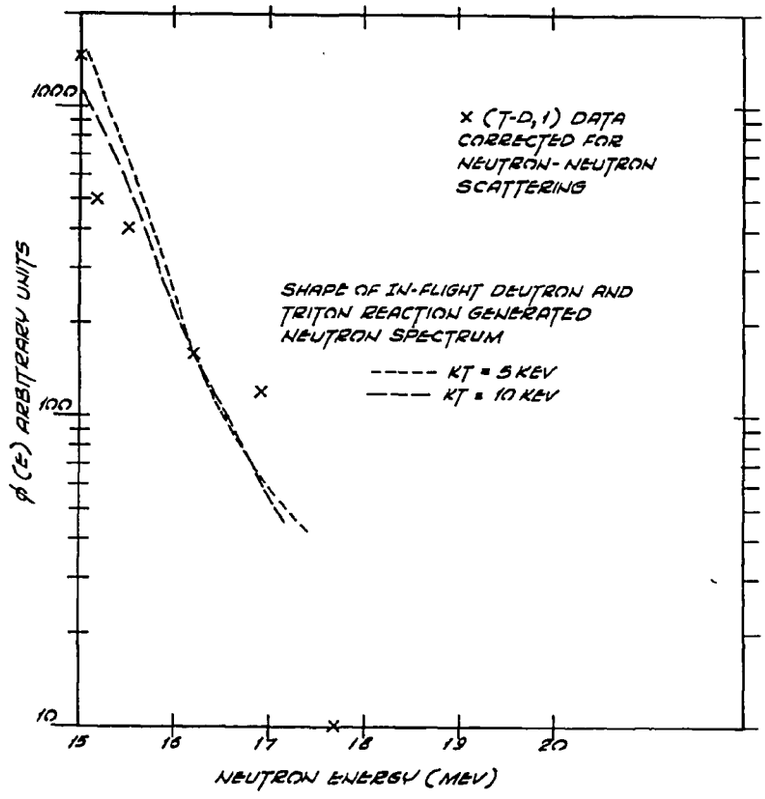

Fig. A-2. The (D-T,1) spectrum corrected for presumed neutron-neutron scattering. The fitted curve was derived considering only those deuterons and tritons that had slowed to 1 MeV before reacting with thermal ions. The curve derivation assumed that below 1 MeV, the neutron producing reaction proceeded isotropically in the laboratory system; this assumption is incorrect but when including the slight angular anistropy at these lower energies the shape of the calculated curve should not be affected very greatly. We have concluded from this figure that in-flight deuteron and triton generated neutrons are dominant in the 15-17 MeV region.

2. Resonance Parameters of ^{238}Pu. (M. G. Silbert; J. R. Berreth (Aerojet Nuclear Co.)) Relevant to Requests 439, 440, 441 NCSAC-35.

Final values have been obtained for 49 resonances observed in $^{238}Pu + n$. A preliminary report was presented in report NCSAC-31 (May 1970). By combining the resonance fission fragment yields, proportional to the fission cross section, and the resonance gamma-ray yields, proportional to a sum of the fission and capture cross sections, neutron and fission widths were derived for each resonance. The radiative capture width was assumed to be 34 ± 6.8 meV for each resonance. Resonance energies, widths, and errors in the widths are presented in Table A-1.

An s-wave neutron strength function of $(1.2 \pm 0.2) \times 10^{-4}$ is derived consistent with other nuclei reported in this mass region.

TABLE A1

Resonance Parameters for ^{238}Pu

E_o(eV)	Γ_n^o(meV/$\sqrt{eV}$)	Γ_f(meV)
18.6	0.96 ± 0.22	1.6 ± 0.5
32.2	0.012 ± 0.007	$4.8^{+6.7}_{-1.9}$
36.6	0.004 ± 0.002	5.9 ± 4.8
59.8	0.17 ± 0.02	0.67 ± 0.17
70.1	0.30 ± 0.05	7.4 ± 2.2
77.7	0.003 ± 0.002	$9.4^{+19.1}_{-4.2}$
83.0	2.26 ± 0.46	3.5 ± 0.9
96.2	0.0057 ± 0.0031	$4.9^{+5.8}_{-2.2}$
99.6	0.026 ± 0.007	5.1 ± 2.1
110.1	0.54 ± 0.10	4.1 ± 1.1
111.2	0.012 ± 0.006	$3.1^{+2.9}_{-1.3}$

TABLE A1 (CONTINUED)

E_o(eV)	Γ_n^o(meV/$\sqrt{eV}$)	Γ_f(meV)
113.6	1.15 ± 0.18	5.4 ± 1.4
118.6	2.83 ± 0.74	1.6 ± 0.4
122.4	2.71 ± 0.68	8.5 ± 2.2
129	0.019 ± 0.015	1.0 $^{+3.0}_{-0.5}$
132.4	0.074 ± 0.016	5.3 ± 1.8
139.7	0.24 ± 0.03	6.3 ± 1.6
151.1	2.39 ± 0.60	9.2 ± 2.4
165.0	0.017 ± 0.008	10.7 $^{+14.4}_{-4.2}$
171.0	3.58 ± 1.29	0.72 ± 0.17
176.8	0.20 ± 0.03	44.0 ± 17.0
182.9	2.11 ± 0.52	7.1 ± 1.8
192.5	1.12 ± 0.27	130 $^{+413}_{-59}$
203	0.35 ± 0.04	2.2 ± 0.5
216	1.20 ± 0.24	22.8 ± 6.8
221	3.97 ± 1.72	1.20 ± 0.30
232	0.047 ± 0.019	0.84 ± 0.44
245	0.43 ± 0.09	25.3 ± 9.7
252	0.98 ± 0.29	57 $^{+63}_{-21}$
261	0.016 ± 0.010	7.1 $^{+24}_{-3.4}$
285	1.54 ± 0.57	3500 ±500 [a]

[a] Determined by multilevel shape analysis of the fission cross section.

TABLE A1 (CONTINUED)

E_o(eV)	Γ_n^o(meV/$\sqrt{eV}$)	Γ_f(meV)
289	2.21 ± 0.68	23.7 ± 7.5
300	3.20 ± 1.33	102 $^{+161}_{-41}$
305	0.46 ± 0.10	68 ± 36
320	9.6 ±10.5	5.5 ± 1.4
327	1.53 ± 0.37	14.8 ± 4.0
337	0.84 ± 0.15	8.4 ± 2.2
361	0.042 ± 0.028	7.4 $^{+25}_{-3.6}$
368	0.90 ± 0.23	4.4 ± 1.3
382	0.020 ± 0.012	18 $^{+127}_{-9}$
391	0.66 ± 0.15	2.8 ± 0.9
408	0.92 ± 0.18	2.5 ± 0.7
419	2.6 ± 1.3	29.1 ± 11.8
426	2.3 ± 1.0	11.3 ± 3.5
448	0.31 ± 0.08	71 $^{+134}_{-30}$
461	2.31 ± 1.08	6.7 ± 2.1
465	3.97 ± 2.82	6.7 ± 2.1
473	1.06 ± 0.31	2.3 ± 0.7
496	0.42 ± 0.09	6.8 ± 2.2

3. Resonance Parameters (J,K) for ^{233}U, ^{235}U, and ^{237}Np.
G. A. Keyworth, F. T. Seibel, and J.W.T. Dabbs (ORNL)) Relevant to Requests 367, 400, NCSAC-35.

The variation of the K-quantum number in resonance fission of ^{235}U has been reported by Pattenden and Postma (Nuc. Phys. A 167, 225). A strong correlation has been noted between these results and the R-values (ratio of valley-to-peak yield in the fission mass distribution) reported by Cowan et al (Phys. Rev. C2, 615). Unpublished data of Pattenden and Postma for the lowest energy resonance in ^{235}U at 0.28 eV also has been found to show a strong correlation with the fission fragment kinetic energy variation. (Moore and Miller, Phys. Chem. Fission, Vol. I, p. 87, 1965). These results indicate that the K-quantum number is connected with physical properties important to reactor design, and that a meaningful multilevel analysis of resonance cross sections of fissile nuclides can only be made if J and K are used as input.

A measurement of J and K for ^{233}U, ^{235}U, and ^{237}Np is planned on ORELA at Oak Ridge National Laboratory, using a neutron beam polarized by transmission through LMN, and a polarized target. Yields and fission fragment anisotropies will be determined by measuring fission neutrons at 0 and 90° to the target nucleus orientation.

Preparation of an N_pAl_2 sample is in progress and a small sample was quite successful, showing nearly 100% polarization below .05°K. Enriched ^{235}U has been received and delivery of enriched ^{233} is expected at this time. Clayton Olsen (LASL) will prepare samples of US which have been shown to behave similarly to the N_pAl_2. Methods of fabrication of a final target of these highly fragile materials are being explored.

Portions of the LMN system, both electronic and plumbing, are being assembled. The cryogenic system is nearly completed in the LASL shops and will undergo extensive testing. The superconducting coil has still not been tested due to failures in the test dewar but, hopefully, these problems have been circumvented and testing and field mapping will begin.

Plans are being formulated and the hardware built for control and monitoring of much of the apparatus by the PDP-15 computer.

A new 60 K Gauss separable split pair superconducting coil has been ordered for the dilution refrigerator and final design for a new refrigerator cryostat is awaiting exact dimensional information from the coil manufacturer.

Several liquid scintillator and photomultiplier tube combinations are being evaluated for maximum neutron and γ descrimination characteristics. Similarly, several pulse shape discrimination techniques are being evaluated before the final circuits are purchased.

B. VAN DE GRAAFF NEUTRON STUDIES

1. Elastic Scattering and Polarization of Fast Neutrons by Liquid Deuterium and Tritium [J. D. Seagrave, J. C. Hopkins, A. Niiler (Edgewood Arsenal), R. K. Walter (Webb School), R. H. Sherman, and E. C. Kerr] Relevant to NCSAC-35, Request 4.

This paper has been accepted for publication in Annals of Physics. The polarization results have been given on pp. 150-151 of NCSAC-31, and the cross sections on pp. 149-150 of NCSAC-33. The non-absolute scale for 9-MeV n-D scattering has been increased 4.8% over the values previously given on the basis of the logarithmic spline fitting and the known values of the total and nonelastic cross sections. Integral cross section values for deuterium and tritium are given in Tables B1 and B2, and illustrated in Fig. B1.

TABLE B1

Integral Neutron Cross Sections for Deuterium

E_n, MeV	σ_T,[a] mb	σ_{el}, mb	σ_{ne}, mb
5.55	1521±11	1480[b]	50[c]
7.00	1317±10	1267[b]	84[c]
8.00	1210±13	1127[b]	103[c]
9.00	1124±10	1002[b]	122[c]
14.3	806±14	648±83[d]	158±84
18.55	643±12	486±39	157±41
20.50	586±10	442±36	144±37
23.00	523± 7	399±35	124±36
36.00	325± 9	196± 5[e]	129±10
46.3	243± 6	146± 3[e]	97± 7

[a] From 125-datum spline fit.

[b] Normalized.

[c] Smooth curve through direct measurements.

[d] Berick et al., Phys. Rev. 174, 1105 (1968).

[e] Romero et al., Phys. Rev. C2, 2134 (1970).

TABLE B2

Integral Neutron Cross Sections for Tritium

E, MeV	σ_T, mb	σ_{el}, mb	σ_{ne}, mb
6.0	2030±122	2165±119	
9.0	1436± 86	1341± 74	
14.1	965± 20	920 [a]	45± 5 [b]
18.0	754± 47	714± 47	40±66
19.5	690± 40	612± 35	78±53
21.0	635± 40	535± 30	100±50
23.0	579± 40	422± 26	157±48

[a] Estimated

[b] Direct measurement, Mather and Pain, AWRE 047/69.

The new nonelastic data shown by open circles are $\sigma_T-\sigma_{el}$ for deuterium, those shown as solid bars are $\sigma_T-\sigma_{el}$ for tritium, and the point at 14.46 MeV marked σ_{ne}(1971) is the preliminary value obtained by integration of the resolved breakup proton energy spectrum reported in the next section. The open hexagons at 36 and 46.3 MeV are the University of California, Davis, values given in Table B1 which are derived from Seagrave's spline fit to the σ_T data, ignoring the published ad hoc University of California, Davis, σ_T values shown in Fig. B1, which are believed to be too high. Unpublished University of California, Davis, data confirm this interpretation (Paul Brady, private communication). In Fig. B2, the deuterium nonelastic cross section is shown on a linear scale, and compared with the calculations of I. H. Sloan [Nucl. Phys. A168 (1970) 211] and with the curve shown on the log-log plot of Fig. B1, together with earlier data.

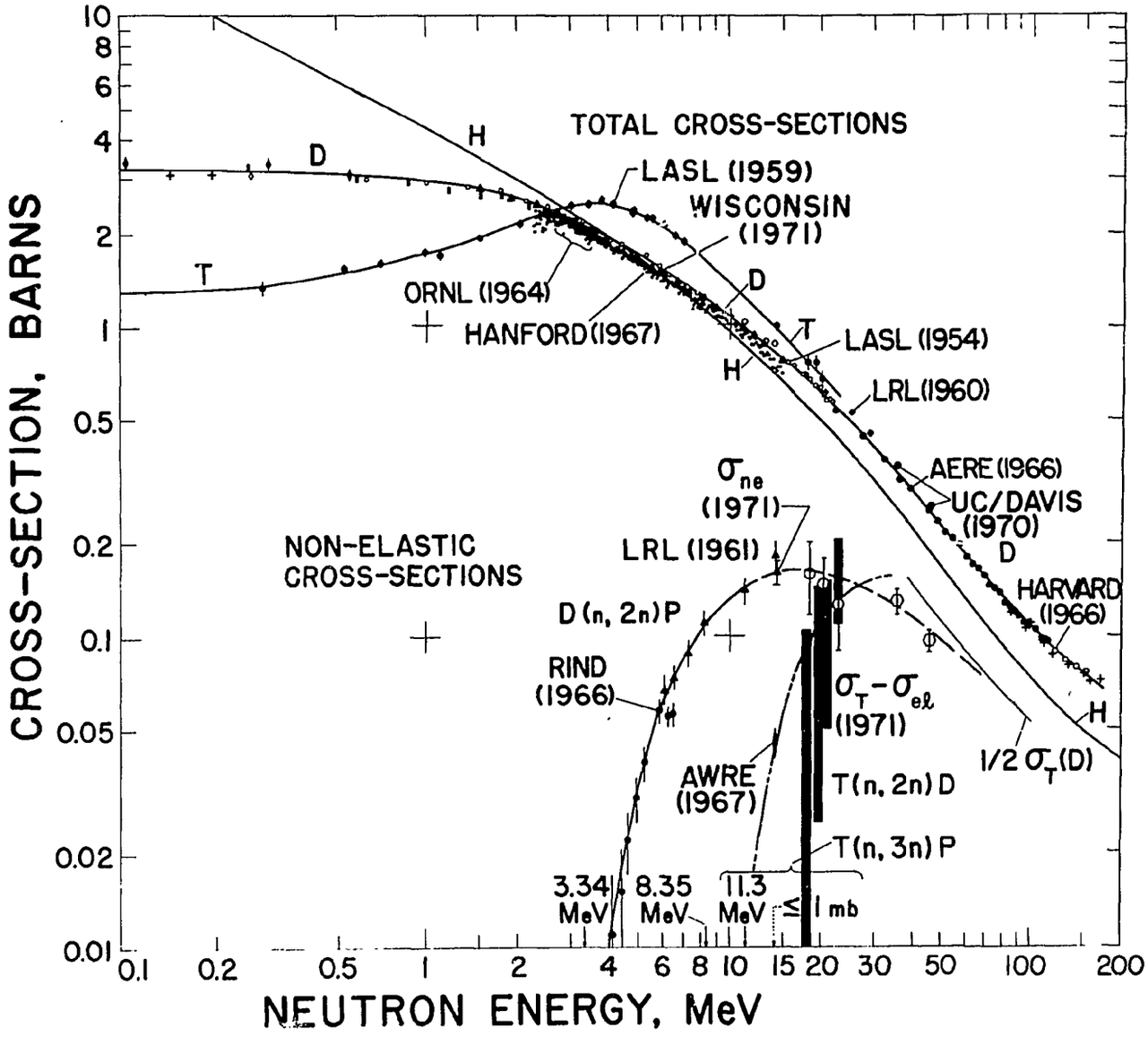

Fig. B-1. Integral (angle-averaged) cross sections for deuterium and tritium.

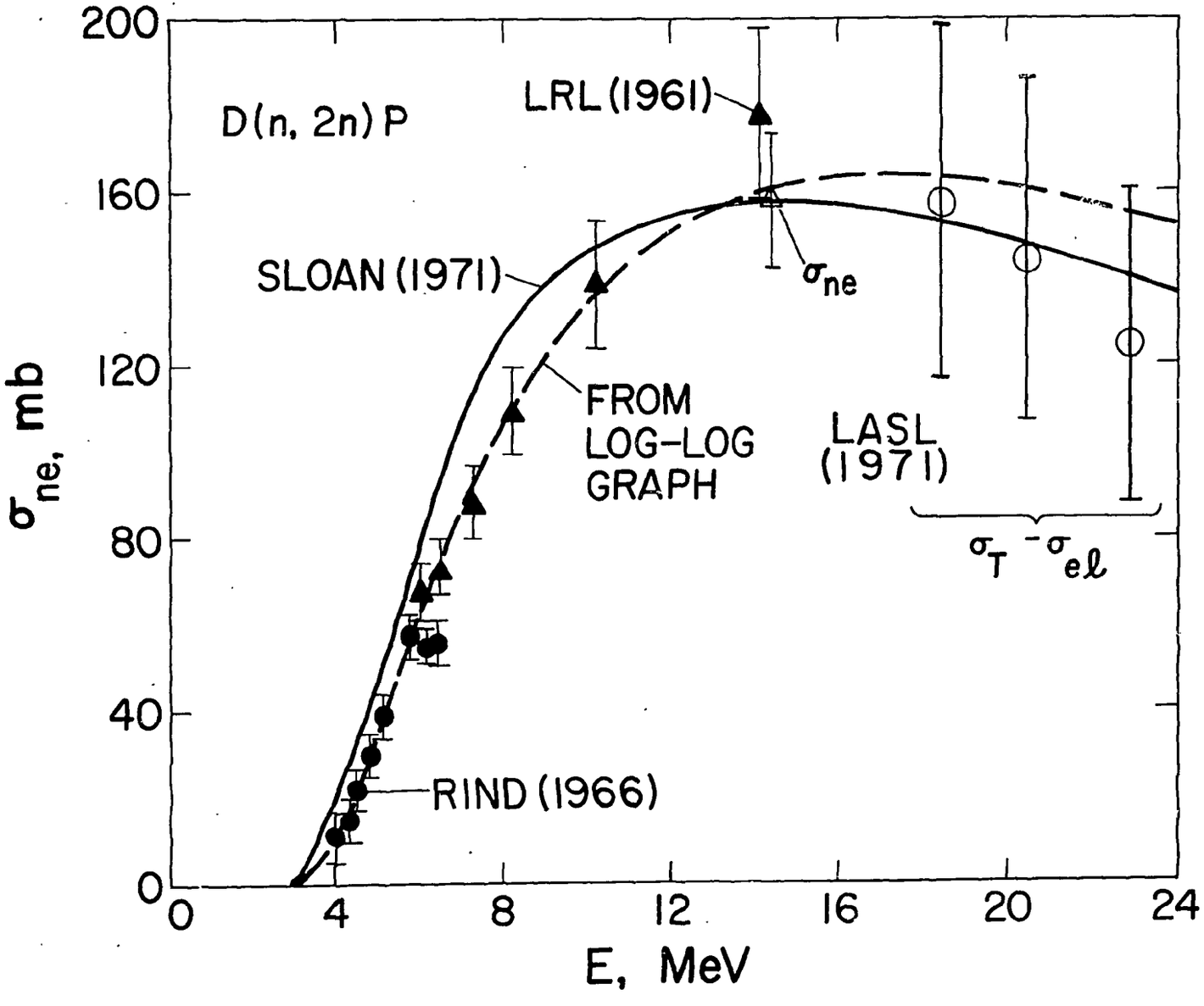

Fig. B-2. Non-elastic cross section for deuterium (linear scale).

2. Breakup Protons from the D(n,2n) Reaction (E. R. Graves and J. D. Seagrave)

The breakup protons from 14.46-MeV neutrons incident on a C_6D_6 scintillator have been separated by pulse-shape discrimination technique from the elastic deuterons down to a proton energy of a little below 3 MeV. The energy spectrum of deuterons has been converted to the angular distribution of elastic scattering and compared with published angular distribution data. The integral of the elastic scattering from the minimum cross section to the forward scattered deuteron has been used to normalize to obtain the cross section for breakup protons. Figure B-3 shows the energy spectrum of breakup protons obtained. The circles and X's represent data points taken with two different energy window widths. A solid line curve has been sketched through the data and extrapolated to zero. The dashed curve is a phase space distribution. It is obvious that the low-energy protons do not follow a phase space distribution, indicating that final state interactions play an important part in the reaction.

The integral of the breakup protons is the inelastic cross section which has been derived by others by subtracting the integrated elastic cross section from the total cross section. In the present method the inelastic value comes from a ratio to the elastic value and does not involve the total cross section at all. It is sensitive to changes in the elastic cross section value in the opposite sense from the values obtained by subtraction.

The integrated σ_{inel} down to the lowest E_p measured is 140 mb. The solid curve sketched gives a complete integral of 158 mb. The dash-dot curve illustrates the assumption that below the lowest measured E_p the distribution approaches the phase space distribution. This extreme assumption yields an integral σ_{inel} of 174 mb. The values obtained at the Los Alamos Scientific Laboratory in the 17-23 MeV range cluster around 150-160 mb as contrasted to a Livermore value at 14 MeV of 180 mb, although the uncertainties are large enough to overlap. An upper limit to the uncertainty in the present value of 158 mb can be taken to be ± 16 mb.

3. Elastic n-^{3}He Scattering (M. Drosg, J. C. Hopkins, D. K. McDaniels, J. T. Martin, J. D. Seagrave, and E. C. Kerr) Relevant to NCSAC-35, Request 7.

Neutrons of 7.9, 12.0, 13.6, 14.4, and 23.7 MeV were elastically scattered from a 0.5-mole sample of liquid ^{3}He. The angular distributions of the scattered neutrons were measured by the time-of-flight method at 14 angles ranging from $\cos\theta_{CM}$ = 0.9 to -0.7.

The absolute scale for the angular distributions was obtained by normalization to the well-known ^{1}H(n,n)^{1}H cross section. The scale factor error is between 3 and 5%.

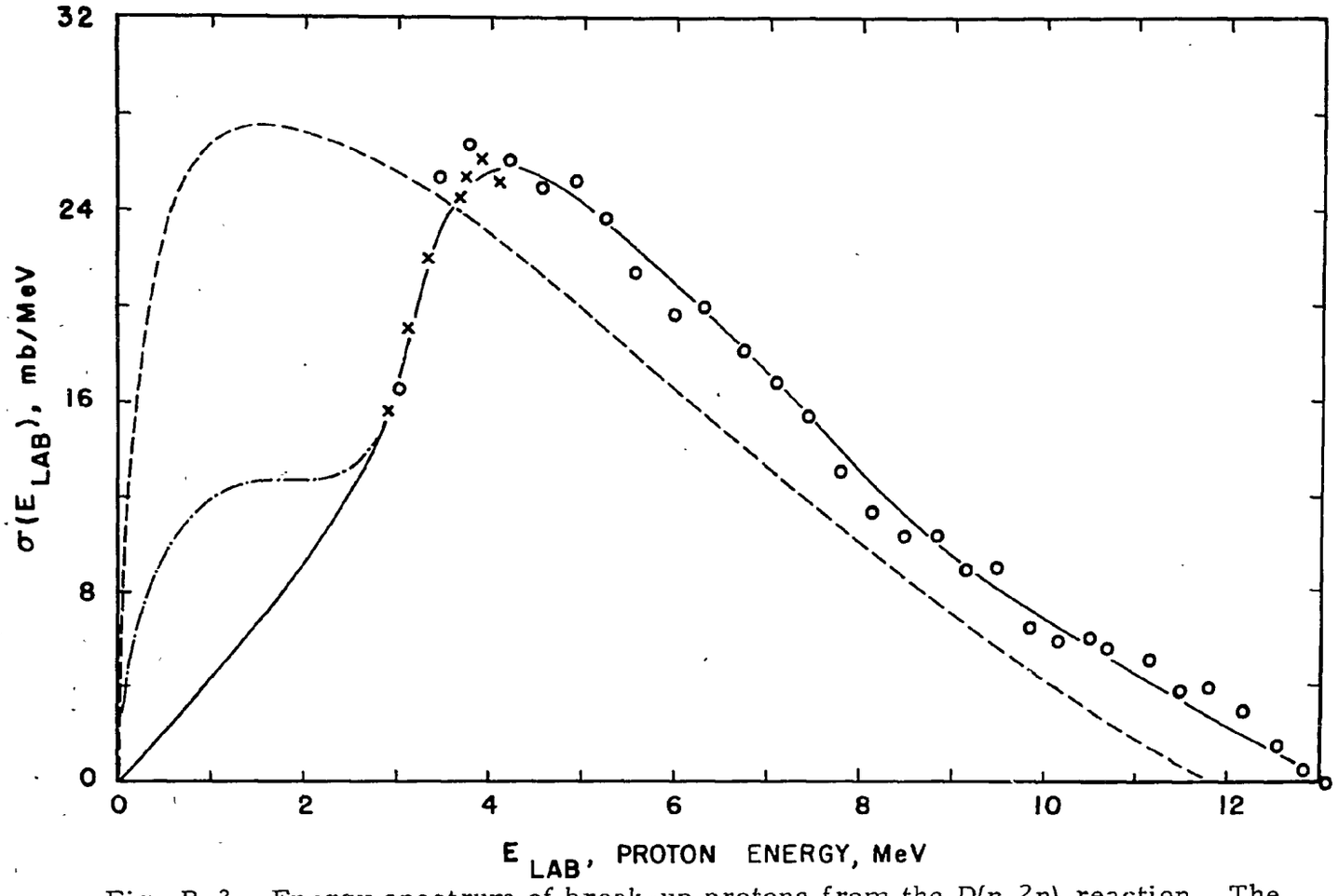

Fig. B-3. Energy spectrum of break-up protons from the D(n, 2n) reaction. The dashed curve is a phase space distribution for three-body breakup.

Multiple scattering corrections must be applied before the final values will be available.

4. Absolute Fission Cross Section for ^{235}U. (R. K. Smith, D. M. Barton, and P. G. Koontz) Relevant to NCSAC-35, Requests 388, 389, 390, 391.)

The fission detector and foil have been mounted in the counter and an attempt has been made to take data closer to the actual experimental conditions. Data have been taken using the on-line computer for data storage and analysis.

The background from room scattering with timing is very low and appears to be mixed with the local scattered neutrons from material at various distances from the fission detector. It is not clear what the scattering correction should be, however, it would appear to be small -- perhaps as small as 0.1% when timing is used.

In connection with the studies made on neutron telescopes for use with the absolute ^{235}U experiment, neutron fluxes have been studied from 1 to 7 MeV.

The experience gained from the flux monitoring in the neutron energy region from 1 to 30 MeV allows one to conclude that by using a special detector that does not have gold and aluminum plating over the glue bonding the silicon to its lavite ring as a first detector and either a second silicon detector and then a 0.25" thick sodium iodide detector, or going directly from the first "special" silicon detector to the 0.25" thick sodium iodide detector, it is possible to look at neutron fluxes with the same neutron telescope and obtain hydrogen foil out backgrounds always less than 10% and in many cases less than 1%. It would appear possible to use the same neutron telescope to measure neutron fluxes below 1 MeV if thinner foils were used.

The first detector in the above described telescope must be used as a separate non-coincidence device for those neutron energies in which the recoil protons do not penetrate into the second detector. If this first detector is 500 microns thick, neutron fluxes in the region from 1 to 7 MeV can be measured as easily as one can measure fluxes with a fission ionization chamber and the room scattered backgrounds are considerably reduced from the neutron flux measurement by the directional effect of the telescope. Perhaps one can use even thicker silicon detectors of this special fabrication and measure neutron fluxes in this simple manner to even higher energies; however, when one uses thin detectors and requires coincidence between two detectors, the CH_2 foil out background is considerably smaller.

5. Study of the Tritium Source Reactions. (D. K. McDaniels, M. Drosg, J. C. Hopkins, J. T. Martin, and J. D. Seagrave)

Both reactions $^{3}H(p,n)^{3}He$ and $^{3}H(d,n)^{4}He$ are convenient sources for monoenergetic neutrons in a wide energy range (depending on the available accelerator). In order to extend the data to higher energies and to resolve a suspected systematic error of the order of 20% in the $^{3}H(d,n)^{4}He$ cross section above 10 MeV, differential cross section measurements at angles between 0° and 140° were performed for particle energies of 6, 7, 10, 11, 12, 13, 14, 15, and 16 MeV. Using both the proton recoil counter telescope technique and the associated particle techniques will allow us to derive the scale factor with an uncertainty of approximately 3%. In a preliminary analysis it was found that the 0° cross sections of the $^{3}H(d,n)^{4}He$ reaction at 11 MeV is about 12% higher than found in previous publications. Besides the energy dependence of this cross section above 10 MeV is much less pronounced than suggested by previous evaluations.

6. Stable Isotope Ratio Determination by Nuclear Methods. (J. D. Seagrave)

In connection with the laboratory's production program for Stable Isotopes of Carbon, Oxygen, Nitrogen, and Sulphur (ICONS), memoranda have been prepared for the ICONS Advisory Committee on nuclear methods for determination of the isotopic ratios $^{12}C:^{13}C$, $^{14}N:^{15}N$, and $^{16}O:^{17}O:^{18}O$ in the near-normal range of dilutions expected in the samples for analysis of a wide variety of possible applications. Some preliminary conclusions may be stated.

a) Since the rarer isotopes are neutron-rich, neutron capture cross sections for these isotopes are small, and direct activation by slow neutrons does not appear useful. However, prompt gamma detection of ^{1}H, ^{13}C, ^{14}N, and ^{34}S is feasible, and may be useful for the detection of compounds with multiple labels which can be concentrated in several-gram samples.

b) Sensitivity of the $^{12}C:^{13}C$ radiative capture ratio method. A carbon isotope ratio determination can be made by comparing the (p,γ) yields from the ^{12}C resonance at 1.70 MeV (width 70 keV) and the ^{13}C resonance at 1.75 MeV (width 0.075 keV). The principal results are:

1. The $^{13}C(p,\gamma)$ yield can be determined to 1% in 2-μA minutes with only 50 nanograms of ^{13}C.

2. Using a 7-keV target thickness of normal carbon, the isotope ratio can be determined to 1% in 4-μA minutes, or to 0.1% in 8-μA hours.

3. For a CO_2 sample, as little as 7 microliters would be required in a 3-mm diameter by 8-mm long cell at 0.1 atm.

4. The proximity and narrowness of the resonances permits scanning the region of interest by modulating the target potential with a 60-cycle ramp or even sine sweep, and gating a sample of the sweep voltage to a pulse-height analyzer when a gamma ray is detected, thus providing a continuous display of the data.

c) A somewhat similar situation exists for comparing $^{14}N(p,\gamma)$ with $^{15}N(p,\alpha\gamma)$.

d) Elastic backscattering of protons exhibits sharp resonances of possible use for isotope identification, especially in combination with the radiative capture technique.

e) For the oxygen isotopes, although the $^{16}O(p,\gamma)^{17}F$ yield is nonresonant, observation of the gamma spectrum near the anomaly at 2.65 MeV has revealed stronger lines from $^{17}O(p,p'\gamma)^{17}O$ and $^{18}O(p,p'\gamma)^{18}O$ which permit determination of the isotope ratios at a fixed proton energy by analysis of the gamma spectrum.

A graphical compilation of relevant charged-particle cross sections is in preparation.

Group A-1 (G. R. Keepin, et al) is investigating experimentally both the thin-target method for carbon near 1.75 MeV and the thick-target method near 0.5 MeV suggested by Ricci (Nucl. Inst. Meth. 94 (1971) 565).

C. FISSION ISOMER STUDIES

1. Excitation Function for the $^{235}U(\alpha,3n)^{236}Pu$ Reaction. (G. Bethune, H. C. Britt and B. H. Erkkila)

The excitation function for the production of ^{236}Pu has been studied by alpha bombardment of ^{235}U targets with energies ranging from 24.0 to 28.0 MeV. The fission cross section for the $^{235}U(\alpha,f)$ reaction has also been measured at these energies. The ^{236}Pu production cross section was measured by detecting the known energy alpha decay groups. The measurement was complicated by the production of ^{236}Np (which then decays to ^{236}Pu) through the (α,t) + (α,dn) + $(\alpha,p2n)$ reactions. The analysis required a least squares fit to the measured growth function using the known 22 h half-life of ^{236}Np. The results are being compared to calculations from a model used to fit fission isomer results from the $^{235}U(\alpha,2n)^{237m}Pu$ reaction.

2. Fission Isomer Studies on Pu Targets. (H. C. Britt, B. B. Back and B. H. Erkkila)

The experimental studies of fission isomers at the tandem have been completed. Excitation functions were obtained for (t,2n), (t,3n),

and (p,2n) reactions on a series of plutonium isotopes. These results are in Figs. C1 and C2 where solid points are the current measurements and open points data for the (p,2n) reaction obtained by the Copenhagen group. The (p,2n) results complement previous measurements and give a new threshold measurement for the $^{244}Pu(p,2n)^{243m}Am$ reaction. The (t,3n) results give a new threshold measurement for the $^{244}Pu(t,3n)^{244m}Am$ reaction and the data on the $^{240}Pu(t,3n)^{240m}Am$ and $^{242}Pu(t,3n)^{242m}Am$ reactions can be compared to data from previous 2n evaporation reactions used to populate the same isomers. A new isomer ^{245m}Am with $T_{1/2}$ = 390 ± 70 nsec was discovered.

D. THERMAL NEUTRON CAPTURE GAMMA-RAY STUDIES

1. $^{12}C(n,\gamma)^{13}C$ (E. T. Jurney)

Three new transitions have been observed in ^{13}C following thermal neutron capture by ^{12}C. Fig. D-1 shows the decay of ^{13}C from the (n,γ) reaction, where the additional γ-rays are those exciting and de-exciting the $1/2^+$ level at 3088 keV. Energies are in keV and preliminary intensities (in parentheses) are in photons per 100 neutrons captured.

D. Kurath and R. D. Lawson (Nucl. Phys. 23, 5 (1961)) quote a value of $(7\pm1) \times 10^{-3}$ for the E1 branching ratio for the de-excitation of the 3684 keV level as arrived at by D. H. Wilkinson from a Breit-Wigner analysis of (p,γ) resonances in ^{13}C. The directly observed ratio is in good agreement with the earlier value.

2. Capture Gamma-Ray Study of ^{188}Re. (E. B. Shera, R. K. Sheline (Florida State Univ.))

New experimental work indicated the existence of several isomeric states in ^{188}Re, including a completely new band at 360.9 keV. A summary of our interpretation of this new data is shown in Table D-1. The calculated Weiskopf hindrance factor, F_w, is shown for each transition. Additional analysis of existing data has revealed the location of the five new rotational bands listed below.

Energy of band head (keV)	K^π	Configuration p	Configuration n
325	4^-	$5/2^+[402]\uparrow$	$\pm\ 3/2^-[501]\uparrow$
556	1^-		
360	5^+	$9/2^-[514]\uparrow$	$\pm\ 1/2^-[510]\uparrow$
480	1^+	$9/2^-[514]\uparrow$	$-\ 7/2^-[503]\uparrow$
582	1^-	(K-2) γ band on G. S.	

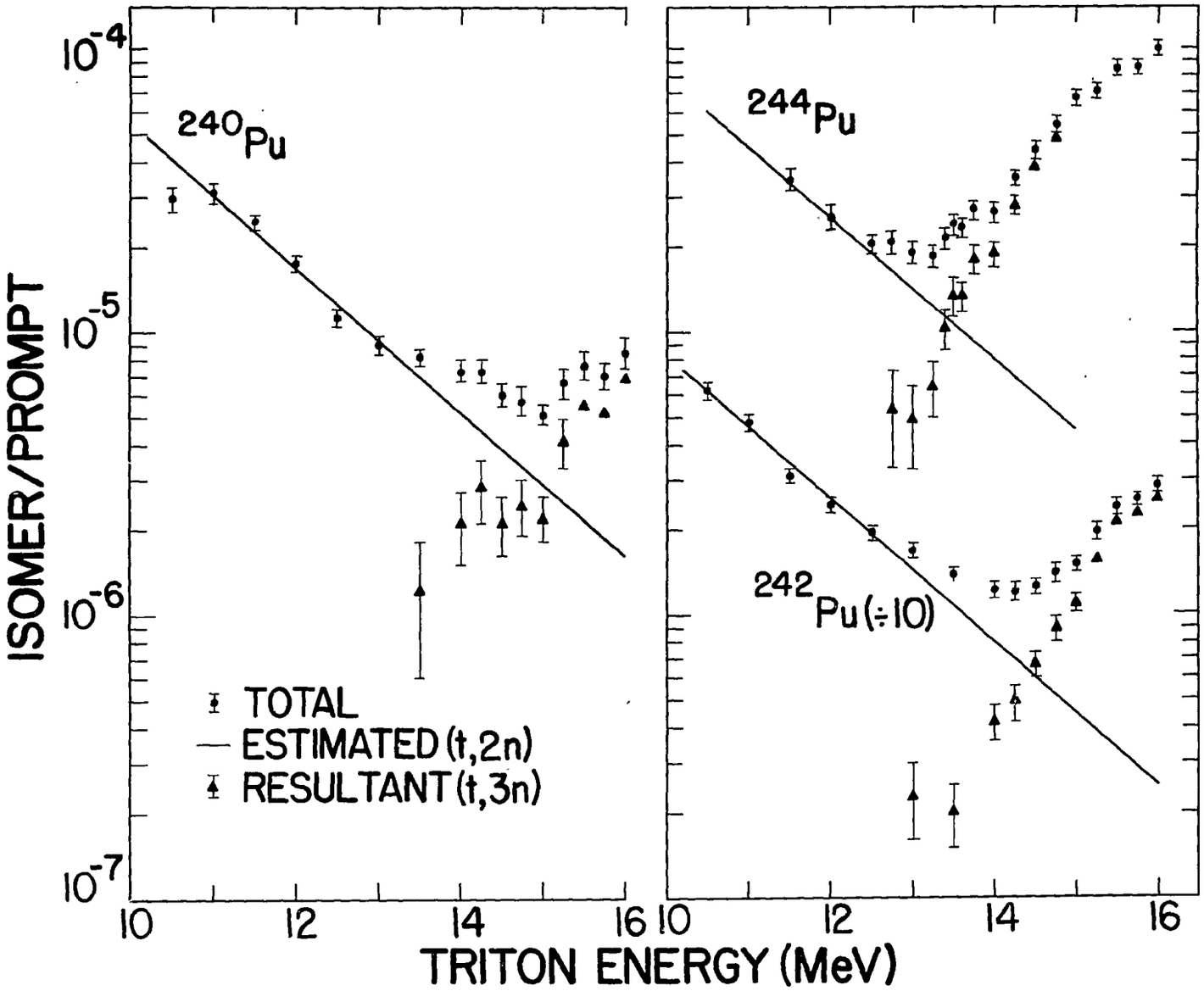

Fig. C-1. Measured isomer/prompt ratios for fission isomers formed by triton bombardment of ^{240}Pu, ^{242}Pu, and ^{244}Pu targets.

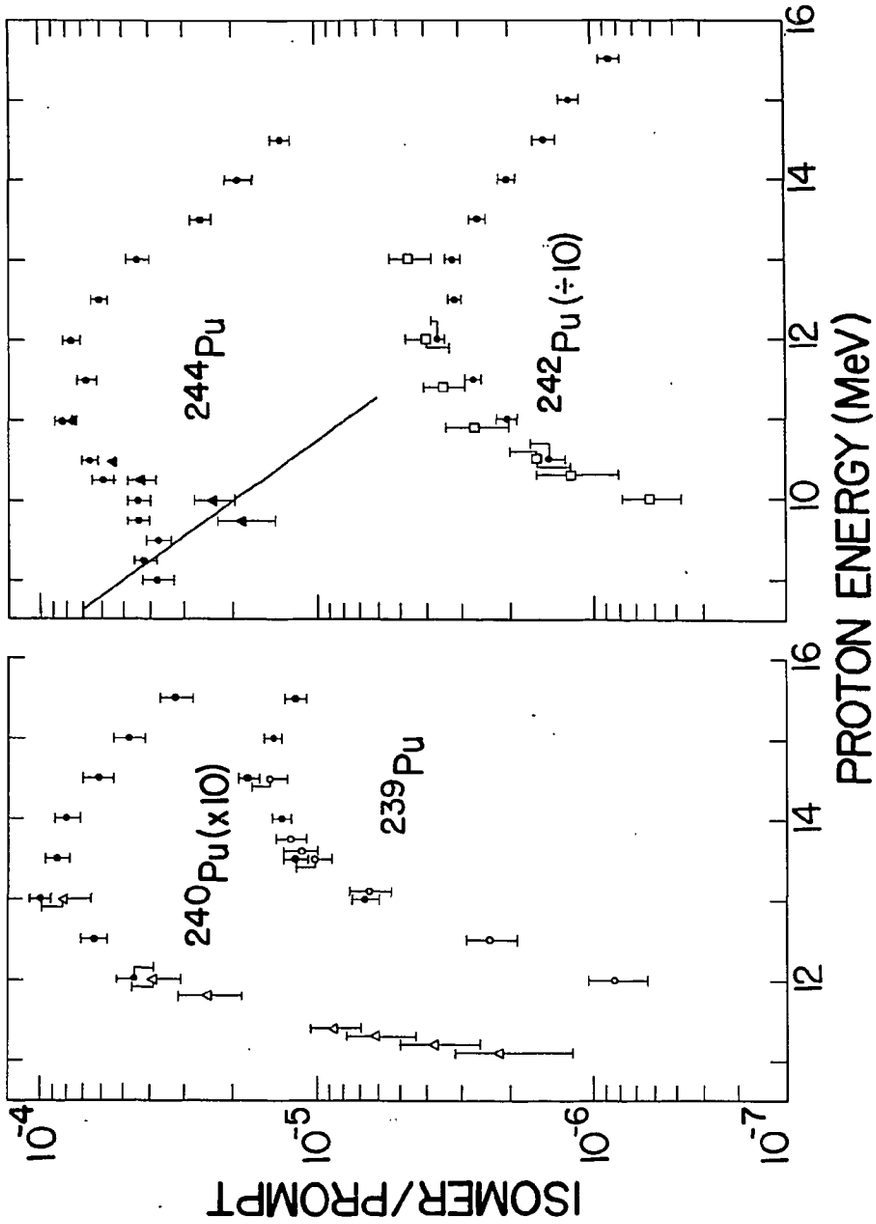

Fig. C-2. Measured isomer/prompt ratios for fission isomers formed by proton bombardment of ^{239}Pu, ^{240}Pu, ^{242}Pu, and ^{244}Pu targets. Open points are previous measurements of the Copenhagen group [N. L. Lark et al., Nucl. Phys. A139, 481 (1969) and G. Sletten, private communication (1970)]. For the ^{244}Pu target the solid line represents the estimated (p, n) contribution and the solid triangle the resultant estimate for the (p, 2n) contribution.

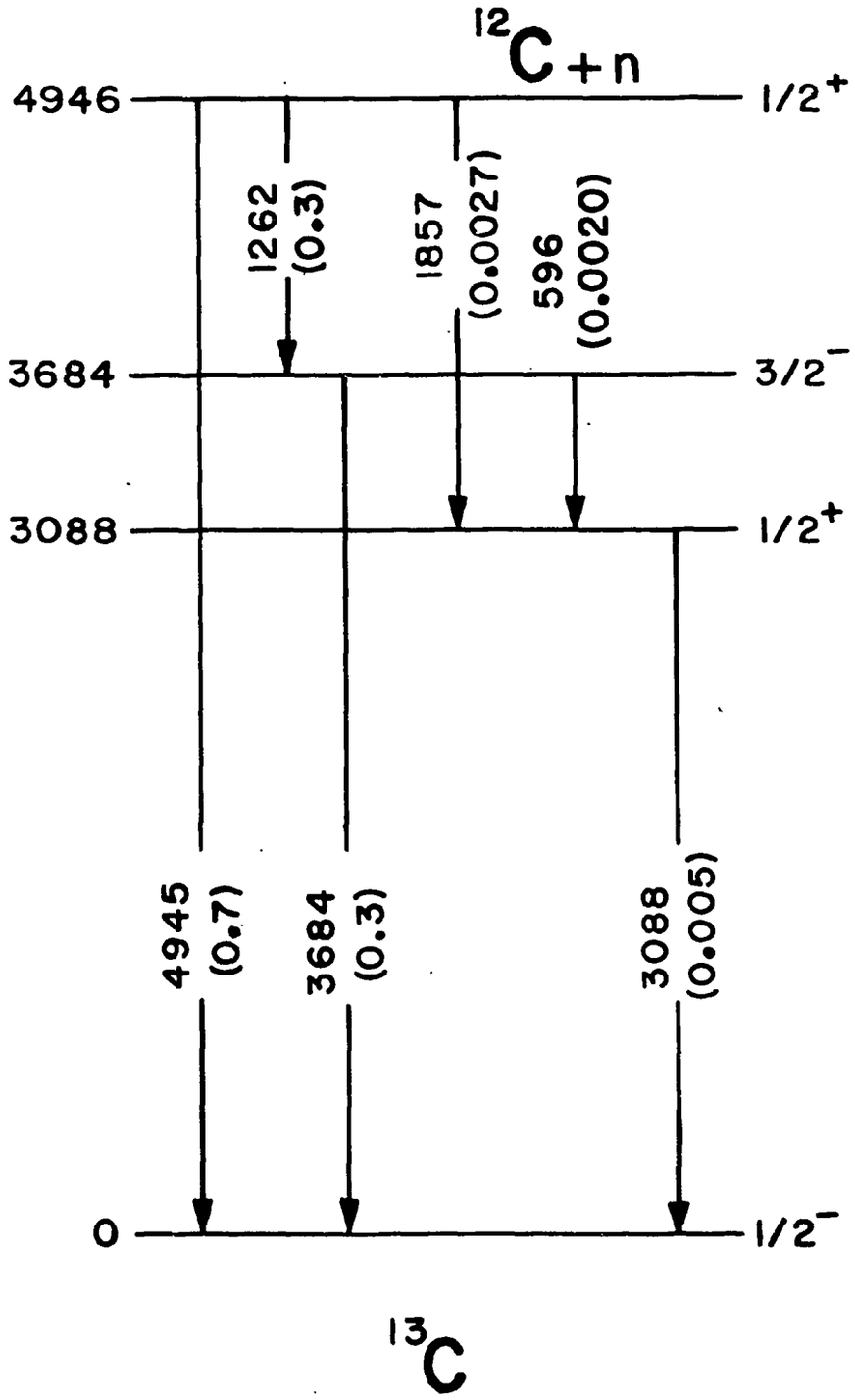

Fig. D-1. Gamma ray transitions observed in ^{12}C+n. Intensities are preliminary values only.

Table D-1. Isomeric States in ^{188}Re. (Shera)

Level (keV)	$T_{1/2}$(exp) of level	Transition energy (keV)	Initial state	Final state	Multi-polarity	$T_{1/2}^{\gamma}$	F_W
172.07	18.7 min	16.03	$5/2^+[402]+7/2^-[503]$	$5/2^+[402]-3/2^-[512]$	M3	3.50×10^{10}s	154
182.76	17.6 ns	13.32	$5/2^+[402]+3/2^-[512]$	$5/2^+[402]+1/2^-[510]$	M1	6.30μs	663
502.34	3.16ns	141.76	$5/2^+[402]-9/2^-[505]$	$5/2^+[402]+3/2^-[512]$	M1	10.8ns	1350
		205.35	"	"	M1	28.6ns	1.1×10^4
207.84	3.20ns	207.85	$9/2^-[514]-9/2^-[505]$	$5/2^+[402]-3/2^-[512]$	E1	3.41ns	1.49×10^5
230.91	21 ns	74.86	$9/2^-[514]-3/2^-[512]$	$5/2^+[402]-3/2^-[512]$	E1	62.5ns	1.28×10^5
		167.3	"	"	E1	56.1ns	1.42×10^6
360.89	5.25ns	129.98	$9/2^-[514]+1/2^-[510]$	$9/2^-[514]+3/2^-[512]$	E2	87.8ns	0.37
		178.13	"	$5/2^+[402]+3/2^-[512]$	E1	30.7ns	8.3×10^5
		188.81	"	$5/2^+[402]+7/2^-[503]$	E1	7.8ns	2.6×10^5

These new findings bring the total of known bands to 15 and the number of assigned states to 41. In these terms, ^{188}Re is now the best understood odd-odd nucleus.

Revised theoretical (d,p) cross-sections have been calculated (by Lanier at LRL) based on the new experimental findings. These new calculations support our interpretation and provide added confidence in the new assignments.

The bands in ^{188}Re which involved the $1/2^-$[510], $3/2^-$[510] and $3/2^-$[512] neutron configurations are expected to be strongly mixed by the Coriolis interaction. To investigate this effect and in particular to see if the experimental energy level spectrum could be accurately predicted by using Nilsson state wave functions with Coriolis mixing, we have performed a series of coupling calculations using a computer code for odd-odd deformed nuclei written by W. Ogle.

Our results indicate that the Coriolis interaction is indeed capable of explaining the observed level energies. The applicability of the Coriolis coupling model has, of course, been repeatedly verified for odd-A deformed nuclei. The present results are interesting because they indicate that the Coriolis interaction plays an important role even in doubly-odd nuclei at the upper mass limit of the rare-earth deformed region.

3. ^{238}U(n,γ)^{239}U (E. T. Jurney)

The γ-ray spectrum from ^{239}U following thermal neutron capture by a ^{238}U target has been re-examined with the objective of determining what fraction of the capture cross section (from $\sigma_c = \Sigma E_\gamma \sigma_\gamma / B_n$) can be accounted for in resolved γ's with currently available resolution. Line intensities have been extracted from the portions of the spectrum from 100 to 1500 keV and from 3250 to Bn = 4802 keV, where 55% of the cross section can be resolved. The ultimate objective of the experiment is to determine the energy dependence of photon production from neutron capture; if a large fraction of the γ-rays can be resolved, then the complicated process of unfolding the residual unresolved continuum would become relatively less demanding.

If one assumes that in the gamma ray spectrum above 1/2 the neutron binding energy all observed gammas correspond to primary transitions, then only 45% of the capture cross section can be accounted for. The observed photon production cross section in 200 keV intervals is given in Table D-2.

Table D-2. Photon production cross sections for thermal neutrons on ^{238}U.

E_γ(keV)	σ(mb)	Line density γ/200 keV	Resolution (keV, FWHM)
2400-2600	148.0	29	2.37
2600-2800	143.0	27	2.51
2800-3000	120.8	27	2.66
3000-3200	124.5	23	2.82
3200-3400	70.2	9	2.97
3400-3600	107.7	11	3.11
3600-3800	77.2	7	3.27
3800-4000	100.4	6	3.50
4000-4200	311.5	6	3.50
4200-4400	0	0	3.70
4400-4600	0.5	1	3.83
4600-4800	11.8	3	3.95

The improved resolution has made it possible to observe high energy transitions which we either missed or incorrectly determined in our earlier work on ^{239}U (R. K. Sheline, et al., Phys. Rev. 151, 1011 (1966)). A weak primary transition to the $1/2^+$ member of the $1/2^+[631]$ band is now observed. New transitions are seen to levels at 294, 350, 723, and 735 keV. The transition we reported to the 754 keV level excited in the (d,p) reaction does not appear to exist. A re-examination of the low-lying level structure of ^{239}U incorporating the present data appears to be in order; the greatly improved low energy data should be especially important in resolving the large number of energy degeneracies we reported in the de-excitation of the low-lying levels.

E. EVALUATION.

1. Neutron and Gamma Ray Production Cross Section Evaluations for Nitrogen, Oxygen, and Aluminum. (P. G. Young and D. G. Foster, Jr.)

Complete evaluations of the neutron and gamma ray production cross sections for nitrogen (P. G. Young and D. G. Foster, Jr., LA-4725, to be published), oxygen (P. G. Young and D. G. Foster, Jr., LA-4780, to be published), and aluminum (D. G. Foster, Jr. and P. G. Young, LA-4726, to be published) have been completed for the neutron energy range 10^{-11} MeV to 20 MeV. The evaluations are in ENDF/B format and have been submitted to the Radiation Shielding Information Center at Oak Ridge for inclusion in the Defense Nuclear Agency Military Applications Cross Section Library. In addition, the data have been submitted to Brookhaven for consideration for Version III of ENDF/B.

The nitrogen data represents a complete re-evaluation of all neutron and gamma ray production experimental data including an R-matrix theory analysis of the experimental elastic scattering angular distributions. The oxygen and aluminum data sets are regarded as preliminary since further improvements are planned. Particular emphasis is placed in all three data sets on the evaluation of the total, elastic, inelastic, and gamma ray production cross sections, and recent experimental data were incorporated in the three evaluations.

2. Evaluated Neutron Cross Sections for ^{3}He, ^{6}Li, and ^{10}B. (M. E. Battat, R. J. LaBauve, L. Stewart, and P. G. Young) Evaluated neutron cross sections for ^{3}He, ^{6}Li, and ^{10}B have been prepared in current ENDF/B format by LASL and submitted to the National Neutron Cross Section Center (NNCSC) for inclusion in Version III of ENDF/B.

The ^{3}He results are based upon an unpublished evaluation by L. Stewart (1968) which was partially prepared in ENDF/B format by M. Drake of NNCSC. This evaluation has been extended to 20 MeV and modified somewhat between 7 and 15 Mev.

The ^{6}Li data represent a revision of an earlier ENDF/B evaluation (MAT1115). Improvements include revisions of the total and some partial cross sections to account for recent experimental data, re-evaluation of the elastic scattering angular distributions, and extension of the complete data set to 20 MeV.

The ^{10}B data are a revision of the previous ENDF/B evaluation (MAT1009). The (n,α) cross section below 150 keV was adjusted to agree with the recent work of Sowerby et al (AERE-R6316, 1970). In addition, the elastic scattering cross sections below 150 keV were modified to agree with the measurements of Asami and Moxon (AERE-PR/NP14, 1968, and AERE-R 5980, 1969).

3. Gamma Ray Production Cross Sections for ^{239}Pu, ^{240}Pu, ^{235}U and ^{238}U. (R. E. Hunter (Valdosta State College), and L. Stewart.

Evaluations of prompt gamma ray production from neutron reactions on ^{239}Pu, ^{240}Pu, ^{235}U and ^{238}U have been prepared for the DNA Cross Section Library. These cross sections include gamma ray production from radiative capture, from fission within the first 100 nsec, and from inelastic scattering. Results have been documented in internal LASL reports; these memos are currently being expanded into two LA reports which will be distributed at a later date.

4. Neutron Cross Sections for ^{239}Pu, ^{235}U and ^{238}U (R. E. Hunter (Valdosta State College), L. Stewart, and T. A. Pitterle, Westinghouse)

Low and medium energy neutron cross sections for ^{239}Pu, ^{235}U and ^{238}U from current ENDF/B files are being integrated with medium and high energy neutron cross sections from the Theoretical Design Division Cross Section Library. New experimental data are being included in the evaluations. The resulting data sets are being tested against reliable critical experiments, and will be submitted to RSIC for inclusion in the DNA Cross Section Library. These evaluations will also be used to update the files in the TD Cross Section Library.

NATIONAL BUREAU OF STANDARDS

A. NEUTRON PHYSICS

1. MeV Neutron Total Cross Sections (R. B. Schwartz, R. A. Schrack, and H. T. Heaton II)

Figure A-1 shows our results for the total cross section of oxygen; these are the data which were referred to in the April 1971 NCSAC report. The data were obtained by measuring the transmission of single crystals of quartz (S_iO_2) relative to semiconductor grade silicon. After allowing for differences in resolution, these results are in quite good agreement with the Karlsruhe data and with the results of Fowler, et al. In particular, our measured (resolution-corrected) value for the minimum at 2.35 MeV is 120 mb, in excellent agreement with the ORNL and Karlsruhe results. In view of the agreement among the three sets of data, we consider that the question of the value of the minimum in the oxygen cross section is now settled.

Figure A-2 shows our measured total cross section for calcium. These data (and the oxygen data) were taken with an energy resolution which varied from about 0.2 nsec/m at the low energy end to about 0.1 nsec/m at the high energy end. The statistical precision was generally 2% or better per point.

2. KeV Cross Sections (R. B. Schwartz, R. A. Schrack, H. T. Heaton II, and J. Menke)

We are currently working on two neutron detectors to measure cross sections in the energy range from a few keV to ~ 500 keV. One detector is based on a lithium loaded glass scintillator, and the other is based on a boron-vaseline mixture, à la Harwell. Work on these detectors is progressing satisfactorily.

3. Intermediate Structure Studies (R. A. Schrack)

A paper entitled "Self-Correlation Analysis of Total Neutron Cross Sections" has been submitted for the Conference on Statistical Properties of Nuclei, held in Albany last August. The abstract follows:

The total cross sections of Al, Ca, Ti, Fe, Ni, Si, and Pb have been measured from .5 MeV to several MeV and analyzed by a self-correlation technique to determine the presence of intermediate structure. The self-correlation function

$$C(\delta) = \frac{1}{N}\sum_{i=1}^{N}\left(\sigma_i - \bar{\sigma}(\delta)\right)^2$$

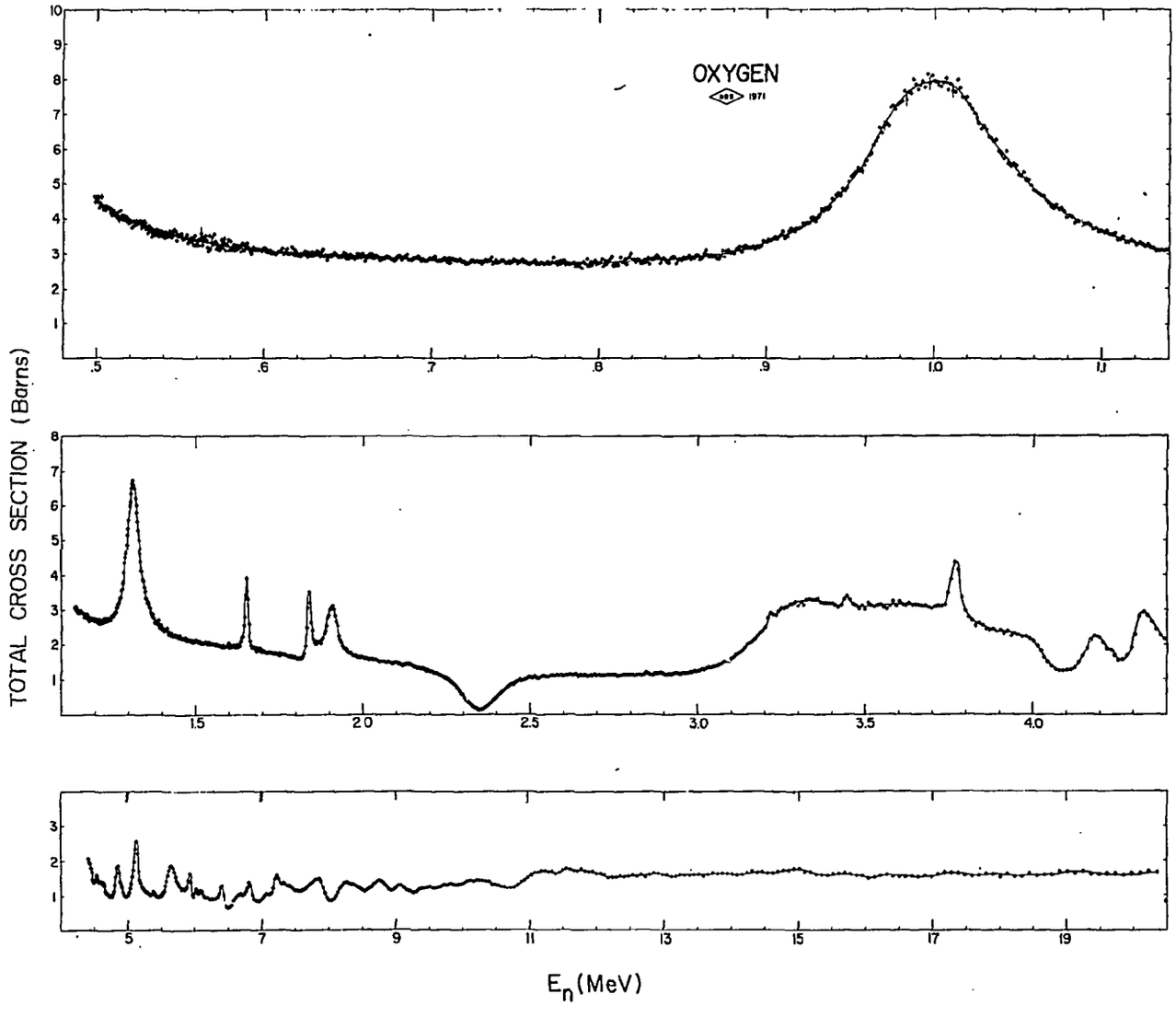

Fig. A-1

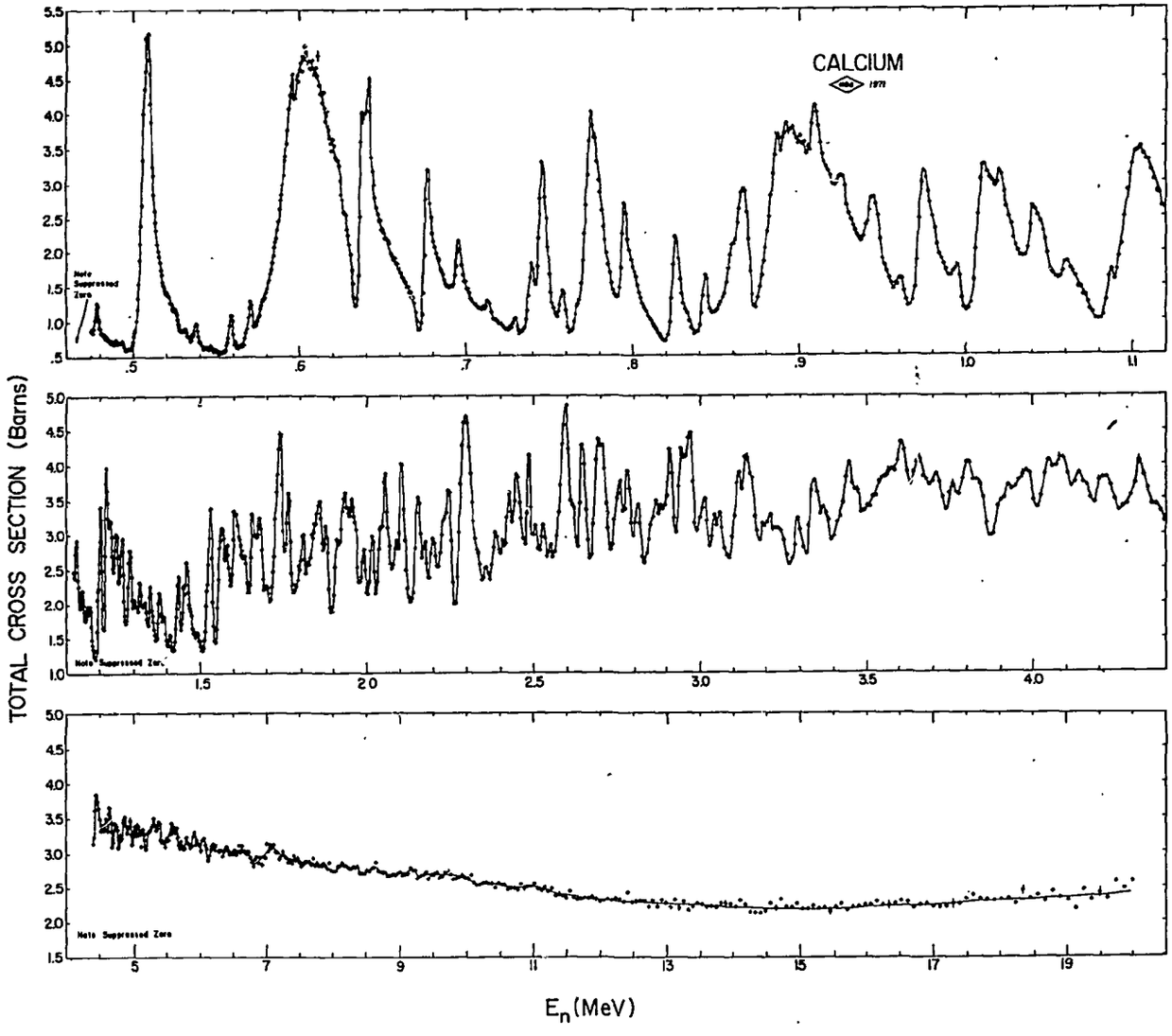
CALCIUM
TOTAL CROSS SECTION (Barns)
Note Suppressed Zero
E_n(MeV)

Fig. A-2

has been modified to be used with time-of-flight data having unequal energy intervals. Pappalardo proposed that the existence of a plateau in the plot of $C(\delta)$ vs δ would be indicative of intermediate structure. The calculation of $C(\delta)$ over a finite range of data (FRD) causes the $C(\delta)$ to exhibit oscillations that mask the existence of the intermediate structure criterion. The effect of different weighting functions in the calculation of $\bar{\sigma}(\delta)$ has been investigated and it has been shown that FRD oscillations can be eliminated by using a Gaussian weighted $\bar{\sigma}(\delta)$. Using both real and synthesized total cross sections the effect of data resolution, regularity of resonance spacing, and regularity of data spacing have been determined.

"A code to synthesize total cross section data from random distributions in width and spacing has been developed to determine how frequently intermediate structure will occur in randomly generated spectra. The fraction of cases in which intermediate structure appears in the randomly generated spectra is comparable to the fraction of cases it occurs in the seven natural spectra measured at NBS."

4. Average Fission Cross Section Ratios for ^{235}U and ^{239}Pu Fission Neutrons (J. A. Grundl)

An oral report of measurements in progress was presented in August 1971 at the IAEA Consultant's Meeting on the Status of Prompt Fission Neutron Spectra. Both differential and integral techniques of measurement were represented by participants at the meeting, and the report was prepared in order to encourage discussion and criticism of integral methods. The abstract for the written summary which will appear in the Proceedings of the meeting is as follows:

"Average fission cross section ratios, $\bar{\sigma}_f(^{235}U)/\bar{\sigma}_f(^{238}U)$, have been measured for ^{235}U and ^{239}Pu fission neutrons. A cavity fission source, a single fission ionization chamber, and a redundant determination of fission foil weight ratios were employed for the measurements. The result for ^{235}U fission neutrons is 3.81±0.17, a value which confirms earlier integral microscopic measurements and remains discrepant with predictions based on differential microscopic data to the extent of 10 to 17%. The measured ratio of average cross section ratios, χ_{235}/χ_{239}, is 0.970±0.012. This value represents a departure from unity which is less than one-half that predicted by differential microscopic data. The measurements described are in progress."

Measured values of $\bar{\sigma}_f(^{235}U)/\bar{\sigma}_f(^{238}U)$, presently available, and obtained for ^{235}U fission neutrons with cavity fission sources are

(1) fission ionization chamber, 20 cm diameter cavity:

3.81±0.17 (present work)

(2) fission track recorders, 50 cm diameter cavity:

3.78±0.18 (Ref. 1 and 2)

(3) fission foil activation calibrated with monoenergetic neutrons, 10 cm diameter cavity:

3.85±0.23 (Ref. 3) .

If the constraints on ^{235}U and ^{238}U fission cross sections provided by ratio measurements are accepted,[4,5] predicted values for the ratio are in the range 4.2 to 4.5.

5. Forced-Reflection Neutron Collimators (L. V. Spencer)

An approach to neutron collimator design has been suggested by L. V. Spencer and S. Woolf in which wall-emergent background neutrons are forced to reflect from each of a number of (tapered) segments beyond the point of first emergence. Simple Monte Carlo and approximate analytic studies have been made using an isotropic scattering model. In these studies several designs with two and three segments were intercompared in the context of a proposed neutron-neutron scattering experiment. A talk at the fall meeting of the American Nuclear Socity has been given on this subject and a paper to be published in Nuclear Instruments and Methods is in press.

B. DATA COMPILATION

1. Photonuclear Data Center (E. G. Fuller, H. Gerstenberg)

During the last year a study was made of the magnitude of effort required to publish a compendium of evaluated photonuclear cross section and related data for the entire periodic table. This study was in part generated by the needs for such data that have been expressed by the AEC's Nuclear Safeguards and Shielding Programs. A 2.8 man-year effort

---

[1] A. Fabry, M. De Coster, G. Minsart, J. C. Shepers, P. Vandeplas, "Nuclear Data for Reactors," Conference Proceedings, Helsinki (1970).

[2] A. Fabry, Nukleonik 10, 280 (1967).

[3] J. A. Grundl, Nucl. Sci. Eng. 31, 191 (1968).

[4] W. E. Stein, R. K. Smith, and J. A. Grundl, Conference on "Neutron Cross Sections and Technology," Washington, D. C. (1966).

[5] J. A. Grundl, Nucl. Sci. Eng. 30, 39-53 (1967).

expanded over a two-year period would be required to publish such a compilation giving the basic information required by a wide-range of fields: Nuclear Physics, Nuclear Safeguards, Shielding, Activation Analysis, Medical Physics, etc. Considerable progress has been made on laying a foundation for this work by building up a library of computer compatible digitized cross section data for over 76 nuclei. There are approximately 190 nuclei and natural element samples for which data are available. In addition, the Center is maintaining its searching, abstracting activities current with the published literature. The third supplement to the Photonuclear Data Index will be published during the second half of FY 72.

2. Photon Cross Sections (J. H. Hubbell, G. L. Simmons)

As an NSRDS-NBS "X-Ray Attenuation Coefficient Information Center" we are continuing to extract from the literature and systematize measured and theoretical photon cross section data over the energy range shown in Fig. B-1 for all processes indicated except photonuclear absorption which is the province of the NSRDS-NBS Photonuclear Data Center (E. G. Fuller).

A manuscript "Survey of Photon Attenuation Coefficient Measurements 10 eV - 100 GeV" has been accepted for publication in Atomic Data, with the following abstract:

"A bibliography of 290 references containing measured absolute-value photon total cross section data above 10 eV is presented, covering the period 1909 to June 1971. An index by element (Z = 1 to 94) and energy range, characterizing experiments according to source, detector and number of data-points, is included. Graphs are presented for 17 elements (Z = 1 to 92) over the energy-range 0.1 keV - 10 MeV comparing some recent attenuation coefficient tabulations (by the Lawrence Radiation Laboratory (Livermore), National Bureau of Standards, Los Alamos Scientific Laboratory and others) with the above documented data-points."

One of the graphs is shown in Fig. B-2.

An intercomparison and evaluation of existing quasi-independent photon cross section compilations (NBS, Livermore, Los Alamos, Sandia, Kaman, and Gulf General Atomic) is in progress under sponsorship of DNA(DASA).

Through participation in the Shielding Subcommittee of CSEWG (Cross Section Evaluation Working Group, AEC) we are continuing to examine, update and expand the ENDF/B photon cross section library tape.

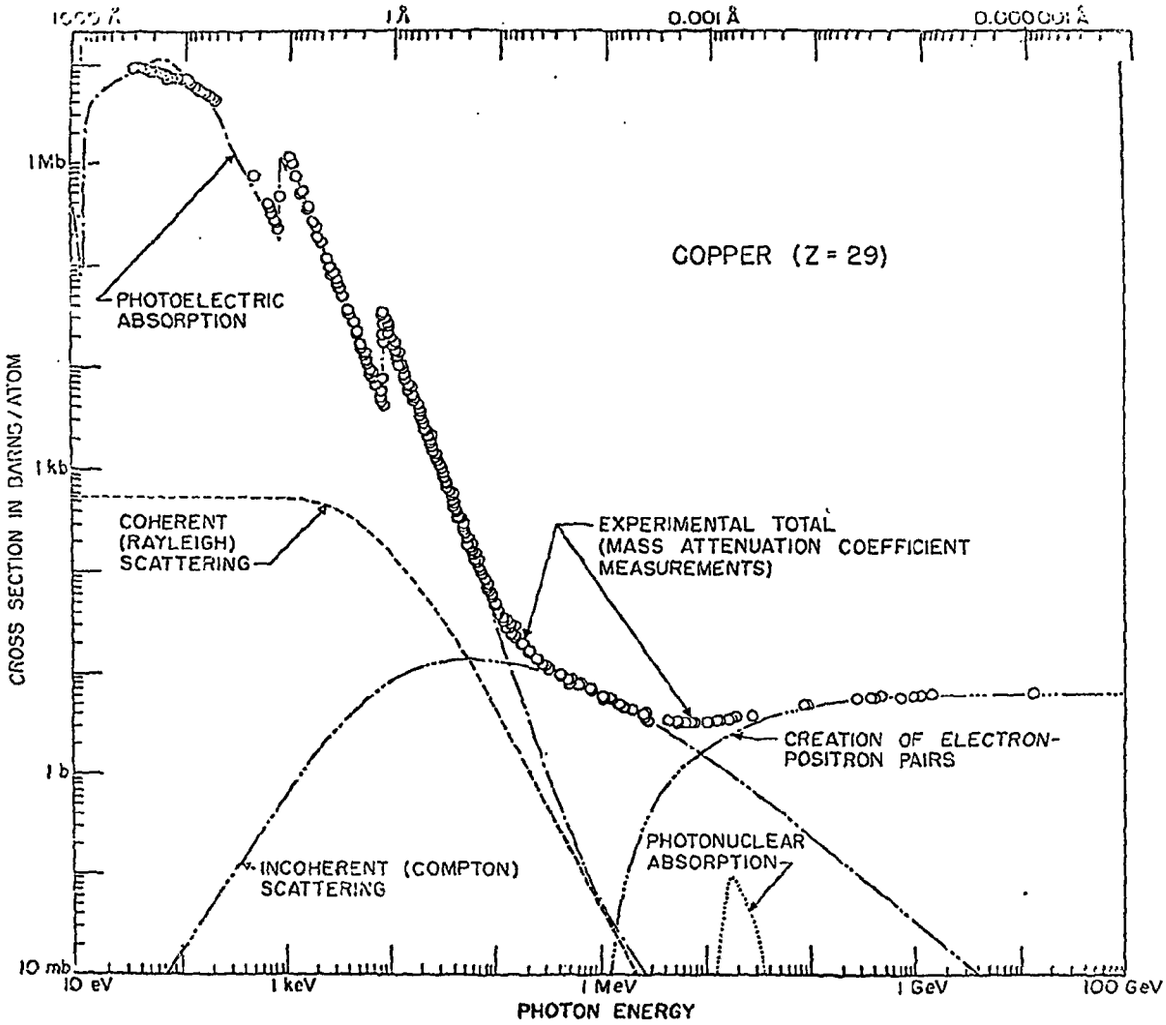
1 Å
0.001 Å
1 Mb
1 kb
1 b
10 mb
CROSS SECTION IN BARNS / ATOM
COPPER (Z = 29)
PHOTOELECTRIC ABSORPTION
COHERENT (RAYLEIGH) SCATTERING
EXPERIMENTAL TOTAL (MASS ATTENUATION COEFFICIENT MEASUREMENTS)
CREATION OF ELECTRON-POSITRON PAIRS
PHOTONUCLEAR ABSORPTION
INCOHERENT (COMPTON) SCATTERING
10 eV
1 keV
1 MeV
1 GeV
100 GeV
PHOTON ENERGY

Fig. B-1

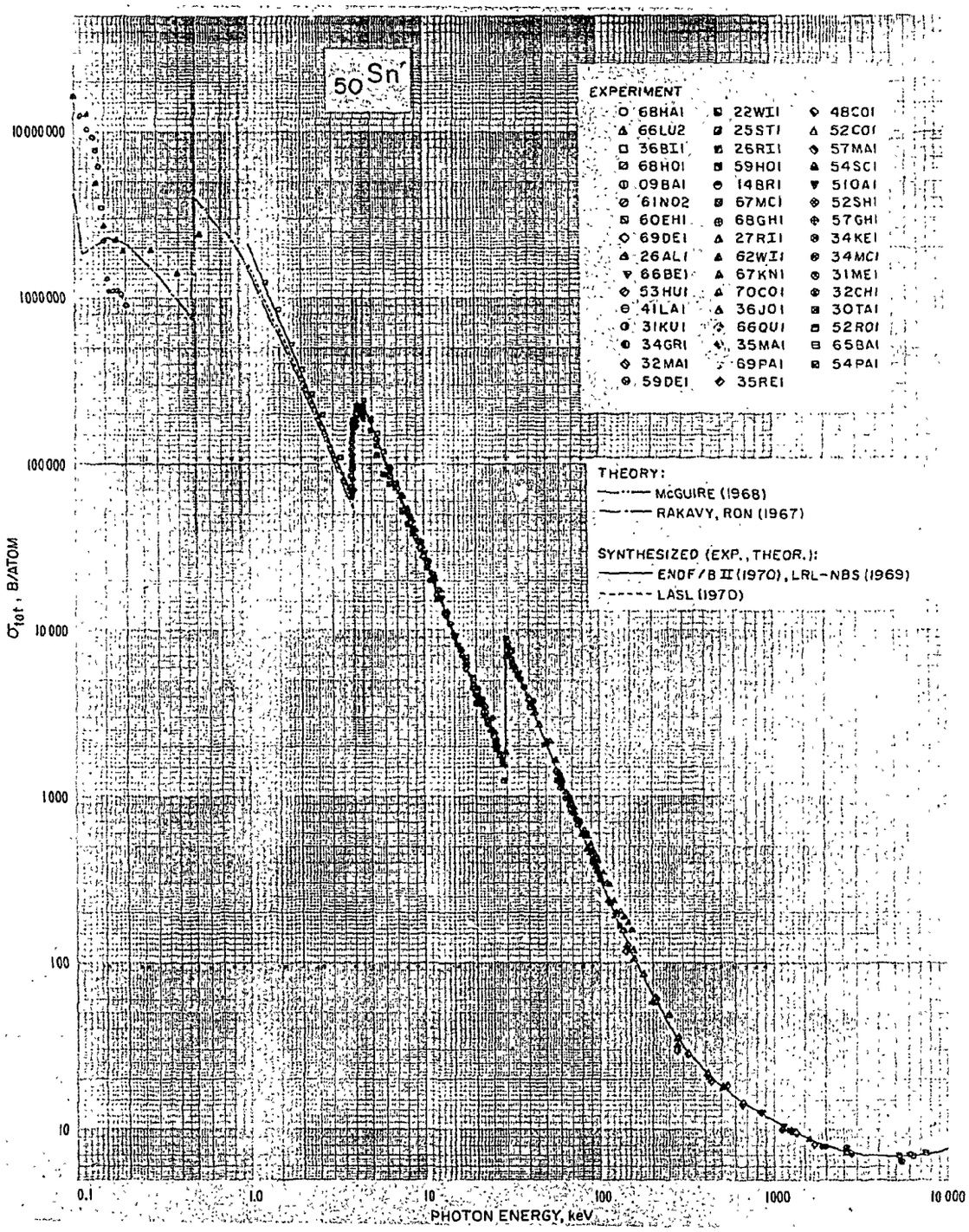
50 Sn
EXPERIMENT
68HA1
66LU2
36BI1
68HO1
09BA1
61NO2
60EH1
69DE1
26AL1
66BE1
53HU1
41LA1
31KU1
34GR1
32MA1
59DE1
22WI1
25ST1
26RI1
59HO1
14BR1
67MC1
68GH1
27RI1
62WI1
67KN1
70CO1
36JO1
66QU1
35MA1
69PA1
35RE1
48CO1
52CO1
57MA1
54SC1
51OA1
52SH1
57GH1
34KE1
34MC1
31ME1
32CH1
30TA1
52RO1
65BA1
54PA1
THEORY:
McGUIRE (1968)
RAKAVY, RON (1967)
SYNTHESIZED (EXP., THEOR.):
ENDF/B II (1970), LRL-NBS (1969)
LASL (1970)
10 000 000
1 000 000
100 000
10 000
1000
100
10
0.1
1.0
10
100
1000
10 000
PHOTON ENERGY, keV

Fig. B-2

C. FACILITIES

1. Linac Above-Ground Neutron Facility (S. Penner)

Construction of the above-ground neutron facility for the NBS linac is now well underway with completion of construction expected in spring 1972 and operation expected in summer 1972. Many of the beam handling components are on hand, and the remainder have been designed.

2. 3-MeV Van de Graaff Facility (M. Meier)

Installation of the 3-MeV Van de Graaff formerly used by Alan Smith's group at Argonne National Laboratory is nearing completion with first beam expected in November. Modifications to the building for access, installation of a new crane, and cutting and flanging of the KN-3000 pressure vessel to permit use of the accelerator in the existing rather small accelerator room are complete. Installation of some new beam handling system components and alignment remains to be done. This accelerator will be used for a program on keV neutron flux and benchmark neutron cross sections.

TEXAS NUCLEAR

A. NEUTRON PHYSICS

1. Elastic and Inelastic Scattering and Gamma-Ray Production on N, O, Al, Si, Ca and Fe at 9 and 11 MeV (W. E. Tucker, D. O. Nellis, P. S. Buchanan, T. C. Martin and G. H. Williams)

   (Work pertinent to requests 39, 40, 43, 44, 60, 61, 65, 66, 71, 72, 97, 100 NCSAC-35)

A report covering the elastic and inelastic scattering of 9 and 11 MeV neutrons from the above elements is being prepared. Gamma ray production cross sections are included for a few of the elements. This report covers the measurements undertaken at the Los Alamos Tandem Facility.

2. Compilation of Neutron-Induced Gamma-Ray Cross Sections (P. S. Buchanan, D. O. Nellis and W. E. Tucker)

The compilation of cross sections and angular distributions of gamma rays from (n,xγ) reactions has been completed and issued as Texas Nuclear Report ORO-2791-32. This compilation includes revision of some of the earlier values and contains measurements from 1961 to the present. The data have also been submitted to the National Neutron Cross Section Center for inclusion in the CSISRS data library.

3. Prompt Gamma-Ray Production From 14.8 MeV Neutrons in Carbon, Nitrogen and Oxygen (D. O. Nellis, P. S. Buchanan, J. B. Ashe, and W. E. Tucker)

   (Work pertinent to requests #35, #42, #46 NCSAC-35)

A paper with the above listed title has been prepared for submission to Nuclear Science and Engineering.

4. Neutron Induced Gamma-Ray Production in ^{208}Pb
(D. O. Nellis, I. L. Morgan, and E. L. Hudspeth)

A paper having the title above has been prepared for submission to Physical Review.

OAK RIDGE NATIONAL LABORATORY

A. NEUTRON PHYSICS

1. Total Cross Sections

a. High-Resolution Total Cross-Section Measurements on ORELA*
(J. A. Harvey, W. M. Good, N. W. Hill, R. F. Carlton†, and R. M. Feezel‡)

High-resolution transmission measurements have been made using several ^{6}Li glass scintillation detectors and a $\frac{1}{4}$-nsec EGG clock at both the 80- and 200-meter flight stations. Three sample thicknesses of ^{242}Pu metal cooled to liquid nitrogen temperature were used for measurements in collaboration with Idaho Nuclear Corporation up to 10 keV. The 30 nsec electron bursts which were used in these measurements resulted in an energy resolution < 0.1%. The following enriched isotopes with areas varying from 1 cm^2 to 5 cm^2 have been measured at 80 meters with 5 nsec electron bursts (< 0.1% energy resolution): ^{40}Ca, ^{42}Ca, ^{43}Ca, ^{44}Ca, ^{54}Fe, ^{56}Fe, ^{57}Fe, ^{98}Mo, ^{120}Sn, ^{203}Tl, ^{205}Tl, ^{204}Pb, ^{206}Pb, and ^{207}Pb. The 200-meter measurements with an energy resolution ~ 0.03% were made up to ~ 500 keV for ^{120}Sn and ^{209}Bi. The data are being processed to obtain resonance parameters and the analysis is almost completed for only ^{120}Sn. Many changes have had to be made to the processing and analysis programs to handle the large amounts of data. Transmission measurements are in progress upon thick samples of pure iron to measure the cross sections of the windows.

---

*Related to NCSAC-35 No. 72 and descrepencies, Appendix E, Item No. 14, p. 89 Minutes, NCSAC, May 4-5, Duke University.
†Research participant from Middle Tennessee State University, under appointment with Oak Ridge Associated Universities.
‡Undergraduate student, Auburn University.

b. Neutron Total Cross Sections of Si^{29}, Ti^{47}, Ti^{49}*
(W. M. Good and J. A. Harvey)

Studies are continuing at ORELA on the measurement of total cross sections in the energy range from about 1 keV to several hundred keV. The purpose is to obtain an increased amount of information on such matters as strength functions, width distributions, spacing distributions, etc. for those nuclides whose level densities do not exceed one or two levels per keV. Considerable new information should still be obtainable for such nuclides because a) there are separated isotopes which are only now available in quantities sufficient for adequate measurements and b) there are nuclides which have been studied previously with results which showed a need for the 10 fold superior resolution presently available.

As examples of the cases just cited, information has been obtained at ORELA using a special small sample facility. This facility consists at present of a flight station at 80 meters, and a sample station at about 10 meters which includes a collimation system for producing beams of diameters in the range $\frac{1}{4}$" to 1". The neutron burst durations for the energy range of interest depend markedly upon moderation time for the moderated photo neutrons from the tantalum target; the detector consists of an array of ^{6}Li glass scintillators 4.5 in. diameter and 0.5 in. thick. Accordingly, it turns out that $\Delta E/E$ is roughly a fixed quantity with a value $\lesssim 1/1000$.

The samples used in the preliminary measurement reported here, were appropriate in thickness for energies below ≈ 30 keV. The new results are tabulated in Table A-1. Stated in words, the present thin samples indicate: a) that for target Si^{29}, for which no previous measurements seem to exist only three rather narrow resonances are evident in the energy range up to ≈ 350 keV and b) that for Ti^{47}, i) the resonance which was reported at 8.21, consists of two resonances, ii) that in addition to the seven resonances previously reported below 30 keV, five new ones are observed which are too narrow to have been observed before, and c) that for Ti^{49}, no new resonances appear to exist below 30 keV, in addition to the seven already reported.

TABLE A-1

New Resonances for Neutrons Incident on Si^{29}, Ti^{47}, Ti^{49}

Isotope	Resonance Energies (keV)
Si^{29}	40.3, 166, 335
Ti^{47}	4.20, 8.11, 8.33, 12.6, 17.7, 19.1, 21.6
Ti^{49}	None below 30 keV

These measurements are continuing to obtain better statistics and for additional information attainable from thicker samples.

---

*Submitted Int. Conf. on Statistical Properties, Albany, New York, August 23-27, 1971.

c. 200-Meter Neutron Time-of-Flight on ORELA
(L. A. Galloway†, C. H. Johnson, J. A. Harvey, N. W. Hill, and J. L. Fowler)

We have activated the recently completed 200-meter flight station at ORELA for neutron total cross section measurements in the ~ 0.5 to 3.0 MeV energy region. Since we had available careful measurements of the total cross section of ^{16}O[1)] in this energy range, we used BeO and compensating Be samples to check out the apparatus. The observed neutron counting rates indicate that, using an array of ~ 7 5" dia organic

scintillators, we should obtain adequate counting rates at 400 meters where the theoretical resolution should be ~ 200 volts at 1 MeV. At 200 meters, even without pulse shape discrimination against gamma rays, we found backgrounds are small. They seem to arise principally from the capture of neutrons slowed down in the organic detector.

---

†Centenary College of Louisiana.

[1]J. L. Fowler, C. H. Johnson, F. X. Haas, and R. M. Feezel, Proceedings Third Conference on Neutron Cross Sections and Technology, Knoxville, Tennessee, March 15-17, 1971.

2. Radiative Capture Cross Sections and Spectra

a. Program for Measuring Radiative Capture Cross Sections (R. L. Macklin and B. J. Allen†)

The neutron capture cross section facility at ORELA has operated well during the year. Samples run from April thru September 20, 1971, include: ^{23}Na, ^{28}Si, ^{40}Ca, ^{42}Ca, ^{63}Cu, ^{65}Cu, ^{90}Zr, ^{91}Zr, ^{92}Zr, ^{94}Zr, ^{110}Cd, ^{111}Cd, ^{122}Te, ^{123}Te, ^{124}Te, ^{125}Te, ^{126}Te, ^{130}Te (Request Numbers 58, 59, 129, 169, 171, 176, 180, 185, 187, 192, 194). Data reduction to cross sections has been completed for some of these but a comprehensive computer program is still under development. The energy range covered is generally from 3 keV to 500 keV or the first inelastic threshold if higher. In cases of particular interest for capture, the first few hundred keV above the inelastic threshold can be covered by raising the bias (from .15 MeV) or correcting for the inelastic gamma yield where the inelastic cross sections are known.

---

†On assignment from Australian Atomic Energy Commission.

b. P-Wave Neutron Capture Spectra from ^{98}Mo*
(G. W. Cole†, S. F. Mughabghab†, M. Bhat†, O. A. Wasson†, R. E. Chrien†, and G. G. Slaughter)

Recent measurements of radiative neutron capture with a ^{98}Mo target[1)] by the BNL fast chopper group have demonstrated the validity of the valency neutron model[2)] at resonance neutron energies below 1.0 keV. The energy region has been extended to ~ 5 keV using the Oak Ridge Linear Accelerator (ORELA) with a nominal time-of-flight resolution of 2.5 nsec/meter. Capture γ-ray spectra from resonances have been analyzed and compared to the valency neutron model.

The success of the model for resonances below 1 keV in ^{98}Mo is related to the large reduced widths of these resonances. If the final state has a strong single particle component, then for these resonances

a simple description of the capture process may reasonably be expected to apply. Above 1 keV in ^{98}Mo, the resonances have significantly smaller widths and statistical processes are expected to dominate the capture reaction.

The results of the present work, in which 21 resolved resonances were studied, confirm these expectations. Spectra for the 12, 429, 612, and 818 eV resonances are in substantial agreement with the previously reported values for the widths of six primary transitions to low-lying s and d states in ^{99}Mo.

However, the regularities expected from the valency neutron model are not observed in the spectra obtained from resonances between 1.0 and 4.0 keV, and the widths predicted by the model are not in agreement with experiment.

Above 4 keV an increase in the P-wave neutron strength function is observed[3]. Agreement with the model is obtained for the p 3/2 resonance at 4842, with $\Gamma n^{1)}$ = 0.71 eV. The observed ground state radiation width of 11.8 ± 3 mev compares to a predicted value of 11.0. Other transitions of this resonance are not in such good accord with the model.

Examination of the primary γ-ray spectra has led to spin and parity assignments for previously unassigned resonances of ^{98}Mo, as indicated in Table A-2.

---

*Submitted Int. Conf. on Statistical Properties of Nuclei, Albany, New York, August 23-27, 1971.

†Brookhaven National Laboratory, Upton, New York.

[1]S. F. Mughabghab, R. E. Chrien, O. A. Wasson, G. W. Cole, and M. R. Bhat, Phys. Rev. Letters 26, 1118 (1971).

[2]J. E. Lynn, The Theory of Neutron Resonance Reactions, (Clarendon Press, Oxford), p. 330 (1968).

[3]H. Weigmann, G. Rohr, and J. Winter, Third Neutron Cross Section Technology Conference, Knoxville (1971).

TABLE A-2

E_r (eV)	401	1122	2170	2623	2950
l	1	1	1	1	1
j	3/2	3/2	1/2	(3/2)	(1/2)
	3260	3792	4013	4571	4842
l	1	1	1	1	1
j	(1/2)	(1/2)	3/2	(1/2)	3/2

c. The 5.5 Anomalous Radiation in $^{205}Tl(n,\gamma)^{206}Tl^{*}$
(E. D. Earle†, M. A. Lone†, G. A. Bartholomew†, B. J. Allen‡, G. G. Slaughter, and J. A. Harvey)

An enhancement at 5.5 MeV in the gamma ray spectra following thermal and fast neutron capture[1] in the mass region $180 < A < 208$ represents a significant departure from the statistical model. Since this effect is strong in ^{206}Tl we have studied its magnitude and variation with resonance energy in the $^{205}Tl(n,\gamma)^{206}Tl$ reaction.

Two complementary experiments were performed with the Oak Ridge Electron Linear Accelerator. 1, High resolution gamma ray spectra were recorded for the strong resonances up to 30 keV with a 36 c.c. Ge(Li) detector at a 10 m. station and with a neutron time resolution of 4 nsec/m. 2, The capture cross-section, resonance parameters and a measure of the relative intensity of gamma rays above and below ≈ 4 MeV for neutron energies up to 70 keV were studied with a "Total Energy Detector"[2] at a 40 m. station with approximately 0.2% energy resolution.

The magnitude and details of the 5.5 MeV γ-ray anomaly are most clearly seen in the γ-ray spectra from two strong s-wave resonances at 2.80 and 3.05 keV. The intensities of all observed γ-rays above 2.5 MeV from these resonances are shown in Fig. A-1. Since the low-lying levels of ^{206}Tl are well known[3] it can be shown that all these γ-rays > 2.5 MeV are E1 primaries and that the only unobserved E1 primary in the anomalous region is at 5.852 MeV. Gamma rays to levels $2.5 \rightarrow 4.5$ MeV below the binding energy are not observed although there are many states in this energy region.

Assuming that the target configuration is predominantly π; $\nu = s_{\frac{1}{2}}^{-1}$; $p_{\frac{1}{2}}^{-2}$ and adopting recent calculations[4] of the ^{206}Tl low-lying state wave functions we conclude that the γ-ray intensity distribution is not consistent with a simple particle-hole neutron transition with unperturbed target. The data require that at least 2p-1h neutron doorway states participate. The unobserved E1 primary is to an excited proton hole state at 0.652 MeV and implies that excited proton configurations do not have significant amplitudes in these two resonances. However a strong transition to this state is observed from several other resonances which also exhibit a strong anomaly, indicating that excited proton configurations are important in these cases.

Two weaker resonances at 0.044 and 1.44 keV are believed to be p-wave because of their decay to known 3^- states and therefore most of the observed transitions from these states are M1(E2) primaries. The 5.5 MeV γ-ray anomaly is much less evident from these resonances implying that the anomaly is predominantly due to E1 transitions after s-wave capture.

The neutron capture data taken with the total energy detector at the 40 m. station provided accurate resonance energies and for many resonances a measure of the neutron and radiative widths. The ratio of intensity above a 4 MeV bias to that below was determined for all

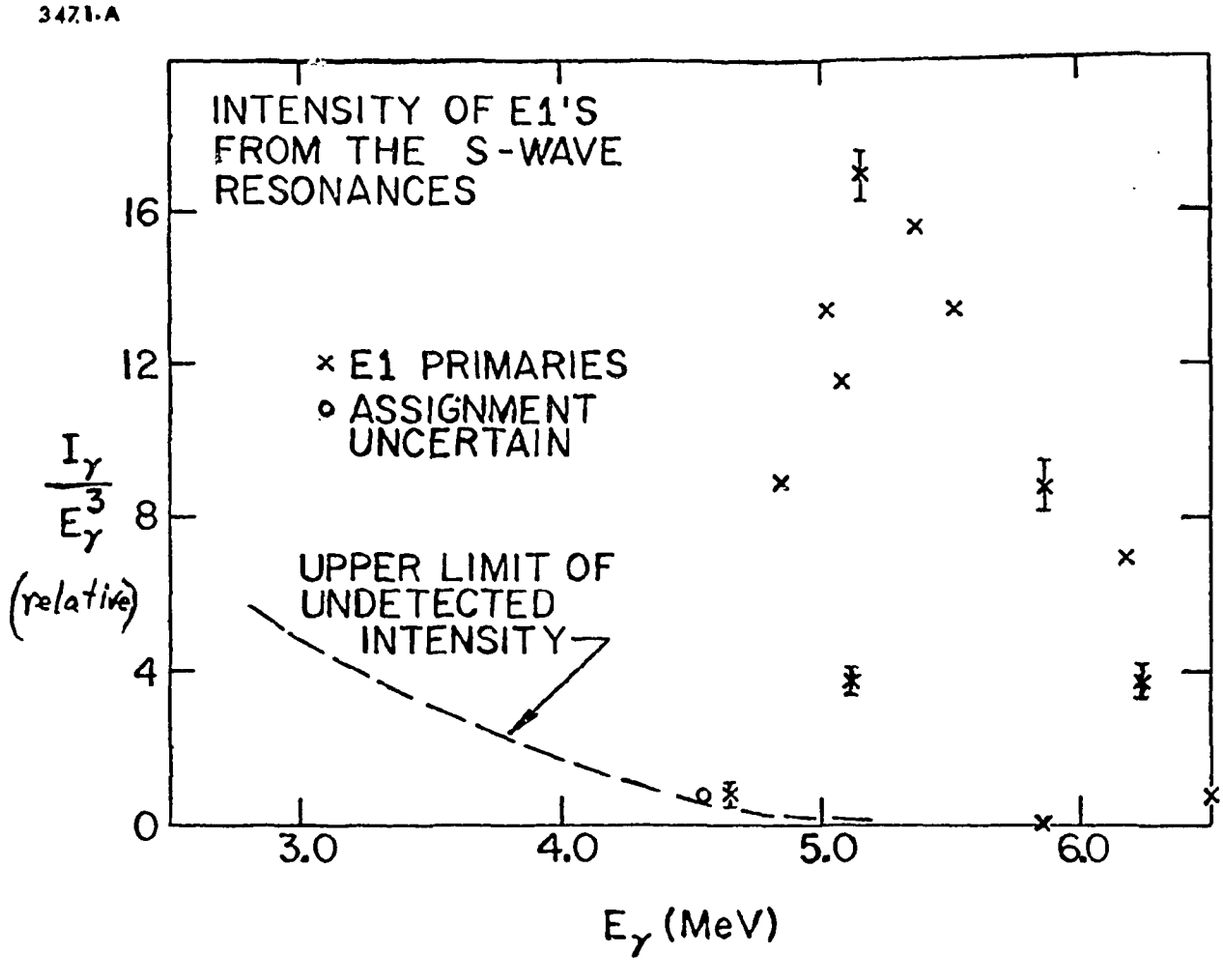

Figure A-1. Distribution of Strengths of γ-Rays with Energies above 2.5 MeV as Observed in the 2.80 keV and 3.05 keV Resonances of $^{205}Tl(n,\gamma)$

resonances. This ratio will be large for resonances with a large 5.5 MeV anomaly. Most of the observed resonances have ratios as large as the s-wave resonances shown in the figure while a few have values lower than the two p-wave resonances. It is clear that the anomaly is present in most s-wave resonances in $^{205}Tl(n,\gamma)^{206}Tl$. Correlation coefficients between the reduced neutron width, the radiative width and the relative strength of the anomaly are being determined. See Fig. A-1.

---

*Submitted Int. Conf. on Statistical Properties of Nuclei, Albany, New York, August 23-27, 1971.

†Chalk River Nuclear Laboratories, Chalk River, Canada.

‡On assignment from Australian Atomic Energy Commission.

[1]G. A. Bartholomew, Proc. Int. Conf. Neutron Capture γ-Ray Spectroscopy, Studsvik 1969, IAEA (1969) 553.

[2]R. L. Macklin and B. J. Allen, Nucl. Instr. and Meth. 91, 565 (1971).

[3]M. B. Lewis and W. W. Daehnick, Phys. Rev. C1, 1577 (1970).

[4]G. H. Herling and T. T. S. Kuo, private communication from G. H. Herling.

d. Width Correlations in Tm-169*
(R. E. Chrien†, G. W. Cole†, and G. G. Slaughter)

Correlations between neutron widths and partial radiative widths were reported[1)] in Tm-169 a number of years ago and submitted as evidence that the statistical decay assumption for the compound nuclear states at an excitation of ~ 6.5 MeV was violated. The limited sample size of the previous experiment has been extended by increasing the number of resonance studied by a factor of three. For this purpose the 10 meter station

at the ORELA has been used. Spin assignments were made based on the examination of low-energy γ-radiation. The results, which tend to support recent Harwell measurements[2], show a lower correlation coefficient than previously reported in ref. 1. The significance of these results will be discussed as well as their bearing on the general problem of width correlations in the 4s giant resonance.

---

*Abstract Tucson Meeting, APS, November 4 6, 1971.
†Brookhaven National Laboratory, Upton, New York.
[1]M. Beer et al., Phys. Rev. Letters 20, 340 (1968), M. A. Lane et al., Phys. Rev. 174, 1512 (1968).
[2]Bruce Thomas, Int. Conf. on Statistical Properties of Nuclei, Albany New York 1971 (in press).

e. Prompt Gamma Rays Emitted in the Thermal Neutron Induced Fission of ^{235}U*
(Frances Pleasonton and H. W. Schmitt)

A 4-fold coincidence experiment has been carried out to determine the average energy and average number of prompt gamma rays emitted as a function of fragment mass in thermal neutron-induced fission of ^{235}U. Measurements are made of the correlated energies of the fission fragments, the energy of the coincident gamma ray (from 0.09 - 10.0 MeV), and the time between detection of one fragment and the gamma ray. The fragment detectors and target are viewed, on axis, by a 5"x4" NaI crystal at a distance of 89 cm from the target. This arrangement permits coincidences registered with prompt neutrons to be distinguished from those associated with prompt gamma rays. Results indicate a saw-tooth dependence on fragment mass for both the average number and the average energy of the gamma rays. The average total number of prompt gamma rays emitted per fission is 6.41 ± 0.3 and the average total energy emitted per fission is 6.31 ± 0.3, giving 0.98 ± 0.07 MeV as the average energy per quantum per fission.

---

*Abstract Tucson Meeting, APS, November 4-6, 1971.

3. Elastic and Inelastic Scattering Cross Sections

a. Elastic and Inelastic Scattering of Neutrons from Carbon in the Energy Range of 5.2 - 8.7 MeV*
(F. G. Perey and W. E. Kinney)

We have acquired data on elastic and inelastic scattering of neutrons on carbon in the energy range of 5.2 - 8.7 MeV. Angular distributions (data at 18 angles) were obtained at least every 100 keV in the energy range and when the resonance structure required, at every 50 keV.

We hope that these data will be adequate to present the resonance structure of elastic and inelastic scattering in this energy region and plan to do an R matrix analysis of this data.

---

*Relevant to Requests No. 31, 33, 34, and 35. NCSAC-35.

b. On a Possible Resolution of the Nitrogen Nonelastic Cross-Section Discrepancy Below 9 MeV*
(F. G. Perey and W. E. Kinney)

New measurements of differential elastic-scattering cross sections of neutrons from nitrogen at six energies between 6.0 and 8.5 MeV yield nonelastic cross sections which are in essential agreement with the sum of the measured nonelastic partial cross sections. The new data give results which are systematically lower than those obtained from p evious measurements, thereby removing the discrepancy in the nonelastic cross sections of nitrogen below 9 MeV.

---

*Relevant to Requests No. 38, 39, and 40. NCSAC-35, submitted to Nucl. Sci. and Eng. for publication.

c. Scattering of Neutrons from Fe, Cu, and Pb*
(F. G. Perey and W. E. Kinney)

Neutron inelastic-scattering data have been obtained every 500 keV from 5.5 - 8.5 MeV for ^{54}Fe, ^{63}Cu, ^{65}Cu, ^{206}Pb, ^{207}Pb, and ^{208}Pb. Complete angular distribution data of both elastic and inelastic scattering were obtained for ^{54}Fe, ^{63}Cu, ^{65}Cu, and ^{208}Pb at 5.5, 7 and 8.5 MeV.

---

*Relevant to Requests No. 97, 98, 100, 101, and 338. NCSAC-35.

4. Neutron Reactions and Gamma-Ray Production Cross Sections

a. Al(n,xγ) Reactions for $5.3 \leq E_n \leq 9.0$ MeV*[1,2]
(J. K. Dickens)

Interactions of neutrons with aluminum have been studied by measuring gamma-ray-production cross sections. Spectra were obtained for incident mean neutron energies E_n = 5.35, 5.85, 6.4, 6.9, 7.45, 7.95, 8.5, and 9.0 MeV. The gamma rays were detected using a coaxial Ge(Li) detector of 30 cm^3 active volume. Data were obtained for gamma-ray angles of 55° for all E_n, for 90° for all E_n except 5.35 MeV, and 75° for E_n = 6.4 and 7.45 MeV. Time-of-flight was used with the detector to discriminate against pulses due to neutrons and background radiation.

Absolute cross sections for production of gamma rays were obtained for the incident neutron energies quoted above. The cross sections have

been compared, where possible, with previous measurements with good agreement. The spectra were studied for gamma rays which could be associated with de-excitation of nuclear levels having unknown decay modes. Gamma rays were found having energies appropriate for ground-state decay of levels at excitation energies E_x = 5.155, 5.414, 5.434, 6.514, 6.821, 6.956, 7.920, 7.411, 7.471, 7.56 (doublet), 7.655, 8.148, and 8.184 MeV.

Figure A-2 exhibits production cross sections for prominent gamma rays compared with previous gamma-ray data (LASL, Ref. 3; CEA, Ref. 4) and estimates based on neutron inelastic scattering data (Ref. 5). The present data are in generally good agreement with the CEA data, and agree well with the (n,n') estimations for lower values of E_n. For E_n > 6 MeV the gamma-ray data indicate increasing strength of the cascade from levels with E_x > 4.8 MeV.

---

*Relevant to Request No. 63. NCSAC-35.

[1]Research sponsored jointly by the Defense Nuclear Agency and the U.S. Atomic Energy Commission under contract with the Union Carbide Corporation.

[2]J. K. Dickens, ORNL-TM-3284 (January 1971); submitted also for publication in Physical Review.

[3]D. M. Drake, et al., Nuc. Sci. Eng. 40, 294 (1970).

[4]A. Bertin et al., Centre de'Etudes de Lumeil Rapport CEA-R-3803 (1969).

[5]W. E. Kinney and F. G. Perey, Al Neutron Elastic- and Inelastic-Scattering Cross Sections from 4.19 to 8.56 MeV, ORNL-4517 (1970).

b. Ca(n,xγ) Reactions for $4.85 \leq E_n \leq 8.05$ MeV*[1,2]
(J. K. Dickens and F. G. Perey)

Gamma-ray spectra have been obtained for reactions involving neutron interaction with a sample of natural calcium. Gamma rays were observed which are associated with the reactions $^{40}Ca(n,n'\gamma)^{40}Ca$, $^{40}Ca(n,p\gamma)^{40}K$, $^{40}Ca(n,\alpha\gamma)^{37}Ar$, and $^{42,44}Ca(n,n'\gamma)^{42,44}Ca$. Incident neutron energies were E_n = 4.85, 5.4, 6.45, 7.0, 7.5, and 8.05 MeV, and the scattering angle was $\theta_\gamma = 125^\circ$. The gamma rays were detected using a 45 cm^3 coaxial Ge(Li) detector placed at 100 cm from the sample; time-of-flight was used with the gamma-ray detector to discriminate against pulses due to neutrons and background gamma radiation. The sample was 20 g of natural calcium metal in the form of a right circular cylinder. The incident neutron beam was produced by bombarding a deuterium-filled 20 g of natural calcium metal in the form of a right circular cylinder. The incident neutron beam was produced by bombarding a deuterium-filled gass cell with the pulsed deuteron beam of appropriate energy from the ORNL 6-MV Van de Graaff. The resulting neutron beam was monitored using a scintillation counter; a time-of-flight spectrum from this detector was recorded simultaneously with the gamma-ray data. These data have been studied to obtain absolute cross sections for production of gamma rays from Ca for the incident neutron energies quoted above.

More than 50 gamma rays were correlated with transitions among the residual nuclei; these assigned gamma rays have > 90% of the total

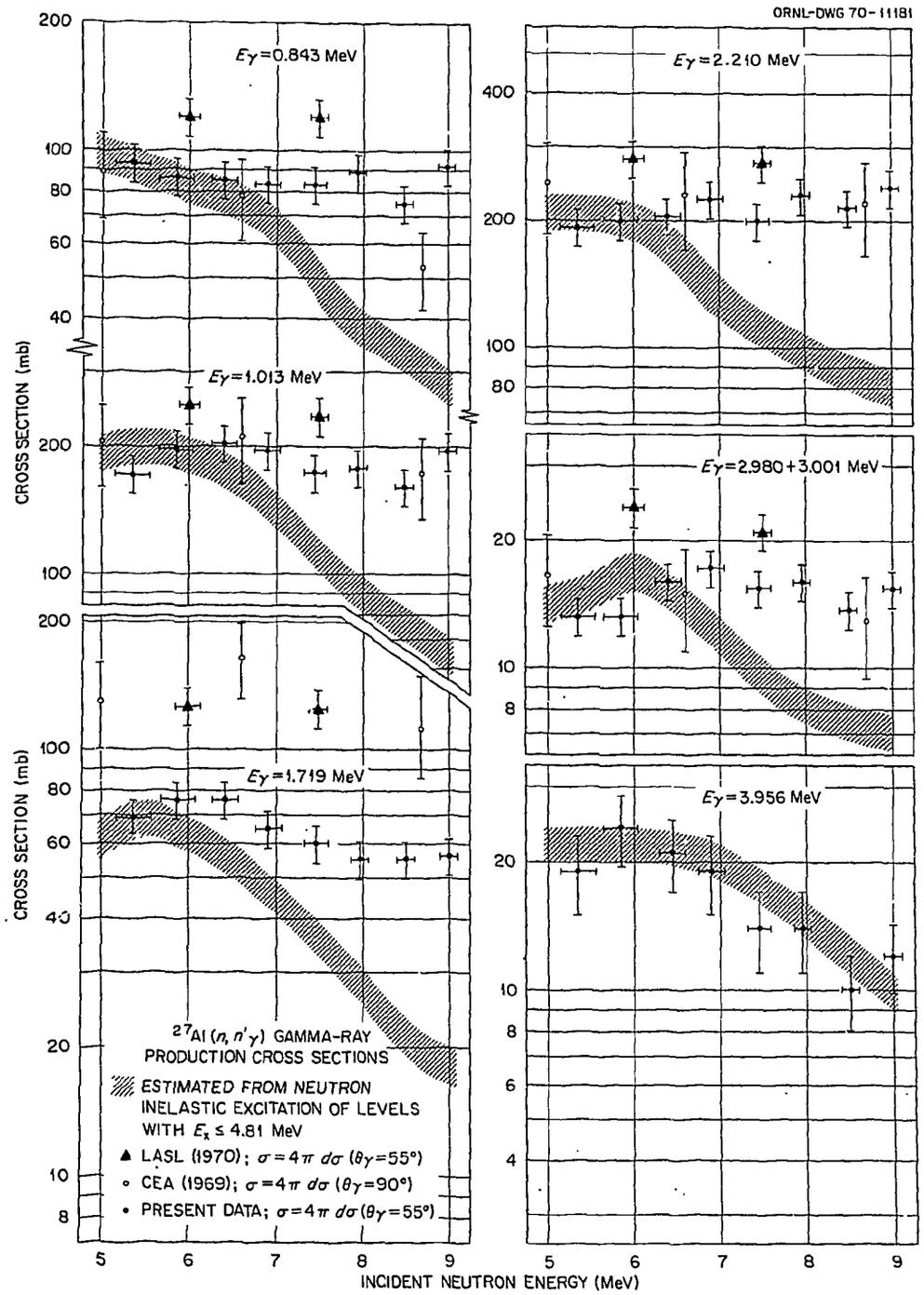

Figure A-2. Gamma-Ray Production Cross Section of ^{27}Al

gamma production cross section for $E_n \leq 6.45$ MeV. All unplaced gamma rays have small cross sections and are most likely associated with transitions in ^{40}K. The cross sections have been compared, where possible, with previously measured values and with results of the most recent evaluation for calcium with generally good agreement. Several important differences with previous data are discussed.

---

*Relevant to Request No. 73. NCSAC-35.
[1]Research sponsored jointly by the Defense Nuclear Agency and the U. S. Atomic Energy Commission under contract with the Union Carbide Corporation.
[2]Submitted to Nucl. Sci. and Eng. for publication.

c. Fe(N,xγ) Reaction for E_n Between 4.9 and 9.0 MeV*[1]
(J. K. Dickens and F. G. Perey)

Study of production cross sections of gamma rays produced by the interaction of neutrons with Fe, first reported last year[2], has continued. Emphasis has been on obtaining data for gamma rays with energy > 3.6 MeV. In addition, several spectra were obtained for an Fe sample enriched to 97% in the isotope ^{54}Fe. These data are being studied to obtain accurate cross sections for gamma rays seen in the spectra using ^{nat}Fe due to the 6% ^{54}Fe isotope.

---

*Relevant to Requests No. 104 and 105. NCSAC-35.
[1]Research sponsored jointly by the Defense Nuclear Agency and the U. S. Atomic Energy Commission under contract with the Union Carbide Corporation.
[2]J. K. Dickens and F. G. Perey, Neutron Phys. Div. Ann. Progr. Rept. May 1970, ORNL-4592, p. 32.

d. Pb(n,xγ) Reactions for E_n Between 4.9 and 8.0 MeV*[1]
(J. K. Dickens)

Spectra of gamma rays produced by neutrons interacting with Pb have been obtained for $4.9 \leq E_n \leq 8.0$ MeV in approximately 0.5-MeV steps for $\theta_\gamma = 125°$. Three samples were used: a 67-g sample enriched in ^{208}Pb, a 136-g sample enriched in ^{207}Pb, and a 67-g sample of radiogenic Pb (88% ^{206}Pb). These spectra were obtained using a 48-cc Ge(Li) detector and appear to be of good quality. Discrete high-energy gamma rays are observed in the ^{208}Pb spectra, in particular $E_\gamma = 4.085$, 4.839, and 5.286 MeV. Spectra for ^{206}Pb and ^{207}Pb do not exhibit strong, discrete, high-energy gamma rays, but indicate a "continuum" of unresolved, weakly excited gamma radiation with energies between 3 and 5 MeV.

---

*Relevant to Requests No. 339 and 340. NCSAC-35.
[1]Research sponsored jointly by the Defense Nuclear Agency and the U. S. Atomic Energy Commission under contract with the Union Carbide Corp.

e. Survey of (n,xγ) Gamma Production Cross Sections for E_n = 6 MeV*[1]
(J. K. Dickens)

A survey study of gamma rays produced by 6-MeV neutron interactions with samples having priority I request[2] was initiated. Samples studied include Ti (^{nat}Ti, and samples enriched in ^{46}Ti and ^{48}Ti), Ni (^{nat}Ni and ^{60}Ni), Cu(^{63}Cu and ^{65}Cu), Zn(^{64}Zn and ^{68}Zn), Nb and Bi. The samples of ^{nat}Ti, ^{63}Cu, ^{65}Cu, ^{nat}Ni, ^{60}Ni, and Bi were metallic cylinders. The Nb sample was a metallic plate. However, the material enriched in ^{46}Ti, ^{48}Ti, ^{64}Zn, and ^{68}Zn could be obtained only in oxide form. The samples were fabricated by compacting the powder in thin-walled aluminum cans. A similar sample fabricated with BeO powder was used to provide the background data. This sample revealed a number of background lines which may interfere with weaker transitions in the element under study.

---

*Ti relevant to Requests No. 78, 79, and 80; Ni relevant to Requests No. 122 and 123; Cu relevant to Request No. 127; Zn relevant to Request No. 134; and Nb relevant to Request No. 209. NCSAC-35.
[1]Research sponsored jointly by the Defense Nuclear Agency and the U. S. Atomic Energy Commission under contract with the Union Carbide Corp.
[2]Compilation of Requests for Nuclear Cross Section Measurements, Los Alamos Siientific Laboratory Report NCSAC-35 (March 1971).

f. Ta and C(n,xγ) Cross Sections for $1 < E_n < 15$ MeV*[1]
(G. L. Morgan, T. A. Love, and C. E. Burgart)

Gamma-ray spectra have been obtained for C and Ta using a 5-in. NaI detector at ORELA for neutron energies of 1 to 15 MeV. The data are presently being unfolded.

---

*Relevant to Requests No. 35 and 322. NCSAC-35.
[1]Research partially supported by the Defense Nuclear Agency under Union Carbide Corporation's contract with the U. S. Atomic Energy Commission.

5. Fission

a. Multilevel Analysis of the ^{235}U Fission and Capture Cross Sections*
(G. de Saussure, R. B. Perez, and W. Kolar[1])

The ^{235}U fission and capture cross section data[2] obtained in 1966 at the Renssalaer Polytechnic Institute linac have been analyzed in the energy region up to 60 eV by using the Reich and Moore multilevel formalism[3] and the computer program MULTI developed at LASL by Auchampaugh[4]. There are three main motivations for this analysis:

1. Multilevel parameters are required to extrapolate statistically the behavior of the cross sections to the unresolved resonance region[5].

Multilevel parameters for ^{235}U are requested with Priority I in the 1971 Compilation of Requests for Nuclear Cross Sections[5,6].

2. The R-matrix parameters are transformed into equivalent Kapur-Peierls parameters through the expansion of the R-matrix[7]. The Kapur-Peierls parameters so obtained can then be compared with the previously reported parameters[7] obtained directly by the Adler and Adler formalism[8]. The comparison will indicate to what extent the data define a unique set of Kapur-Peierls parameters.

3. The resonance parameters obtained by analyzing RPI linac data will be used as "initial guesses" for a fit to new data recently obtained at ORELA. The new data have a better energy resolution and a higher precision than the earlier data, but they were not yet fully reduced when this analysis started.

Figure A-3 shows some preliminary results obtained in this analysis. The dots in the figure are the capture and fission cross sections obtained from the linac data. The solid lines are computed cross sections. Two open fission channels were assumed. The levels were not divided into two spin groups, as sufficient information for such a division is not yet available. It is clear that for the energy region covered by Figure A-3 the resonance parameters describe the fission and capture cross sections with an accuracy comparable to that of the data.

An interesting test of the validity of the analysis is illustrated in Figure A-4. The data on that figure are from the measurement of the fission cross section made at Saclay[11] at a sample temperature of 77°K. The line was obtained from the same parameters as in Figure A-3 with a Doppler broadening corresponding to the Saclay experimental conditions. The consistency between the calculation and the experimental data is fair.

A set of Kapur-Peierls parameters was deduced from the R-matrix parameters and compared with Kapur-Peierls parameters obtained directly by the Adler and Adler formalism. It is interesting to note that there were rather large differences between the two sets of Kapur-Peierls parameters.

---

*Extracted from Neutron Physics Division Annual Progress Report for Period ending May 31, 1971, ORNL-4705, UC-34-Physics.

[1]Central Bureau for Nuclear Measurements, Euratom, Geel, Belgium.

[2]G. de Saussure et al., Simultaneous Measurements of the Neutron Fission and Capture Cross Sections for ^{235}U for Incident Neutron Energies from 0.4 eV to 3 keV, ORNL-TM-1804 (1967).

[3]C. W. Reich and M. S. Moore, Phys. Rev. 111, 929 (1958).

[4]G. F. Auchampaugh, Los Alamos Scientific Laboratory Report, LA-4633 (to be published). We are indebted to D. R. Winkler for making the MULTI program operational on the ORNL IBM-360/91 computer and to G. F. Auchampaugh for his many helpful suggestions.

[5]M. S. Moore, private communication.

[6]Compilation of Requests for Nuclear Cross Section Measurements, LA-4652-MS, Request No. 400 (March 1971).

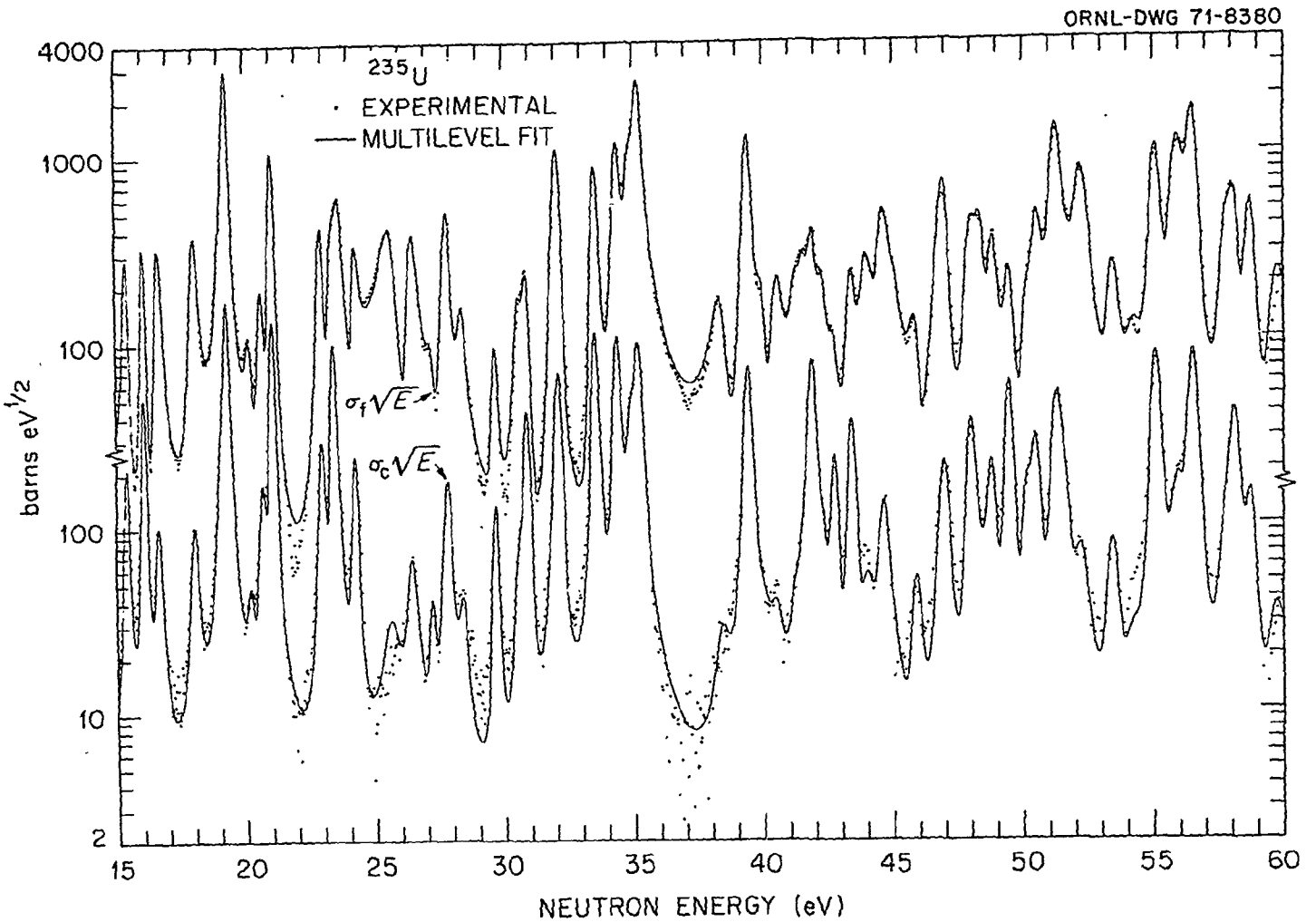

Figure A-3. Fission Cross Section ^{235}U (ORNL)

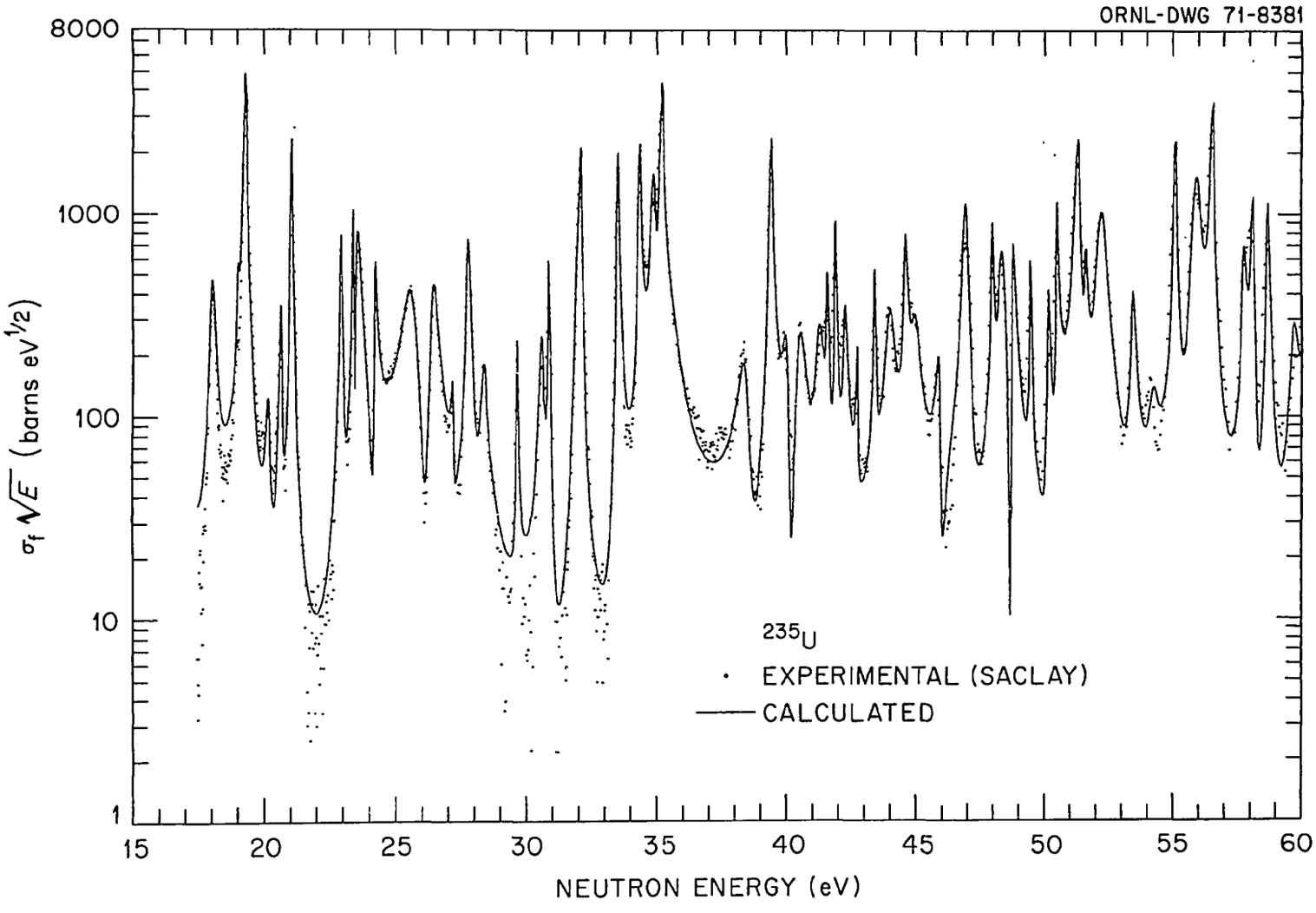

Figure A-4. Fission Cross Section ^{235}U at Low Temperatures (Saclay)

[7]G. de Saussure, and R. B. Perez, POLLA, A Fortran Program to Convert R-Matrix-Type Multilevel Resonance Parameters for Fissile Nuclei into Equivalent Kapur-Peierls-Type Parameters, ORNL-TM-2599 (1969).
[8]D. B. Adler and F. T. Adler, Proc. Conf. on Breeding Economics and Safety in Large Fast Power Reactors, October 1963, ANL-6792, p. 695.

b. Measurements of the Neutron Absorption and Fission Cross Sections of ^{239}Pu and ^{235}U over the Energy Range from 0.02 eV to 500 keV*
(R. Gwin, E. G. Silver, R. W. Ingle[1], and H. Weaver)

Experiments have been performed in which the neutron absorption rates of ^{239}Pu and ^{235}U were measured over the energy region from 0.02 eV to 400 keV. The main goal of this investigation was to provide values of $\bar{\alpha}$, the ratio of the average neutron capture cross section $\bar{\sigma}_c$ to the average neutron fission cross section $\bar{\sigma}_f$, for ^{239}Pu over the neutron energy region of interest for fast breeder reactors. The full energy region from 0.02 eV to 400 keV was covered in one measurement, enabling a single normalization of the data, and values of $\bar{\alpha}$ for ^{239}Pu are given over this energy region. An additional object of the experiments was to provide values of the ratio of the ^{239}Pu fission cross section to the ^{235}U fission cross section in the energy region from 10 to 100 keV. A knowledge of neutron cross sections which is consistent with critical experiments. Values of the ^{235}U neutron fission cross sections $\bar{\sigma}_f$ are also presented for the energy region from 10 to 80 keV.

These measurements are a continuation of those reported previously[2]. A pulsed source of neutrons produced by the Oak Ridge Electron Linear Accelerator (ORELA) is collimated to strike a sample centered in a beam tube in the large liquid scintillator ORELAST[3]. Prompt gamma rays resulting from neutron absorption in the sample are detected by ORELAST. In these experiments the samples were ^{239}Pu and ^{235}U contained in ionization chambers. Absorption events detected by ORELAST which are in coincidence with pulses from the ionization chamber are fission events, while absorption events not in coincidence with pulses from the fission chamber correspond to capture events plus those fission events not recorded by the ionization chamber.

Figure A-5 shows values of $\bar{\alpha}$ of ^{239}Pu obtained at ORELA for energy intervals extending from 0.1 to 400 keV. Also included in Figure A-5 are the results of the ENDF/B II evaluation for ^{239}Pu (Mat-1104)[4], the ORNL-RPI results, and the data from the Van de Graaff measurements of Lottin et al[5]. Values of $\bar{\alpha}$ for ^{235}U are shown in Figure A-6.

The results from the measurements on ^{235}U and ^{239}Pu, together with those from similar measurements, have been combined to yield the ratio of the average fission cross section for ^{239}Pu to that for ^{235}U. The present ORELA values for the region above 10 keV are compared with the ENDF/B II values[4] and the results of Szabo et al[6] in Figure A-7. The ORELA results are about 8 to 10% higher than the ENDF/B values. This may be

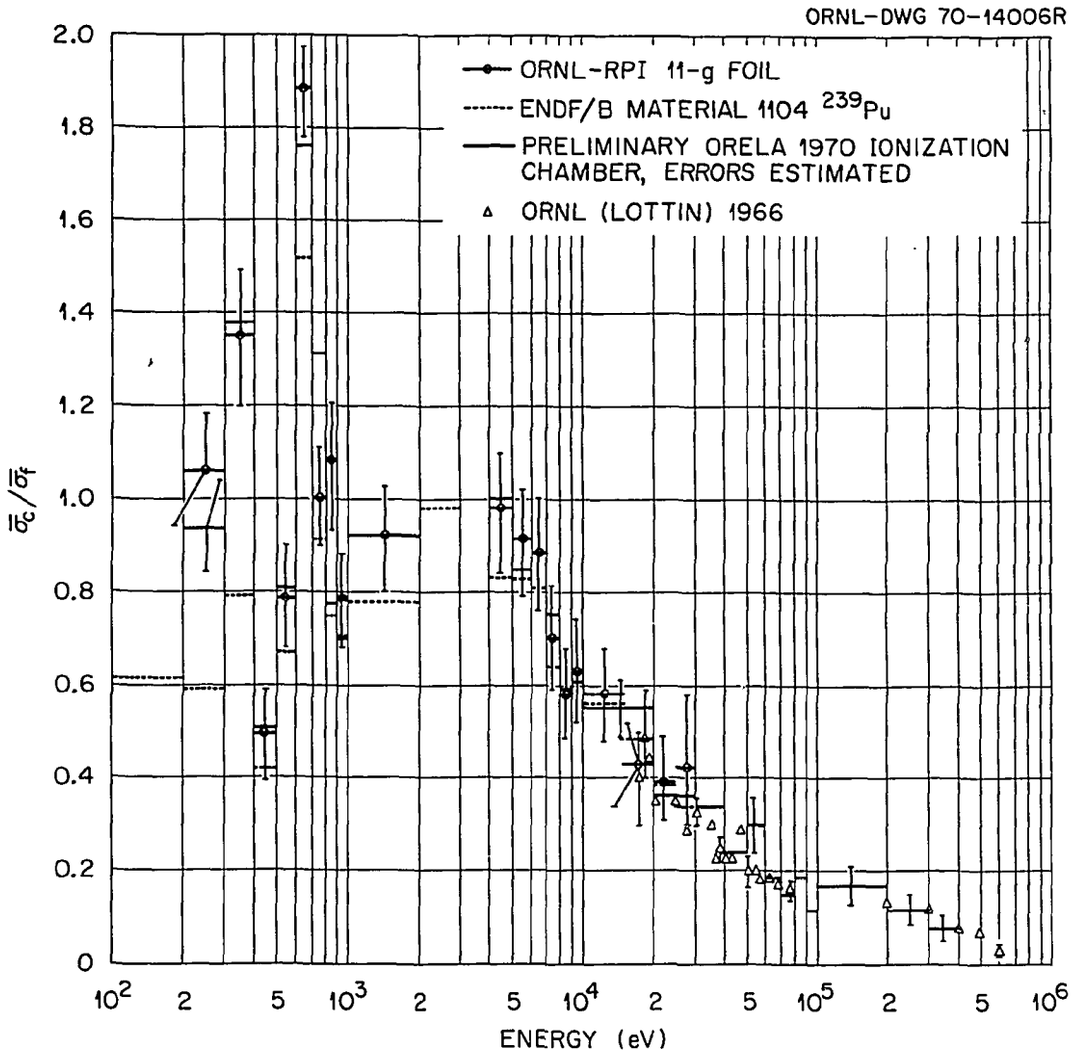

Ratio of the Average Value of σ_c to the Average Value of σ_f for Energy Intervals Between 0.1 and 400 keV.

Figure A.5. Capture to Fission Ratio $\bar{\sigma}_c/\bar{\sigma}_f$ for ^{239}Pu

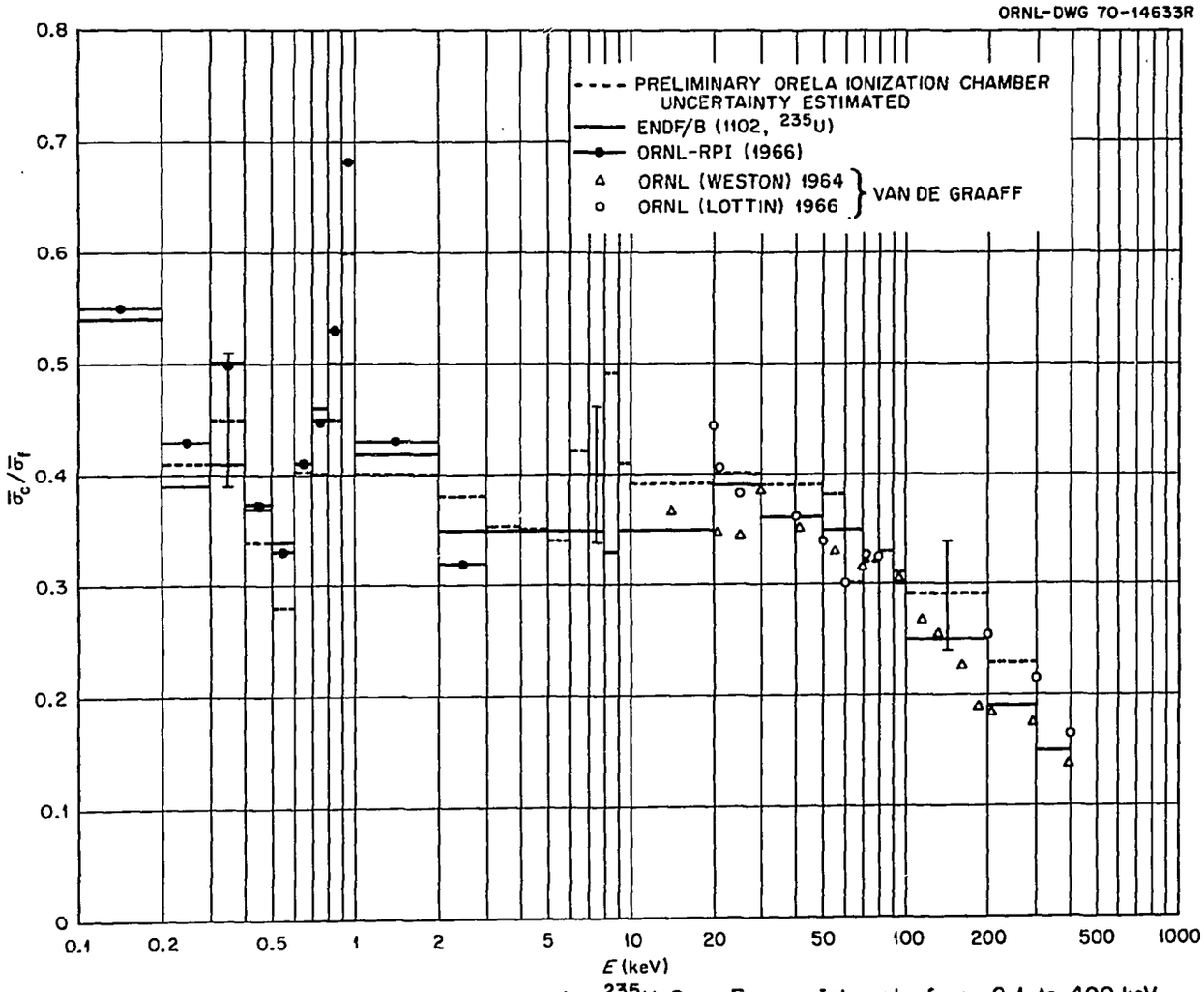

Ratio of the Average Value of σ_c to σ_f for ^{235}U Over Energy Intervals from 0.1 to 400 keV.

Figure A-6. Capture to Fission Ratio $\bar{\sigma}_c/\bar{\sigma}_f$ for ^{235}U

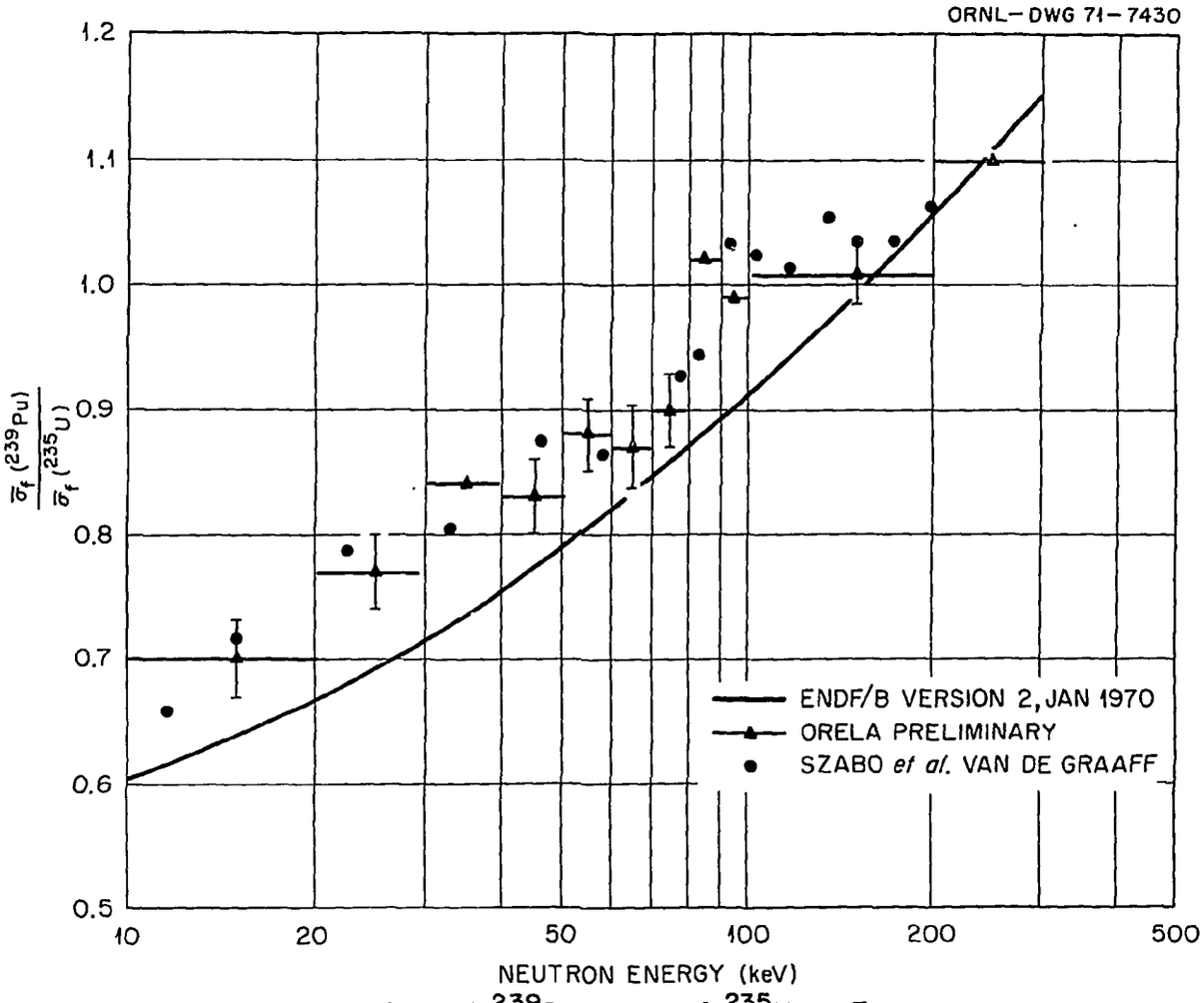

Ratio of $\bar{\sigma}_f$ of ^{239}Pu to $\bar{\sigma}_f$ of ^{235}U vs Energy.

Figure A-7. Ratio $\sigma_f(^{239}Pu)/\sigma_f(^{235}U)$ vs Neutron Energy

partially attributable to a difference in the thicknesses of the Al plates used in the ^{239}Pu and ^{235}U ionization chambers. The plates in the ^{239}Pu chamber were 0.005 in. thick, whereas those in the ^{235}U chamber were only 0.001 in. thick. Since there are prominent Al resonances at 35 keV and at above 85 keV, no uncertainty has been assigned to the present ratio between 30 and 40 keV nor above 80 keV.

Figure A-8 shows average values of the neutron fission cross section for ^{235}U as obtained in these experiments for energies between 10 and 80 keV. Also shown are the ENDF/B II evaluation for ^{235}U (Mat-1102) and the results of the recent measurements of Lemley et al[7] and Szabo et al[6]. The experimental data in the figure are in general lower than the ENDF/B values for ^{235}U. The interpretation of the present data in terms of an absolute neutron cross section in the keV region is complicated both by fluctuations in the energy dependence of the neutron flux and by instrumental difficulties in the measurement of the neutron flux. For these reasons the neutron fission cross section for ^{235}U is not given above 80 keV. The present data and that of Szabo et al suggest that the ENDF/B II results are too high and that this is reflected in the ratio of the fission cross section of ^{239}Pu to that of ^{235}U.

In summary, it can be stated that the present experiments have provided values of the neutron absorption and fission cross sections for ^{239}Pu and ^{235}U over an energy interval which extends from 0.02 eV to 80 keV and gives values of $\bar{\alpha}$ to 400 keV for ^{239}Pu. In general the values of $\bar{\alpha}$ measured for both ^{239}Pu and ^{235}U are in reasonable agreement with the corresponding ENDF/B II results. For the neutron energy region above 10 keV, the neutron fission cross section of ^{235}U and the ratio $\bar{\sigma}_f$ (^{239}Pu)/ $\bar{\sigma}_f$(^{235}U) as derived in these experiments are not consistent with the EANDF/V II evaluation. The present experiments yield a lower fission cross section for ^{235}U and a higher ratio of the ^{239}Pu fission cross section to that of ^{235}U than the ENDF/F II results. Recent measurements by Lemley et al[6] and Szabo et al[5] also yield lower values of the ^{235}U neutron fission cross section than the results given by ENDF/B II for Mat-1102.

---

*Extracted from Neu. Phys. Div. Ann. Prog. Rept. for Period Ending May 31, 1971, ORNL-4705, UC-34-Physics.

[1]Instrumentation and Controls Division.

[2]R. Gwin et al, "Measurements of the Neutron Fission and Absorption Cross Sections of ^{239}Pu Over the Energy Region 0.02 eV to 30 keV, Part II," Sec. 1.1 in Neutron Phys. Div. Ann. Progr. Rept. May 31, 1970, ORNL-4592.

[3]E. G. Silver, J. H. Todd, and J. Lewin, "Assembly and Initial Operation of the ORELAST," Sec. 1.11 in Neutron Phys. Ann. Progr. Rept. May 31, 1969, ORNL-4443.

[4]Evaluated Nuclear Data File (ENDF/B) of the National Neutron Cross Section Center (NNCSC), ^{239}Pu data, Material (MAT) 1104 and for ^{235}U data Material (MAT) 1102, Tape 201 (revised April 1970). A detailed list of the evaluators for the ENDF/B information is given in File 1 of the data tape which is available from NNCSC. The code SUPERTOG was used to obtain the data on the ENDF/B tape.

[5]A Lottin et al in Proc. Intern. Conf. on Fast Critical Experiments and Their Analysis, p. 22, ANL-7320 (1966).

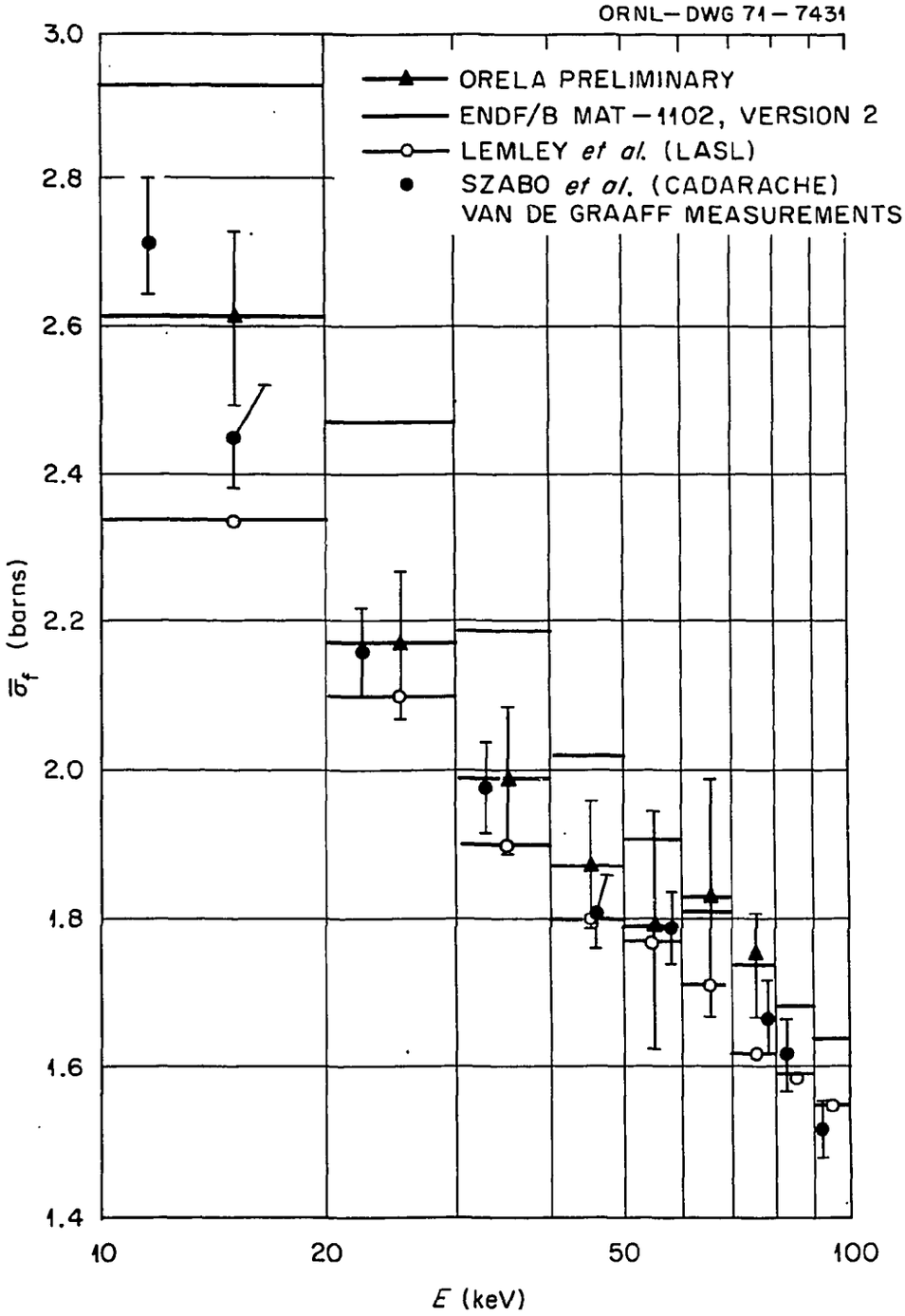

Fig. A-8. ^{235}U Neutron Fission Cross Section vs Energy.

[6]I. Szabo et al, "^{235}U Fission Cross Section from 10 keV to 200 keV," paper presented at Third Conf. on Neut. Cross Sections and Technology, March 15-18, 1971, Knoxville, Tennessee.
[7]J. R. Lemley, Nucl. Sci. and Eng. 43, 281 (1971).

c. Fragment Shell Influences in Nuclear Fission*
(Ulrich Mosel† and H. W. Schmitt)

Potential energy surfaces and shell correction energy surfaces for nuclei in the A ≅ 200 region and for actinide nuclei (A ≳ 230) have been calculated in the improved Two Center Model. These surfaces are shown in a two dimensional representation as a function of the elongation and the constriction of the nuclear shape. Both the groundstate shell corrections and the fission barriers in the A ≅ 200 region agree well with experiment. It is found that the saddle point position in this region is shifted significantly towards smaller deformations compared with the Liquid Drop Model prediction, this shift arising from a very pronounced valley in the shell correction surface, at the position of the Liquid Drop Model saddle point. The implications of this finding for a nuclear mass formula and for the application of the Liquid Drop Model to fission of these nuclei are discussed. In both mass regions (A ≅ 200 and A ≳ 230) the shell corrections alone show pronounced structure which changes slowly with mass number. At small deformations, up to the region of the second maximum in the potential, this structure is determined by the compound-nucleus shell structure. At larger deformations this structure is shown to arise from the shell structure of the nascent fragments, thus establishing the importance of fragment shells early in the fission process for the entire mass region A ≳ 200. As a consequence of these studies the regions of validity for the Liquid Drop Model in describing nuclear fission are explained. Finally it is shown that the recently observed symmetry in the mass distribution of ^{257}Fm is due to the approach to the nucleus ^{264}Fm which can split symmetrically into the two energetically strongly favored ^{132}Sn nuclei.

---

*Abstract of paper submitted to Phys. Rev.; presented at Seattle Meeting, APS, August 25-27, 1971.
†University of Tennessee, Knoxville, Tennessee.

d. High Resolution Cross Section Measurements for ^{234}U(n,f) and ^{236}U(n,f) at Neutron Energies Between 0.7 and 2 MeV
(Helmut Rosler*, Franz Plasil, and H. W. Schmitt)

Preliminary results for the ^{236}U(n,f) cross section in the energy region around the fission threshold have been obtained by time of flight measurements using the Oak Ridge Electron Linear Accelerator as a pulsed neutron source. The fission events are detected in a multi-plate ionization chamber, the neutron flux is monitored independently by a Naton 136 scintillator and a ^{235}U ionization chamber.

Figure A-9 shows the measured cross section normalized to 0.805 barns at 2 MeV. The ^{235}U fission spectrum, in its smooth behavior, has been normalized to the values of the BNL 325 Report. The error triangles give the error bars along both axis. The energy resolution is 8 keV at 1 MeV. Improved short rise time preamplifiers have recently been developed and will, in future experiments, allow a resolution of 4.5 keV at 1 MeV.

The aim of the experiment is to look for fine structure in the fission cross section, which may be interpreted in terms of the double-humped fission barrier. Estimated completion date is October 1971.

---

*Guest assignee (NATO Fellowship) from Reaktorstation Garching, Munich, Germany.

e. High Resolution Cross Section Measurement for $^{236}U(n,f)$* (H. Rosler†, F. Plasil, and H. W. Schmitt)

High resolution measurements of the cross section for neutron-induced fission of ^{236}U in the energy range from 0.5 to 6 MeV have been initiated and first results obtained. The neutron energies are separated by time of flight, using the Oak Ridge Electron Linear Accelerator (ORELA) as a pulsed neutron source. The fission events are detected in an ionization chamber containing 11 aluminum plates, which are electroplated on both sides with 0.5 mg/cm^2 ^{236}U. Every second plate is connected to a separate fast preamplifier the output signal of which starts the time-to-amplitude-converter. The first experiment was carried out at a flight path length of 33 m and achieved a total energy resolution of 8 keV FWHM at 1 MeV neutron energy. The neutron flux is monitored independently in a ^{235}U fission chamber and a Naton 136 fast plastic scintillator. The results achieved up to now confirm the known fine structure at 0.95 and 1.4 MeV which is superimposed on the smooth rise in cross section at the fission barrier. In addition the experiment seems to indicate similar but less prnounced structures at lower energies and also resolves the fine structure into separate lines. Insufficient beam collimation and rise time capability of the preamplifiers as well as structure in the energy distribution of the neutrons from air scattering in the beam tube render these results somewhat uncertain. New current sensitive preamplifiers have been developed and permit a resolution of 6 keV at 1 MeV. With these the experiment is presently being repeated using additional collimators and an evacuated flight tube.

---

*Submitted to Conf. on the Statistical Properties of Nuclei, Albany, New York, August 23-27, 1971.

†Guest assignee (NATO Fellowship) from Reaktorstation, Garching, Munich, Germany.

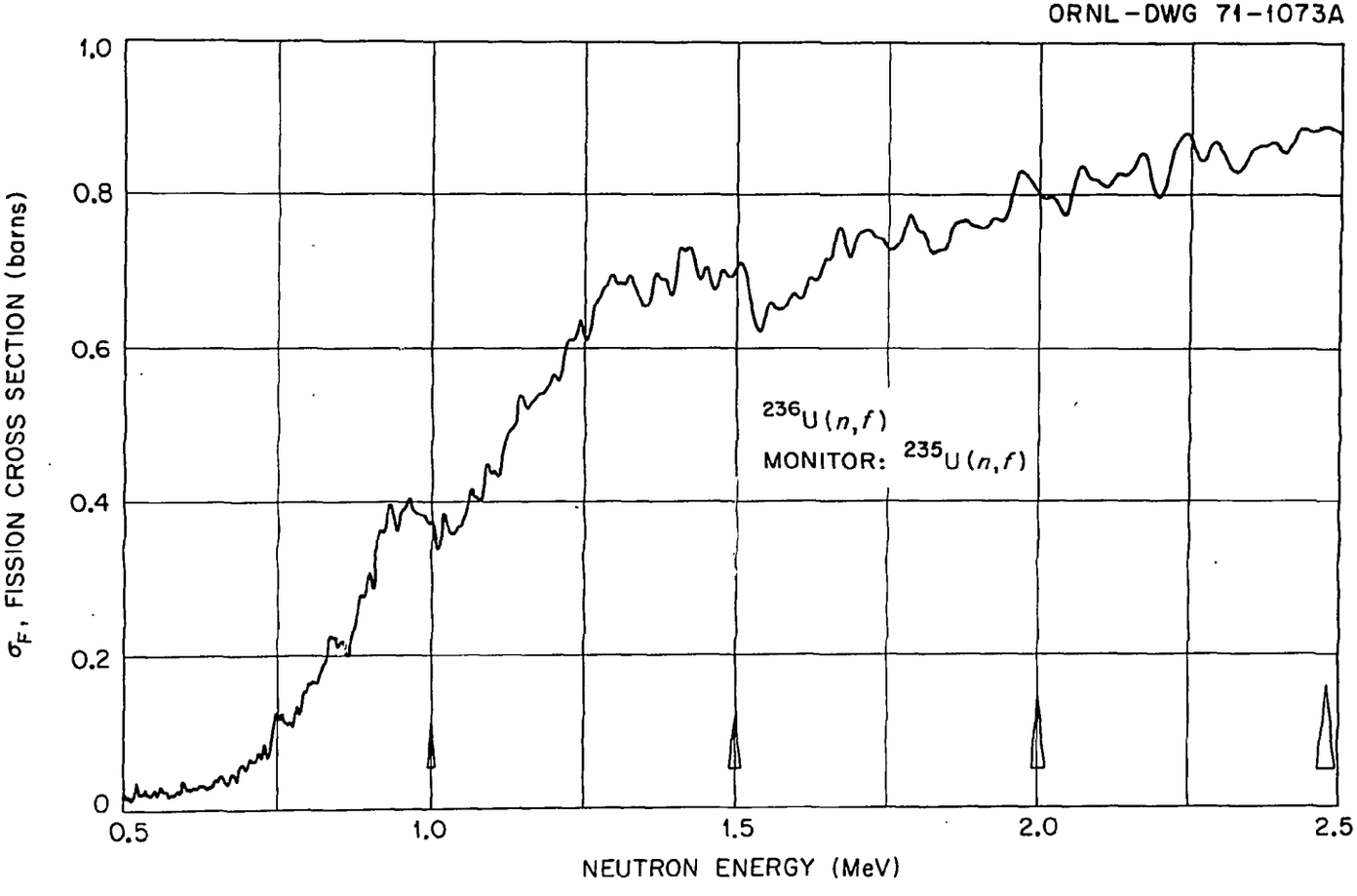

Figure A-9. Fission Cross Section ^{236}U vs Neutron Energy

7. Instruments and Techniques

a. Oak Ridge Electron Linear Accelerator (ORELA)
(J. A. Harvey and F. C. Maienschein)

During the past year ORELA has been operated on a 24-hour, 7-day basis for a total of 5133 (83% of scheduled hours) productive experimental hours. During this time period, there was an operational outage time of about 8 weeks due to a failure of the closure clamp on the gun tank. Klystron life time has been very good with 3 klystrons having been in operation 10,000 hours each. Four electron guns have been used this past year thus yielding an electron gun mean life of about 1400 hours. A new replacement gun tank with modular circuit components is undergoing its final tests and is scheduled for installation in December.

The on-line computer data acquisition system has proved itself satisfactory this past year; usually 4 to 6 experimenters are collecting data simultaneously. The Data Analysis System with interactive graphics was delivered by Digital Equipment Corporation in April 1971. The extended acceptance tests are scheduled to be completed in November 1971 but it will be many months before the system is of maximum value to the experimenters.

---

b. Fast Timing from a Fission Ionization Chamber*
(H. Rosler† and N. W. Hill)

The timing resolution of a ^{252}Cf-loaded fission ionization chamber connected to a new current preamplifier has been tested by looking at coincident fission fragment pulses and pulses from fission γ-rays which are detected in a plastic scintillator. A time resolution of 1 nsec FWHM could be achieved.

---

*Paper submitted for publication, Nucl. Instr. and Methods.
†Guest assignee with ORNL Phys. Div. from Reaktorstation, Garching, Munich, Germany.

c. Deterioration of Large Ge(Li) Diodes Caused by Fast Neutrons
(P. H. Stelson, J. K. Dickens, S. Raman, and R. C. Trammell†)

The large Ge(Li) gamma-ray detector has become a powerful tool for the investigation of nuclear reactions. Unfortunately these detectors are quite susceptible to fast neutron damage and this makes it difficult to decide whether or not to risk using a detector to study reactions at accelerators where fast neutrons are inevitably present. After ruining several detectors we decided to study the problem in a controlled way.

A 30 cm^3 true coaxial doide was systematically irradiated by neutrons from a plutonium-beryllium source. An increase in the width of the 2.614-MeV gamma-ray from ThC" was first detected after an irradiation of $5 \times 10^7 n/cm^2$. When the total irradiation had reached $6 \times 10^8 n/cm^2$, the peak width had increased by more than 50 percent. The irradiated detector was then reprocessed to remove the damage. The diode was again subjected to neutron irradiation. The second curve of resolution deterioration as a function of neutron flux was quite similar to the first one. The procedure was repeated a third time with similar results. Thus, reprocessing a detector effectively removes the neutron damage at a cost of only about 10 to 15 percent of the original price. A method was also developed for using the gamma-ray spectrum to evaluate the amount of neutron flux incident on the detector. The number of counts in the 693-keV peak (from (n,n') reaction with the ^{72}Ge in the detector) can be multiplied by 20 to get a rough measure of the neutron flux in n/cm^2.

---

*Paper submitted for publication, Nucl. Instr. and Methods.
†ORTEC, Inc., Oak Ridge, Tennessee.

d. Self-Absorption of Gamma Rays Produced in Large Cylindrical Samples*
(J. K. Dickens)

An exact expression is derived for the self-absorption of gamma rays produced uniformly throughout large cylindrical samples (i.e., diameter > 1 mean-free path). The calculated self-absorption of gamma rays emitted by ^{110m}Ag is compared with observed absorption by a 2-cm diameter Pb sample. Calculated self-absorption of gamma rays produced by 7-MeV neutron interaction with ^{208}Pb agree with estimates based upon Monte Carlo computations.

---

*Paper accepted for publication, Nucl. Instr. and Methods.

e. Energies and Intensities of Gamma Rays Emitted by a ^{226}Ra Source*
(J. K. Dickens)

Energies and intensities of 64 gamma rays emitted by ^{226}Ra and its decay products have been measured for gamma-ray energies between 186 and 2979 keV. Results are tabulated which are of primary use for efficiency calibration of Ge(Li) detectors.

---

*J. K. Dickens, ORNL-TM-3509 (to be published).

8. Evaluation

a. Cross Section Evaluations for Na, Ca, Fe, and Pb*
(C. Y. Fu, W. E. Kinney, F. G. Perey, and S. K. Penny)

Complete evaluations with ENDF/B format of neutron and photon production cross sections have been made for Ca (Mat. 1152), Fe (Mat. 1124) and Pb (Mat. 1136) and submitted to CSEWG for review and consideration for inclusion in the Version III data set being presently assembled at BNL. For Na (Mat. 1156) a complete evaluation of photon production cross sections has been made in a format compatible with the neutron cross section evaluation currently being performed at WARD in order to have a complete evaluation for the Version III data set.

These evaluations are pertinent to some of the requestors of the following requests since they may partially meet their needs:

Na - requests 55, 56, 57
Ca - requests 71, 72, 73
Fe - requests 97, 98, 99, 100, 101, 103, 104, 105
Pb - requests 338, 339, 340

---

*Research partially supported by the Defense Nuclear Agency Under Union Carbide Corporation's contract with the U. S. Atomic Energy Commission.

B. CHARGED PARTICLES

1. Equilibrium Quadrupole and Hexadecapole Deformations in ^{230}Th and ^{238}U*

(F. K. McGowan, C. E. Bemis, Jr., J. L. C. Ford, Jr., W. T. Milner, R. L. Robinson, and P. H. Stelson)

Large contributions to the excitation of 4+ rotational states from electric hexadecapole (E4) transitions have been observed in precision Coulomb excitation experiments with ^{4}He projectiles for even-even targets in the mass range $230 \leq A \leq 252$. The values of $B(E4,0 \rightarrow 4)$ deduced from an analysis of the Coulomb excitation probabilities for ^{230}Th and ^{238}U are 1.10 ± 0.44 e^2b^4 and 1.26 ± 0.52 e^2b^4, respectively. β_{40} deformation parameters are 0.110 ± 0.027 and 0.100 ± 0.028 for ^{230}Th and ^{238}U, respectively.

---

*Submitted for publication, Phys. Rev. Letters.

2. Ground-State Rotational Bands in Even-Even Actinide Nuclei*
(M. Schmorak, C. E. Bemis, Jr., M. J. Zender, N. B. Gove, and P. F. Dittner)

The gamma-ray spectra following the α-decay of several even-even actinides were studies. The deduced level energies of the ground-state rotational bands were compared with the collective model and the VMI model. The VMI model gave an excellent fit to the experimental levels; no phase transitions were observed in the actinide region, in contrast to the situation in the rare-earth region.

---

*Paper submitted for publication, Nucl. Phys.

3. Coulomb Excitation of ^{232}Th*
(W. T. Milner, F. K. McGowan, R. L. Robinson, and P. H. Stelson)

Twenty states in ^{232}Th have been observed by direct E2 and E3 Coulomb excitation with 5.5 MeV protons and 18 MeV ^{4}He ions. Reduced transition probabilities B(E2), B(M1), B(E3), and B(E1) have been deduced from γ-ray yield and angular distribution measurements. Level energies in keV (J^{π},B(Eλ,0 $\rightarrow$ J) in single particle units) are: 774.1(2+,0.83), 785.3(2+,2.88), 1072.2(2+,0.05), 1322.3(2+,0.04), 1386.9(2+,0.19), 1477.0 (2+,0.18), 1554.0(2+,0.56), 774.1(3-,18.8), 1105.7(3-,9.4), and 1182.3 (3-,1.6). Interband B(E2) branching ratios for decay of the 774- and 785-keV states are not consistent with band mixing to first order. The B(E3,0 $\rightarrow$ 3) are in good agreement with the microscopic description[1)] of octupole vibrational states. The B(E1) branching ratios for transitions to the ground state rotational band imply that the Coriolis interaction between octupole states is important.

---

*Paper, Tucson Meeting, APS, November 4-6, 1971.

4. Precise Coulomb Excitation (BE2) Values for First 2^{+} States of the Actinide Nuclei*
(J. L. C. Ford, Jr., P. H. Stelson, C. E. Bemis, Jr., F. K. McGowan, R. L. Robinson, and W. T. Milner)

Precise transition probabilities have been measured for the first 2^{+} states of ^{230,232}Th, ^{234,236,238}U, ^{238,240,242,244}Pu, ^{244,246,248}Cm, and ^{252}Cf by Coulomb excitation with 17 and 18 MeV alpha particles. Comparison is made with theoretical values. An excitation energy of 44.0 $\pm$ 0.5 keV was measured for the first excited level of ^{252}Cf. The essential results of the study are shown in Figure B-1.

---

*Submitted for publication, Phys. Rev. Letters.

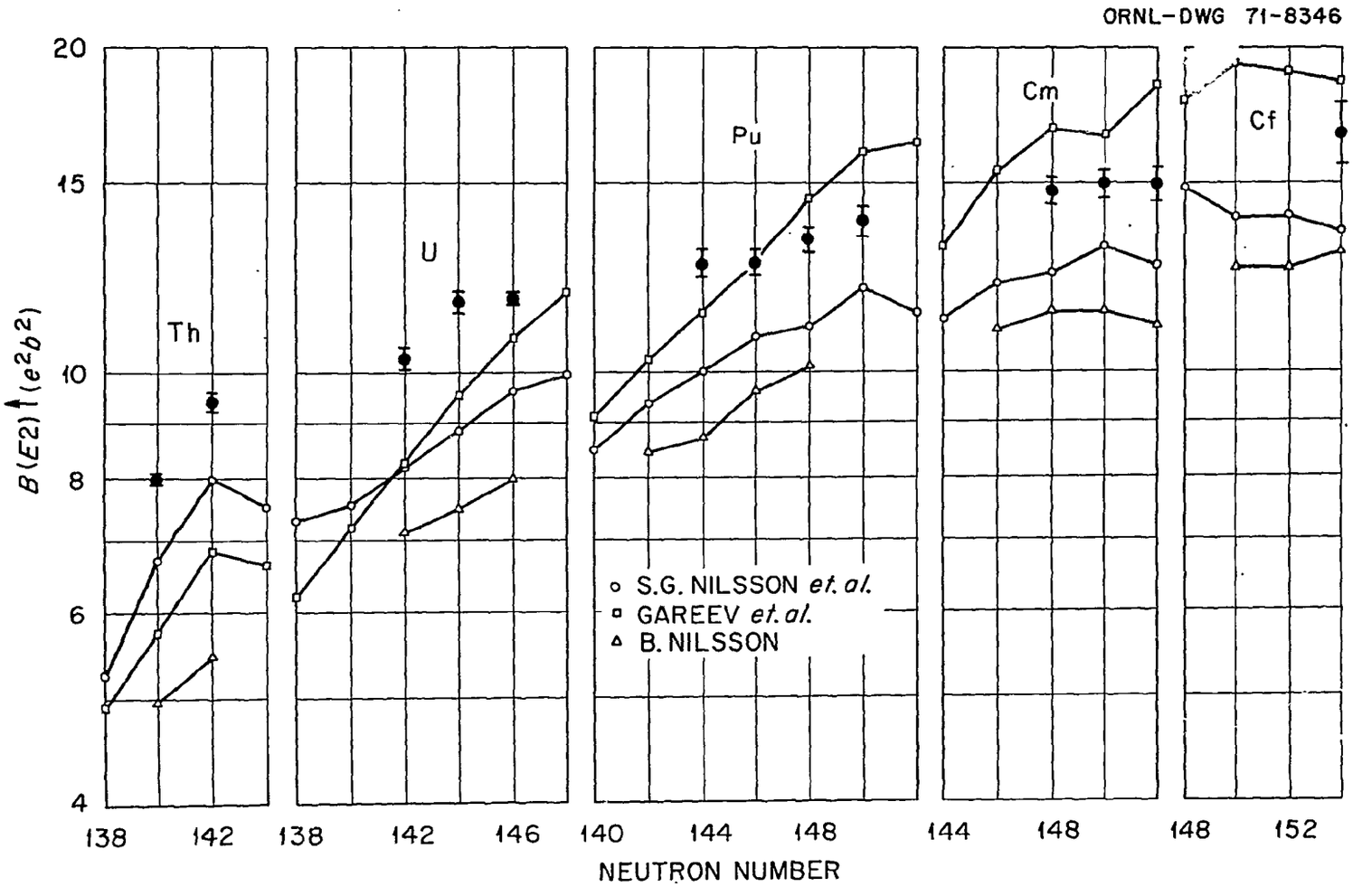

Figure B-1. Comparison of Observed B(E2)'s with Theories for Actinide Nuclei

RENSSELAER POLYTECHNIC INSTITUTE

A. CROSS SECTION MEASUREMENTS

1. Neutron Capture and Total Cross Sections of ^{240}Pu*

(R. W. Hockenbury, W. R. Moyer and R. C. Block)

The present status of the ^{240}Pu capture and transmission measurements is as follows. Resonance parameters were obtained from 20 eV to 500 eV and published[1]. The s-wave neutron strength function determined from these parameters and the level spacing is $(1.10 \pm 0.27) \times 10^{-4}$, in good agreement with previous transmission measurements[2]. The average radiation width from our data ($\bar{\Gamma}_\gamma = 0.0295 \pm 0.0015$ eV) is about 25% larger than that reported by Weigmann[3]. The present results are summarized in Table A-1.

The keV capture cross section results have been sent to the National Neutron Cross Section Center. Using the theory of Lane and Lynn,[4] the keV capture cross section has been calculated and is compared to the measured values in Fig.A-1. Here the RPI average resonance parameters for

Table A-1

$D_{J=\frac{1}{2}}^{\ell=0}$	= 13.7 eV	S_o	$= (1.10 \pm 0.27) \cdot 10^{-4}$
$\langle \Gamma_n^o \rangle_{J=\frac{1}{2}}^{\ell=o}$	= 1.508 meV	$\langle \Gamma_\gamma \rangle^{\ell=0}$	$= 0.0295 \pm 0.0015$ eV

s-wave neutrons (Table A-1) and the p-wave parameters of Ref. 5 have been used. The importance of the p-wave contribution in the keV region is evident in Fig. A-1. Calcuations to obtain a best fit to the measurements are still in progress.

2. MeV Total Neutron Cross Sections on H, D, and ^{7}Li

(P. Stoler, J. M. Clement, and C. A. Goulding)

Since the last report we have completed measurements f total neutron cross sections on hydrogen, deuterium and i. The neutron energy ranged from less than 1 MeV to

---

*Pertinent to Requests 468, 469 and 471

1. R. W. Hockenbury, J. D. Boice, W. R. Moyer and R. C. Block, Proc. 3d Conf. Neutron Cross Section and Tech., Vol. 2, 721 (1971).
2. W. Kolar and K. H. Bockhoff, Nucl. Energy 22, 299 (1968).
3. H. Weigmann and H. Schmid, Nucl. Energy 22, 317 (1968).
4. A. M. Lane and J. E. Lynn, Proc. Phys. Soc. LXX, 557 (1957).
5. S. Yiftah, J. J. Schmidt, M. Caner and M. Segev, Fast Reactor Physics I, 123, IAEA, Vienna, 1968.

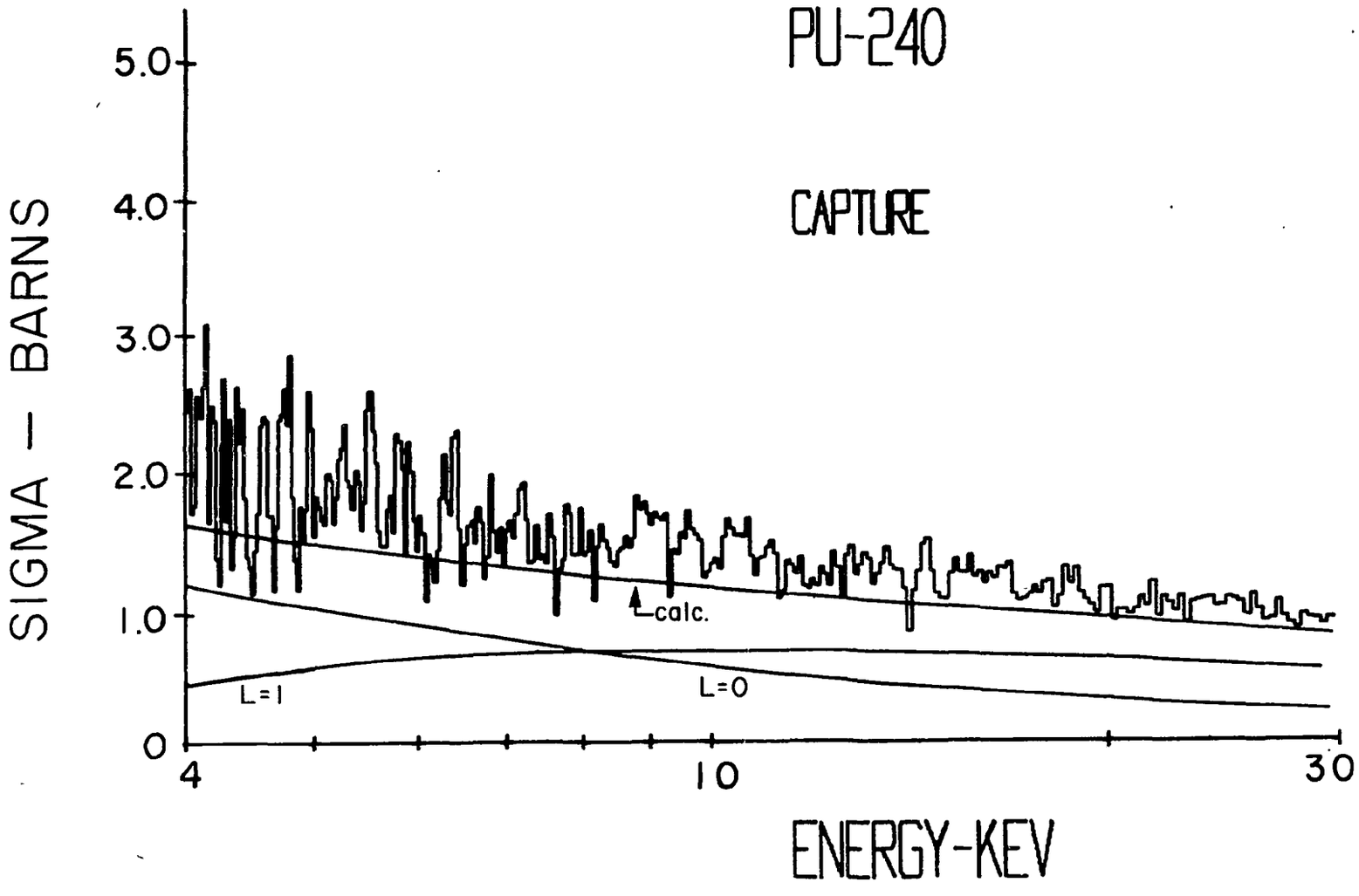

Fig. A-1. Measured and calculated capture cross sections for ^{240}Pu.

greater than 30 MeV. The experimental arrangement has been previously described, but a short recapitulation follows. A pulsed electron beam of approximately 70 MeV was used to produce a white source of neutrons. The collimated neutrons after passing through the transmission sample were energy analyzed using a 250 m time-of-flight spectrometer. The minimum electron beam burst width of 10 ns, combined with the intrinsic detector resolution of a few ns, produce an overall resolution capability of 0.05 ns/m. However, due to the smoothness of the cross sections, wider beam bursts were usually employed.

The hydrogen and deuterium samples were in gaseous form under high pressure ($\sim$100 atm), and the ^{7}Li was an encapsulated metalic cylinder.

The hydrogen, deuterium, and part of the ^{7}Li results are shown in figs. A-1 to A-3. Due to comparisons between the present hydrogen results, with those of other recent measurements and evaluations, it is felt that the overall accuracy of these measurements is in the 1% range.

3. <u>The Differential Elastic Scattering Cross Sections of KeV Neutrons from Natural Iron</u>*
(R. Zuhr and K. Min)

The differential elastic scattering cross sections of keV neutrons from natural iron has been measured at six scattering angles. The least square fits of the Legendre polynomial, expansion $\sigma(\theta) = \sum_{n=o}^{2} a_n P_n (\cos \theta)$ were made through the data points. The results at

---

* Pertinent to Request 97

1. RPI Linear Accelerator Project Progress Report, RPI-328-226, p 35 (1971)

2. A. Langsdorf, R. O. Lane and J. E. Monahan ANL-5567, Argonne National Laboratory (1956)

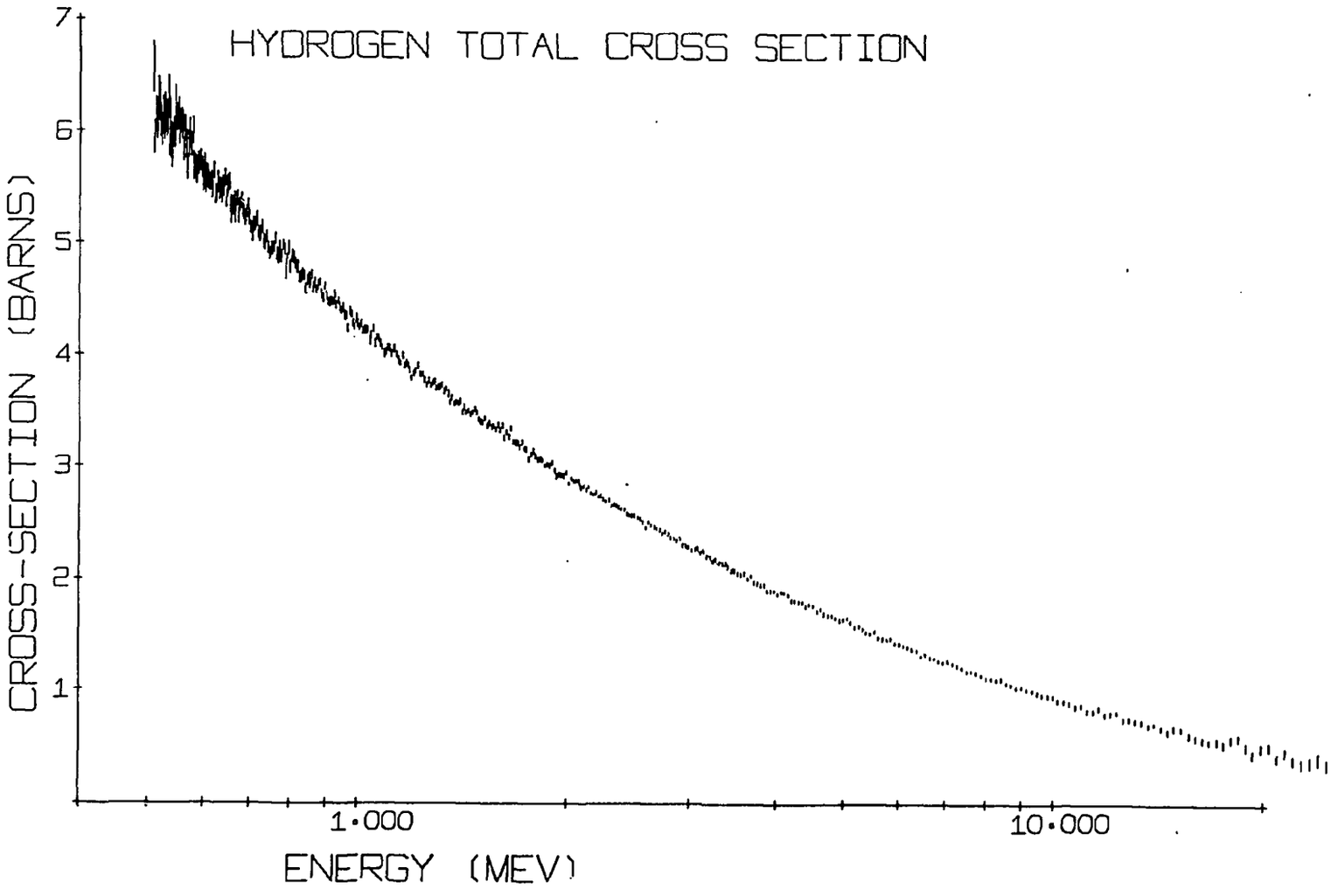

Fig. A-2. Hydrogen total neutron cross section.

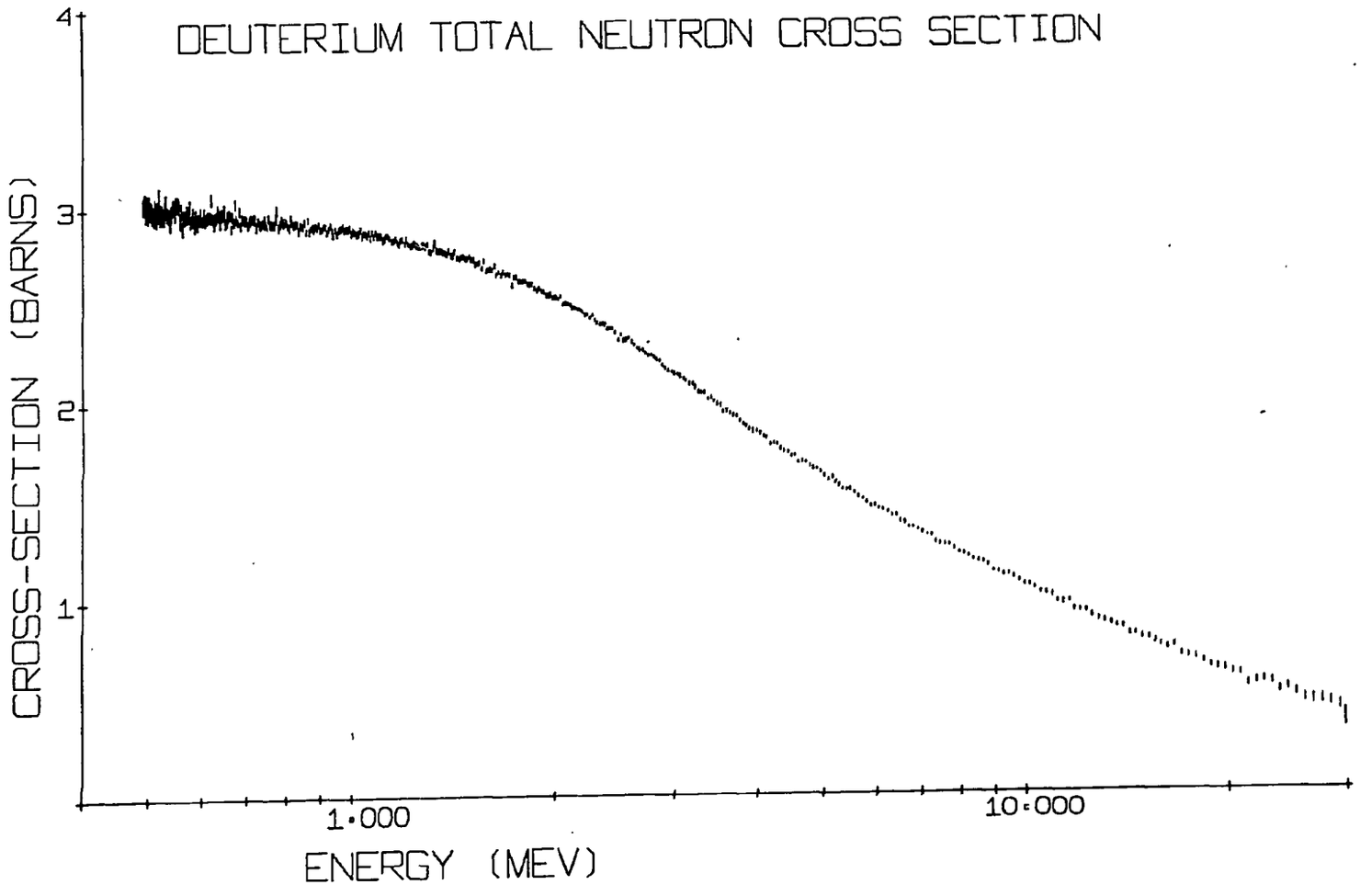

Fig. A-3. Deuterium total neutron cross section.

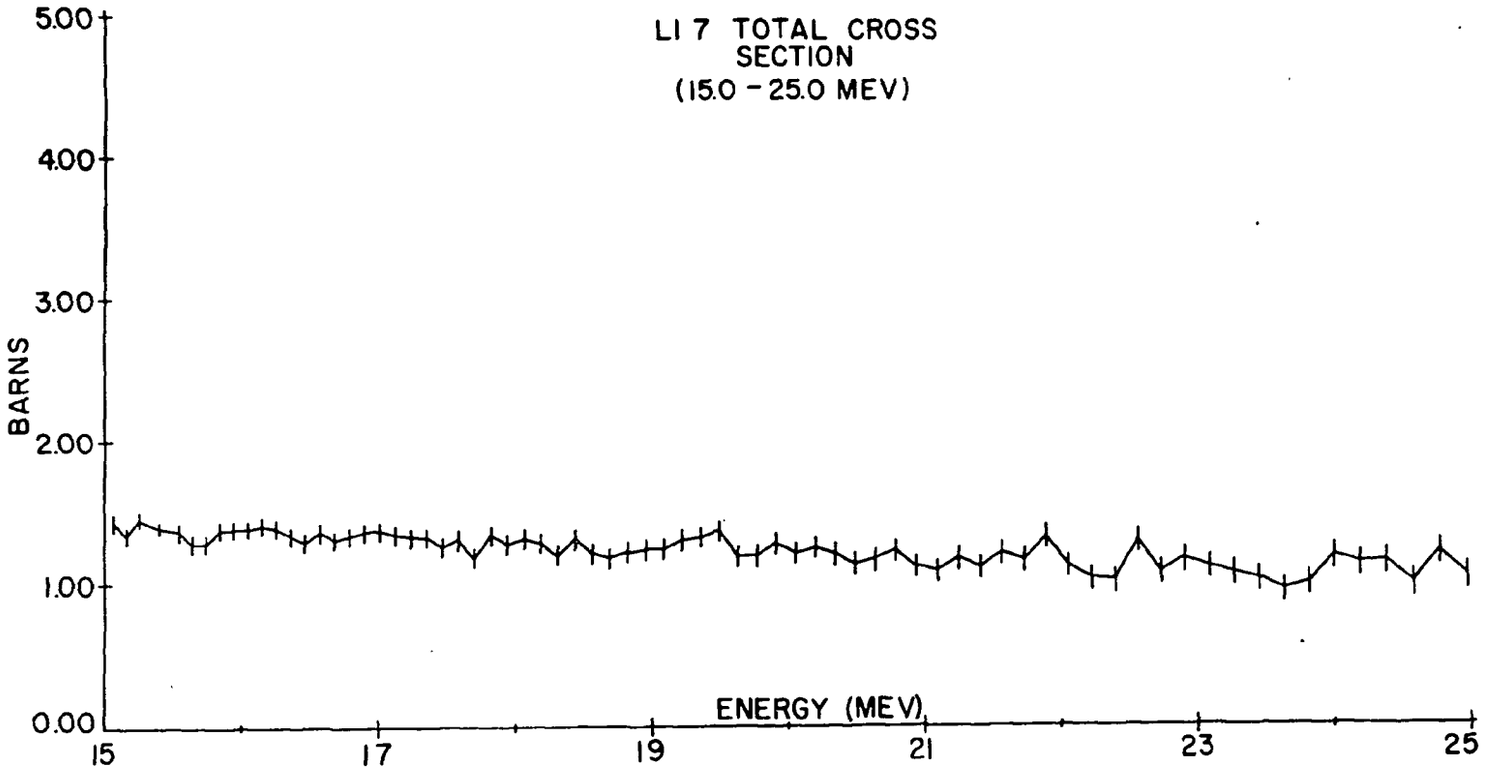

Fig. A-4. A portion of the ^{7}Li total neutron cross section.

eleven neutron energies were previously reported in a progress report.[1] Prior to further data analysis, the total scattering cross sections averaged over a relatively large neutron energy interval, $\Delta E_n = 100$ keV, were obtained to compare with the previously published results of comparable resolution.[2] This is shown in Fig. A-5, where comparison is also made with the total cross sections averaged over the same energy interval.

4. Neutron Capture Measurements On ^{54}Fe, ^{58}Fe, ^{61}Ni*
(R. W. Hockenbury, N. N. Kaushal, B. Ward and R. C. Block)

Capture measurements have been made on enriched samples of ^{54}Fe and ^{58}Fe from 20 eV to about 300 keV using the 1.25 meter scintillation detector. The data show many p-wave resonances and a few s-wave resonances, as has been observed[1,2] in measurements of other Fe and Ni isotopes. The ^{54}Fe sample will also be measured at a higher resolution from 35 keV to about 400 keV. Samples of ^{61}Ni and ^{64}Ni are now being prepared for capture measurements.

5. Measurement of Nubar for ^{235}U and ^{233}U**
(R. C. Reed and R. C. Block)

Instrumentation improvements for the nubar measurements have progressed. The fast current amplifiers have been finished and are in the final testing. New photomultiplier bases have been designed, built, and placed in the system. A 100-Megahertz scaler has been built for the logic unit in order to decrease the deadtime correction. Gamma flash and other gain shifts will be corrected for by taking ^{252}Cf nubar data simultaneously with the uranium data and normalizing the uranium nubar relative to the ^{252}Cf nubar.

---

* Pertinent to Requests #102,106,107,111,120 and 126

1. R. W. Hockenbury, Z. M Bartolome, J. R. Tatarczuk, W. R. Moyer and R. C. Block, Phys. Rev. 178, 1746 (1969)

2. R. G. Stieglitz, R. W. Hockenbury and R. C. Block, Nucl. Phys. A163, 592 (1971)

** Pertinent to Requests 361 and 395

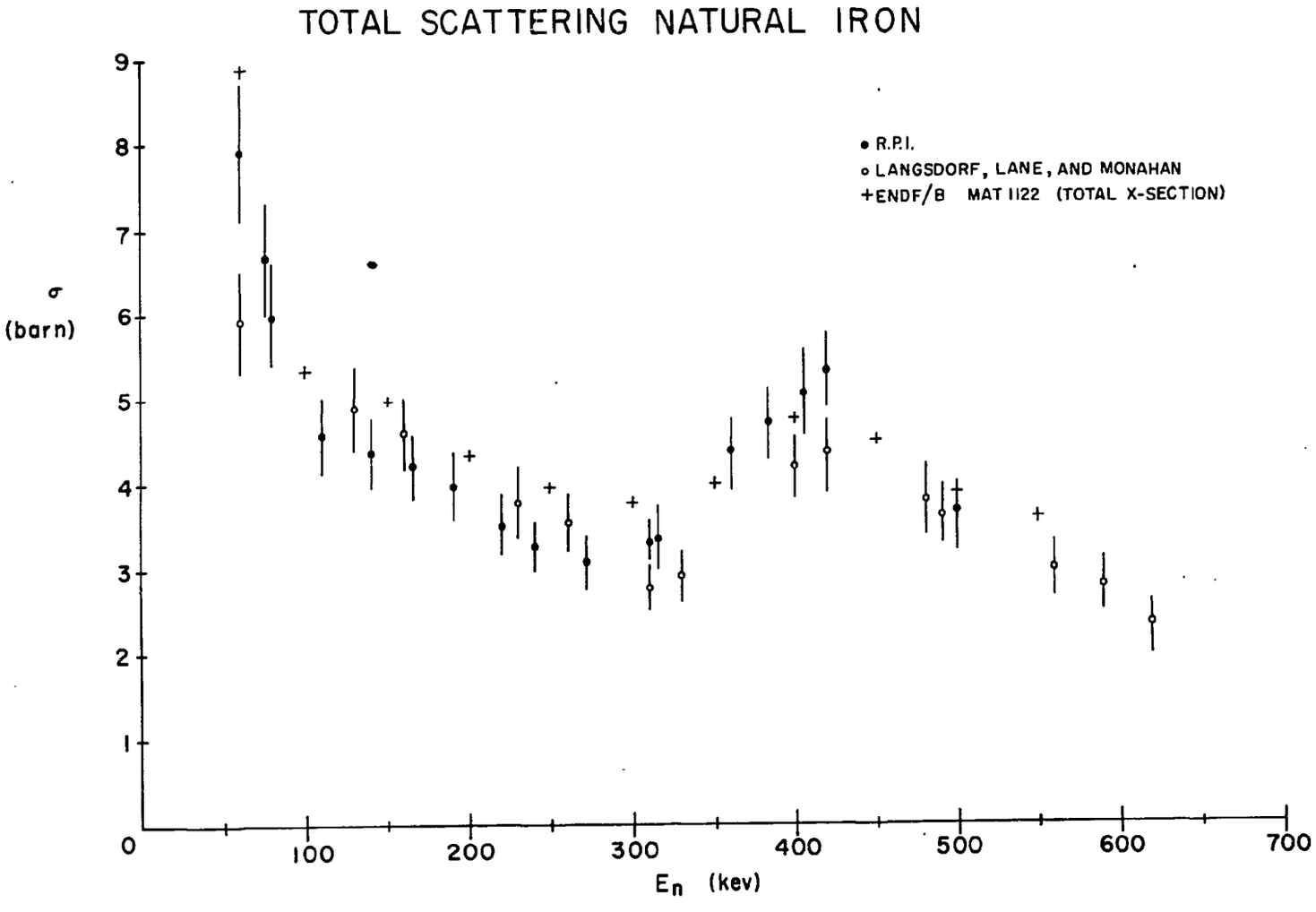

Fig. A-5. The total scattering cross section of natural iron.

6. The Application of Resonance Filtered Beams to Neutron Time of Flight Experiments
(R. C. Block, R. W. Hockenbury, P. J. Turinsky, and K. Alfieri

The success of resonance-filtered reactor beams has led to the speculation that this technique could be adapted to time-of-flight experiments. A 14-inch thick filter of iron (steel type C1108) was placed into the beam between the neutron target and the 25 meter ^{10}B-NaI detector. The observed time-of-flight spectrum is plotted in Figure A-6. The interesting feature of this figure is the rather well-resolved maxima which correspond to the interference minima in the ^{56}Fe total cross section. In particular the peak counts at 24.7 keV is 500 times background and it appears feasible to use filtered beams to carry out low-background precision experiments.

One experiment that was carried out was the measurement of the iron cross section minimum at 24.7 keV. A 6-inch thick sample of iron (C1108 steel) was oscillated in and out of the 14-inch iron filtered beam. The observed total cross section "σ_t" (not yet corrected for resolution) is shown in Fig. A-7. We obtain a minimum cross section of 0.50±0.03 barns. However, there is still the presence of 0.7% Mn which probably gives rise to the 23.7 keV 'bump' in Fig. A-7; additional experiments are underway with low Mn iron and separate Mn samples to determine both the iron minimum cross sections and the precise energy relationship between the Mn resonance peak and the iron minimum.

7. The Strength Function for P-Wave Neutrons
(R. C. Block and R. W. Hockenbury)

The p-wave neutron strength function for nuclei near mass 55, 90 and 180 has been determined at RPI during the course of several capture cross-section measurements.[1,2,3] These results are summarized in Table A-2, where the p-wave strength function S_1 is defined as

$$S_1 = \frac{\sum_{i=1}^{N} (g\Gamma_n / \sqrt{E_o}\, v_1)_i}{3\Delta E} \qquad (1)$$

The sum is determined over the N resonances observed in the neutron energy region ΔE (usually spanning from 0 to about 50 or 100 keV), the product of the statistical weight factor g times the neutron width Γ_n is determined from the capture

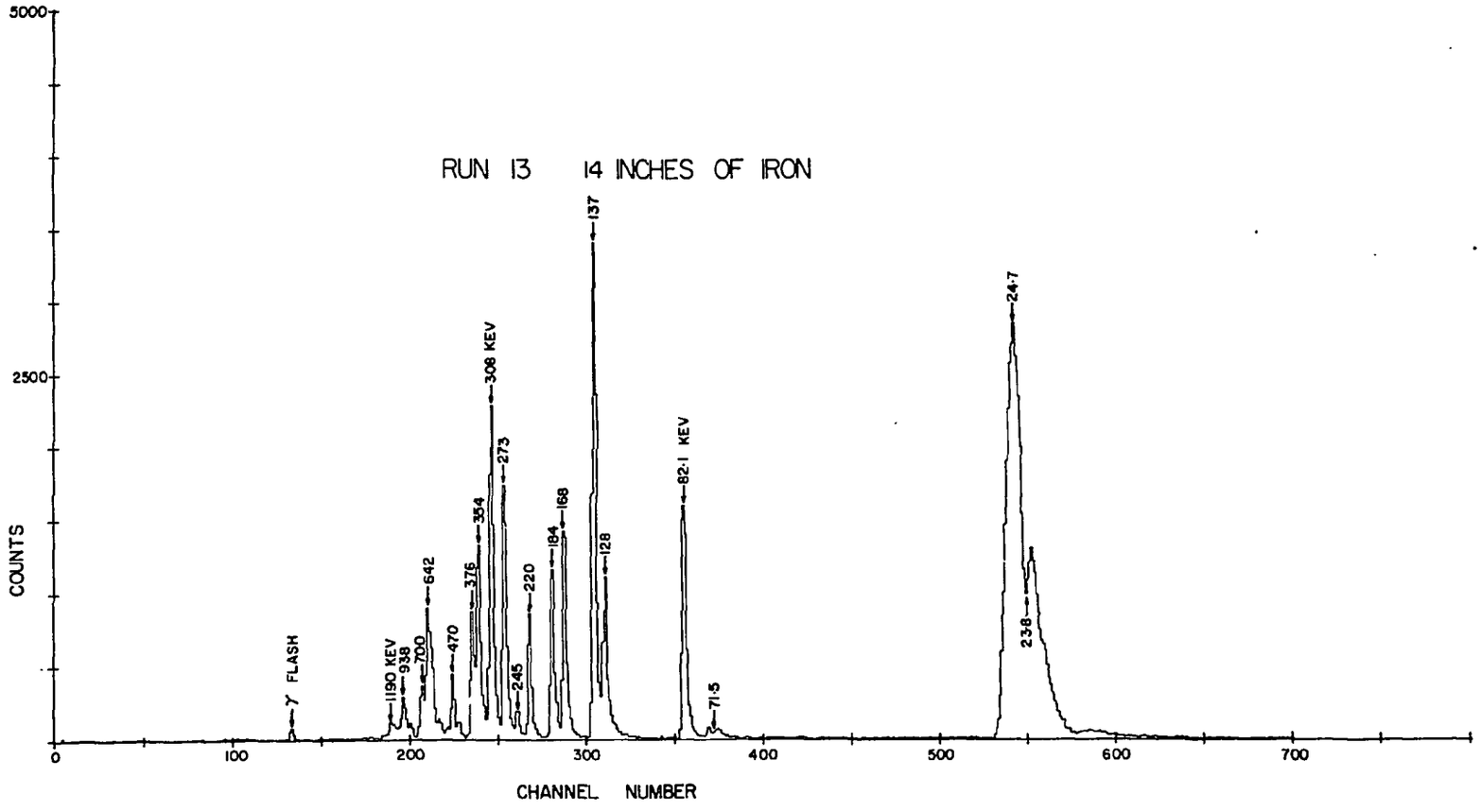

Fig. A-6. Counts vs time of flight for neutrons filtered through 14 in. of iron.

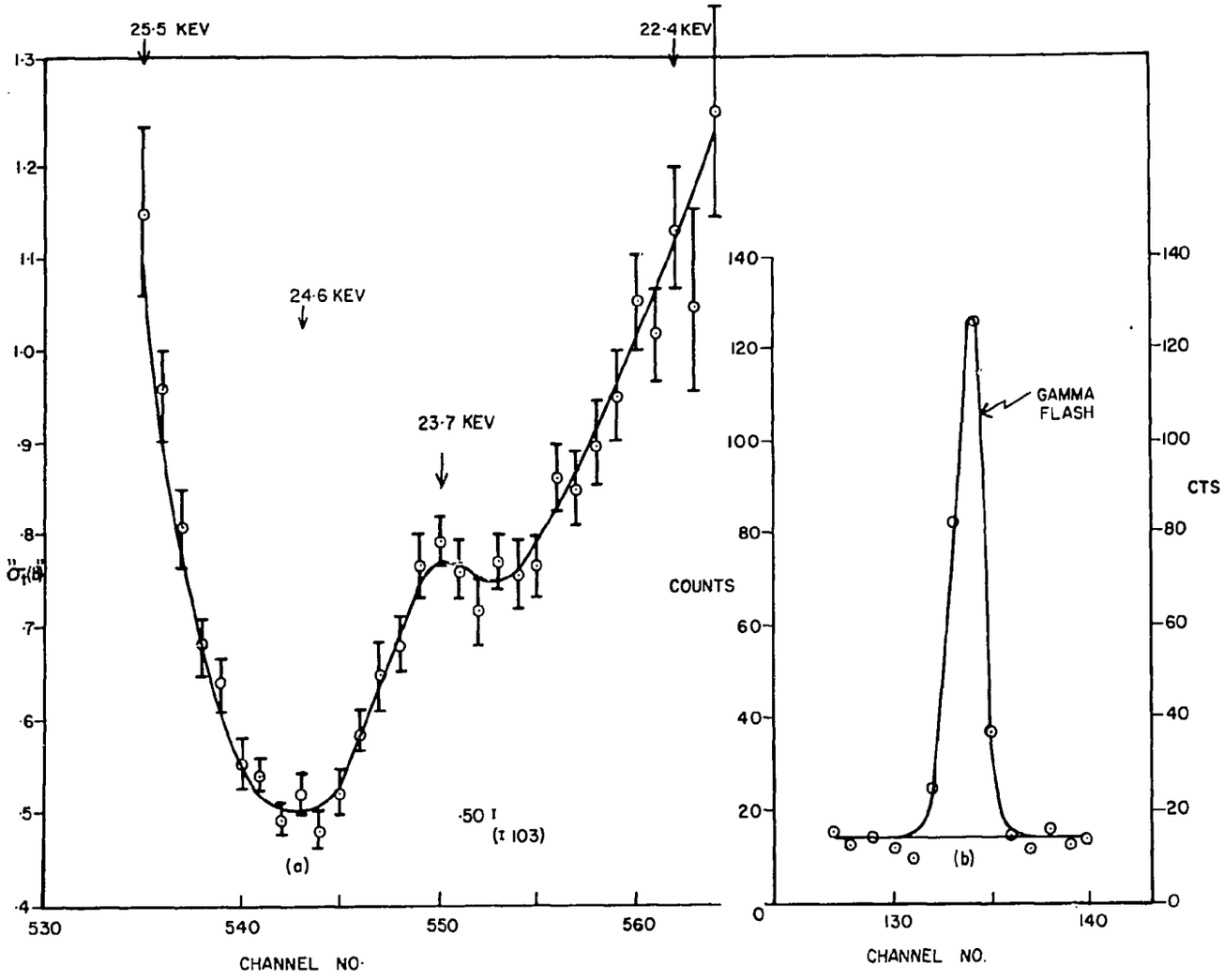

Fig. A-7. (a) The total cross section of iron near the 24.7-keV minimum.
(b) The gamma flash profile from the linac.

Calculations are now being carried out to fit the experimental p-wave strength function over the entire mass range.

TABLE A-2

Target Nucleus	S_1 (in units of 10^{-4})	Reference
^{51}V	0.08 ± 0.04	3
^{50}Cr	0.26 ± 0.15	3
^{52}Cr	0.05 ± 0.02	3
^{53}Cr	0.07 ± 0.05	3
^{54}Cr	0.04 ± 0.02	3
^{56}Fe	0.10 ± 0.04	1
^{58}Ni	0.04 ± 0.03	1
^{60}Ni	0.08 ± 0.03	3
^{90}Zr	7 ± 4	2
^{91}Zr	3 ± 2	2
^{92}Zr	7 ± 5	2
^{94}Zr	4 ± 2	2
$^{182,184,186}W$	$0.28 {}^{+0.52}_{-0.15}$	2

area under the resonance, E_o is the resonance energy (in eV), and v_1 is the p-wave penetrability factor. The factor of 3 in the denominator is from a $(2\ell+1)$ term in the definition of S_1.

The results summarized in Table A-2 are plotted in Fig. A-8 along with results from other laboratories. Figure A-8 was obtained by adding to Perey and Buck's[4] p-wave strength function vs. atomic mass plot (Fig. 2 of Ref. 4) the experimental results from RPI and from Geel[5] and the diffuse edge optical model predictions of Moldauer.[6] The solid curve in Fig. is the p-wave strength function for a spherical optical model potential and the dashed curve is for a collective model potential; both of these curves appear in Ref. 4. The dot-dashed curves are from Ref. 6 with a spin-orbit potential of 7 and 14 MeV depth.

The most striking feature of Fig. A-8 is the very low values which the experimental points reach near mass numbers 50 and 170, about 8% and 20% respectively of the black nucleus value of $\sim 10^{-4}$. These deep minima are not predicted by either the spherical or collective model calculations of Perey and Buck. The dot-dashed curve from Moldauer[6] does predict a minima of about 0.25×10^{-4} near mass 50, but this is still a factor of three larger than the experimental values. Moldauer did not extend his calculation beyond mass 120, but a calculation by Jain[7] using a surface absorption optical potential predicts a minimum of about 0.35×10^{-4} near mass 160. This is in reasonable agreement with the experimental results of about 0.25×10^{-4} near mass 170; however, Jain[7] also predicts a minimum near mass 60 of about 0.35×10^{-4} which is about a factor of four larger than the experimental values.

1. R. W. Hockenbury, Z. M. Bartolome, J. R. Tatarczuk, W. R. Moyer and R.C.Block, Phys.Rev. 178, 1746 (1969)
2. Z. M. Bartolome, R.W. Hockenbury, W. R. Moyer, J.R. Tatarczuk and R.C.Block, Nucl.Sci.Eng. 37, 137 (1969).
3. R. G. Stieglitz, R.W. Hockenbury and R.C. Block, Nucl. Phys. A163, 592 (1971).
4. B. Buck and F. Perey, Phys.Rev. Letters, 8, 444, (1962).
5. H. Weigmann, J. Winter and H. Schmid, Second Conf. on Neutron Cross Sections and Technology, p. 533 (1968).
6. P. Moldauer, Nucl. Phys. 47, 65 (1963).
7. A. P. Jain, Nucl. Phys. 50, 157 (1964).

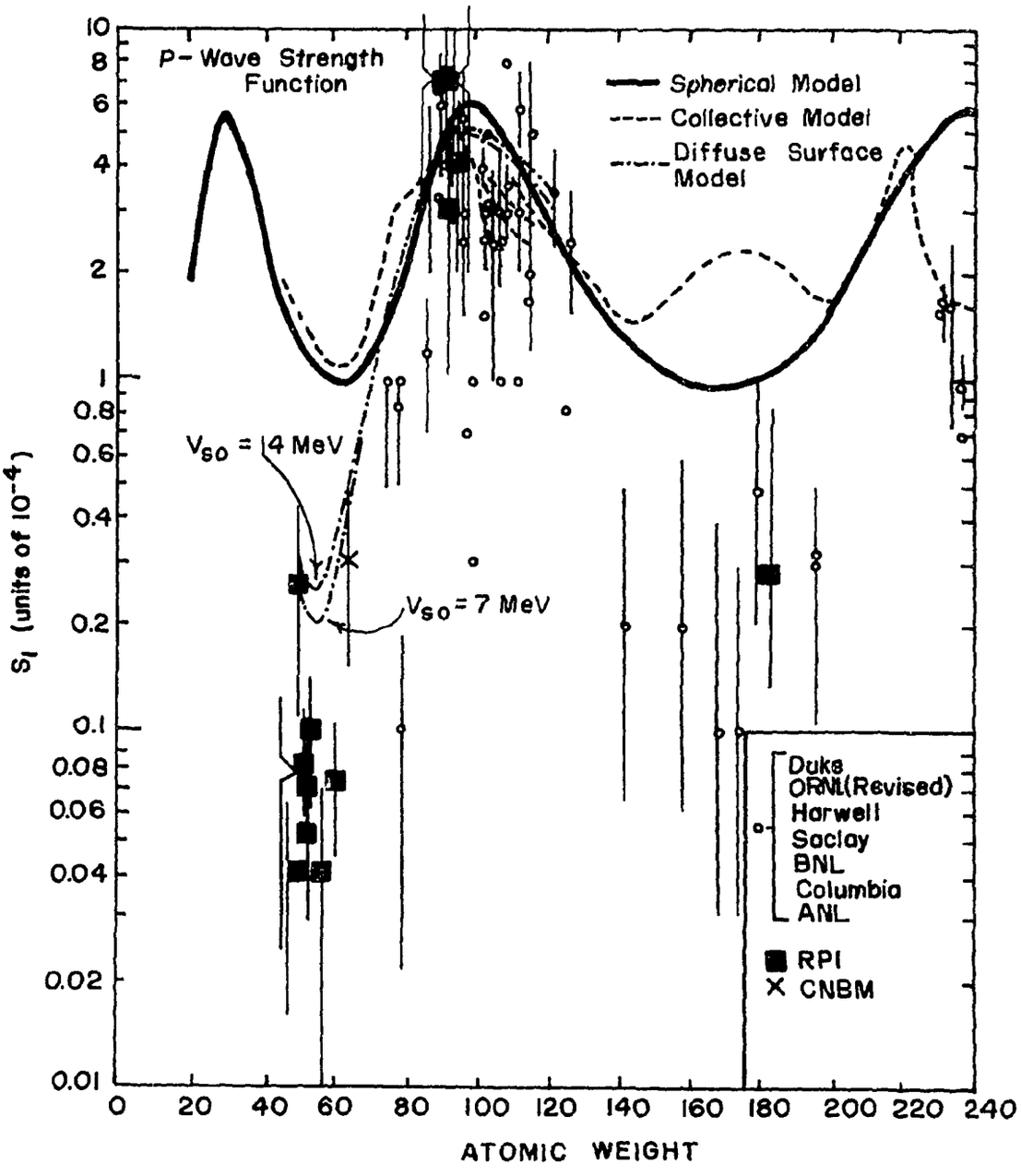

Fig. A-8. The p-wave neutron strength function S_1 vs the atomic weight. The solid and dashed curves are from Perey and Buck[4] and the dot-dashed curves from Moldauer.[6]

8. Temperature-Dependent Transmission and Self-Indication Measurements Upon Depleted Urznium in the Unresolved Region
(T. Y. Byoun and R. C. Block)

Room temperature transmission and self-indication measurements have been carried out up to 100 keV upon samples of depleted uranium varying in thickness for less than 1 mm to about 1.5 cm. A new vacuum furnace has been built and tested to carry out the 1200°K measurements and the 78°K and 1200°K measurements will be carried out this winter.

B. INTEGRAL CHECKS OF CROSS-SECTION DATA

1. Fast Reactor Physics Studies (E. R. Gaerttner, N. N. Kaushal, B. K. Malaviya and M. Becker)

Integral checks of differential microscopic data based on the study of fast neutron transport in bulk media has been continuing. Time-of-flight-measured fast neutron angular flux spectra at different positions in simple homogenous systems have been analyzed using transport theory codes and standard data files. Definite conclusions have been obtained as to the adequacy of current cross section data files on iron and depleted uranium. These were reported in the last report. Preliminary analysis of the aluminum data indicates disagreements between experimental and calculated neutron spectra. These disagreements can be attributed to errors in the inelastic cross section data in the region above 1 MeV; however, the analysis is not yet completed.

The main experimental effort at present is being devoted to readying a 6-ft-cube metallic sodium assembly for fast neutron spectrum measurements. The assembly consists of a double walled steel vessel filled with sodium and then sealed under a positive pressure of dry nitrogen which acts as the cover gas. A number of reentrant channels are provided for extraction of the neutron flux from various points in the assembly. Preliminary measurement of neutron spectra from the sodium assembly show anisotropic effects to be quite strong and we can expect to see a large sensitivity to the anistropy in the cross sections in the course of our analysis of the data.

TRIANGLE UNIVERSITIES NUCLEAR LABORATORY

A. NEUTRON AND FISSION PHYSICS

1. Resonance Cross Section Measurements with Continuous Beam (J. Malan,* W. F. E. Pineo,** E. G. Bilpuch, H. W. Newson)

R-matrix analysis of the total cross section of natural Sr (82% Sr^{88}) has been continued. The interpretation is very difficult and the resulting parameters are not necessarily unique. However, up to 500 keV, the value of $\Sigma_{gJ}\Gamma_n^{\ell}$ is probably accurate enough for p-wave strength-function and doorway-state studies. Above 500 keV there appears to be serious incoherent overlapping, and analysis can be continued (up to 800 keV) only on the assumption (expected from the optical model) that all strong resonances are due to s- and p-waves. The results of this analysis were presented at Washington[1,2] and at the Albany Conference where they were shown to agree with doorway state calculations. Efforts to prove that d-waves are unimportant are now underway.

2. Resolved Neutron Total Cross Sections and Intermediate Structure (W.F.E. Pineo, M. Divadeenam,+ H. W. Newson)

The cross sections for natural silicon (92% Si^{28}) as measured at NBS[3] have been analyzed with our R-matrix code. The results are given in Table A-1 (all energies are in keV). In this case there is no confusion between p- and d-waves up to 1400 keV. These widths indicate one or more strong p-wave doorways near 1 MeV. It is known that s-wave strength below 500 keV is small. These results were reported at Albany.

---

* Now at the Atomic Energy Board of the Republic of South Africa

** North Carolina A and T University, Greensboro, N. C.

\+ North Carolina Central University, Durham, N. C.

1 W. F. E. Pineo, E. G. Bilpuch, H. W. Newson and J. G. Malan, Bulletin of the American Physical Society, 16, 495 (1971)

2 M. Divadeenam, E. G. Bilpuch, and H. W. Newson, Bulletin of the American Physical Society, 16, 495 (1971)

3 R. B. Schwartz, R. A. Schrack, and H. T. Heaton, II, Bulletin of the American Physical Society, 16, 495 (1971)

Table A-1

E_o	Γ_n	E_o	Γ_n
(s-wave)		(p-wave)	
190	~6.0	531	0.5
1160	2.5	565	10.0
1186	1.8	591	0.4
1252	7.0	813	28.0
		845	0.8
(p- or d-wave)		964	80.0
1480	3.0	910	2.5
1528	2.7	1042	0.8
1580	0.1	1202	15.0
		1264	1.0
		1407	12.0
		1594	0.15

3. Averaged Cross Sections, Strength Functions, and Intermediate Structure (W. F. E. Pineo, M. Divadeenam, E. G. Bilpuch, H. W. Newson)

Preparation of papers on this topic based on the theses of M. Divadeenam and W. F. E. Pineo is still in progress. Data for natural Barium (50 to 875 keV) and Radiolead (1.3 - 1.9 MeV) are to be analyzed for strength functions by our average cross section technique. Mo + n data indicate intermediate structure which is probably not due to 2p-1h states. However there is evidence that p-wave doorway effects may be apparent in Differential Scattering Cross Sections even when resolution is very poor compared to total cross section measurements; attempts to identify this effect are still underway.

4. Shell Model and Particle-Vibration Model Calculation of Neutron Resonances and Intermediate Structure (M. Divadeenam, W. P. Beres,* H. W. Newson)

Following an initial success of the 2p-1h doorway interpretation[1,2] of Sr^{88}, Zr^{91} and Ca^{49} resonances, we have extended the calculations to the s-d shell

---

* Wayne State University, Detroit, Michigan

[1] M. Divadeenam, W. P. Beres, and H. W. Newson, Annals of Physics (in press)

[2] M. Divadeenam, E. G. Bilpuch, and H. W. Newson, Bull. Am. Phys. Soc. 16, 495 (1971)

nuclei in spite of the scarcity of the neutron resonance levels. As a test case $S^{33}(S^{32} + n)$ is considered in an attempt to predict s- and p-wave doorway state energies and their neutron escape widths. A stronger mixing of the 2p-1h basis states is required to reproduce the experimental results in terms of the sum rule $\Sigma\gamma_n^2 = \gamma_\ell^2$. The alternate model (particle + vibration model) fails in that it overestimates the escape widths considerably.

Recent neutron total neutron cross section measurements[3] on Si^{28} at NBS and their subsequent R-matrix analysis by Pineo suggest the possible presence of a p-wave doorway (or doorways) below 1 MeV. These results were discussed by Newson[4] at the recent Albany meeting. A 2p-1h model calculation is planned for the Si^{28} + n case.

Assuming that the two extra $1g_{9/2}$ protons in the ground states of ${}_{42}Mo^{92}_{50}$ and ${}_{42}Mo^{98}_{50}$ are coupled to 0^+, a 2p-1h diagonalization for $J^\pi = 1/2^+$ is being performed in compound nuclei Mo^{93} and Mo^{99}. The predictions will be compared with the available experimental data.[5] An extension to the p-wave doorways is planned. In addition the applicability of the particle + vibration model will be tested for these nuclei.

A preliminary report of our 2p-1h calculations for Ni^{57} and Ni^{61} have been presented by Newson[4] at the Albany conference. Detailed discussion will be published as a paper.

The nucleus Ca^{40} being doubly magic might be suitable for doorway state investigation. A 2p-1h diagonalization in Ca^{41} predicted two $1/2^+$ doorways (below 1 MeV), which might be interpreted as responsible for the observed Ca^{40} s-wave neutron resonances in the keV region.[4] The doorway escape widths are not yet estimated.

An extension of the particle-vibration model to all possible $1/2^+$ doorways in Pb^{209} and Pb^{207} has been carried out and the results were reported[6] at the

---

[3] R. B. Schwartz, R. A. Schrack, and H. T. Heaton, II, Bull. Am. Phys. Soc. 16, 495 (1971) and Bull. Am. Phys. Soc. 16, 595 (1971)

[4] H. W. Newson, in Proceedings of the International Conference on Statistical Properties of Nuclei (Albany, 1971)

[5] M. Divadeenam, E. G. Bilpuch, and H. W. Newson, Bull. Am. Phys. Soc. 15, 568 (1970)

[6] M. Divadeenam and W. P. Beres, in Proceedings of The International Conference on Statistical Properties of Nuclei (Albany, 1971)

Albany meeting. The results are summarized below in Table A-2 and Fig. A-1. The positions of the predicted doorways agree well with experiment, while the two sets of calculated reduced widths agree with the experimental reduced widths equally well.

Table A-2

Configuration[b]	Pb^{209} Theory E_d	γd^2 c	γd^2 d	Pb^{209} Expt.[1,14] E_{res}	γn^2	Pb^{207} Theory E_d	γd^2 c	γd^2 d	Pb^{207} Expt.[1] E_{res}	$\Sigma\gamma_n^2$
$4^+ \otimes 2g_{9/2}$	0.365	37.8	22.2	0.500	22.5	0.361	37.1	23.6	~.43	23
$6^+ \otimes 1i_{11/2}$	1.265	3.2	2.4	1.314	1.7	1.159	3.7	2.8	no data	
$2^+ \otimes 3d_{5/2}$	1.700	11.8	6.6	{1.735, 1.87}	{12.5, 2.6}	1.691	9.1	5.7	avail-	
$2^+ \otimes 3d_{3/2}$	2.670	5.5	3.1			2.661	4.2	2.7	able	
$4^+ \otimes 2g_{7/2}$	2.865	13.0	8.9			2.863	12.9	9.4		

a) Predicted doorway and experimental resonance energies are in MeV, while the reduced widths are in keV. b) The symbol ⊗ represents the coupling of two angular momentum states. c) Widths calculated using Hamamoto's parameters for the continuum neutron. d) Buck and Perey's parameters used for the continuum neutron.

The Pb^{209} p-wave and d-wave doorways have also been considered. The results will be presented in the near future.

An extension of the above model to the Pb^{207} + n case is underway.

Recent (n, γ) and (γ, n) reaction data indicate that the neutron doorways act as common doorways for the neutron and γ-channels. An additional test of the particle + vibration model will be attempted in calculating the neutron capture $\Gamma_{n\gamma}$ escape widths for the particle + vibration doorways in Pb^{209} and Pb^{207}. In particular a calculation of the Γ_{n_γ} for the $(4^+ \otimes g_{9/2})_{1/2+}$ doorway is planned.

5. Charged Particle Fission (F. O. Purser, J. R. Boyce, Jr., D. E. Epperson, T. D. Hayward, E. G. Bilpuch, H. W. Newson, H. W. Schmitt*)

a. Cross Section Measurements

The differential cross section measurements for proton induced fission

* Oak Ridge National Laboratory, Oak Ridge, Tennessee

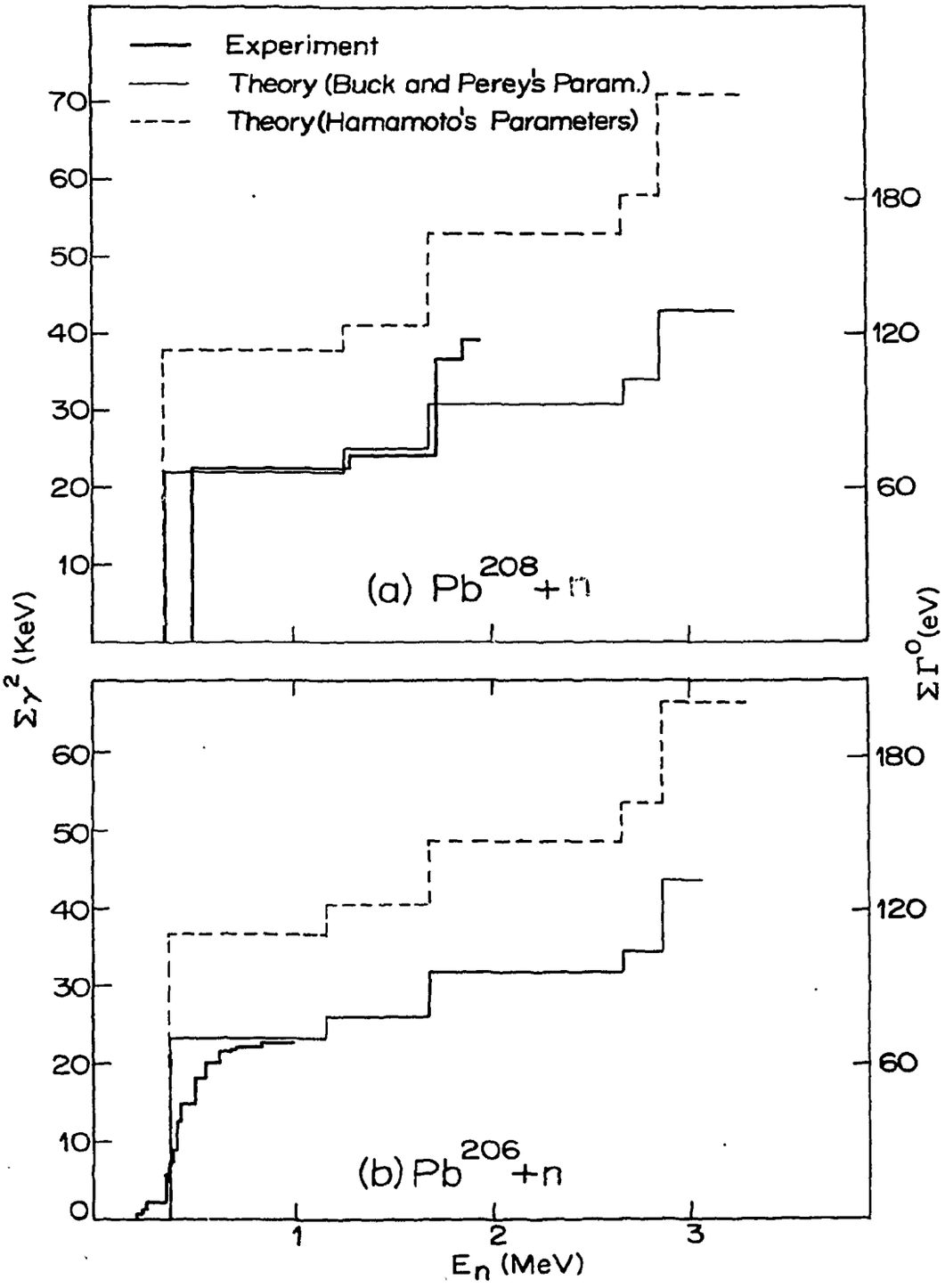
Experiment
Theory (Buck and Perey's Param.)
Theory (Hamamoto's Parameters)
(a) Pb208 + n
(b) Pb206 + n
Σγ2 (KeV)
ΣΓ0 (eV)
En (MeV)
70
60
50
40
30
20
10
0
180
120
60
1
2
3

Fig. A-1

of ^{233}U and ^{234}U have been extended to lower proton energies, 4.5 MeV and 5.0 MeV, respectively. Extending the energy range was necessary to assess quantitatively the contribution to the total fission cross section made by the opening of the second and third chance fission channels.

Below the coulomb barrier, which is about 14 MeV for protons in Uranium, the measured fission cross sections are dominated by coulomb penetrability. The logarithmic cross section increase with energy essentially masks any moderate variation in the measured cross sections. Underlying structure in the data can be displayed by calculating from these cross sections a fission probability as a function of energy. This probability may be defined as Γ_F/Γ_T and may be approximated by σ_F/σ_R where σ_R is a reaction cross section calculated by an appropriate model. Proton optical model parameters for the severely distorted actinide nuclei are not available in the literature and we have undertaken extensive optical model calculations to determine a range of energy dependent parameters appropriate to the region. Because of the extended excitation energy range covered by our data boundary conditions to the reaction cross section may be established by the available (d,p,f) data for low excitation energies and by elastic angular distributions measured at this laboratory. Preliminary analysis of the fission probability data for the five Uranium isotopes in this manner display distinctively the opening of the competing fission channels (p,n,f) and (p,2nf) with the (p,2nf) channel decreasing in importance as A decreases. Analysis is proceeding with the view of extracting accurate fission thresholds and barrier heights for Neptunium nuclei $232 < A < 239$. *

b. Angular Distributions

Analysis of 113 fission fragment angular distributions from proton induced fission of the Uranium isotopes is proceeding. Preliminary results indicate that in certain cases the measured anisotropies $(\omega(0°)/\omega(90°))$ undergo reasonably rapid changes (2 - 3 MeV wide) with little effect upon the total fission cross section. Effects of this nature could be expected from double peaked fission barriers and are being investigated further.

c. Mass and Kinetic Energy Distributions

Measurements of fragment mass and kinetic energy distributions using E_1, E_2 correlation techniques have been obtained for $^{235}U(p,f)$ and (d,f) and

---

* Additionally the available data may be adequate to obtain mutually consistent determinations of Γ_F/Γ_n for all the isotopes over a reasonably wide range of excitation energies.

$^{236}U(p,f)$ and (d,f) with the intention of attempting to unfold the effect of second and higher chance fission and to obtain permanent mass and energy data for a single isotope fissioning at a high excitation energy. Analysis is in its preliminary stages.

6. Analysis of Nucleon-^{4}He Scattering below 20 MeV (Th. Stammbach,* R. L. Walter)

An R-matrix analysis of all available n-^{4}He and p-^{4}He cross-section and polarization data has been made to give a new parameterization of these scattering processes. Phase shifts have been derived and polarization tables are compared to earlier reports. This work has been submitted to Nuclear Physics.

7. Polarization in (^{3}He,n) Reactions on ^{9}Be, ^{11}B and ^{13}C Below 4 MeV (R. S. Thomason,** L. A. Schaller,+ Th. Stammbach, R. L. Walter)

A paper entitled "Neutron Polarization Produced in $^{9}Be(^{3}He,n)$ Reactions for ^{3}He Energies from 2.1 to 3.9 MeV" has been submitted to Nuclear Physics. The analysis of the ^{11}B and ^{13}C data will be reconsidered along with the data obtained in Section 8 of this report.

8. Polarization in (^{3}He,n) Reactions at from 8 to 20 MeV (T. C. Rhea, R. A. Hardekopf, P. W. Lisowski, J. M. Joyce,‡ R. L. Walter)

Preliminary measurements indicated that the counting rates for obtaining polarization data on neutrons produced in (^{3}He,n) reactions were sufficient to investigate such phenomena with the low (< 2 μa) intensity beam from tandem accelerators. The first reaction studied was the $^{12}C(^{3}He,n_0)$ reaction. Polarization and cross-section distributions were obtained at 8, 10, 12, 14, 16 and 18 MeV. Effects of resonance structure may die out above 14 MeV, but it is too early to draw conclusions. Some DWBA calculations are planned.

9. Neutron Polarization from (d,n) Reactions on ^{24}Mg, ^{28}Si, and ^{40}Ca (J. Taylor,‡‡ Th. Stammbach, R. L. Walter)

A manuscript was prepared for publication but a recent paper on $^{28}Si(d,p)$ effects some of the conclusions. Until more DWBA checks are made, the manuscript

* Now at Schweiz. Inst. f. Nuklearphysik, Zurich, Switzerland
** Now at G. E. Co., Miss. Test Facility, Bay St. Louis, Mississippi
\+ Now at LASL, Los Alamos, New Mexico
‡ Now at East Carolina University, Greenville, N. C.
‡‡ Now at Armed Forces Institute of Pathology, Washington, D. C.

will be withheld from submission.

10. Polarization of Neutrons from ^{10}B, ^{11}B, and $^{13}C(d,n)$ Reactions (M. M. Meier,* R. L. Walter)

These measurements were carried out for energies from 2.8 to 3.0 MeV. A report on this work was submitted to Nuclear Physics.

11. The j-dependence in the $^{11}B(d,n_0)$ and $^{11}B(d,n_1)$ Polarizations (J. Taylor, G. Spalek,** Th. Stammbach, R. A. Hardekopf, R. L. Walter)

A paper on this work done for deuteron energies from 7 to 12 MeV is nearly completed for submission. This data and analysis supplements the work in Section 10 of this report. A preliminary report was given at the Madison Polarization Symposium.

12. Remeasurement of the Neutron Polarization from the $^{7}Li(p,n)^{7}Be$ Reactions for 3 to 4 MeV Protons (R. A. Hardekopf, J. M. Joyce, G. L. Morgan,+ C. E. Hollandsworth,‡ R. L. Walter)

This work has appeared in Nuclear Physics A167 (1971) 49.

13. The $^{9}Be(d,\vec{n})$ Reaction from 3 to 4 MeV (G. Spalek, J. Taylor, R. A. Hardekopf, Th. Stammbach, R. L. Walter)

The polarization from the $^{9}Be(d,n)$ reactions for five neutron groups has been compared to DWBA calculations. As most of the reactions are 1p transfers, these reactions are a good test of the sensitivity to Q-value. Optical model fits were made to $^{9}Be(d,d)$ data obtained from 3 to 4 MeV. Preliminary results were presented at the Madison Polarization Symposium. A paper for publication is intended but little progress has been made since the last report.

14. Polarization of Neutrons from the D(d,n) Reaction from 6 to 22 MeV (G. Spalek, R. A. Hardekopf, J. Taylor, Th. Stammbach, T. C. Rhea, J. M. Joyce, R. L. Walter)

A measurement of the D(d,n) neutron polarization was carried out from

* Now at National Bureau of Standards, Gaithersburg, Md.
** Now at Medical Physics Div., University of Wisconsin, Madison, Wisconsin
‡ Now at NEL, Edgewood, Maryland
\+ Now at Oak Ridge National Laboratory, Oak Ridge, Tennessee

6 to 14 MeV on the tandem accelerator and was reported at the Madison Polarization Conference. A second phase, using the pulsed beam of the Cyclo-Graaff, extended these measurements to 22 MeV. The polarization at 45° c.m. was found to be around 0.35 above 16 MeV in disagreement with earlier values reported around 0.24. Thus the reaction is the most useful source of polarized neutrons for 16 MeV < E_n < 22 MeV and the only measured source between 18 and 22 MeV. A brief report on the second part is being prepared for publication. A final analysis of the first part is still underway and will be published along with the data discussed in Section B-14.

15. (p,n) Experiments with Chopped Beam (S. M. Shafroth, A. A. Jaffe,* G. A. Bissinger,** T. G. Dzubay, F. Everling, D. W. Miller, D. A. Outlaw, E. J. Ludwig, A. Watkins, P. Nettles)

a. The data on ^{80,82}Kr(p,n) have been presented at the International Conference on Nuclidic Masses at Teddington, England.

b. The ^{36}Ar(p,n)^{36}K threshold data have been published in Physical Review C 3, 2489 (1971).

c. A study of the ^{36}Ar(p,n)^{36}K → β^+ ^{36}Ar*(γ) reaction has been made primarily to investigate the anomalous log ft in the $\Delta T = 0$, $\Delta J = 0$ $2^+ \rightarrow 2^+$ transition from ^{36}K to ^{36}Ar(6.613). As a result it was found that the log ft is normal (3.5). These data were presented at the Washington meeting of the American Physical Society and are part of the Ph.D. thesis of D. W. Miller. They are being prepared for publication.

d. (p,n) Excitation Functions. The studies of (p,n) excitation functions by observing delayed β-decay with the computer-controlled beam chopper have been suspended pending installation of new radiation shielding for the target area. Background radiation from the chopped beam during the counting cycle was too high to allow reliable β-yield measurements. With the new shielding walls, additional studies are anticipated.

---

* Now at Hebrew University, Jerusalem, Israel

** Now at Rutgers University, New Brunswick, N. J.

B. CHARGED PARTICLE REACTIONS

1. Fine Structure of Isobaric Analogue States in Medium-Weight Nuclei

(T. Dittrich, J. D. Moses, W. C. Peters, N. H. Prochnow,* W. M. Wilson, J. F. Wimpey, G. E. Mitchell, H. W. Newson, E. G. Bilpuch)

a. The Chromium Isotopes

A paper has been published on the questions of enhancement of neutron decay of analogue states in ^{55}Mn and ^{65}Cu: "A High-Resolution Investigation of the (p,n) Reaction Through Isobaric Analogue Resonances", Nuclear Physics A168, 406 (1971).

A paper covering measurements on the isotopes ^{50,52,54}Cr entitled "Fine Structure of Analogue States in ^{51}Mn, ^{53}Mn and ^{55}Mn" has been accepted for publication in Nuclear Physics. The following is the abstract of that paper:

> "Excitation functions were measured for proton elastic scattering from ^{50,52,54}Cr, inelastic scattering from ^{50}Cr and the (p,n) reaction on ^{54}Cr. Using the TUNL 3 MV Van de Graaff accelerator and high-resolution analyzer-homogenizer system, a total resolution of 300-400 eV was achieved for thin solid targets of enriched chromium isotopes. Eleven analogue states were observed; six of these showed well-developed fine structure patterns. Spins, parities, and partial widths were determined for approximately 330 resonances. Spectroscopic factors and Coulomb energy differences were extracted for the eleven analogue states."

b. Analysis of Fine Structure Distributions of Isobaric Analogue States

The distributions of the fine structure reduced widths versus energy for analogue states measured in this Laboratory over the past several years are being fit to the general form

$$S(E) = S_0 \frac{(E-E_\lambda-\Delta) + \omega^2/4}{(E-E_\lambda)^2 + \pi^2/4}$$

Here S(E) is the local strength function $S = \langle \frac{\gamma^2}{D} \rangle$ and S_0 is the background strength function, E_λ and Δ are the energy and displacement of the analogue state, Γ is the spreading width, and ω^2 is a parameter which indicates the effects of other open

---

* Now at Wisconsin State University, River Falls, Wisconsin

channels; it should vanish in the one-channel case. The fitting first averages both the data and the theoretical distribution using either a gaussian or a square weighing function, then is done by an automatic search code which varies any or all of the above parameters to minimize X^2. Studies are underway to determine the interdependence of the parameters and uniqueness of fit. This analysis is made difficult by the fact that the proton strength functions away from the analogue states are typically small and inaccurately measured, and that in most cases the analogue states have too few fine structure resonances for reliable fitting. Preliminary results on favorable cases indicate that the analogue state energy E_λ is well determined by this procedure, and that spreading widths can be extracted with approximately 25% accuracy. (The spreading widths in the mass region 50-65 are typically less than 10 keV.) The other parameters are less well determined, but approximate values should be obtainable.

c. The Iron Isotopes

A paper entitled "Fine Structure of Analogue States in ^{55}Co, ^{57}Co and ^{59}Co" has been published in Nuclear Physics A168, 37 (1971).

Analysis of the elastic scattering data for ^{58}Fe above 2.6 MeV has been completed. A paper entitled "Fine Structure of an Analogue State in ^{59}Co" is almost ready to be submitted for publication. The following is the abstract of that paper:

> "Differential cross sections were measured at four angles for proton elastic scattering from ^{58}Fe at energies from 2.65 - 3.11 MeV. Using the TUNL 3 MV Van de Graaff accelerator and high resolution analyzer-homogenizer system, a total resolution of 300 - 350 eV was achieved for thin solid targets of enriched iron ^{58}Fe. The analogue of the $3/2^-$ third excited state of ^{59}Fe shows a fine structure pattern. The spectroscopic factor and Coulomb energy difference were extracted for this analogue state. Spins, parities and widths were determined for approximately 125 resonances."

2. Statistical Properties of Nuclei Via Proton Resonance Reactions (E. G. Bilpuch, G. E. Mitchell, N. H. Prochnow, H. W. Newson, J. D. Moses)

We have almost completed our measurements of the high resolution proton elastic scattering excitation functions for all the even-even targets with $40 \lesssim A \leq 64$. These excitation functions extend over a proton energy range of about 1.5 MeV (1.8 MeV $\leq E_p \leq$ 3.3 MeV). In these isotopes we have observed about 40 analogue states. The observed fine structure is related to the level density of the particular compound nucleus. Statistical information can be obtained from these excitation functions for species of levels that have spin and parity different from that of the analogue state. Even for levels with the same spin and parity as that of the analogue state, one can obtain level density information in the vicinity of the analogue state as well as statistical information for the levels away from the analogue state.

In general the types of statistical information that one can obtain from these measurements are:

1. Level density variation with energy for states of a particular spin and parity.
2. The effect of the density change on the spacing distribution.
3. The effect of the density and strength function changes in the width distribution.
4. Energy dependence of the strength functions (for a particular spin and parity).
5. Dependence of the average strength function (for a particular spin and parity) on the neutron excess.

3. $^{50}Ti(d,p\gamma)^{51}Ti$ and $^{48}Ca(\alpha,n\gamma)^{51}Ti$ Angular Correlation Measurements (G. P. Lamaze, C. R. Gould, N. R. Roberson, D. R. Tilley)

Angular correlation studies have been completed on the excited states of ^{51}Ti using the reaction $^{50}Ti(d,p\gamma)^{51}Ti$. Studies of the levels have also been made with a 30 cc and 80 cc Ge(Li) detectors using the reaction $^{48}Ca(\alpha,n\gamma)^{51}Ti$ to populate the excited states. Both n-γ and γ-γ coincidence measurements were made. New levels have been observed at 2346, 2733, 2755, 2922, 3235, 3473, 3636 and 5440 keV excitation energies. Branching ratios have been obtained for the decays of many of the levels. Some spin assignments have also been made. A paper was presented at the 1971 Washington meeting of the American Physical Society. A paper is being prepared for submission to Nuclear Physics.

4. Mean Lifetimes in ^{27}Si (E. C. Hagen, C. R. Gould, N. R. Roberson, D. R. Tilley)

The mean lifetimes of the first six excited states of ^{27}Si have been investigated by use of the Doppler shift attenuation method. The γ-rays from the $^{24}Mg(\alpha n\gamma)^{27}Si$ reaction were observed at angles between 50° and 143° in coincidence with neutrons at 0°. The following mean lines were determined: τ(0.781 MeV state) > 5 psec, τ(0.957) = 1.73 ± 0.30 psec, τ(2.164) = 34 ± 15 fsec, τ (2.65) < 80 fsec, τ(2.86) = < 34 fsec, and τ (2.91) = 70 ± 16 fsec. The transition strengths are being compared with the predictions of an excited-core model.

5. Lifetimes in ^{37}Ar Using Doppler Shift Techniques (C. E. Ragan III, C. R. Gould, N. R. Roberson, G. E. Mitchell, D. R. Tilley)

These results have been published in The Physical Review C3, 1152 (1971). In addition a measurement on the 1.61 MeV level using the recoil distance method gave a mean life of 6.02 ± 0.29 nsec. This measurement has been reported in Physical Review C3, 2076 (1971).

6. Lifetime Measurements in ^{42}Sc (C. R. Gould, J. D. Hutton, G. E. Mitchell, N. R. Roberson, D. R. Tilley)

Levels in ^{42}Sc are currently being investigated by means of Ge(Li)-Ge(Li) coincidence measurements with the $^{40}Ca(^{3}He,p\gamma\gamma)^{41}Sc$ reaction. This technique has confirmed the presence of a number of weak branches seen in previous work at Liverpool and Utrecht and also confirms the presence of a new level at 2.297 MeV. In a separate experiment, the angular correlation of the 1844→ 1587 keV γ-ray has been investigated and indicates the 1844 level to have spin 1, 2 or 3 with the decay proceeding by a pure dipole transition. This is consistent with a negative parity assignment for this level.

7. Electromagnetic Studies in ^{57}Ni (C. R. Gould, N. R. Roberson, G. E. Mitchell, D. R. Tilley)

Gamma ray angular distribution measurements have been used to investigate properties of levels at 2.443 and 3.003 MeV in ^{57}Ni using the $^{54}Fe(\alpha,n)^{57}Ni$ reaction. A spin parity assignment δ, 5/2 was made for the 2.443 MeV level. The 3.003 MeV level was found to have possible spins δ 3/2 or 5/2 and a mean lifetime δ 11 ± 6 gs. These results have been submitted for publication in The Physical Review.

8. Location of the 0^+, T = 1 Analog State in ^{26}Al and 3.7 MeV (G. Bissinger, C. R. Gould)

Attention has recently been focussed on the location of the second 0^+ T = 1 state in ^{26}Al, the analog of the levels at 3.58 MeV in 3.32 MeV in ^{26}Mg and ^{26}S: respectively. Fortune et al.[1] claimed to have located this level at 3.72 MeV, contradicting an earlier assignment[2] of J = 1 to this state. We have performed a high resolution study of the decay modes of levels in ^{26}Al using $^{24}Mg(^3He,p\gamma)^{26}Al$. there the decay γ-rays were observed at 90° in an 80 cc Ge(Li) detector in coincidence with protons emitted at 180°. A level at 3721 keV clearly decays to the 0^+ first excited state at 223 keV and cannot therefore be the missing 0^+ T = 1 level. On the other hand the level at 3.75 MeV is found to be a doublet with energies of 3750 and 3754 keV. The upper member decays only to the lowest 1^+ T = 0 level at 1058 keV whereas the lower member decays to the 2^+ T = 1 at 2069.5 keV. The first of these two decay modes is the more reasonable for a 0^+, T = 1 level, involving as it does a $\Delta T = 1$, M1 transition. Therefore the level at 3754 keV may be the missing 0^+ T = 1 analog state in ^{26}Al.

9. The $^{90}Zr(p,\gamma)^{91}Nb$ and $^{51}Cr(p,\gamma)^{52}Cr$ Reactions (S. M. Shafroth, J. M. Joyce, G. J. F. Legge,* H. Ejiri,** T. Hain, W. McEver, E. J. Ludwig)

This work is inactive at present.

10. Gamma Ray Studies (S. M. Shafroth, P. H. Nettles, T. White+)

a. The 9" x 9" crystal is being used to investigate the $^{27}Al(p,\gamma)$ reaction at bombarding energies above the giant dipole resonance. New electronics and better anti-coincidence shielding are under construction.

b. The 80 cc Ge(Li) detector is being used by the high resolution group to study the gamma decay of analog resonances. It has recently been used to study the gamma decay of ^{36}Ar following β decay of ^{36}K, and to study ^{51}Ti and ^{26}Al. (See Sections B-3 and B-8.)

* Visiting scientist from the University of Melbourne, Melbourne, Australia
** Visiting scientist from the University of Washington, Seattle, Washington
\+ Furman University, Greenville, S. C.

1 H. T. Fortune, R. R. Belts, P. Neogy and D. J. Pullen, Phys. Letters 36B, 215 (1971)
2 G. A. Bissinger, P. A. Quinard, P. R. Chagron, Nucl. Phys. A115, 33 (1968)

11. X-Ray Studies (G. A. Bissinger,* S. M. Shafroth, A. B. Baskin, P. H. Nettles, W. Scates, A. W. Waltner, J. M. Howard, D. Peterson)

a. Characteristic Ag X-Rays Produced by ^{16}O Bombardment

Absolute cross sections and energy shifts have been measured as a function of beam energy for the characteristic K and L x-rays of Ag produced by ^{16}O bombardment. The PWBA predictions for K x-ray cross-sections are in rather poor agreement with the measurements, even after corrections were made for coulomb and binding-energy effects. Additional measurements are planned to confirm the absolute scale for the experimental cross sections. The PWBA predictions for the L x-ray cross section is in very poor agreement with the measurements. The problem of coulomb and binding energy effects for these predictions is under study, but no results are available at this time. A paper describing these measurements is in preparation.

b. 2 - 30 MeV Protons on Ag

A paper has been submitted to Physical Review entitled "Yields of K and L x-rays from 2 - 30 MeV proton Bombardment of Ag".

c. 0.5 - 3.0 MeV Protons on Au

A paper is being prepared entitled "Relative Intensity Variations and Centroid Shifts of L_α, L_β, L_γ X-Ray Peaks vs. E_p for 0.5 - 3.0 MeV Protons on Au." A new mechanism is proposed to explain the observed shifts.

d. 2 - 30 MeV Protons on Au

A paper concerning yields of L x-rays arising from 2-30 MeV bombardment of Au is nearly ready to submit for publication. Data have been obtained on the yield of Au K x-rays from 3 - 15 MeV protons using a borrowed ORTEC Ge(Li) detector for the x-rays.

e. Angular Distributions

Data were taken on the angular distribution of Ag K and L x-rays and Au L x-rays at E_p = 2.2 MeV. Much of the above data has been presented at a small international meeting "Inner Shell Ionization and Atomic Collisions II" at

---

* Now at Rutgers University, New Brunswick, N. J.

Amsterdam in July by Dr. Merzbacher.

12. ^{3}He Scattering and Polarization Studies (E. J. Ludwig, T. Clegg, R. L. Walter)

A paper has recently been submitted to Nuclear Physics describing measurements of ^{3}He cross sections and polarizations in elastic scattering from ^{9}Be, ^{12}C and ^{16}O. These data represent part of the thesis work performed by W. S. McEver.

Polarization measurements have also been obtained for 21 MeV ^{3}He particles scattered from ^{27}Al. The analysis of these data is almost complete and a report of the results was made at the Washington, D. C. meeting of the American Physical Society.

13. A Study of (d,t) and (d,^{3}He) Cross Sections and Polarizations (A. Watkins, E. J. Ludwig, T. Clegg, T. G. Dzubay)

The analysis has been completed of the angular distribution of ^{3}H and ^{3}He particles resulting from the bombardment of ^{32}S, ^{14}N and ^{10}B targets by beams of 15 MeV deuterons. The differential cross section agrees well with initial theoretical predictions made with code DWUCK, although the measured vector asymmetries for ^{14}N(d,t)^{13}N and ^{14}N(d,^{3}He)^{13}C disagree substantially with theory. ^{3}H and ^{3}He angular distributions appeared quite similar for "mirror" states except for some of the excited "mirror" states populated in these reactions. The vector asymmetries to comparable states differed in magnitude, a fact which might be explained by the different coulomb interactions in the outgoing channel.

An abstract has been submitted to the Southeastern Section meeting of the American Physical Society describing these results.

14. Measurements of The Analyzing Power for T($\vec{p}$,p)T and T($\vec{p}$,d)d (R. A. Hardekopf, P. Lisowski, T. C. Rhea, T. B. Clegg, R. L. Walter)

The polarized proton beam from the TUNL Lamb Shift source has been used to study asymmetries of the protons and deuterons from the T($\vec{p}$,p)T and T($\vec{p}$,d)D reactions. The deuteron asymmetry, equivalent to the proton polarization in the inverse reaction, has been compared with neutron polarizations resulting from the charge symmetric D(d,n)^{3}He reaction at equivalent deuteron bombarding energies from 3 to 14 MeV. A preliminary report was presented at the Few-Nucleon Conference in Budapest in July 1971. A phase-shift analysis of the elastic-scattering data is in progress.

15. The $^{28}Si(^{3}He,\alpha)^{27}Si$ Reaction at 21 MeV (J. Joyce, E. J. Ludwig)

The analysis of cross-section data corresponding to the lowest 11 excited states of ^{27}Si has continued using the DWUCK distorted wave program with the inclusion of finite range corrections in the calculations. The best agreement with the data was obtained when α-particle potentials were chosen to be about 50 MeV deeper than the ^{3}He potentials. The orbital angular momentum transfers have been determined in most cases and these appear to complement angular correlation work on this nucleus. This work is being prepared for publication.

16. The $^{54}Fe(p,t)^{52}Fe$ Reaction (R. O. Nelson, N. R. Roberson, C. R. Gould)

This work is being prepared for publication.

17. $Mg^{24}(d,t)Mg^{23}$ and $Mg^{24}(d,He^{3})Ni^{23}$ Reactions (R. O. Nelson, N. R. Roberson)

The reactions $^{24}Mg(d,t)^{23}Mg$ and $^{24}Mg(d^{3},He)^{23}Na$ have been studied using the 21.1 MeV deuteron beam of the TUNL Cyclo-Graaff. Angular distributions from 12° to 85° were measured for thirteen states below 5.4 MeV excitation energy in each of the mirror nuclei ^{23}Mg and ^{23}Na. To explain the cross sections an analysis in progress employs the coupled channel Born approximation (CCBA) which includes effects from multi-step processes in the entrance and exit channels. The results will be compared with previous calculations using the direct distorted Born approximation (DWBA).

18. Inelastic Deuteron Scattering from ^{24}Mg, $^{208,206}Pb$ (R. A. Hilko, R. O. Nelson, N. R. Roberson)

Inelastic deuteron angular distributions were measured using mass-identification with a solid-state ΔE-E telescope having a resolution of about 55 keV. Spectra from 12° to 155° in the laboratory was taken on ^{24}Mg with 21.1 MeV deuterons from the TUNL Cyclo-Graaff. Spectra from 25° to 90° were taken on ^{208}Pb with 23.0 MeV deuterons and spectra were taken on ^{206}Pb at 40° and 50°. Deformation parameters assuming a rotational model are being calculated using DWBA and the Coupled-Channel method.

19. $^{208}Pb(p,p)^{208}Pb$ (R. A. Hardekopf, T. B. Clegg, G. A. Bissinger)

Measurements of the cross section and polarization for protons scattered from ^{208}Pb are underway in the energy range 7 MeV $< E_p <$ 15 MeV. These consist at present of two excitation curves for cross sections over the energy range and

angular distributions at 10, 11, 12, 13, and 14 MeV. Polarization measurements will be made. Optical model parameters which describe the measurements will be extracted.

20. $^{207}Pb(d,p)^{208}Pb$ Asymmetry Measurements (R. A. Hardekopf, T. B. Clegg, G. A. Bissinger, W. J. Thompson, T. C. Rhea)

Measurements of the left-right asymmetry of protons from the reaction $^{207}Pb(d,p)^{208}Pb$ with an incident vector polarized deuteron beam are underway. These measurements are being made as a function of energy over the center-of-mass energy range corresponding to the position of the first analog resonances observed in $^{208}Pb(p,p)^{208}Pb$ elastic scattering. This asymmetry shows resonance behavior, though more data are desired to determine its shape more clearly. It is expected that a simple resonance-term addition to the usual optical model potential can account for this when used in a DWBA calculation.

21. A Study of T = 3/2 States in ^{41}Sc by ^{40}Ca + p Elastic Scattering (T. A. Trainor, T. B. Clegg, E. J. Ludwig)

To try to confirm the location of the lowest T = 3/2 state in ^{41}Sc, excitation curves for the cross section and polarization in ^{40}Ca + p elastic scattering are being taken in the energy range $4.900 \leq E_p \leq 4.928$ MeV in energy steps as small as 2 keV. The state at 4.899 MeV first seen by Brown[1] is tentatively assigned $3/2^+$ on the basis of his work and is thus thought to be the analogue of the ^{41}K and ^{41}Ti ground states. We have measured cross section excitation curves at θ_{lab} = 45.3°, 53.5°, 55.9°, 61.5°, 81.7°, 88.5°, 113.5°, 121.1°, 125.3°, 135.9°, 141.7°, 148.5° and polarization excitation curves at θ_{lab} = 53.5° and 133.5°. Analysis of these data is in progress and is expected to confirm the level parameters for this resonance.

22. $^{208}Pb(p,p')^{208}Pb$ (P. Nettles, E. J. Ludwig, J. M. Joyce, E. Klema*, H. W. Newson)

An effort has begun to obtain excitation curve data for protons inelastically scattered from ^{208}Pb in the energy range of 19 MeV $\leq E_p \leq$ 30 MeV. The study of the yield to excited states of ^{208}Pb may reveal variations in the cross sections at energies where single particle + excited core states are likely to be found. The initial part of the investigation was carried out with an overall resolution of about 30-40 keV using the TUNL Cyclo-Graaff. Particle identification techniques were

---

* Tufts University, Medford, Massachusetts

[1] Ph.D. Thesis, Rice University (1963), unpublished

used to separate deuteron and triton groups from the (p,d) and (p,t) reactions. These groups might be expected to resonate at energies corresponding to certain particle-hole excited core + single particle states.

23. Charge Asymmetry Measurements in $^{32}S(d,^{3}He)^{31}P$ and $^{32}S(d,t)^{31}S$ Reactions (T. G. Dzubay, R. V. Poore)

Simultaneous measurements of $^{32}S(d,^{3}He)^{31}P$ and $^{32}S(d,t)^{31}S$ cross sections have been made at beam energies of 17.7, 20.8, and 23 MeV. The experimental angular distributions and charge asymmetries are adequately described by the DWBA. Spectroscopic factors are found to be the same for (d,t) and (d,^{3}He) reactions within an accuracy of 5 per cent. Cross-section ratios for transitions to the ground states are found to decrease from 4.6 at 17.7 MeV to 2.6 at 23 MeV. A T = 1 isospin impurity of 1 per cent in the ground state of ^{32}S is able to account for a factor of 1.8 in the ratio, and this factor decreases very slowly with increasing beam energy.

C. DEVELOPMENT

1. Accelerator Improvements (F. O. Purser, T. D. Hayward, J. R. Boyce, Jr, H. W. Newson, R. L. Rummel, M. T. Smith, T. G. Dzubay, E. G. Bilpuch, J. D. Moses, G. E. Mitchell, D. Epperson)

a. Tandem Accelerator

The tandem accelerator has generally run satisfactorily since the last report. Such instabilities as have been encountered have usually been associated with improper positioning of the charging screens which tend to wear away from the belt resulting in a need for periodic opening to replace them.

We have encountered erratic behavior of the tungsten filaments used in the duoplasmatron source. Apparently identical filaments and source conditions can frequently give widely varying arc conditions resulting in unpredictable and sometimes unsatisfactory source performance. The conditions can normally be corrected by a change of filament. The problem is being investigated.

The major electrical components and controls for the direct extraction negative ion source are complete. Work has been started in the machine shop to fabricate the necessary parts for assembling and testing this source. We anticipate placing this source in operation, principally in connection with the tandem high resolution studies during January 1972.

b. The Injector Cyclotron

The injector cyclotron experienced its first serious down time during the past report period. A short circuit in the oscillator precipitated various surge-power related failures in the anode supply which required nearly two weeks to isolate and repair. It has been back in satisfactory operation for two months.

The central dee geometry has been modified to render possible more accurate positioning. Following this modification, both high resolution (0.5 ns burst length) and high intensity operation has shown improvement.

A singlet quadrupole is being installed between the cyclotron and tandem to improve over all beam transmission. This quadrupole will be valuable principally for the neutron polarization group which would like high deuteron beam currents ($> 4\mu A$) on target.

The pulse suppression system for time-of-flight work and the external dee-voltage feedback system have been held up by other projects and lack of personnel. It is hoped that they can be completed and placed in routine use within the coming report period.

The possibility of using the cyclotron to produce moderate quantities of medically useful short-lived isotopes is being investigated. The isotope program would occupy approximately 30% of the cyclotron running time which is at present utilized for about 40% of the available time as an injector in the Cyclo-Graaff. Isotopes produced would be supplied to Duke University Medical Center which would process them for use in their nuclear medical program.

c. Improved Beam Energy Resolution for The Tandem Accelerator

This program is continuing with the emphasis upon improving overall resolution and ensuring reproducibility of results. A total overall resolution of about 1 keV was obtained for the $T = 3/2$ resonance in carbon at 14.233 and is presently being analyzed. Repeated runs over a known analogue resonance region in ^{92}Mo indicate that early problems in making accurate energy steps of less than 500 eV and reproducing energy calibrations to 1 keV have been solved. The limit on attainable resolution with the present equipment remains Doppler broadening of the HH^+ beam in the source exchange canal. Installation of a well regulated direct extraction source should remove this limitation and allow us to reach the resolution region governed principally by target Doppler effects.

2. Pulsed Beams (F. O. Purser, T. D. Hayward, D. E. Elliott, H. W. Newson, R. O. Nelson, R. A. Hilko, T. G. Dzubay, N. R. Roberson, P. Nettles, E. J. Ludwig, S. M. Shafroth)

a. Cyclo-Graaff Time-of-Flight System

This program has been held in abeyance for this report period due to the press of other projects. The chopper plates for the fast pulse suppression systems have proven quite useful in chopped beam experiments measuring decay curves (slow chopping).

b. Particle Identification by Time-of-Flight

This program is continuing utilizing the Cyclo-Graaff deuteron beam. Overall time resolutions of 800 ps have been obtained.

3. Polarized Source Improvements (T. B. Clegg, T. A. Trainor, T. C. Rhea, P. W. Lisowski, R. H. Hardekopf)

There have been several problems which appeared with ion source operation. They are listed below with comments on the solutions found or tried.

(1.) There has been considerable trouble with poorly regulated high voltage power supplies for the lenses and electrostatic mirrors. A regulation circuit was constructed which reduced the long term voltage drifts to about ±25 volts out of 50 kV. There still is considerable problem with power supply ripple and a new regulation circuit is under construction to regulate against voltage drifts and ripple.

(2.) The magnetic field for the "spin filter" must be uniform to ±0.2G over a 10" long axial distance. If this is not true, poor spin state selection results. Because poor selection was observed the magnetic field was carefully remeasured and coil currents were adjusted slightly to reestablish the uniform field. Provisions were made to monitor the coil currents to check the field uniformity in the future.

(3.) To determine the exact direction of the spin quantization axis at the scattering chamber, it is necessary to know the energy of the polarized beam as it passes through the spin precession solenoid and the current in the solenoid. Apparatus has been built to monitor the beam energy and the solenoid current continuously. Calculations have been made to establish the solenoid current required to precess the spin quantization axis through the desired angle for any polarized beam energy at the ion source.

(4.) The deionized water cooling system for the ion source has been troublesome because it is open and the water loss from evaporation is substantial requiring frequent refilling. A closed heat exchanger has been purchased and will be installed during October. The system can then be operated closed to prevent evaporation.

(5.) The polarized beam currents remain ~ 1-10 nA on target. The causes of these low beam currents (relative to the 100 nA usually achieved by the similar Los Alamos group with their polarized source) are uncertain, but probably there are two major contributions:

(a.) The positive ion duoplasmatron at LASL produces more H^+ beam than the one at TUNL, by maybe a factor of 5.

(b.) The beam optics for the Los Alamos source has been designed so that a larger percentage of the polarized beam is accelerated through the tandem and reaches the target. The first of these ideas has been investigated by changing the extraction geometry and magnetic lens for the positive ion beam. This investigation has not yet improved the beam substantially, but is continuing.

4. Rotating Scattering Chamber (P. W. Lisowski, T. B. Clegg, E. J. Ludwig, F. O. Purser)

To facilitate measurements with the polarized deuteron beam, a rotating seal system with new support stands has been designed for the scattering chamber now installed on the 52° beam leg after the first analyzing magnet. When installed this system will allow easy measurement of deuteron vector and tensor analyzing powers by rotating the chamber in 90° intervals around the beam axis. It is expected that the shop work on the necessary parts will start soon and that the rotating chamber will be available within the next six months.

5. New High-Intensity Positive Ion Duoplasmatron (T. A. Trainor, T. B. Clegg)

To try to increase the H^+ beam used in the Lamb-shift polarized ion source, work has begun on a new duoplasmatron. The design has been adapted slightly from one tested successfully at Oak Ridge by the plasma physics group.[1] It differs from the duoplasmatron now installed on the TUNL polarized ion source in that the arc current to be used will probably be 25-40 A versus 13A in the present source. It also utilizes a multi-aperture electrode to cover the plasma expan-

[1] Thesis, O. B. Morgan, University of Wisconson (1970), unpublished

sion cup. A similar multi-aperture electrode aligned carefully with the first will serve as the extraction electrode. Finally a heated thoriated tungsten grid immediately after the extraction electrode will serve as a source of electrons to space-charge neutralize the positive beam.

The hardware and electronics for the source are approximately halfway completed. It is expected that testing of the source may begin early in 1972.

6. Development of a High Resolution System for The 4 MeV Van de Graaff Accelerator (D. Flynn, F. O. Purser, G. E. Mitchell, H. W. Newson, L. W. Seagondollar, E. G. Bilpuch)

In order to devise a system with which to perform elastic (p,p) scattering at energies up to 5 MeV and with energy resolution of the order of 400 eV, we have modified our standard high resolution system.

In the new system the energy of the central beam (HH^+) is changed by changing the potential applied to a water vapor stripper which dissociates the HH^+ beam just before it enters the electrostatic analyzer. Normally the electrostatic analyzer can only measure energies up to 3 MeV. By using the dissociated beam (which will have half the energy of the primary ^+H beam) the analyzer can effectively measure accelerated proton energies up to 6 MeV. Using the electrostatic analyzer to measure energy changes, and the stripper to change the energy, we have devised a negative feedback system which keeps the dissociated beam centered at the analyzer exit slits and thereby gives directly (from the negative value of the stripper voltage) the fluctuations of the beam energy. This system has the advantage of cancelling time dependent energy fluctuations while requiring only half the normal analyzer voltage as compared to the system used on our 3 MeV accelerator where the full voltage is put on one plate to measure the energy of the HH^+ beam.

Known resonances of ^{60}Ni + p in the vicinity of 2.21 MeV were observed, and the width of the energy resolution--both with and without the new homogenizer control circuit--was estimated. The resolution without homogenizing was ~ 2 keV. The resolution was also measured directly by observing the peak-to-peak voltage fluctuation on the stripper. With homogenization, the resolution was ~ 600 to 700 eV.

It is expected that better collimation, a better analyzer voltage supply, and a new corona stabilizing system can further improve the energy resolution obtainable with the 4 MeV accelerator making it more nearly competitive with that of the 3 MeV accelerator (~ 300 eV).

7. Computers and Programming (R. J. Eastgate, S. E. Edwards, C. R. Gould, R. A. Hardekopf, R. A. Hilko, R. O. Nelson, W. C. Peters, N. R. Roberson)

a. Data Acquisition And Analysis

The two DDP-224 computers have operated reliably during the last six months with little downtime. The acquisition of fast, fixed head disc or drum memory is being considered for both computers. This will facilitate data analysis on the 8K off-time computer and the handling of large data arrays on the 16K on-line computer in connection with multi-counter telescope and fission experiments.

b. IBM 360 and DDP-224 Programming

The programs JIB 3, SNOOPY, BANDMIX, DWUCK-2, M2, CORPAR and FTAU continue to be used at TUCC on the IBM 360 model 165 computer. In addition, an improved version of T. Tamura's JUPITOR I code has been received from G. W. Schweimer of the Karlsruhe cyclotron laboratory, Germany. This version renormalizes the calculated wave function exponent if this becomes greater than the exponent range on a given computer and also has a new search routine. Both single and double precision versions are currently running.

The code MARS, written by T. Tamura, has also been adapted for the IBM 360. Using the coupled channel Born approximation, the program calculates differential cross sections for reactions including multistep processes as well as the direct contribution. The program is currently being used for the analysis of reactions on several deformed nuclei.

An automatic gradient-search program for the elastic scattering of spin 1/2 on spin 1/2 particles is running on the 8K DDP-224 off-line computer. The program, called CPHASE, fits cross sections and polarizations for up to 30 angles and outputs results on the line printer and on the display oscilloscope. Singlet and triplet complex phase shifts are calculated for up to four ℓ-waves and mixing parameters for p- and d-waves.

A modified version of the optical model code OPTICS has been used to generate reaction cross sections for proton elastic scattering on Uranium near the Coulomb barrier in connection with current fission studies. The code will also be used to provide normalized optical wave functions needed in a distorted wave stripping code.

Data analysis by the 3 MeV high resolution, γ-ray spectroscopy

group is performed with the programs RAND, LINCOR and MULTEYE. LINCOR calculates the multiple correlation coefficients between given sets of numbers and RAND determines the confidence level (percent) of the coefficients. MULTEYE is a multilevel, single channel R matrix code for fitting elastic scattering data. The code can fit up to ten levels simultaneously.

D. GENERAL

1. Radioactivity Studies with The 80 cc Ge(Li) Detector (T. Hain, J. G. F. Legge, J. Montgomery, S. M. Shafroth)

This work is inactive at present.

2. 24" Scattering Chamber

The new 24" scattering chamber which allows detectors to be placed at completely arbitrary scattering angles has now been completed and will soon be installed after the high-resolution magnet system. This general purpose chamber will have freon-cooled detectors and will be especially useful for excitation curve work.

E. THEORY

1. Optical-Model and Phase-Shift Analysis of $^4He(d,d)^4He$ (W. J. Thompson)

Our previous analyses up to 52 MeV d energy have been re-examined and will now include all measured cross sections, vector and tensor polarizations. The total of more than 3000 data points has been plotted for comparison purposes. Improved optical-model potential parameters will be used to give starting parameters for a complete phase-shift analysis. Calculations for use in absolute deuteron vector polarization determinations with the TUNL Lamb-shift source will then be made.

2. Description of $^{9}Be(p,p)^{9}Be$ and $^{9}Be(p,p')^{9}Be^{*}$ (M. F. Werby,** S. Edwards+ W. J. Thompson, H. J. Votava, E. J. Ludwig, T. B. Clegg)

The optical-model analysis for 6 to 30 MeV protons which was made by the first three authors has been published in Nuclear Physics A169, 81 (1971). The recently-completed measurements at TUNL of elastic and inelastic cross sections up to 30 MeV, polarizations up to 15 MeV and excitation functions from 6 to 15 MeV have so far revealed a probable, previously-unreported, resonance near 7 MeV p energy.++

3. Energy and Isospin Dependence of the Optical-Model Potential from Proton Bombardment Below the Coulomb Barrier (J. S. Eck,‡ W. J. Thompson)

Recently-obtained polarization data from University of Wisconsin and cross section data from TUNL (T. B. Clegg and R. A. Hardekopf) have been analyzed and show that the energy dependence of the optical-model potential at low energies is more rapid than that indicated from higher-energy analyses, a result in agreement with that from low-energy (p,n) reactions investigated at ORNL. Theoretical analysis of the energy dependence expected from the Fermi-gas model with Pauli correlations (SES-APS Abstract) agrees with the low-energy results. Work on the isospin dependence of the optical potential is in progress.

4. Spin Precession in the Nuclear Potential (H. J. Votava, W. J. Thompson)

Final checkout of the program for spin-1/2 precession during elastic scattering in the nuclear potential (SNOOPSPN) has been completed and is being applied to scattering by realistic optical-model potentials with spin-orbit coupling. Graphics routines are being incorporated to allow pictorial representations to help clarify spin phenomena in nuclear interactions.

5. Alpha Clustering and Elastic Alpha Scattering (W. J. Thompson)

A paper showing that alpha clustering in the target nucleus is not responsible for the backward enhancement in alpha elastic scattering from some nuclei near A = 40 is to be published in Particles and Nuclei.

** Florida State University
+ Florida State University
++ See Tucson, American Physical Society Meeting Abstract
‡ Kansas State University

6. Heavy-Ion Elastic and Inelastic Scattering Calculations (W. J. Thompson, R. H. Siemssen*)

The coupled-channels code JUPITOR-1 (T. Tamura, ORNL-4152) has been adapted to the ANL, CDC-3600 computer, and is being used to analyze data from Argonne. A version for the IBM 370/165 at TUCC is now running. Subroutines to calculate Coulomb-excitation contributions have been debugged and will be incorporated in JUPITOR-1 to increase accuracy while reducing computing time.

7. Optical-Model Absorption Cross Sections and Proton-Induced Fission (R.J. Eastgate, J. R. Boyce, Jr., W. J. Thompson)

Stringent tests on the DDP-224 optical-model program OPTICS were made in modifications to calculate total absorption (reaction) cross sections at low energies and to relate these to (p,f) total cross sections. However, for many fissionable nuclei, it can be shown by explicit calculation that Coulomb excitation is probably the dominant contribution to the low-energy proton absorption cross section.

8. Nuclear Theory Computer Programs (B. H. Choi, S. K. Datta, R. J. Eastgate, D. A. Payne, W. J. Thompson)

Final versions, updates and documentation for the following programs for use in analyzing nuclear-structure data from TUNL experiments are at, or near, completion:

(1.) SNOOPT2 - A new version of the optical-model and phase-shift analysis code is on on-line disk at TUCC.

(2.) JUPITOR-1 - A double-precision version of the coupled-channels code for collective-model analysis of elastic and inelastic scattering, at TUCC.

(3.) BSEF - Bound-state energy eigen-value or well-depth search program with oscilloscope display of wave function and potential, at TUNL.

(4.) OPTICS - On-line optical-model analysis program for elastic and compound-elastic scattering analyses, with oscilloscope display of cross sections and polarizations, at TUNL. A description of this code is in preparation for Computer Physics Communications.

---

* Argonne National Laboratory

(5.) DWBA Code for Zero-Range Analysis of Transfer Reactions - The few available DWBA codes are poorly documented, difficult to modify and do not calculate all relevant polarization quantities. The codes BSEF and OPTICS are being used in writing a new code for use at TUCC, and at TUNL when large-capacity addressable storage (e.g. drum) becomes available.

(6.) Moshinsky Bracket Subroutine - Documentation of this subroutine, which is very useful for shell-model and Hartree-Fock residual interaction calculations, is nearing completion.

(7.) Angular Momentum Coefficients in Prime Notation - The 3n-j coefficients can be expressed exactly as square roots of quotients of prime numbers. Algorithms and programs have been written to perform prime-number arithmetic, and will be used for the 3n-j coefficients for angular-momentum coupling.

In general, for flexibility of usage, we require that our programs for the TUNL, DDP-224 will also run at TUCC without reprogramming.

A 4000-track disk pack has been rented from Memorex Corporation at a saving of a factor of 40 over TUCC rental. The pack will serve as a large-capacity ($3.5*10^6$ word) program and data library, thus minimizing computer input-output time.

U. S. Army Aberdeen Research and Development Center

RADIATION DIVISION
BALLISTIC RESEARCH LABORATORIES

A. SMALL-ANGLE ELASTIC SCATTERING OF FAST NEUTRONS (C. Hollandsworth, W. Bucher, R. Lamoreaux, A. Niiler, and R. Sankey)

The measurements of the small-angle elastic neutron scattering from carbon, oxygen, and nitrogen at 7.55 and 9.5 MeV have been completed and the final results were presented at the Tuscon Meeting of the American Physical Society. The following abstract was submitted:

"A new technique has been developed for the measurement of small-angle elastic scattering of 6-10 MeV neutrons. By using a scattering geometry which is the inverse of that normally employed for small-angle measurements, several advantages are realized. The increased counting rate and sensitivity (signal-to-background ratio) permit measurements for low A nuclei. The results of measurements of the differential cross sections for scattering from C, N, and O in the angular range 2° to 15° will be presented. In some cases the small-angle cross sections are found to be 20% to 40% higher than would be inferred from existing data."

Table A-1 summarizes the results of these measurements and a plot of the carbon data is shown in Figure A-1. The angular resolutions are ± 0.7, ± 0.9, ± 1.2, and ± 1.5 degrees for the scattering angles 2.6, 6.6, 10.4, and 14.2 degrees, respectively. The energy spread of the incident neutrons is ± 60 and ± 50 keV at 7.55 and 9.50 MeV, respectively. The uncertainty in the mean neutron energy is estimated to be 30 keV. Further small-angle data for the above elements have been taken at 7.40, 8.56, and 9.00 MeV. These data are complete and will be processed in the near future.

Since all the above small-angle measurements with the special-purpose collimator were made, as a matter of convenience, relative to the cross section of lead, the latter cross section was determined for the purpose of normalization by auxiliary measurements carried out in ring geometry. Such data for lead was obtained at 7.55, 8.0, 8.56, and 9.0 MeV for the angular range 3.5 to 15 degrees. Only the 7.55 and 9.0 MeV data have been processed and these are shown in Figure A-2.

Future work will involve an extension of the C, N, and O measurents to the 10-14 MeV energy range and measurements for Be, Aℓ, Fe, Cu, Sn, and W at 7.55 MeV in the angular range 2-15 degrees. (Pertinent to Requests #31, #33, # 39, #40, and #44; NCSAC-35).

TABLE A-1 Results

CARBON

θ_L	θ_{cm}	7.55 MeV σ_{cm}(mb)	7.55 MeV % error	9.5 MeV σ_{cm}(mb)	9.5 MeV % error
2.6°	2.82°	681	9	472	7
6.6	7.15	600	5	427	5
10.4	11.26	566	5	407	5
14.2	15.37	514	5	369	5

NITROGEN

θ_L	θ_{cm}	7.55 MeV σ_{cm}(mb)	7.55 MeV % error	9.5 MeV σ_{cm}(mb)	9.5 MeV % error
2.6°	2.79°	593	13	499	14
6.6	7.07	524	11	371	12
10.4	11.14	506	10	389	9
14.2	15.20	369	10	368	9

OXYGEN

θ_L	θ_{cm}	7.55 MeV σ_{cm}(mb)	7.55 MeV % error	9.5 MeV σ_{cm}(mb)	9.5 MeV % error
2.6°	2.76°	340	18	385	17
6.6	7.01	260	17	320	13
10.4	11.05	221	18	285	13
14.2	15.08	155	18	242	11

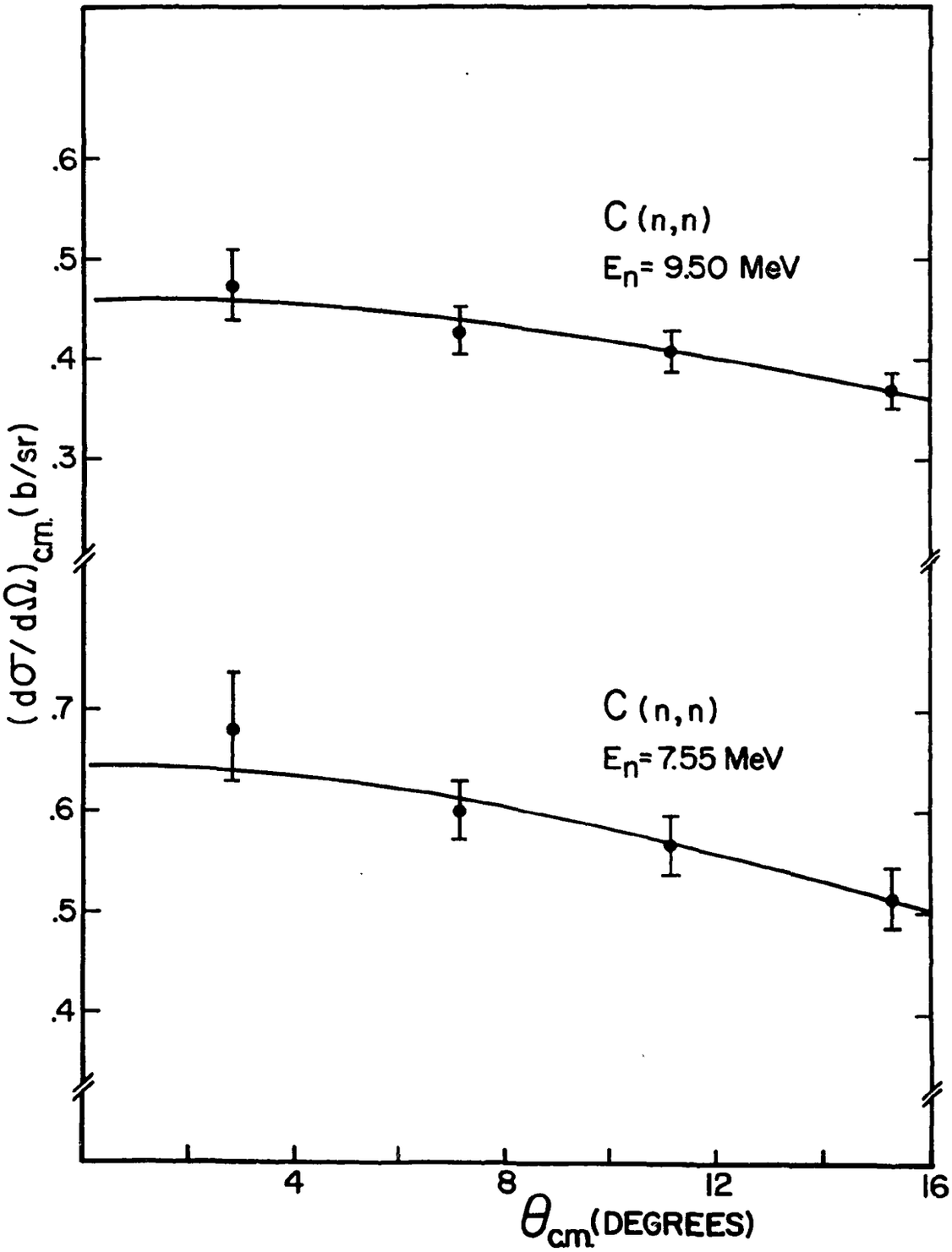
C (n,n)
E_n= 9.50 MeV
C (n,n)
E_n= 7.55 MeV
.6
.5
.4
.3
.7
.6
.5
.4
$(d\sigma/d\Omega)_{cm.}$ (b/sr)
4
8
12
16
$\theta_{cm.}$(DEGREES)

Fig. A-1

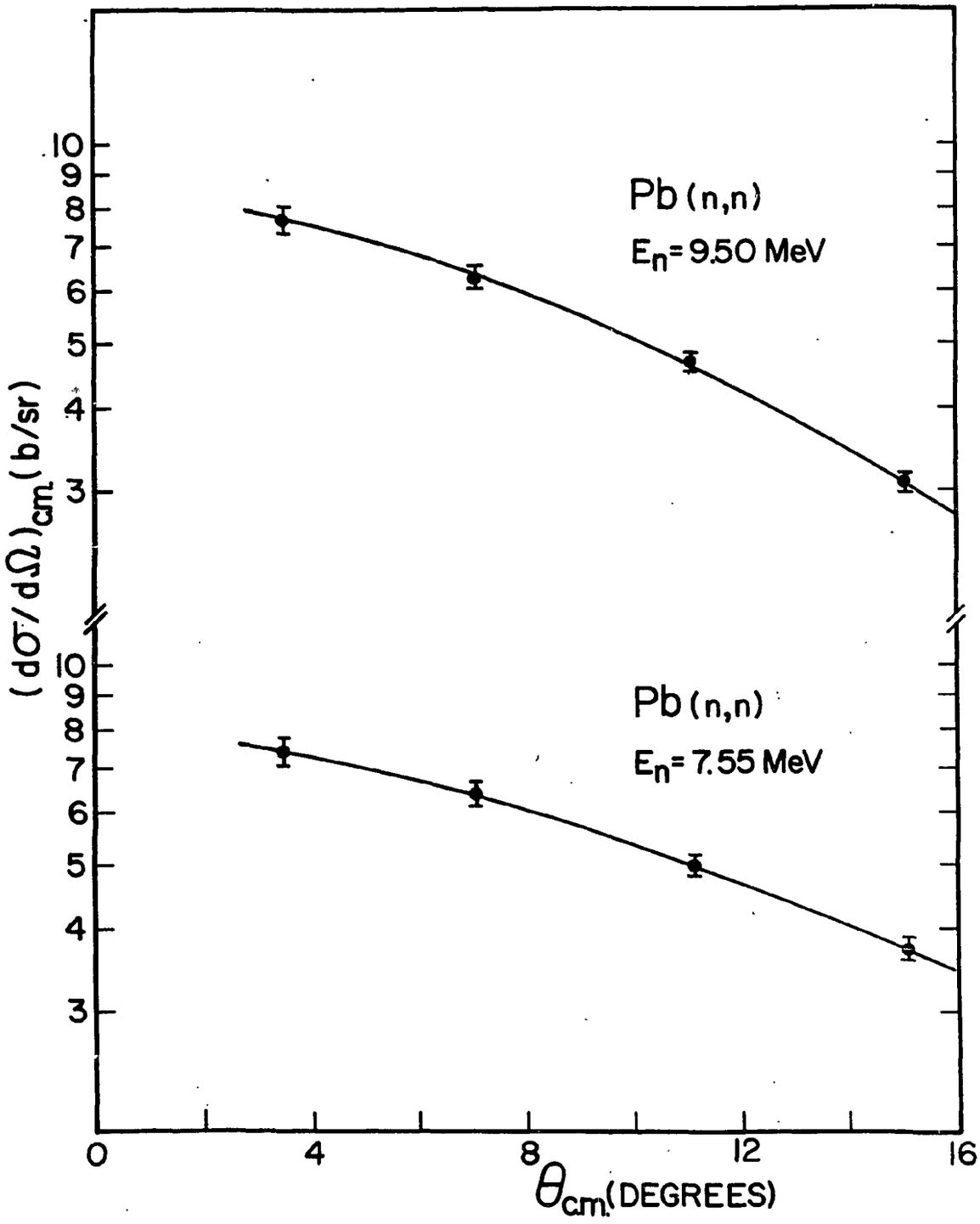
Pb (n,n)
E_n= 9.50 MeV
Pb (n,n)
E_n= 7.55 MeV
$(d\sigma/d\Omega)_{cm}$ (b/sr)
10
9
8
7
6
5
4
3
0
4
8
12
16
θ_{cm} (DEGREES)

Fig. A-2

YALE UNIVERSITY

A. FAST NEUTRON POLARIZATION STUDIES (F.W.K.Firk, H.L. Schultz, R.J. Holt, R. Nath and F.D. Brooks (visitor from University of Cape Town S.A., 1970-71))

1. Polarization in $\vec{n}$-p Scattering

Measurements of the left-right asymmetry in $\vec{n}$-p scattering in the energy range 5-20 MeV have been completed using an anthracene crystal as a combined proton target-neutron polarimeter. The source of polarized neutrons was the reaction $^{12}C(n,\vec{n})^{12}C$ at 50°: measurements of the source polarization are now in progress. The neutron energies were measured with a resolution of 0.3 ns. m^{-1}.

2. Absolute Polarization of Neutrons in n-^{12}C Scattering Between 2 and 5 MeV

An absolute determination of the polarization of neutrons elastically scattered from ^{12}C at a laboratory angle of 50° has been made as a continuous function of energy between 2 and 5 MeV using a neutron double-scattering technique. The neutron energies were measured with a time-of-flight resolution of 0.7 ns.m^{-1}. As a refinement, the neutron spin-precession method, recently developed at Yale for use with a continuous energy spectrum of neutrons was used to reduce systematic errors to negligible amounts. From an intensity point of view, the present experiment involves "quadruple-scattering" namely: $(e^-,\gamma)\rightarrow^{238}U(\gamma,n)\rightarrow^{12}C(n,\vec{n})\rightarrow^{12}C(\vec{n},n)$. It is only feasible now that peak electron currents of approximately 10A are available in the short pulse mode of the electron linac.

The observed values of P(E) ' P(E-ΔE) obtained using two identical graphite scatterers, each 15 cm long x 7.5 cm wide x 1.5 cm thick, are shown in Fig. A-1(a). Here, ΔE is the energy loss in n-^{12}C scatterings at 50°. The values of the polarization, P(E), deduced from the double-scattering measurements are shown in Fig. A-1(b). In order to calculate these polarizations, a starting value of P(E) = 0.47 is obtained at 2.25 MeV where the polarization is essentially constant

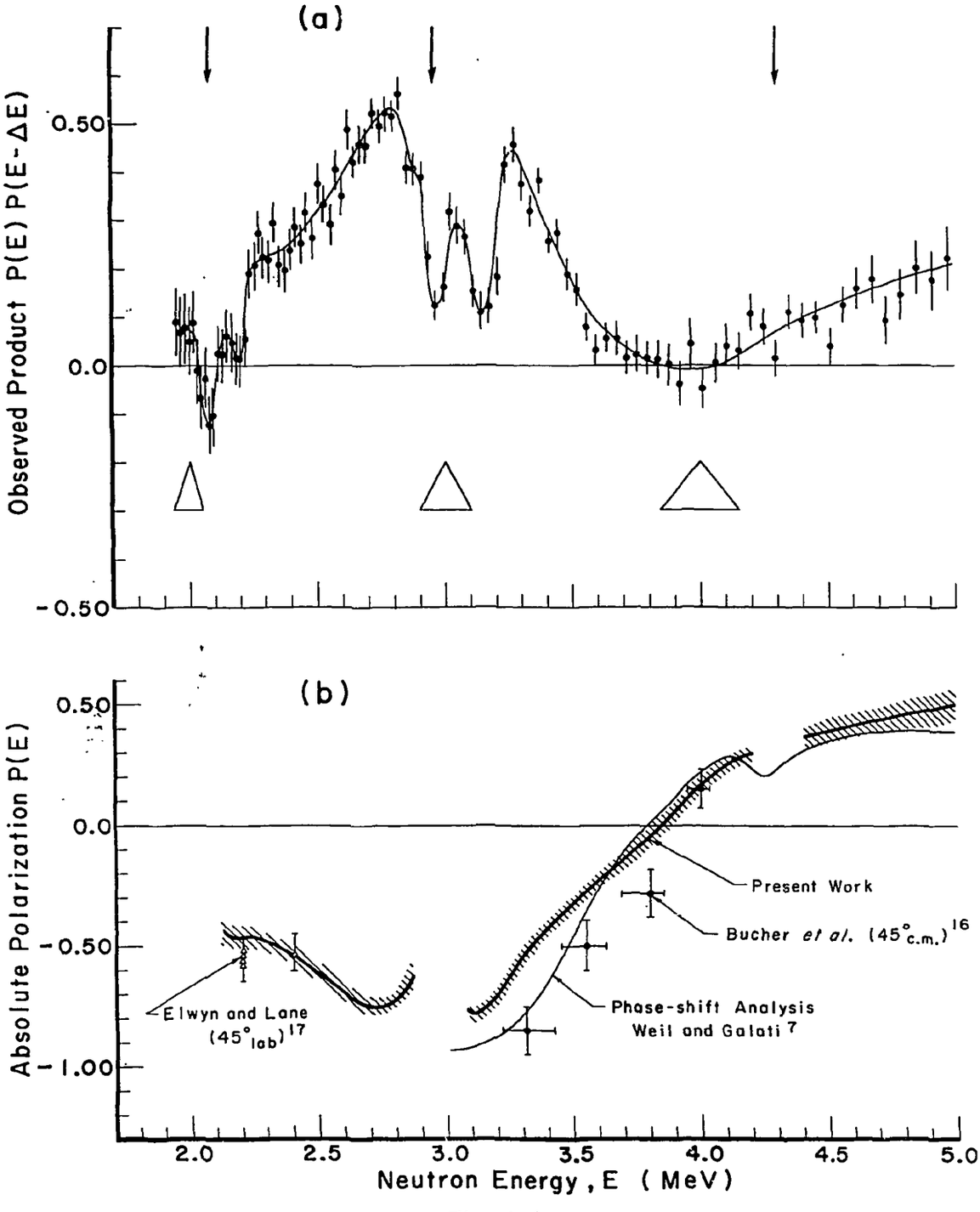
(a)
Observed Product P(E) P(E-ΔE)
0.50
0.0
-0.50
(b)
Absolute Polarization P(E)
0.50
0.0
-0.50
-1.00
Present Work
Bucher et al. (45°c.m.)16
Phase-shift Analysis
Weil and Galati 7
Elwyn and Lane
(45°lab)17
2.0
2.5
3.0
3.5
4.0
4.5
5.0
Neutron Energy, E (MeV)

Fig. A-1.

over the range of the energy loss (116 keV at 2 MeV). (The values of the polarizations in the immediate vicinities of the resonances at 2.08, 2.96 and 4.3 MeV have been omitted from Fig. 1b due to uncertainties in the corrections for the resolving power of the spectrometer).

Previous measurements of the polarizations, obtained by traditional methods, are shown for comparison. At 2.2 and 2.4 MeV, the agreement with the results of Elwyn and Lane is very good. However, between 3.2 and 3.9 MeV, the present values indicate significantly less polarization than those reported by Bucher _et al_. The phase-shift analysis of Weil and Galati is also shown.

When used with the intense pulsed primary photoneutron sources available on modern high-powered electron linacs or with the primary $\vec{(p,n)}$ sources available on cyclotrons, the reaction $^{12}C(n,n)^{12}C$ provides a useful source of polarized neutrons in the MeV-region which has the virtues of technical simplicity and very low cost.